PROGRESSIVE COLLAPSE ANALYSIS AND PROBABILISTIC MODELS FOR ANALYSIS AND DESIGN OF MULTI-STOREY BUILDINGS SUBJECT TO BLAST LOADING

A Thesis Submitted

In Partial Fulfilment of the Requirements

for the Degree of

DOCTOR OF PHILOSOPHY

by

Barri Chinna Seethayya

DEPARTMENT OF CIVIL ENGINEERING

INDIAN INSTITUTE OF TECHNOLOGY GUWAHATI

GUWAHATI – 781039

JUNE 2023

CERTIFICATE

This is to certify that the work contained in the thesis entitled *"**PROGRESSIVE COLLAPSE ANALYSIS AND PROBABILISTIC MODELS FOR ANALYSIS AND DESIGN OF MULTI-STOREY BUILDINGS SUBJECT TO BLAST LOADING**"* is the result of investigations carried out by **Mr. Barri Chinna Seethayya** under my supervision and is an authentic record of the results obtained from the research work carried out at the Department of Civil Engineering, Indian Institute of Technology Guwahati, India for the award of degree of Doctor of Philosophy. This work has not been submitted elsewhere for a degree.

Thesis Supervisor

Dr. Hrishikesh Sharma

Associate Professor

Department of Civil Engineering

Indian Institute of Technology Guwahati, India

Guwahati

June 2023

DECLARATION

I, Barri Chinna Seethayya, a PhD Scholar of Indian Institute of Technology Guwahati declare that the content of this entitled *"**PROGRESSIVE COLLAPSE ANALYSIS AND PROBABILISTIC MODELS FOR ANALYSIS AND DESIGN OF MULTI-STOREY BUILDINGS SUBJECT TO BLAST LOADING**"* submitted here is a partial fulfilment for the requirement of awarding the Degree for **Doctor of Philosophy** and submitted to Indian Institute of Technology Guwahati, India. This thesis is the documentation of the research work carried out by me at the institute in a period of **July 2016 to June 2023** under the supervision of ***Dr. Hrishikesh Sharma,*** Associate Professor, Department of Civil Engineering, Indian Institute of Technology Guwahati, India. This work has not been submitted elsewhere for any degree or diploma of any institute or university to the best of my knowledge and belief.

In keeping with the general practice of reporting scientific observations, due acknowledgements have been made wherever the work described is based on the findings of other observations.

Barri Chinnaseethayya

Guwahati **BARRI CHINNA SEETHAYYA**

June 2023 Roll No. 166104023

ACKNOWLEDGEMENTS

The gratification and happiness on the successful completion of any task would be incomplete without mentioning the people who made it possible and; whose constant guidance and encouragement crowned my effort with success. I want to grab this opportunity to acknowledge the kindness of all those who guided and helped me to complete MY THESIS.

First of all, I would like to express my sincere thanks to my guide **Dr. Hrishikesh Sharma** for his co-operation, suggestions and esteemed guidance thorough critical reviews of my work. I am a big fan of his Courage, Commitment and Confident towards work and academic challenges.

Secondly, I want to thank all the other members of my Doctoral Committee Prof. Konjengbam Darun Kumar Singh, Prof. L. Boeing Singh and Prof. Vinayak Kulkarni (Department of Mechanical Engineering) for their faith and believe over my work. Besides, I would like to thank all the teachers who helped me with their advice and encouragement which I needed. My heartfelt special thanks to my inspiration, Missile Man and Ex-president of India, Dr. A.P.J Abdul Kalam who changed my perception at LEAD INDIA-2020 movement.

Finally, I want to thank MY PARENTS for their unconditional love and support, and friends specially Durgarao P, Satyanarayana K for their help When I needed the most, and Jaswanth G for his enormous support throughout the completion of MY THESIS.

"My Humble Thanks to IIT Guwahati and Government of India"

BARRI CHINNA SEETHAYYA

ABSTRACT

Concrete and steel rigid frame structures are the most utilised civil engineering structures in building constructions. The rigid frame buildings can experience to blast loads (lateral loads) during their lifetime. This research presents a finite element simulations of charge shapes and their spherical equivalents, the validation of the Multi-Material Arbitrary Lagrangian Eulerian (MM-ALE) approach and the analysis of an RC frame subject to internal blast loading. This research develops a novel quadratic blast profiles and response spectra for both quadratic and exponential profiles, and presents the numerical validation of blast profile. This research also develops the multi-storey rigid frame structures' critical load factors analysis, probabilistic models of critical load factors, and the peak loads of multi-storey buildings, and presents their validation. This research also presents the dynamic analysis of multi-storey buildings subject to blast loading, eigen modal analysis, generalised equation of motion, development of modified shape function, and validation of the modified shape function. This research illustrates the framework for designing multi-storey buildings subject to blast loading and the member design approach, equivalent SDOF design method, and multi-storey building design procedure. This research also presents the methodology and framework to quantify the required resistance of multi-storey buildings to mitigate progressive collapse. This research also develops the probabilistic models for collapse resistance factors for the series of top and bottom column removal in the multi-storey buildings. Finally, this research presents a simple, accurate and probabilistic framework for the analysis and design of multi-storey building subject to blast loading. The MATLAB code is used to develop the quadratic blast profiles. The SAP2000 and LS-DYNA softwares are used to carry out the simulations of RC frame subject to blast loading. The OriginPro is used to develop probabilistic models of progressive collapse resistance and peak load factors. The limitations of building shape function, peak loads of multi-storey buildings, the charge shape and progressive collapse

methods are addressed to enhance the blast resistant design techniques. This study is limited to the rigid frame multi-storey buildings subject to blast loading only.

TABLE OF CONTENTS

TABLE OF FIGURES

TABLE OF TABLES

CHAPTER 1 INTRODUCTION

1.1 General

The intensity of terrorist attacks has grown in the last decade, and it has been noticed that there has been a substantial increase in death tolls due to these frequent events, with global consequences (Shirbhate and Goel 2020; Elsanadedy et al., 2014; Kennett et al., 2005; Chen, Lu, and Wu 2023). The number of nations in which at least one person died due to terrorism in a given year is shown in Fig.1.1. It is also worth noting that the number of countries affected by the rise in terrorism is growing. Terrorism results in economic losses due to structural flaws, but more crucially, it results in the loss of priceless lives. The economic impact of terrorism, GDP losses, property destruction, and injuries are depicted in Fig.1.2.

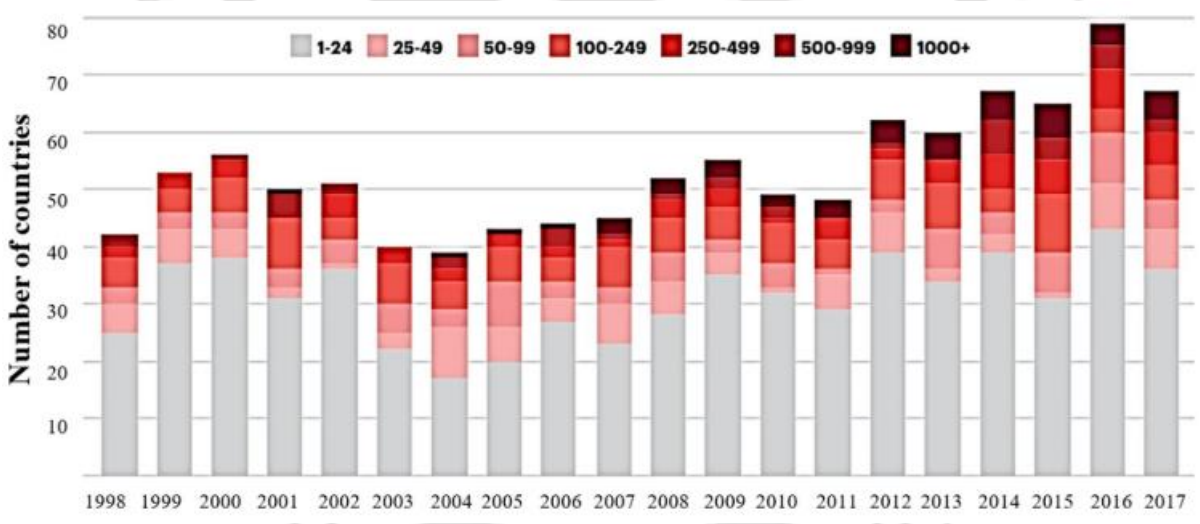

Fig. 1.1. Deaths from terrorism and number of countries affected, 1998–2017 (Shirbhate and Goel 2020).

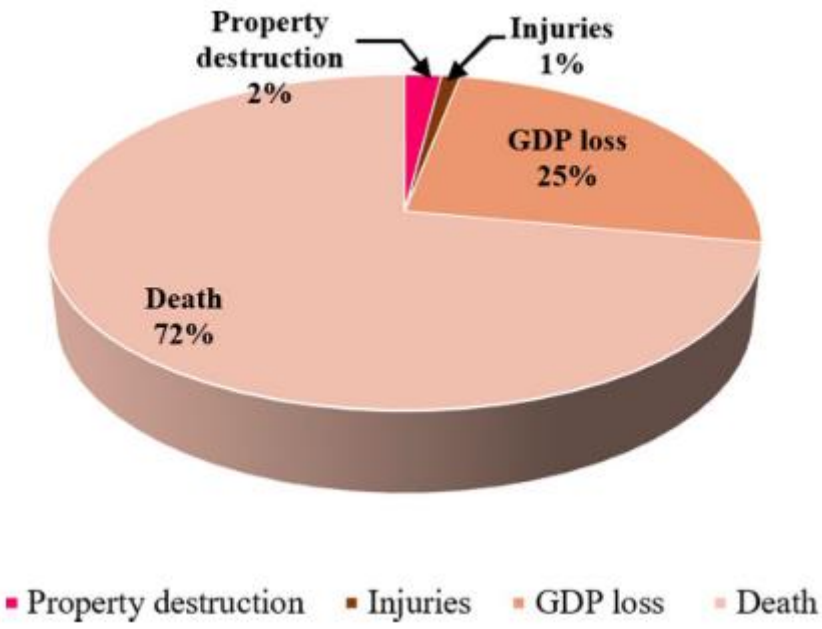

Fig. 1.2. The economic impact of terrorism (Shirbhate and Goel 2020).

Explosions are among the most common causes of natural and man-made disasters that result in significant economic damage and fatalities. As a result of uncontrolled gas leaks, car or aircraft strikes, and terrorist attacks, such low probability and high consequence catastrophes can occur in civil and industrial structures. The Jewish Community Centre in Argentina in 1994 and the WTC twin tower bombing in Sri Lanka in 1997 are two recent instances. Near-field incidents like the Murrah building bombing (Fig. 1.3) in the United States in 1995, the Central Bank bombing in Sri Lanka in 1996, and the Khobar Towers attack in Saudi Arabia in 1996, on the other hand, had the potential to damage and destroyed the structural integrity of the structures. These incidents have been accompanied by a substantial number of casualties in several situations. Recent events such as the Lahore city bombing in 2009 and the Baghdad bombings on foreign embassies in 2010 highlight the need to investigate building structures' responses to a near-field blast to safeguard lives and property.

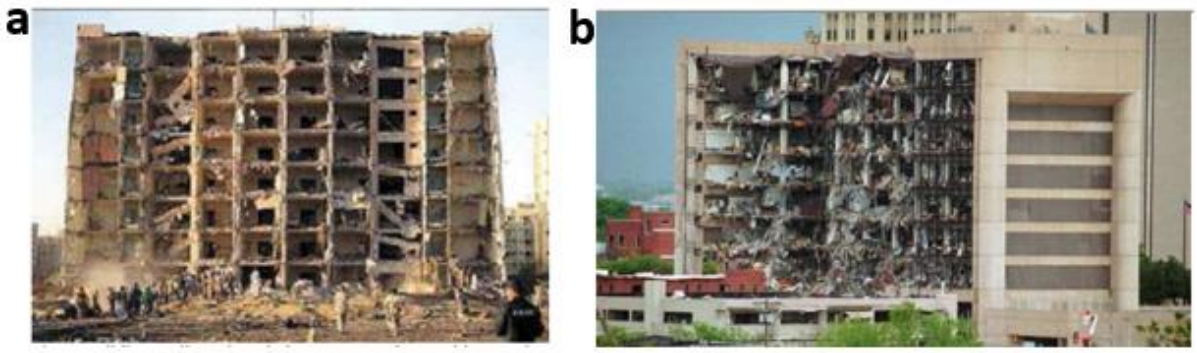

Fig. 1.3. (a) Building collapse in Khobar Towers due to blast action (1996) (b) Building of Federal Murrah Building after blast attack (1995) (Crawford et al., 2015)

Terrorism is a menace to every nation, as evidenced by the casualty analysis of these incidents. Essential structures such as government buildings, hospitals, public meeting places, retail malls, theatres, mass transportation networks, and stadiums, among others, should be engineered to withstand blast-induced dynamic loads.

However, the political instability in some areas of the world and the frequent occurrence of various natural disasters and extreme events damage structural members and even lead to progressive collapse of entire structures. This phenomenon needs extensive attention and research. The problem of progressive collapse poses higher requirements for the design method of a Reinforced Concrete (RC) structure (Zhang and Li 2020; Kiakojouri et al., 2020). Over the few past decades, progressive collapse studies have become increasingly popular. Considerable literature has been published on progressive collapse: Initial studies were technical reports on the failure of existing buildings ending with suggestions on possible code prescriptions; after 9/11 event, the scientific literature focused on structural failure and robustness. Due to the complexity in dealing with such phenomena, threat-dependent approaches are generally adopted by codes and guidelines with the underlying assumption on blast as triggering event (Kiakojouri et al., 2021b; Ravikumar 2021). However, the general

ideas, concepts and definitions have been merely changed over the past twenty years. The failure of vertical members under extreme events, such as blast and impact, is a highly dynamic phenomenon. In such situations sudden column loss represents a more appropriate design scenario, which considers the dynamic influences but is event-independent.

Despite the existence of numerous guidelines for the design of buildings against blast loads, such as those published by the US Department of the Army, US Department of Defence, US General Services Administration (GSA), FEMA, and the American Society of Civil Engineers (ASCE), there are only a few design codes that provide the necessary recommendations for blast resistance design of multi-storey buildings. The National Cooperative Highway Research Program (NCHRP) has provided some design information based on simplified methods; however, the failure behaviours of multi-storey buildings under explosions have not been incorporated. The Federal Highway Administration (FHWA) also gave state-of-the-art guidelines on security planning, blast phenomenology, the blast reaction mechanism of the bridge's structural components, material performance, and protective design suggestions. Table 1.1 summarises existing recommendations for blast design of buildings based on single-degree-of-freedom (SDOF) assessments from multiple design guides.

Table 1.1. Summary of the current guidelines for blast loading on structures (Zhang et al., 2020)

Guideline	Remarks and notes
TM-5-855-1	Provides design and analysis procedures for the protective structures exposed to the effects of conventional weapons and tor use in designing hardened facilities
TM-5-1300	Provides design approaches for structures to resist the effects of blast waves and fragments by considering blast load parameters and structural response modes
UFC 3-340-02	Prediction of idealized close-in and far-field blast loads using shock and gas considering dynamic increase factors (DIFs), which provide both flexural and shear failure-based design approaches
UFC 4-010-01	Provides appropriate, implementable, and enforceable measures to establish a level of protection against terrorist attacks for all depart of defence and military buildings
FEMA 428	Predicting the expected overpressure on buildings using explosive weight and standoff distance in both horizontal and vertical distances arising from various vehicle explosions
ASCE 1997	Provides a structural design guideline for blast resistance of petrochemical facilities
ASCE/SEI 59-11	Considers dynamic increase factors for structures for only far-range blast loads using SDOF analysis which provides flexural failure-based design approaches
ASCE 7-10	Provides the concepts and analysis methods of progressive collapse of integrated and redundant structural systems under explosions

IS 4991-1968	Provides criteria for blast resistant design of structure for explosions above ground

1.2 Motivation of Research

Accidental gas leaks and terrorist attacks against civilian or commercial structures are the most common source of explosive occurrences. Accidental incidents happen, such as explosions in storage facilities or gas explosions. As a result, it is critical to evaluate and anticipate the impact of explosions and create solutions to safeguard structures from explosive occurrences. Current blast load prediction procedures are confined to spherical or hemispherical charge geometries (UFC 2005/TM 5-1300), and there is limited research on cylindrical charge shapes (Tyas et al., 2019; S.E. Rigby et al., 2021). The blast-resistant design manuals in Table 1.1 are only for single-story and multi-bay structures (UFC 2005/TM 5-1300). The shape function of buildings is only used for the first mode in the literature (Chopra 2012; Taranath et al., 2005; Paz and Halperson 1980). There has been no significant research on the relationship between positive and negative phase peak overpressures. There is little research on the relationship between positive and negative phase durations (Cormie et al., 2019; UFC 2005). When the negative phase effect is considered in the study, the indefinite blast Friedlander's profile with wave decay parameter produces aberrant findings in the time-history analysis (Gantes and Pnevmatikos 2004). Experiments with detonating explosives are frequently expensive and dangerous. As a result, numerical modelling is a practical and effective method of studying blast loads caused by explosions, particularly in complex contexts. The ability to predict blast loading is an important first step in evaluating the efficacy of protective systems and vital infrastructure in the face of explosions. There is a pressing need to understand better the underlying mechanisms regulating the formation of blast loads on a

structure and subsequent structural reaction to equip engineers with simple forecasting tools based on physically sound concepts.

1.3 Overview of Existing State of Art and Limitations

When a spherical explosive detonates, the wave front hits all of the explosive's edges simultaneously, and the blast wave extends in a spherically symmetric way into the air. In contrast, the detonation wave in a cylindrical charge will not reach all sides of the explosive at the same time, resulting in a highly complex blast wave pattern. Spherical equivalency factors can still be calculated for near-field cylindrical and other explosives. Instead of the idealised spherical or hemispherical explosives considered in commonly used semi-empirical techniques, realistic explosion situations frequently include detonating non-spherical high explosive charges. There is limited literature available on charge shapes like spherical and cylindrical. An explosive carrier bears an unexpected charge shape to target the buildings. As a result, simplified engineering-level tools must integrate the impacts of charge shape and the associated loading quantification and distribution (Rigby et al., 2021).

The negative phase's influence, particularly on light cladding and glass panels, has piqued people's curiosity in recent years. This might be due to an increasing understanding of the relevance of well-designed glass in reducing infrastructure damage and injury to building occupants in the case of an explosion. A quick surge in pressure is frequently followed by an exponential decline in the pressure during blast loading. The characteristics of this pressure pulse are critical for design and may be found in a variety of blast design textbooks (Cormie et al., 2019) in the public domain. The blast wave decay coefficient 'b' is a dimensionless parameter that characterises the rate at which pressure values decline. It is used to build the pressure-time history curve. Depending on whether the curve is for the incident or reflected blast wave, different coefficient values should be utilised when creating the pressure-time history. Friedlander's blast profile, on the other hand, is an indefinite profile that produces

abnormal findings for the negative phase effect in the time-history analysis. Only a small amount of study has been done on the blast wave decay parameter to account for the negative phase impact of blast loading. A simple, precise, and dependable blast time-history profile is required to eliminate the restrictions in the literature blast profiles.

In the design of blast resistant structures, rigid frame structure architecture is chosen because it enables open internal space while also providing strong resistance to lateral loads. Furthermore, due to the gradual growth of plastic hinges up to the structure's ultimate capacity, this style of design has intrinsic energy absorption capabilities. Under the action of horizontal and vertical blast loads, each element in a frame is exposed to combined bending moments and axial stresses. On the other hand, a simple analysis cannot determine the phasing between critical axial force and bending moment values. For trial beam-column design, it is advised that the peak axial loads and moments produced are considered to act simultaneously. The typical blast resistant design guides, such as TM 5-1300, UFC 2005, and the Department of Defence, are only applicable to single storey and multi-bay structures. A framework for the analysis and design of multi-storey buildings subjected to blast loads is required.

The consequences of higher modes should be considered for moderate- to high-rise structures (Taranath et al., 2005). A multi-degree-of-freedom system is transformed into an analogous single-degree-of-freedom system using generalised coordinates. Any arbitrary function that meets the boundary criteria can be used to describe the deformed structure. The effectiveness of this method will be determined by how well the postulated shape function approximates the dynamic system's actual displacements. Because the deflections in the first mode are all of the same sign, the fundamental mode of a multi-story building or a single-span beam is straight-line to comprehend. The mode shape of more complicated systems, on the other hand, may be difficult to comprehend, and even a shape function determined from the static deflections owing to the structure's self-weight may be inadequate. Only the first mode

of shape functions is advised for high-rise, mid-rise, and low-rise structures (Paz and Halperson 1980). The straight-line design indicated for the mid-rise structure is used in most seismic construction regulations. As a result, a building shape function must be developed to account desired mode shape in multi-storey building analysis and design.

The following objectives are carried out in this research based on the limitations and research gaps mentioned in the available literature.

1.4 Objectives

The objective of this study is to develop a framework for analysing and designing multi-storey buildings that are subject to blast loading by using an equivalent SDOF analysis with a modified shape function and critical load and progressive collapse resistance factors, incorporating the charge shape effect in blast load quantification, and developing a simple, reliable, and accurate blast profile.

The following tasks are completed to attain the proposed objective.

- The effect of charge shapes on structural response is investigated, and the spherical equivalent quantities for the pressure and deformation of the RC frame subject to blast loading are determined.
- The effect of the blast wave decay parameter on structural response is investigated, and a new blast load profile for the time-history analysis of SDOF systems subject to blast loading is developed.
- Development of probabilistic models to predict the critical load and collapse resistance factors of multi-storey rigid frame structures (midrise buildings) subject to blast loading.
- A modified shape function is developed for accurate SDOF analysis of multi-storey buildings for the intended mode shape when subject to blast loading.

- ❖ A detailed methodology for analysis and design of multi-storey buildings is presented based on the developed models of blast load profile, probabilistic models to predict the critical load, collapse resistance factors and modified shape function.
- ❖ A user-friendly Capacity Based Design Software (CBDS) is developed with a graphical interface for designing a structural member subject to blast loading.
- ❖ Probabilistic models for collapse resistance factors for multi-storey building is developed.

1.5 Work Plan and Methodology

The following work plan and approach is adopted to attain the proposed objective.

- ➢ Finite element simulations are performed using the Multi-Material Arbitrary Lagrangian Eulerian (MM-ALE) method of the LS-DYNA hydro-codes to determine the pressure and deformation equivalents between spherical and other charge shapes such as cylindrical, rectangular, conical, and cubical.
- ➢ A new, simple, dependable, and accurate blast time-history is developed using different blast wave decay parameter values. Analytical and numerical approaches are used to compare the novel blast profile to existing literature profiles. The SAP2000 software is used for numerical validation.
- ➢ A numerical technique based on SAP2000 software is adopted to generate a database for the development of probabilistic models to predict critical load and collapse resistance factors of multi-storey rigid frames subject to blast loading. The developed probabilistic models account for the uncertainties such as blast direction and position. OriginPro software is used to develop probabilistic models to predict critical load and collapse resistance factors.
- ➢ A modified shape function is developed for the multi-storey shear buildings. The Eigen and numerical approaches are used to validate the natural time periods

generated by the modified shape function. The SAP2000 software is used for numerical validation. The developed shape function gives an accurate result of the response of multi-story building subject to blast loading.

- A detailed methodology for analysis and design of multi-storey building is presented based on the developed models of blast load profile, probabilistic models to predict the critical load, collapse resistance factors and modified shape function. The response spectrum from the novel blast profile and charge shape effect in blast load calculations are applied to assess and design multi-storey buildings subject to blast loading. A user-friendly Capacity Based Design Software (CBDS) is developed with a graphical interface for designing a structural member subjected to blast loading.
- Probabilistic models for collapse resistance factors of multi-storey buildings are developed. The developed probabilistic collapse resistances factors (axial, shear and bending) of multi-storey rigid frame constructions can be used to design and mitigate the progressive collapse of the multi-storey buildings.

This research contributes to our understanding of multi-storey building responses to blast loads, the design of buildings subjected to blast loads, the progressive collapse resistance and critical load factors, and the development of equivalent SDOF methods for evaluating concrete and steel multi-storey building performance against explosive loads.

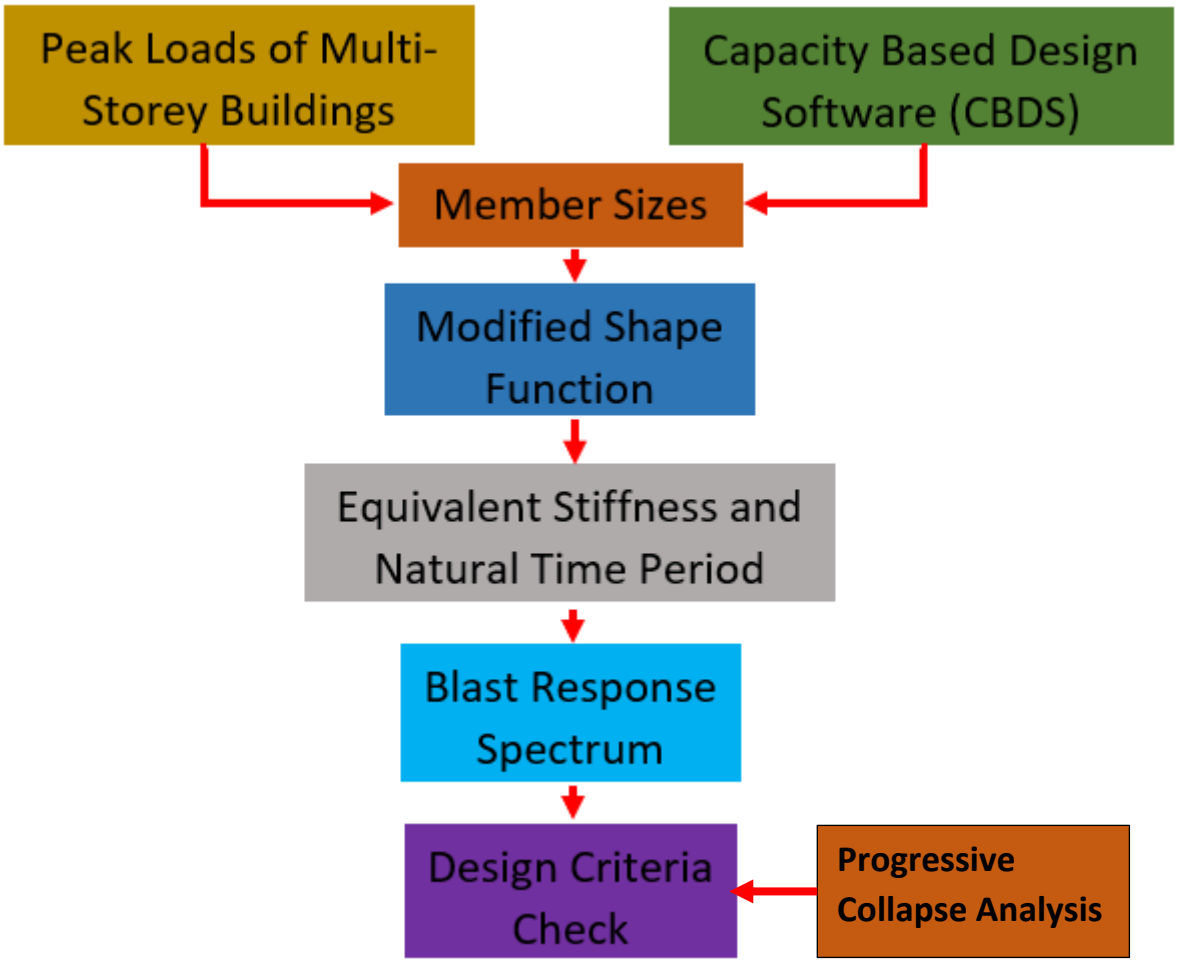

Fig. 1.4. Flow chart of the proposed framework

1.6 Scope of Research Work

This research thesis's scope can be stated as follows:

- The critical load factors include only multi-storey rigid frame constructions for multi-storey buildings subject to blast loads.
- The critical load factors can be used to design crucial load-bearing members (columns) for both steel and concrete multi-storey rigid frame constructions.
- The progressive collapse resistance factors can be used to quantify the minimum resistance required to mitigate progressive collapse in multi-storey buildings.

- The novel blast profile can be employed in time history analyses of structures to comprehensively examine blast effects, including positive and negative phase effects.
- The new blast profile does not require the blast wave decay parameter's calculation.
- The cylindrical, cubical, conical, and rectangular charge shapes are used to determine the spherical equivalent quantities for pressure and deformation. These equivalents can be used to calculate the blast load for a specific charge shape.
- The charge shape's orientation influence is not considered in this report.
- The modified shape function can be used only for shear-type multi-storey buildings.
- The simplified standard equivalent SDOF approach for the required mode shape can be utilised to analyse and design shear-type multi-storey buildings with this report.

1.7 Organisation of the Thesis

This research thesis report is divided into nine chapters in general. The first chapter explains the need for the research, the motivation, an overview of the existing state of art and limitations, the objectives to be achieved and the scope of research work. State of the art for the blast load and buildings is presented in the second Chapter. The third chapter covers finite element simulations of charge shapes and their spherical equivalents, the validation of the Multi-Material Arbitrary Lagrangian Eulerian (MM-ALE) approach and the analysis of an RC frame subject to internal blast loading. The fourth Chapter develops quadratic and other types of blast profiles and response spectra for both quadratic and exponential profiles and numerical blast profile validation. The fifth chapter develops multi-storey rigid frame structures' critical load factors, probabilistic models of critical load factors, peak loads of multi-storey buildings, and research methodological validation. The dynamic study of multi-storey buildings subject to blast loading, eigen modal analysis, generalised equation of motion, derivation of modified

shape function, and validation of the modified shape function are developed in the sixth chapter. The seventh chapter develops the framework for designing multi-storey buildings subject to blast loading and the member design approach, equivalent SDOF design method, and multi-storey building design procedure. The eighth chapter develops the methodology and framework to quantify the required resistance of multi-storey buildings to mitigate progressive collapse and develops collapse resistance factors for the series of top and bottom column removal in the multi-storey buildings. The summary, conclusions, and proposed future study are presented in the ninth chapter. Finally, the study concludes with a list of references and an appendix.

CHAPTER 2 BLAST LOAD AND BUILDINGS: STATE OF ART

2.1 General

An explosive is a chemical compound substance or a mechanism that emits a significant quantity of energy in the form of heat, light, sound, or shock waves. The explosive must be detonated in order to have an impact other than heat. Because explosives are easy to make, are small, and strong, they are frequently utilised as weapons in terrorist operations. Due to explosives, the significant sources of threat are hand-delivered and vehicle-based weapons. The features of the explosive material have an impact on blast load; thus, it is essential to understand the different types of explosives and their physical characteristics. The blast wave and its effect on the structure are characterised by the weight, substance, shape, and distance of the explosives from the structure.

There are many reinforced concrete structures in the urban environment, as part of the infrastructure and as various types of civilian and military facilities. Many studies on the effects of blast loading on reinforced concrete elements have been reported in the literature. Engineers require a precise and concise procedure to provide reliable and fast results. As a result, several academics have recently focused on creating reliable, efficient, and simple blast resistant design and analysis approaches. Explosives, blast phenomena, and blast impacts on buildings all require a thorough understanding of blast-resistant structures' study and construction. Therefore, it's essential to compile a literature evaluation on explosives, blast phenomena, blast wave interaction, and structural response to blast loads.

2.2 Charge Shape and Structural Response

The detonation process is limited by the explosive qualities, including the molecular structure (monomolecular, bimolecular, etc.) of the explosive, form and dimensional features, and the physical composition (solid, liquid, gas) of the charge. Due to these restrictions, either a high- or low-order detonation occurs. The process concludes typically with a high-order detonation, resulting in the highest-pressure output for the given kind and amount of material. On the other hand, if the explosion is partial, with the initial reaction not passing through the material mass, deflagration consumes a considerable amount of the explosive, lowering the blast pressure. Other than hemispherical TNT, blast parameters for explosives detonated on the ground surface include uncased and cased high explosives, propellants and propelling charges, and pyrotechnic mixes. Fig. 2.1 depicts the various shapes of explosive materials.

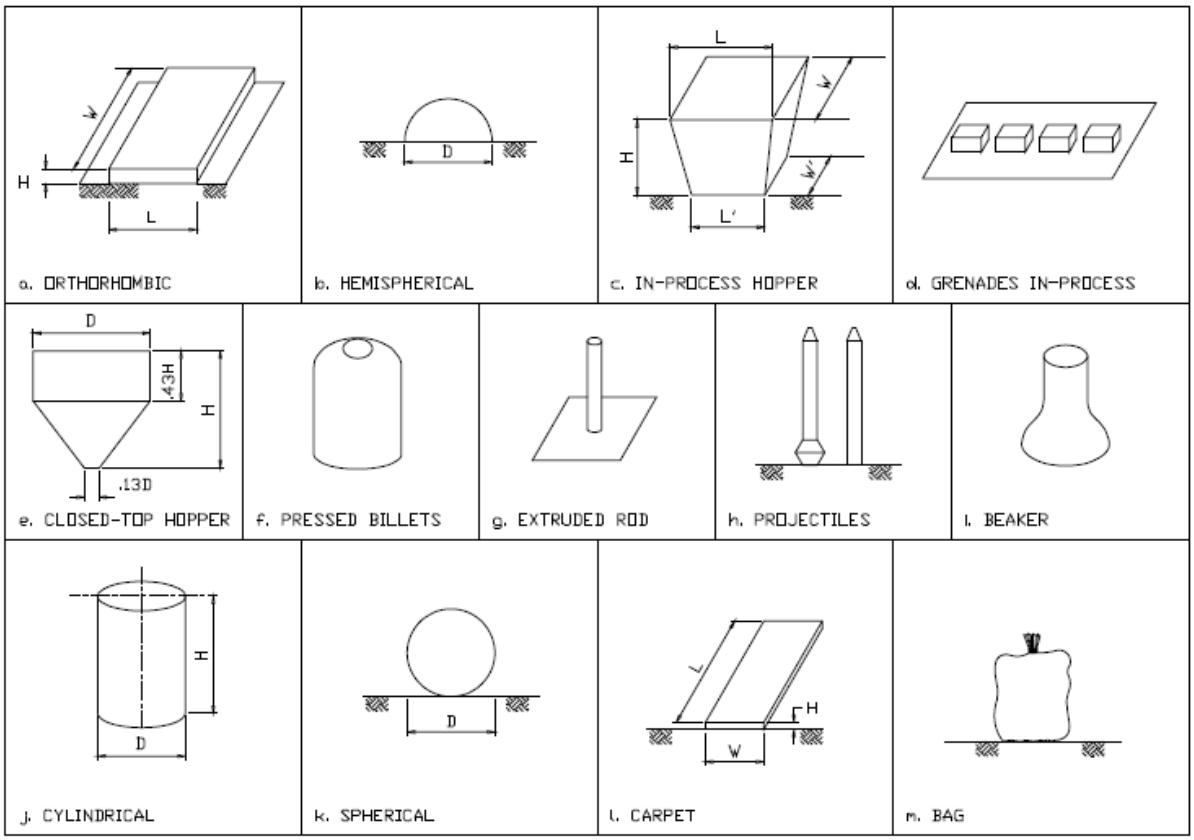

Fig. 2.1. Explosive shapes (UFC 2005).

Instead of the idealised spherical/hemispherical explosives considered in commonly used semi-empirical techniques, realistic explosion scenarios frequently entail detonating non-spherical high explosive charges. As a result, simplified engineering-level tools must integrate the impacts of charge shape and the associated loading distribution. An energy equivalent formulation has been devised to determine spherical equivalence factors, with the approach presented for the case of a cylindrical explosive charge detonated in the centre. The LS-DYNA explicit solver has been used for all numerical studies (Abedini et al., 2020; Feng et al., 2021; Nouri et al., 2021; Choubey et al., 2020). The reaction of plates under blast loading from various forms of explosive detonated at varying stand-off distances (SODs) has been studied using a two-stage uncoupled analytical technique. An axisymmetric, multi-material Arbitrary Lagrangian-Eulerian (MM-ALE) framework has been used to analyse the detonation process, blast wave production, and blast wave interaction with the target structure (Zhang et al., 2020).

The first stage in designing protective systems is to quantify the size and distribution of the blast load acting on structural elements placed near an explosive charge (Cankaya et al., 2020). Simple prediction approaches that do not account for charge shape are inadequate in this case since the shape of the charge is known to influence the imposed load considerably. Such simplified tools must be supplemented by physically accurate changes to represent the consequences of charge shape.

A set of numerical near-field blast load distributions have been developed that were all found to have the same normalised shape. The new method allowed analysts to quickly compute the distribution of specific impulses across the loaded face of various target sizes and near-field scaled distances. It also served as a benchmark for data-driven modelling approaches to capture blast loading phenomena in more complex scenarios. The usefulness of data-driven predictive techniques for blast load prediction has been established. More sophisticated, machine learning-assisted ways to simulate a more complicated array of situations and input

factors, such as explosive type (TNT equivalency), charge shape effects, and blast wave clearing, might be added to the methodology (Pannell et al., 2021).

The effect of cylindrical charge features on blast loads (peak overpressure and maximum impulse), such as length-to-diameter ratio, orientation, and starting configuration have been investigated (Xiao et al., 2020). Three potential initiation configurations have been considered in the middle, at one end, and both. For the spherical and cylindrical charges, numerical models have been built. The peak overpressure (highest impulse) in the near field created by centrally started cylindrical charges can be overestimated by a factor of up to three if the charge shape impact is ignored. As a result, in numerical simulations for the blast-resistant design of protective structures subjected to near-field detonations, the cylindrical charge form should be explicitly simulated. A probabilistic framework has been proposed to predict the failure probabilities of steel columns under blast loading. The framework considers the uncertainties in the blast phenomenon, the demands imposed on the column, and the capacities of the column for the limit states of flexure, and global buckling. The blast load models are used to predict the structural demands such as maximum internal moment and deflections imposed by the blast on a column. The results highlighted the importance of the explosive weight and column axial load on the failure probabilities (Singh et al., 2020).

A statistical study of two blast wave characteristics, maximum overpressure and pressure-time diagram decay coefficient, was done based on field testing of the cylindrical TNT charge free-air explosion. A simple numerical simulation has also been performed to compare the obtained maximum overpressure with the field test data. The impact of the air mesh size on the maximum free-field overpressures has been investigated using a comparison of the maximum free-field overpressures (LUKIC et al., 2020; Liao et al., 2022; Vapper and Lasn 2020). For a rapid blast load estimate for further structural parts analysis, expressions for blast wave parameters have been utilised. Their exact determination provides a more realistic blast

analysis and safer design. The TNT (trinitrotoluene, trotyl) charge is shaped like a cylinder, and it has been exploded at each measurement. Fig. 2.2 depicts the charge geometry and detonator capsules.

Fig. 2.2. Charge geometry and detonator capsules filled with lead azide (LUKIĆ et al., 2020).

The damage to structural components caused by a close-in explosion is influenced by charge configuration. A blast loading model has been developed that takes charge shape and detonation configuration into account (Hu et al., 2018). Close-in explosions triggered at both ends of an explosive cylinder (double-end-initiation) have been tested in the field. The effects of charge shape, diameter-to-length (D/L) ratio, scaled distance, and detonation position have been studied on the overpressure and impulse. The orientation of the explosive, in addition to its shape, plays an essential part in determining the amount of the overpressure and impulse; as a result, the explosive's posture in each test has been meticulously altered.

A computational model has been created to investigate the impact of the geometry of a high-explosive on the dynamics of the pressure wave generated (Artero-Guerrero et al., 2017). The impact of the HE's pre-detonation shape on the subsequent blast wave has been studied, and the five shapes indicated in Fig. 2.3 have been used. The impact of the high-mass

explosive's shape on the dynamics of the produced blast wave has been explored and correlated through the investigation of peak pressures, time of arrival, and impulse. Formex F4HV samples of constant mass hemispherical, cylindrical, and flat-shaped have been used in the tests.

Fig. 2.3. Generic shapes of the high-explosives used in the numerical models: (a) hemispherical, (b-d) cylindrical and (e) flat (Artero-Guerrero et al., 2017).

Characterisation of Blast Loading (CoBL) laboratory at The University of Sheffield has produced experimental research that provides a geographical and temporal map of reflected pressure in the extreme near field (Langran-Wheeler et al., 2017). A preliminary set of long cylinder and spherical charge experiments utilising CoBL have been reported. The impact of charge shape on loading methods and magnitudes has been examined. The results reveal that the cylindrical charge's orientation impacts the distribution of peak overpressures and particular impulses compared to an idealised spherical charge shape. When compared to a sphere of the same mass, a lateral 7:1-cylinder charge in the near-field twice the total impulse delivered over an area with the same diameter as the length of the cylinder.

A fully coupled 3D multi-material arbitrary Lagrangian-Eulerian (MM-ALE) modelling approach in LS DYNA software has been employed to simulate the cylindrical charge blast loading (Christian et al., 2016). A comparison of spherical and cylindrical charge blast simulations has been performed to demonstrate the impact on peak overpressure and total impulse (Akhlaghi, 2020). The three shapes of TNT charge employed in the numerical analysis are shown in Fig. 2.4.

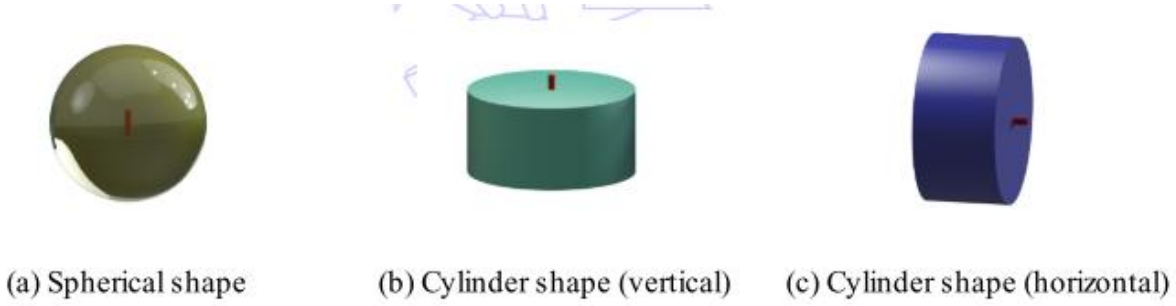

Fig. 2.4. TNT charges with a set detonator (red point) (Christian et al., 2016).

A numerical analysis has been performed that describes the impact of charge shape, charge orientation, and the location of detonation inside the charge on free-field incident overpressures and impulses using a verified and validated computational fluid dynamics model (Sherkar et al., 2016). Analyses have been carried out with cylindrical charges of various aspect ratios and masses, and the findings have been compared to those of a spherical charge baseline analysis. The numerical study reveals that the charge shape significantly impacts the overpressure distributions in the near-field and midfield zones. A cylindrical charge generates more incident overpressures and impulses than a spherical charge. When structural components and frame systems are subject to near-field detonations, ignoring charge shape in the analysis and design can lead to inadequate response estimations and incorrect performance conclusions.

The effect of spherical charge blast loads on the containment chamber and the chamber's estimated reaction have been explored (Clutter and King 2016; Chiquito et al., 2021; Abedini and Zhang 2021). It has been discovered that the more realistic charge design resulted in increased stresses on the vessel walls. The non-ideal arrangement provided a significantly different reaction than the commonly presumed perfect spherical charge. The use of separate charges on shelves increases peak loadings at various points throughout the vessel. While

designing these systems, it is evident that scenario elements such as the actual explosive charge shape and distribution inside the chamber should be considered.

Experiments using an emulsion explosive, TNT, and C4 have been carried out to quantify the shape effect (Simoens and Lefebvre 2015; Zheng and Xu 2021). Unconstrained, centrally started spherical and cylindrical charges with various length-to-diameter (L/D) ratios have been fired. For different decreased distances, the pressure in the median plane has been measured. The pressure field in the median plane of a cylindrical charge changed as predicted, closely related to the L/D ratio. The impact of the explosive mass on cylindrical charges has been researched, and it has been discovered that the similitude parameters, which are typically employed for spherical charges, may be extended to cylindrical charges within the range studied.

The unique features of air under high temperature and high pressure have been considered. A complete set of dimensionless hydrodynamic equations in the Lagrangian distance coordinate system has been established by using the state equations of real air to describe the close-in flow field characteristics and the propagation of shock wave of spherical TNT charge bursting in real air (Zhou et al., 2015; Kumar et al., 2020; Li et al., 2020). The numerical computation has been then simplified using a set of altered hydrodynamic equations in shock moving coordinates. Combining the artificial viscosity approach and the shock fitting methodology has been devised to estimate the whole flow field of TNT exploding in actual air.

An examination of published data (for Composition B and pentolite), as well as data collected for RDX/TNT 60/40 and PE4, has revealed that the impulse from the curved surface of a cylindrical charge of explosive does not appear to be affected by the length to diameter ratio, even though the pressure varies (Knock and Davies 2013; Gao et al., 2021; Jing et al., 2021). As the length to diameter ratio increases for a given distance from a given explosive

mass, the peak pressure increases while the impulse remains constant, implying that the pressure must drop faster behind the peak pressure, indicating a shorter duration shock wave. However, there was insufficient data to confirm this at the time.

When compared to spherical charges, cylindrical charges produce a more substantial close-in explosion. The peak pressure perpendicular to a cylinder's curved side, looked for impulse data for the curved surface of cylindrical charges in the literature for Composition B and Pentolite, and then described experimental work on cylindrical PE4 charges (Zhu et al., 2020; Xiao et al., 2020b; Knock and Davies, 2011). The results of the free-air experiment and literature analysis reveal that a linear connection may be used to forecast the impulse, albeit the best fit cannot be determined based on the available data.

Although the distributions of peak incident overpressure and impulse generated by spherical and cylindrical charges of the same weight can differ significantly close to the point of detonation, spherical charges have been assumed for nearly all explosive-effects computations in modern blast-resistant design standards such as UFC-3-340-02 and ASCE Standard for the Blast Protection of Buildings (Wu et al., 2010; Kristoffersen et al., 2021; Mohammadzadeh et al., 2020). The reflected peak overpressure and impulse distributions as a function of charge shape, direction, and scaled distance have been investigated using blast-testing software. The distributions of reflected peak overpressure and impulse in the immediate area of the explosive have been modified by the ratio of charge length (L) to diameter (D), the orientation of the longitudinal axis of the charge, and the detonation point inside the charge for cylindrical charges. Fig. 2.5 depicts typical spherical and cylindrical charges. The cylindrical and spherical charges were made with pentolite and plastic-explosive boosters.

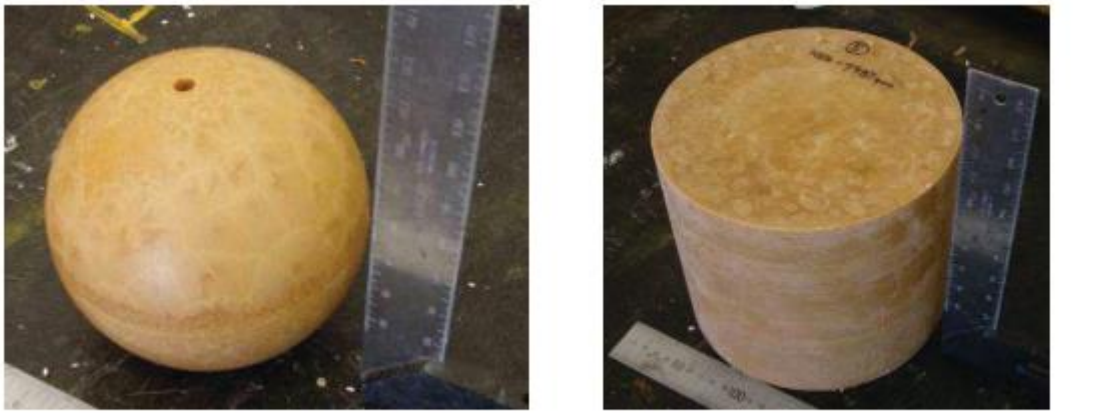

(a) 2.5 kg spherical charge (b) 8 kg cylindrical charge

Fig. 2.5. Typical charge shapes (Wu et al., 2010).

The reflected overpressures and impulse on a target immediately underneath a cylindrical charge with a vertical axis are substantially more significant than those on a spherical and a cylindrical charge with a horizontal axis of the same mass. The peak reflected overpressure could be significantly affected by the placement of the detonation point within a cylindrical charge.

Graphs showing equivalent spherical weights for cylindrical charges with length-to-diameter ratios have been developed using experimental data from the literature (Esparza 1992). The charge weights have been translated to comparable TNT values based on Pentolite spherical charge test data. The peak side-on overpressure and impulse data from Pentolite cylindrical charges initiated at one end have been scaled to standard sea-level circumstances using Sachs' scaling parameters. Then, using typical air blast curves for spherical TNT detonations in free-air, equivalent spherical weights have been calculated. These findings reveal that cylindrical charge shape has a considerable impact on free-air blast loads compared to spherical charges. Much more experimental study and data analysis have been required to define air blast loads from cylindrical and other non-spherical explosive charges. At small-

scaled distances, where the effects of geometry are most relevant, measurements of ordinarily and obliquely reflected pressure and impulse are almost non-existent.

The air blast characteristics, peak overpressure, arrival time, positive duration, and impulse have been shown against scaled distances (C.N Kingery 1980). The parameters' values have been obtained from empirical measurements taken during a series of experiments funded by Canada, the United Kingdom, and the United States as part of the Technical Cooperation Program (TTCP). Surface bursts of TNT have been used for the tests. Small TNT bricks piled in the shape of a hemisphere have been used to make the charges.

In an ideal gas, the problem of a spherical blast in the air has been solved analytically for both strong and weak shocks (Brode 1955). The initial conditions for numerical integration of the differential equations of gas motion in Lagrangean form are the strong-shock, point-source solution, and spherical isothermal distributions. The von Neumann-Richtmyer artificial viscosity has been used to avoid shock discontinuities. Overpressure, density, particle velocity, and location as functions of time and space are among the findings. For various periods and radial distances, the dynamic pressure, positive and negative impulses of both dynamic pressure and static overpressure, positive and negative durations of pressure and velocity, and shock values of all variables are also provided.

2.3 Prediction of Blast Loading and Duration

The close-in regime refers to a loading method in which the explosive is placed very close to the structure. In this situation, the loading period is substantially shorter than the structure's natural period. As a result, the loading is impulsive. The far-field regime comprises loading scenarios with a very long standoff distance. The standoff distance is high enough in the near field regime to generate a blast wave with a duration close to the structure's natural

period. The structure's response is affected by the pressure and the impulse in this type of loading. Table 2.1 depicts the response regime.

Table 2.1. Categorized response regime based on scaled distance (Z) (Abedini and Mutalib 2020)

Scaled distance	Z (mm/kg$^{1/3}$)	Z (ft/lb$^{1/3}$)
Close-in	Z<1190	Z<3
Near field	1190<Z<3967	3<Z<10
Far-field	Z>3967	Z>10

The scaled distance (Z) of detonation from the target, which defines a relationship between equivalent weight (W) and standoff distance (R) of explosive charge, is the most popular criterion for classifying blast loadings based on Hopkinson-Cranz law:

$$Z = \frac{R}{W^{1/3}} \tag{2.1}$$

where R is the standoff distance, and W is the equivalent weight of charge.

Several authors have recommended their formulations for predicting the peak overpressure from conventional explosives. The following are the most widely used formulations (Ullah et al., 2017).

The differential equation of gas motion in Lagrangian form has been analysed and presented the analytical solution for the peak positive over-pressure (P_m) in near-field and medium to far-field conditions as (Brode 1955):

$$P_m = \frac{6.7}{Z^3} + 1 \text{ bar } (P_m > 10 \text{ bar}) \tag{2.2}$$

$$P_m = \frac{0.975}{Z} + \frac{1.455}{Z^2} + \frac{5.85}{Z^3} - 0.019 \text{ bar } (0.1 < P_m < 10 \text{ bar}) \tag{2.3}$$

Newmark et al., (1961) introduced a relationship to calculate the maximum blast overpressure for a high explosive charge detonation at the ground surface as:

$$P_m = 6784 \frac{Q}{R^3} + 93 \left(\frac{Q}{R^3}\right)^{0.5} \text{ (bar)} \tag{2.4}$$

Q is the Charge in tonne-TNT, and R is the stand-off distance (m)

Based on an experimental analysis of extensive explosion data; the following equation has been presented to compute the peak positive over pressure (Kinney et al., 1985):

$$Pm = \frac{808\left[1+\left(\frac{Z}{4.5}\right)^2\right]}{\left\{\left[1+\left(\frac{Z}{0.048}\right)^2\right]\left[1+\left(\frac{Z}{0.32}\right)^2\right]\left[1+\left(\frac{Z}{1.35}\right)^2\right]\right\}^{0.5}} \tag{2.5}$$

Based on the experimental analysis of explosion data; the following equation has been presented to compute the peak positive over pressure (Held 1983):

$$P_m = \frac{2}{Z^2} \text{ (MPa)} \tag{2.6}$$

Based on explosion data analysis; the following equation has been presented to compute peak positive over pressure (Sadovskiy 2004):

$$P_m = \frac{0.085}{Z} + \frac{0.3}{Z^2} + \frac{0.8}{Z^3} \text{ (MPa)} \tag{2.7}$$

Based on numerical simulations; the following equation has been presented to compute peak positive over pressure (made a close accurate match with TM5-1300, which is derived from field experiment results and a good match with Brode's equation) (Izadifard et al., 2010):

$$\log_{10}[\log_{10} P_m] = -0.1319X^2 - 0.3231X + 0.644 \tag{2.8}$$

Where $X = \log_{10} Z$ and P_m is in kPa.

Several authors have also recommended their formulations for predicting the decay of the shock front from peak pressure to zero over pressure of the positive phase of an explosion, i.e., the positive phase duration (t_d).

The following equation has been presented to compute the positive over pressure duration (Henrych 1979):

$$t_d = e^{(-2.75+0.27\log_{10} Z)+\log_{10} W^{1/3}} \tag{2.9}$$

The following equation has been presented to compute the positive over pressure duration (Kinney et al., 1985):

$$t_d = W^{1/3} \frac{980\left[1+\left(\frac{Z}{0.54}\right)^{10}\right]}{\left[1+\left(\frac{Z}{0.02}\right)^{3}\right]\times\left[1+\left(\frac{Z}{0.74}\right)^{6}\right]\times\sqrt{\left[1+\left(\frac{Z}{6.9}\right)^{2}\right]}} (\text{ms}) \tag{2.10}$$

The following equation has been presented to compute the positive over pressure duration (Sadovskiy 2004):

$$t_{\text{d}} = 1.2\sqrt[6]{W}\sqrt{R}(\text{ms}) \tag{2.11}$$

The following equation has been presented to compute the positive over pressure duration (Izadifard et al., 2010):

$$\begin{cases} t_d = W^{1/3}(-64.86\,\text{Z}^4+52.32\,\text{Z}^3-15.68\,\text{Z}^2+1.794\,\text{Z}+0.1034) & Z \le 0.37 \\ t_d = W^{1/3}(4.64\,\text{Z}^2-3.86\,\text{Z}+0.854) & 0.37 < Z < 0.82 \\ t_d = W^{1/3}(-2.7X^3+6.27X^2+0.358X+0.763) & 0.82 < Z < 2.5 \\ t_d = W^{1/3}(0.608X^3-2.38X^2+5.62X-0.22) & Z > 2.5 \end{cases} \tag{2.12}$$

Where $\text{X} = \log_{10} Z$ and t_d is in millisecond.

The standard blast-resistant design manual UFC 2005/TM 5-1300 can be used to predict the structure's behaviour under explosion loads. The effective blast parameters, such as positive and negative phases, can be calculated from Fig. 2.6 and Fig. 2.7 presented in the manual.

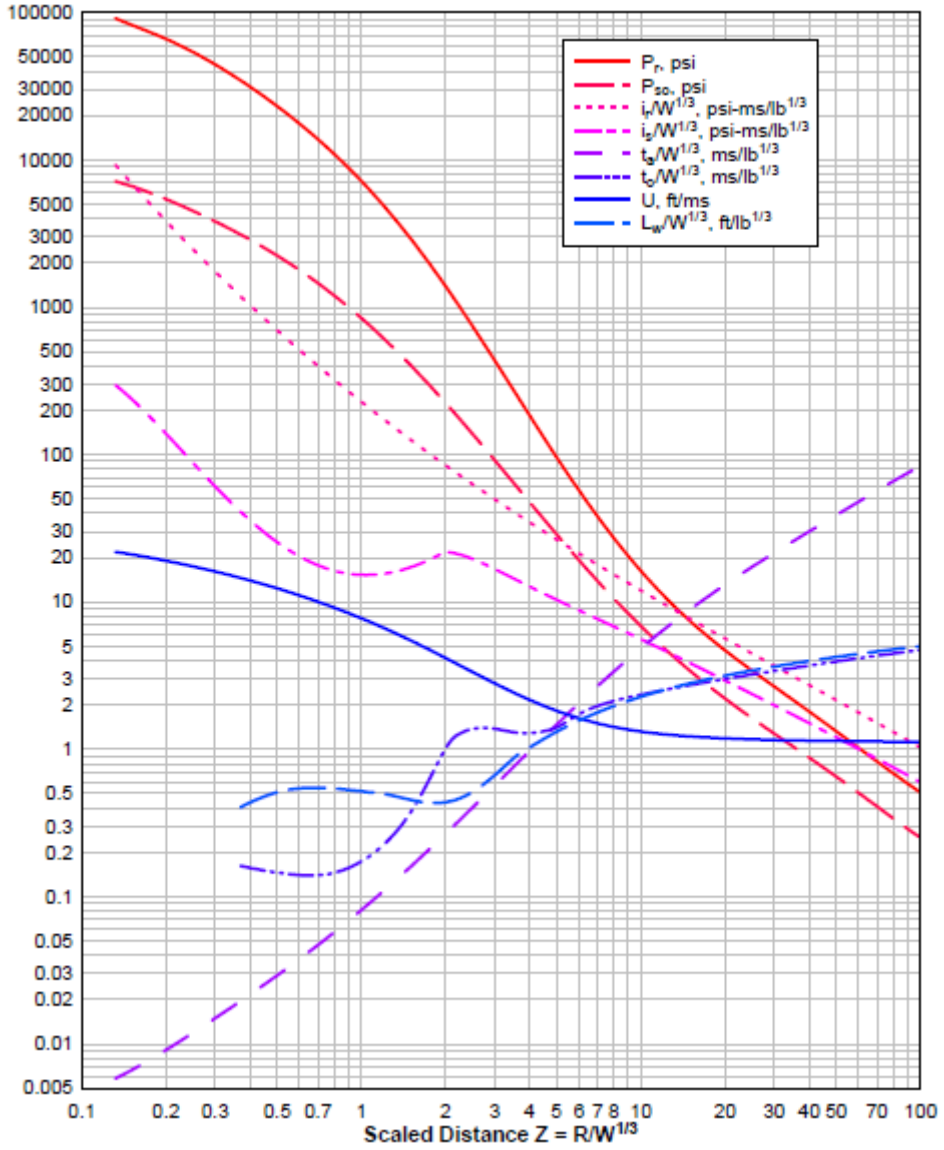

Fig. 2.6. Positive phase shock wave parameters for a spherical TNT explosion in free air at sea level (UFC 2005).

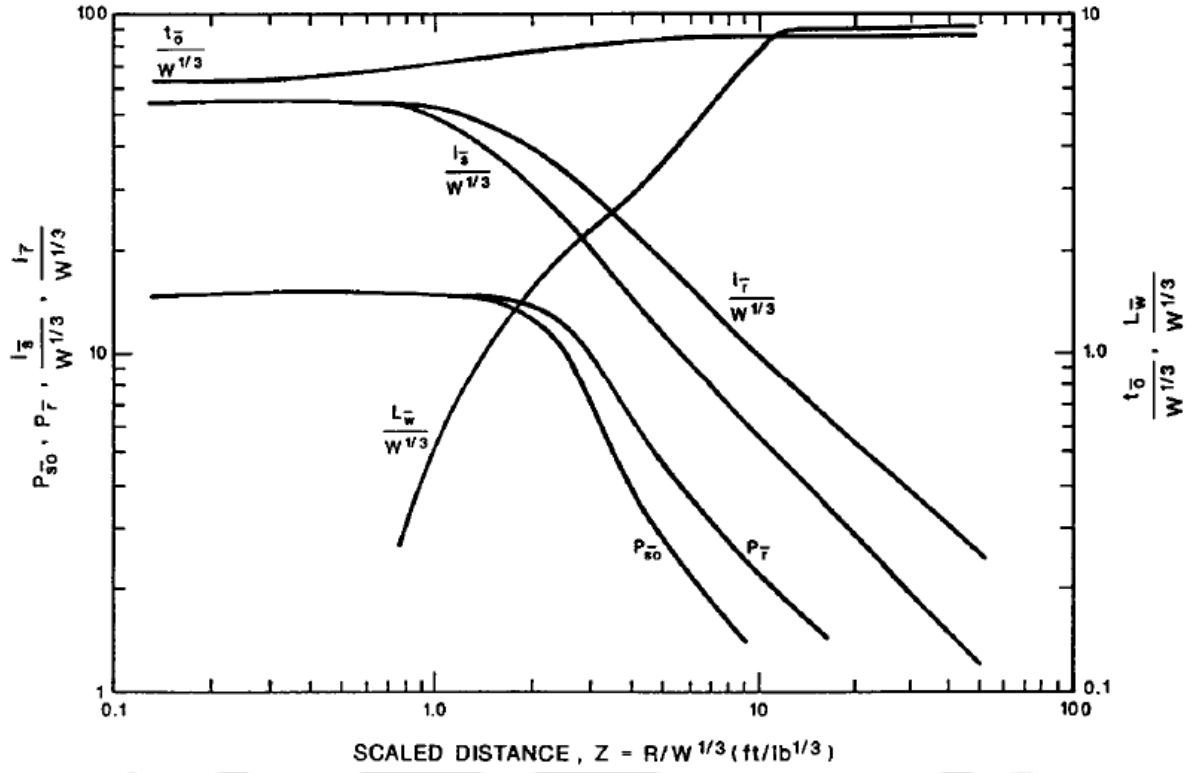

Fig. 2.7. Negative phase shock wave parameters for a spherical TNT explosion in free air at sea level (UFC 2005).

2.4 Blast Profile and Wave Decay Parameter

An exponential decline frequently follows a fast surge in pressure in blast loading. The characteristics of this pressure pulse are critical for design and may be found in a variety of blast design guides available in the literature. The negative phase's impact on light cladding and glass panels has piqued interest in recent years (Shirbhate and Goel 2020; Maazoun et al., 2021; Gholipour et al., 2020). Indeed, it has been argued that most non-fatal injuries caused by terrorist attacks are caused by flying glass pieces or hearing loss caused by broken glass panels.

The blast wave decay parameter (b) is a dimensionless parameter that specifies the rate at which pressure values decline (Cuomo and Lanza 2020). It is required for drawing the pressure-time history profile. Depending on whether the profile is for the incident or reflected

blast wave, different coefficient values should be utilised when creating the pressure-time history. When positive pressure reaches its maximum value, it declines, represented by the wave decay parameter (b). The form of the blast pressure profile is determined by the wave decay parameter, which regulates the blast wave's negative phase. Various approaches for computing the wave decay parameter based on the pressure impulse ratio might be utilised. The parameter (b) may be calculated using the blast wave's area under a pressure-time curve. Kinney and Graham proposed the following relationship between blast impulse and wave decay parameter:

$$p(\mathrm{t}) = p_0\left(1-\frac{t}{t_d}\right)e^{-b\frac{t}{t_d}} \tag{2.13}$$

$$\frac{i_o}{A} = \int_0^{t_d} p(t)dt = p_o t_d\left[\frac{1}{b}-\frac{1}{b^2}(1-\mathrm{e}^{-\mathrm{b}})\right] \tag{2.14}$$

Where i_o = Blast impulse; A = Area under the pressure-time curve; p_o = Positive peak overpressure; t_d = Positive phase duration; and b = wave decay parameter, respectively.

The complexity of explosion loads and their growing frequency in the civil environment underlines the need for models that capture the behaviour of structures under blast loads. A simplified single degree of freedom model has been used to describe the structural system under blast stress to conduct a probabilistic evaluation of the performance of framed reinforced concrete structures (Stochino et al., 2020). The blast load time history has been stated using Friedlander's suggested exponential function of time t for b = 1.8, and the nonlinear equation has been reduced using an analogous triangular time history as follows:

$$p(t) = P_o\left(1-\frac{t}{t_d}\right) \tag{2.15}$$

In this linear scenario, the positive phase duration has been calculated by matching the area under the two curves to provide an equivalent impulse for both models.

An essential component for determining the blast load impulse is the blast wave decay coefficient (b), dependent on the scaled distance (Z). The term "impulse" is crucial for structural design since it refers to the overall force (per unit area) imparted to a structure by a blast load. If the maximum overpressure, the duration of the positive phase, and the impulse are known through field testing, the decay coefficient may be determined iteratively using the Friedlander equation. A list of the most often utilised decay coefficient expressions from various authors have been addressed in the literature (LUKIC et al., 2020).

Most blast-resistant glazing system standards and publications are based on simplified Single Degree of Freedom (SDOF) models and triangular blast pressure time histories with no negative phase (Eslami et al., 2020; Draganić et al., 2021; Zhao et al., 2020). Experiments have shown that pressure-duration or pressure-impulse design curves obtained by SDOF models can be too cautious, particularly in impulsive explosion scenarios. Furthermore, the imposed blast pressure time periods contain both positive and negative phases, which is more realistic than focusing just on the positive phase. It is also demonstrated that the wave decay parameter (b) significantly impacts the blast's impulse and negative pressure. This decay parameter is dependent on several variables, including the scaled distance, the form of the blast wave (spherical or hemispherical), and the pressure type (incident or reflected).

A technical study, which includes values for various blast parameters in diagrams and polynomial form, is one of the most extensively used sources (Kingery CN and Bulmash G 1984). However, it does not provide an equation for computing the blast wave decay coefficient, which is required for creating the pressure-time history of an explosion at a given place. A survey of the technical literature for blast pressure decay coefficient expressions has

been conducted, and pertinent comparisons have been made (Karlos et al., 2016; Anas et al., 2021; Caçoilo et al., 2021; Stewart et al., 2020)). For free-air and surface bursts, new equations characterising the Friedlander equation's decay coefficient have been provided for both incident and reflected instances. These equations are not applicable for close-in detonations since they expressed the decay coefficient in terms of the scaled distance.

The maximum under pressure has been given a new reflection coefficient. The impact of the reflected under pressure phase has been calculated for various systems using a single degree of freedom approach (Teich and Gebbeken 2010). Under pressure dominates the structural reaction considerably, especially for flexible systems subject to modest blast stresses. The traditional triangle technique isn't secure in these situations. The quick reduction of the negative impulse for $b < 1$ has also been demonstrated. However, when $b > 2$, the compressive phase takes over, and the negative impulse fades away. The methods used to derive the form parameter (b) vary even more amongst the various sources. Because most studies only examine the overpressure period when calculating the shape parameter.

The pressure-time functions have been implemented in EUROPLEXUS (Larcher 2008). In addition to this implementation, an external procedure has been created that allows several values of the pressure-time function to be calculated. This tool can be used to compute things like the charge based on given peak pressure and positive impulse, which helps fit experiments to a pressure-time curve. The Friedlander equation's decay or form parameter (b) defines the decay of the pressure-time curve, and it has been computed using the positive phase's impulse. Under spherical or hemispherical circumstances, the proposed equations describe the whole behaviour of an air blast wave.

The existing understanding of blast pressure modelling has been expanded for engineering applications. A parametric study has been conducted using time-history

assessments of simple cantilevered wall models based on pre-defined pressure functions (Lam et al., 2004; Roy and Matsagar 2021; Ardila-Giraldo and Pujol 2021). In response behaviour modelling of the walls, the "corner period" of the velocity response spectrum is the most important governing parameter. The discovery of a direct link between the corner period and the "clearing time" for the blast significantly contributed to this research. A simple but realistic capacity spectrum model has been devised for the design and testing of cantilevered walls' performance under blast loads. The well-known Friedlander wave equation has been developed to describe the rise and decrease of the static over-pressure over time.

Elastic-plastic response spectra have been frequently used in the design of structures that are exposed to stresses caused by explosions. The triangular form of blast pressure with respect to time has been used to compute such spectra already accessible in the literature. The response spectra based on an exponential distribution of blast pressure have been proposed and are more consistent with experimental results (Gantes and Pnevmatikos 2004). In order to do this, analytical formulations of the solutions of the relevant equations of motion have been developed and utilised to conduct a comprehensive parametric investigation. Comparing the proposed approach's spectra to existing ones reveals that the commonly used assumption of triangular blast load evolution with time can be slightly under conservative at times, especially for flexible structural systems, but significantly over conservative at other times, especially for stiffer structures. In the exponential distribution, parameter (b) determines the degree of the negative phase. There is a considerable negative phase when ‘b’ is less than one, but the negative phase becomes less prominent when ‘b’ is more than one. Accordingly, the values b = 1; 2; and 3 have been employed and concluded that the negative phase duration doubles the positive phase duration.

Following the positive phase of an explosion, the negative phase occurs when the pressure drops below atmospheric pressure. While the positive phase of the explosion is widely

recognised, confirmation of the negative phase is uncommon in the literature. As a result, it is frequently addressed erroneously or ignored entirely. The existing approaches have been summarized for approximating the negative phase and gave suggestions based on experimental validation for which form to employ (Rigby et al., 2014). The consequence of erroneously modelling the negative phase has also been demonstrated, and numerical simulations explain its ramifications. A bilinear approximation simulated the negative phase, with a rise time equal to 1/4 of the negative phase duration (UFC 2005).

2.5 Multi-Storey Buildings Subject to Blast Loading

The blast load on a structure has been determined by several factors, including the size of the explosion, the location of the explosion (confinement type), the geometry and orientation of the object, and so on. Dynamics, explosive physics, and physical security procedures are the skills needed to create blast-resistant structures (Sabale and Choudhary 2021; Sharapov et al., 2021). TM5-855-1 is one of the military manuals that explain how to develop defensive systems (restricted for use). This document includes methods for predicting blast wave characteristics and estimating explosive loads on buildings. Another commonly used publication evaluating structural resistance to explosive blast is the UFC 3-340-02.

Blasting demolition is the preferred method for safely and efficiently demolishing high-rise buildings, and numerical simulation is very helpful for the design of complicated blasting schemes (Sun et al., 2020; Gajewski and Sielicki 2020). The stress transients of blasted columns at the bottom of buildings are important boundary conditions. Yet, few works have investigated it and provided a detailed model. After detonation of explosives, the bearing capacity of the column gradually decreases, which takes several milliseconds (Singh et al., 2020). When the bearing capacity reduced to less than the initial axial compressive stress in the column, the initial stress releases linearly, which also takes several milliseconds. The movements of the concrete fragments bent the longitudinal reinforcement bars, which induces

a strong tensile stress in the residual column; their stress-time history curves are triangular (Pathak and Ramana 2020).

There are three forms of interaction between the blast wave and finite structures in the case of limited systems (Catovic et al., 2021; Xu et al., 2022; Ding et al., 2022; Zhang and Abedini 2021). The first, known as diffraction loading, occurs when a large-scale blast wave engulfs an object produced by an explosive charge with a very high yield (Fig. 2.8a). Because of its size, the object's mobility is reduced here (diffraction target). The second type of loading is drag loading, which includes an enormous blast wave acting on a smaller object (Fig. 2.8b). This sort of target (known as a drag target) will be enveloped, but the dynamic pressure translational force will move and do extra damage to the target. The third scenario is a blast wave formed by a relatively modest charge explosion that loads a more significant structure (Fig. 2.8c). The reaction of specific structural components should be examined independently.

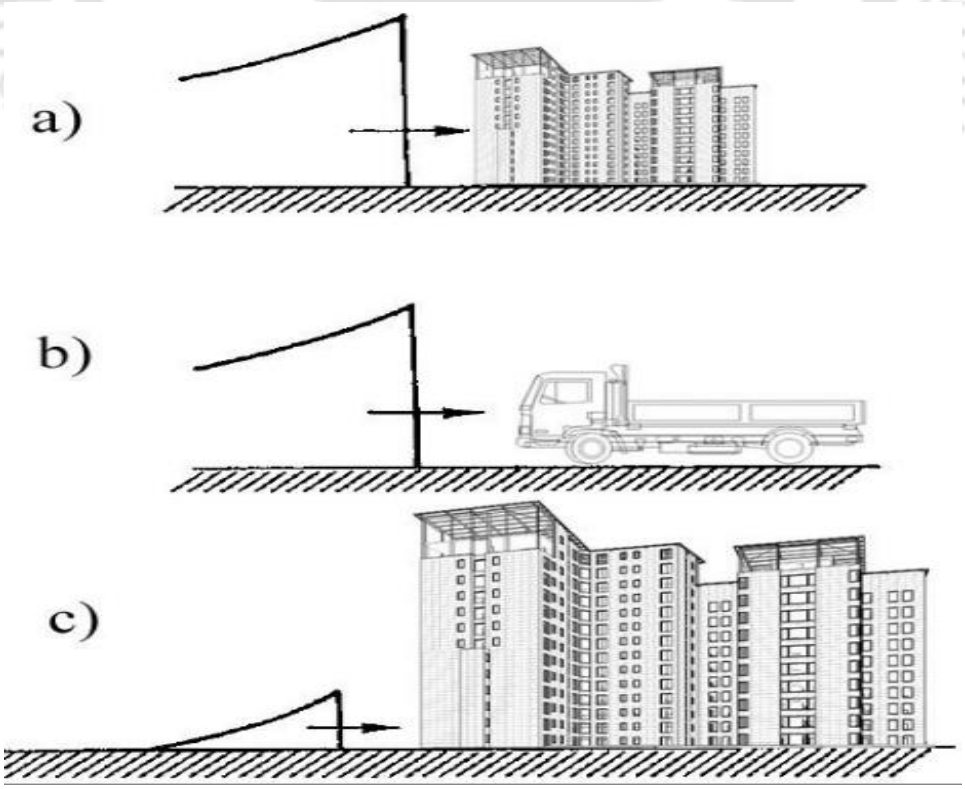

Fig. 2.8. (a) A large explosion and relatively large object; (b) large scale explosion and rel. Small object; (c) small scale explosion and rel. Large object (Catovic et al., 2021).

A probabilistic analysis of the performance of framed reinforced concrete structures has been published according to Italian NTC18 and European EC8 technical requirements (Stochino et al., (2020). A single-degree-of-freedom model of the structural system under blast stress has been created by a spring representing stiffness and a mass expressing inertia can be used to explain the structural behaviour of a mechanical system under blast load (He et al., 2021; Yan et al., 2020). Because the maximum displacement is attained in the first loading cycle, damping may be ignored in this type of issue. This structural model aims to determine the structure's maximum displacement during the collapse. A generalized SDOF system of beams under blast loading has been derived from the conservation law of energy and bending moment-curvature relationship by assuming the smooth material constitutive laws. The predicted deformation demand from the generalized SDOF system has been used to validate the measured demand from the available experimental results (Stochino et al., 2021).

During the design phase, criteria for the application of incidental design loads must be developed in connection to the necessary performance of each system of a process plant. This includes blast loads on essential goods for safety, emergency, and evacuation purposes and any equipment whose failure might lead to escalation, which must be constructed to withstand accidental explosions. The force acting on the object of interest must be estimated for the structural design of supporting structures, process equipment, and pipes in both onshore and offshore facilities, based on the usual features of the pressure wave (magnitude, duration, and shape). A guideline has been proposed that may calculate the force acting on components susceptible to unintentional explosions based on blast loading and the shape, size, and responsiveness of the impacted object, using a set of simplified relations (Ditali et al., 2018).

The majority of structures destroyed by explosives or impact loading were not constructed to withstand blast loads in the first place (Vivek and Sitharam 2020). Because of the extreme fragility of these structures, new requirements and standards for practical

approaches to limit the dangers of explosions are constantly being developed. A rigorous finite element study has been used to evaluate the structural performance of reinforced concrete frames when subject to blast loading (Ibrahim et al., 2017). As a preliminary to providing mitigation advice, the reaction of the structural model under the simulated blast load has been reported, along with two alternative designs. However, the frame did not avoid collapsing, emphasising the need for additional measures in the design when load route redundancy is critical.

The use of beam-column (1D) and plane (2D) finite elements have been discussed in the numerical analysis of planar concrete frames (Radnic et al., 2016). The two numerical models have been presented for nonlinear static analysis of planar concrete structures, one based on beam-column (1D) elements and the other on the plane (2D) finite elements, which can simulate the main nonlinear effects. Two experimental test results have been used to validate the proposed models. The experimental and numerical findings are in good agreement, indicating that both numerical models may be used in real-world situations.

The progressive collapse capacity of steel moment frames have been evaluated using an alternate load path approach, followed by a nonlinear dynamic study of the steel moment frames' reaction under blast and unexpected column loss scenarios (Tavakoli and Kiakojouri, 2013). The building's structural response to a rapid column loss under various methods of column removal, with or without external blast loading, has been studied in depth. According to the findings, the likelihood of progressive collapse is highly influenced by the site of column loss. The loss of a column might impact the structure's overall reaction to external blast loads. The findings shed more light on the impact of abrupt column loss on the dynamic response of steel moment frames subject to blast load.

A novel effective methodology has been introduced for calculating the equivalent uniform blast load for non-uniform blast loads such as close-in explosions of one-way square and rectangular reinforced concrete slabs (Wang et al., (2012). The model has subsequently been verified using experiments and blast tests for square and rectangular slabs utilising a single degree of freedom (SDOF) system. According to the test findings, the model estimates the explosive charge weight and stand-off distance to impose a specific damage level on the tested RC slabs, particularly for close-in blast loads. The novel model proved to be more accurate than traditional SDOF analysis and ran faster than FE analysis. The external virtual work done by the comparable uniform blast load has been equated to the external virtual work done by the non-uniform blast load, such as close-in explosions, to provide an "equivalent" blast load. The same external virtual work has been used to study the transition of the non-uniform dispersed blast load into uniform blast pressure for SDOF analysis. A theoretical formula has been presented for the peak equivalent uniform blast load.

Terrorists have made iconic and prominent structures a universal target for bomb assaults. The majority of these structures have been constructed without regard for their susceptibility to such occurrences (Xiao et al., 2021b; Fahmed et al., 2021). Authorities in planning and construction control have begun to recognise the dangers of these incidents and have included precautions in planning rules to mitigate their impact. The effects of near-field explosions have been investigated on the structural framing system and essential elements such as columns and the material reaction of the components (Jayasooriya et al., 2011). This information can be utilised to develop mitigation methods for the structure's probable catastrophic and gradual collapse. The structural frame system and components have been investigated for global stability and a local residual strength capacity in the linear elastic and non-linear plastic response regimes using a two-stage finite element modelling (FEM) and analytical approach. The approach utilised in this study may evaluate the susceptibility,

damage, and residual strength capacity of building frames and parts exposed to near-field blast events.

A new technique has been introduced for progressive collapse analysis of reinforced concrete (RC) frame structures under blast loading that considered non-zero initial conditions and early damage to neighbouring structural components (Shi Yanchao et al., 2010) . The numerical findings have been compared to those obtained utilising the alternate load path approach and those obtained from full numerical simulations, including the direct application of blast loads to the frame. Because the structure's velocity, displacement, and damage severity after the blast-loading phase are all affected by the blast scenarios, the crucial blast scenarios that destroy some essential structural components and induce progressive collapse must be found first. It should be noted that there might be numerous critical blast scenarios for a particular RC frame, i.e., planting explosives in a few different positions could all result in the collapse of the column under study. In these circumstances, many progressive collapse evaluations under various explosion scenarios should be carried out to understand the RC frame's progressive collapse resistive capabilities fully.

Turbines, moisture separators, and electric generators are all housed in the turbine building, an essential component in nuclear power plants. Turbine buildings are primarily frame constructions that have not been built to withstand blast loads in most situations. The dynamic reactions of reinforced concrete (RC) frame structures when subjected to distant strong surface loadings generated by explosions were numerically studied (Li et al., 2009). The research was expanded to look at the effect of claddings on frame structures when they were subject to blast loads. The dynamic reactions of frame structures with claddings have been shown to be more severe. This is due to the structure's exposure to varying blast forces. Two kinds of blast wave-structure interaction may be distinguished by evaluating the relative distance between the detonation centre and the target structure and the size of the structure

itself, as illustrated in Fig. 2.9. The interaction of a blast wave created by the detonation of a smaller charge loading a target structure at a short standoff distance, which is characteristic of most terrorist acts such as vehicle bombs, falls within the first category. The interaction of a blast wave on a relatively distant structure, such as that which may occur due to an accidental severe surface explosion of petroleum refineries, chemical factories, ammunitions storage locations, and other such systems.

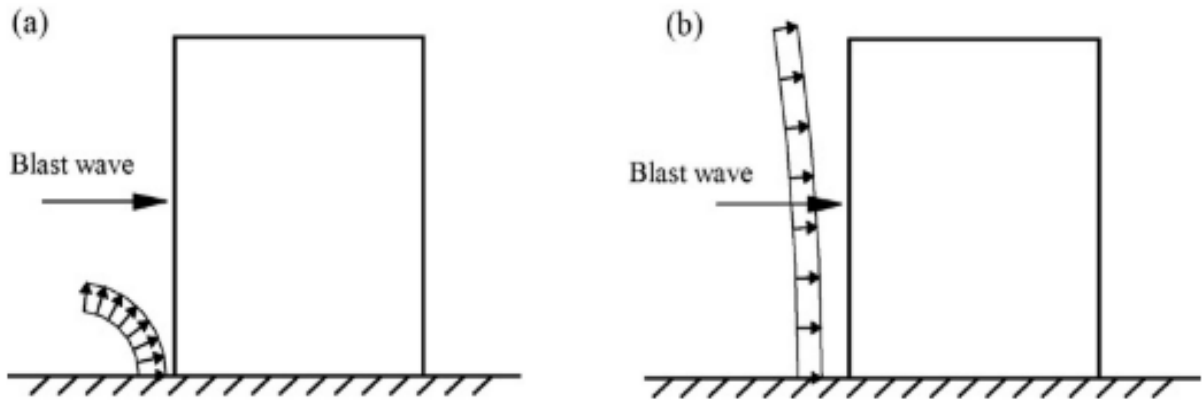

Fig. 2.9. Two classes of blast wave-structure interaction (Li et al., 2009).

When high explosives explode near a structural column, the existence of non-structural outside walls might impact the loads on that column. The influence of external (no wall and solid masonry wall) type on the loads on and response of exterior columns has been studied using numerical models and actual trials (Baylot and Bevins, 2007; Yadav 2021). Both calculations and testing show that, while failing fast, the outer wall substantially impacts the loads on the column and the air blast pressures entering the building. The calculations showed that when the air explosion collides with the collapsing external wall, the impulse imparted to the structural column right in front of the explosives increases significantly. This interaction causes the loads to be high enough to fail the external column when higher pressures.

The blast pressure on a building caused by a nearby explosion usually is quite significant and lasts only a few seconds. Even when impacted parts are simplified using single-degree-of-freedom models, such impulsive loading requires dynamic time-history analysis. Another option is to apply Newmark's empirical equation, which calculates the needed ultimate strength of an element based on the peak blast force, the ratio of the positive phase length to the natural period of vibration, and the target ductility ratio (Schmidt 2007; Ju and Kwak 2021; Datta et al., 2021). The General Services Administration has software that can compute the relevant parameters of the blast load and is available to the public. Structural dynamics principles determine the resistance member's effective mass, stiffness, and strength. The Department of Defence has created comprehensive reaction limitations that correspond to four tiers of protection for various materials and element kinds. As a result, a similar static technique for blast effects analysis and design, especially considering the uncertainties and assumptions that even more complex procedures contain. This technique is viable when the danger is external to the structure of interest and consists of a small to medium explosive at a moderate distance or a big explosive at a significant distance, with few additional reflecting surfaces nearby. Special conditions, such as close-in and restricted explosions, and where surrounding characteristics might drastically modify the blast environment, necessitate a more thorough examination.

A numerical investigation has been presented on performance assessment of multi-storey seismic reinforced concrete frame building under close-in blast loading. The study stated that a decrease in scaled distance raised effective plastic strain and damage index values. Furthermore, simultaneous use of close-spaced transverse steel reinforcement spacing in mid-height and ends of reinforced concrete columns has been found to be effective in reducing both effective plastic strains and damage index values (Abebe and Mohammed 2022; Francioli et al., 2023). The progressive collapse behaviour of high-rise reinforced concrete frame buildings

under blast loading induced by Vehicle-Borne Improvised Explosive Device (VBIED) has been studied with the two retrofitting measures such as fibre reinforced polymer (FRP) and steel plate (SP) (Chen et al., 2023). The damages caused in the building produced due to progressive collapse under blast loading scenario have been investigated. The surface blast effect has been included using simulated air pressure and ground motion produced due to blast (Tolani et al., 2022; Sun et al., 2020). The progressive collapse possibility of an existing RC building has been investigated against blast generated waves. A simple nonlinear dynamic analysis approach has been carried out to examine the progressive collapse possibility of the building when exposed to blast threat events (Elsanadedy et al., 2023). The response of reinforced concrete building subject to blast loading under variable mass of TNT has been discussed. The results indicated that using double reinforced mesh has great influence on reinforced concrete slabs to withstand blast loads and the damage in concrete happened under blast loads in flat slab system (Talaat et al., 2022).

A five full-scale experiments have been conducted to investigate the blast loads on a two-storey reinforced concrete and masonry building with a gable roof. The overpressure time histories have been recorded and used to determine the blast loads on the building (Xiao et al. 2021b). A high-fidelity numerical simulations have been utilized to carry out a detailed investigation of the influence of a building's porosity on its capacity to shield virtual facades located at several distances behind the shielding structure (Dib et al., 2022). The vibration response of the four-storey masonry building has been studied in a typical southwestern mountainous area of China under the blasting load. The results showed that the maximum particle velocity increased to 3rd floor and attenuation occurred on the 4th floor. The higher the floor is, the more concentrated the energy is in the low-frequency domain (Huo et al., 2019). The blasting effects have been presented on the structural response of a 5-storey building considering its columns, shear walls, beams, slabs, raft foundation, masonry walls, and

windows. Stresses, displacements, material status, and pressure due to blasting on some gauge points are presented (Toy and Sevim 2022). The effects of a surface blast on multi-storey buildings of different heights have been extensively investigated by considering the action of the air pressure and ground acceleration separately and both acting simultaneously. The results showed that the relative effects of air pressure and ground shock on the buildings depend upon the height of the building and standoff distance (Tolani et al., 2020a). The performance of two hillside building configurations, i.e., split foundation (SF) and step-back (SB), commonly observed in the seismically active Indian Himalayan region has been evaluated under blast and blast-induced ground motion using an uncoupled approach. It has been observed that the blast on the downhill side was critical for the hillside buildings having a storey ratio of 0.5; whereas, the blast on uphill side was more damaged for the buildings with a storey ratio of 1 and 2 (Kulariya and Saha 2022).

A quantitative procedure for the robustness and progressive collapse assessment of reinforced concrete frames under blast load scenarios has been presented. The global robustness has been evaluated by the damage-presumption approach where the damages have been defined in both typology and extension depending on the blast scenario occurring at the local level (Francioli et al., 2021; Francioli et al., 2023b). A DNA strategy has been reported to identify the perpetrator of a suicide car bombing in front of the Australian Embassy in Jakarta, Indonesia, on 9 September 2004 (Sudoyo et al., 2008). A numerical simulation approach has been proposed and verified by considering the blast and collapse resistant effects of masonry-infilled walls and the collapse resistance of masonry-infilled RC frame buildings has been evaluated under blast loadings. The study concluded that the presence of masonry-infilled walls can efficiently block the blast waves into the building structures and relieve the upward arch of slabs and damage degree of interior columns, and the masonry-infilled walls provide sufficient alternate load paths than the bare RC frame buildings to enhance the

structural robustness and restore the gravity stability of masonry-infilled RC frame buildings after the explosions (Lu et al., 2023). The response and extent of damage in reinforced concrete framed buildings have been investigated under varying blast load pulse shapes. The effect of masonry infill has been included in the in-plane direction of blast loads with varying pulse shapes. Results revealed that the in-plane strength and stiffness of masonry infills have significantly reduced the overall damage in structural components (Fatima et al., 2023).

The progressive collapse possibility of an existing reinforced concrete building has been investigated against blast-generated waves. Data has been collected for a typical RC building constructed in a congested area in Riyadh city. A simple nonlinear dynamic analysis approach has been carried out to examine the progressive collapse possibility of the building when exposed to blast threat events. The progress of damage caused to different structural elements and the state of stress in these elements have been studied (Elsanadedy et al., 2023). The blast response of two-storey masonry structure having varying areas of openings on the frontal wall has been investigated. The nodal-force method has been adopted by applying the blast load on each node of the finite element model. The results have been reported in terms of major principal stress, minor principal stress and direct shear stress. The effect of opening area on blast response of masonry models has been found to be quite significant (Raza et al., 2023). The response of reinforce concrete buildings subject to blast loading under variable mass of TNT and different standoff distance has been discussed. The study has been carried out using the finite element program (ABAQUS) by using two different models i.e., Flat slab system and Solid slab system. The results have been obtained in terms of Von-Mises stresses, deflection and concrete damage against varying mass of TNT. The results revealed that using double reinforced mesh has great influence on reinforced concrete slabs to withstand blast loads (Talaat et al., 2022). The effect of intended explosion to a structural member has been investigated by considering the critical columns of a four storey RC building. The behavioural

changes have been investigated under critical load path of the building subject to a sudden collapse of load bearing member. It has been observed that ground floor columns are most critical for load transfer and joint displacement when subject to blast loading (Goel et al., 2017).

A triangular pyramid explosion risk mode has been established based on the theory of risk which combined the overpressure, duration, and frequency of the explosion scene at the same time. The first principle of acceptable cumulative frequency and the key principle of maximum explosion risk have been formulated. The results revealed that the explosion scene and its frequency, the volume of the obstructed region, and the distance of the explosion source are the key variable that affected the explosive load (Bai et al., 2021). Three experimental research works have been introduced on protective structures against bomb and blast loadings. The effects of reinforcement of the roof, concrete depth and size of an RC wall have been investigated when RC buildings subject to a series of bombing tests. The explosive tests have also been conducted on tunnel shelters to determine the effects upon corners in branch type and mesh type tunnels under blast pressure (Ishikawa and Beppu 2007). A 3D numerical model with the direct simulation of blast load has been proposed to study the real behaviour of a 20-storey tall building under the blast loading. It has been found that due to the uplift and downward pressure working on the slab, the column force under the direct blast simulation method is smaller than that of the alternative path method (Fu 2013; Jayatilake et al., 2004). The progressive collapse behaviour of steel concrete composite buildings subject to ground blast explosion has been investigated using nonlinear dynamic analysis and conventional alternate path approach. The composite slab model based on equivalent area approach and the composite joint model based on Eurocode's component method have been proposed for nonlinear analysis. The results revealed that a heavy blast load may wipe out a series of columns or beams at once instead of a single one and high blast pressure may also induce large lateral drift and lead to significant damage to structural elements spreading over several storeys

of the building (Jeyarajan et al., 2015). The dynamic response of high-rise building subject to blast loading has been presented. The performance of high-rise buildings, blast phenomena and dynamic response of a concrete frame structure under blast loading have been investigated by using SAP2000 software. The moderate explosive energy has been used to control the structural damages due to explosion and for decreasing the façade on surrounding buildings (Vinothini and Elavenil 2016).

The design manual for the Unified Facilities Criteria (UFC 2005) provided rational procedures for performing the preliminary design of blast resistant frames efficiently and preliminary dynamic load factors for establishing equivalent static loads for both the local and overall frame mechanism. In the design of blast resistant structures, rigid frame structure architecture has been chosen because it enables open internal space while also providing strong resistance to lateral stresses. Furthermore, due to the gradual growth of plastic hinges up to the structure's ultimate capacity, this style of design has intrinsic energy absorption capabilities. Under the action of horizontal and vertical blast loads, each element in a frame is exposed to combined bending moments and axial stresses. On the other hand, a simple analysis cannot determine the phasing between critical axial force and bending moment values. For trial beam-column design, it is advised that the peak axial loads and moments calculated from Fig. 2.10 be considered to act simultaneously.

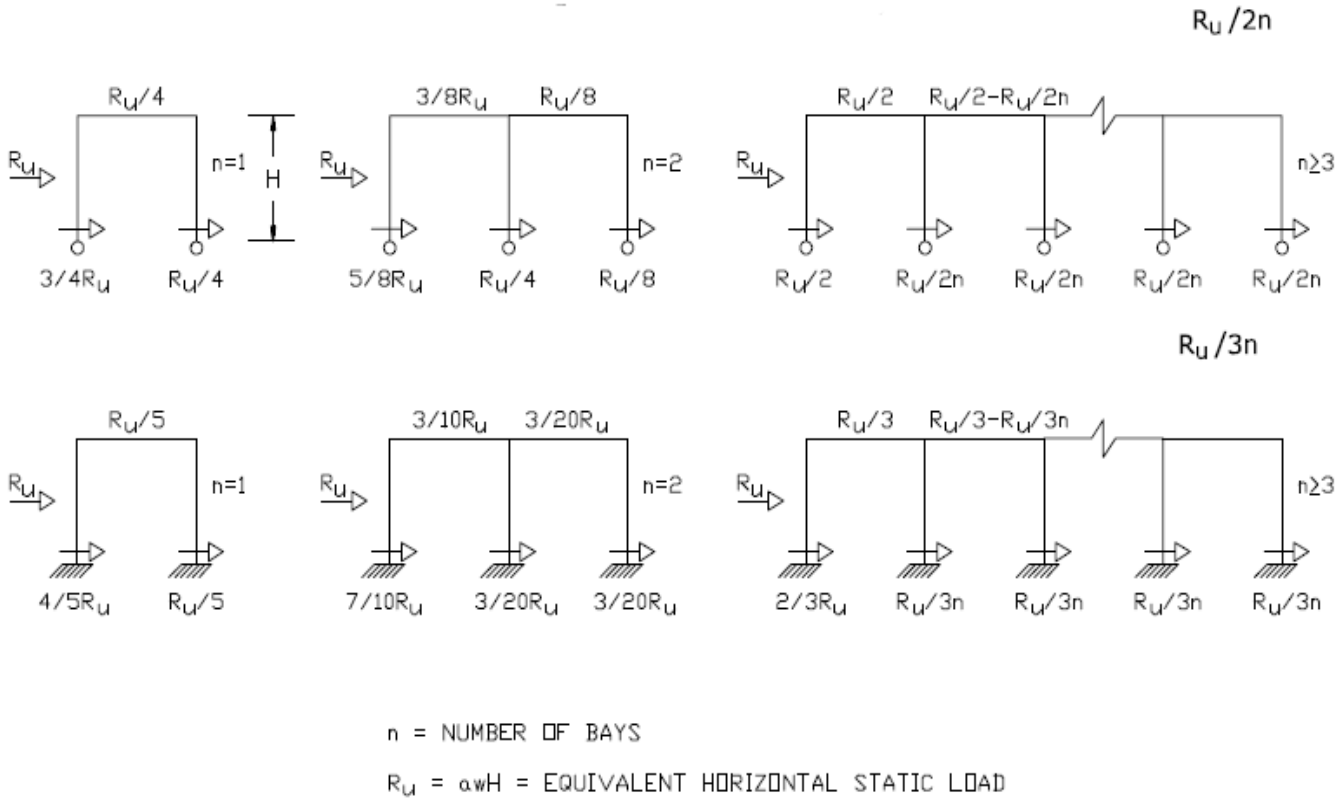

Fig. 2.10. Estimate of Peak Shears and Axial Loads in Rigid Frames Due to Horizontal Loads (UFC 2005).

2.6 Shape Function of Multi-Storey Buildings

Building regulations include static techniques based on a single-mode response with easy modifications to account for higher mode impacts. While the simplified approaches are acceptable for basic regular structures, they do not account for complicated structures' entire spectrum of behaviour. As a result, dynamic analysis is the preferable technique for the design of structures with regular or irregular geometry (Taranath et al., 2004). Single-degree-of-freedom (SDOF) systems represent simple oscillators, whereas multi-degree-of-freedom (MDOF) systems represent complicated oscillators. A single lump of mass on the top end of a vertically cantilevered pole or a mass supported by two columns represents a simple oscillator. The idealised system describes two types of structures: 1) a single-column structure with a

relatively big mass at its top, and 2) a single-story frame with flexible columns and a stiff beam. By lumping storey masses at intervals along the length of a vertically cantilevered pole, buildings may be analysed as multi-degree-of-freedom (MDOF) systems.

A two-dimensional model is usually sufficient for a regular and largely symmetrical building. The consequences of higher modes may be considered for moderate- to high-rise structures. A multi-degree-of-freedom system is transformed into an analogous single-degree-of-freedom system using generalised coordinates (Paz and Halperson, 1980). Any arbitrary function that meets the boundary criteria can be used to describe the deformed structure. The aspect ratio of the structure, defined as the ratio of the building height to the base dimension, is the most relevant consideration for selecting the shape function for building structures.

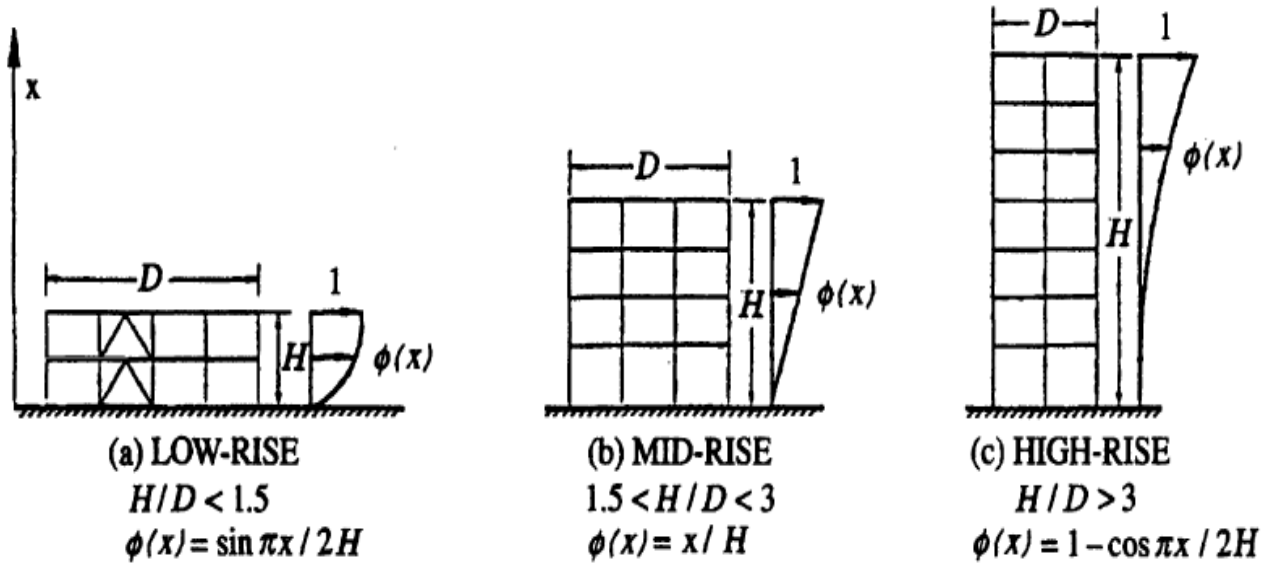

Fig. 2.11. Possible shape functions based on the aspect ratio (Paz and Halperson 1980).

Because the deflections in this mode are all of the same sign, the fundamental mode of a multi-story building or a single-span beam is simple to comprehend (Chopra 2012). However, the mode form of more complicated systems may be difficult to comprehend. A

shape function derived from the structure's static deflections owing to self-weight may not be acceptable.

The shape functions for high-rise, mid-rise, and low-rise structures should only be used in the first mode (Paz and Halperson, 1980). The straight-line design indicated for the mid-rise structure has been used in most seismic construction regulations. After obtaining the dynamic response in terms of the generalised coordinate, the displacements in the structure are determined.

For static and dynamic analysis of symmetric wall-frame buildings, an approximation technique based on the continuum approach and transfer matrix method has been given (Bozdogan 2009). The whole thing was modelled after a sandwich beam. The high-rise structure has been modelled as a discrete lumped mass system for free vibration analysis.

For the computation of the derivative of vibration mode shapes concerning design parameters, four approaches have been presented: finite difference method, modal method, a modified modal method, and Nelson's methods. Depending on the structural system, the mode shape will be bending, shear, or a mix of bending and shear (Camarda 2015). The mode shape of tall buildings can normally be represented by a straight line (Edskär and Edskär 2018). The natural frequencies and mode shapes are essential parameters in evaluating design loads for buildings subject to dynamic loading conditions (Geetha 2017). They are also required for spectrum or mode superposition harmonics or transient analysis. A simple yet precise analytical technique has been devised based on energy principles for rapid computation of natural frequencies and mode shapes of multi-storey structures designed with the framed tube, shear core, and double belt trusses systems; the method is based on the creation of a continuum model that is equal to genuine multi-story structures in significant movements (Malekinejad and Rahgozar 2012).

2.7 Progressive Collapse of Multi-Storey Buildings

After removing a critical load-bearing element in a typical progressive collapse scenario, the connecting spans will deflect until the rotation capacity offered by the neighbouring slabs or beams is exhausted. Because of the presence of frame redundancy, removing a column will not always result in the collapse of RC structures. The structure will disperse the load to nearby columns, which will carry the increased stress exerted on them if not overloaded (Azim et al., 2020).

The key to the research of progressive structural collapse is to perform an in-depth investigation into the structural collapse mechanism at the onset of structural component failure due to accidental events and the demand of progressive collapse resistance for the remaining substructures. However, the most common available methods for analysing progressive collapse adopt the empirical coefficient assumption, which lacks the theoretical basis and neglects the contribution of floor resistance (Zhang et al., 2020; Vieira et al., 2020; Hu and Zhao 2020). A series of static and dynamic loading tests have been performed to investigate the progressive collapse resistance of conventional precast concrete moment frame. The test results showed that the progressive collapse resistance was significantly affected by the connection detail and beam rebar ratio (Feng et al., 2020).

After removing a column, an analytical model for the collapse of traditional 2D framed buildings has been proposed (Masoero et al., 2013; Xiao et al., 2021; Chauhan and Malik 2021). The maximum and lower bounds of the collapse loads, dependent on the activated collapse mechanism, are closed-form expressions under simplified conditions. A quantifiable geometric/mechanical parameter has also been discovered, specifying which collapse process has been activated for a given starting damage. Resistance to progressive collapse initiation has been calculated as the ratio of dynamic collapse load after damage to static collapse load before damage for numerous circumstances. Data from dynamic nonlinear simulations have been used

to compare the results. The suggested analytical technique provides a preliminary robustness-oriented design strategy incorporating particular solutions in terms of redundancy, compartmentalization, and column and beam mechanical characteristics.

A numerical study has been carried out on a framed RC building to evaluate the cost-benefit of designing against progressive collapse over the conventional seismic design. UFC 4-023-03 and Eurocode CEN 8 standards have been used in the design procedure. The results revealed that the seismic design requirements are insufficient for avoiding the progressive collapse of the structure (Ghaderi et al., 2020). A column removal strategy has been used to model and simulate multi-storey buildings' progressive collapse under sudden column removal. The study introduced a failure function and control mechanism of the frame structure (Mourid et al., 2020). The progressive collapse simulations have been presented to assess the robustness of a seismic-resistant building using self-centring moment resisting frames under a sudden column loss scenario. The simulations allowed for the identification of all possible failure modes and the quantification of the contribution of the composite floor to the robustness of the frame. The results showed that the building can withstand the code-prescribed load with a safety factor of 2 and that the structural limit state that triggers progressive collapse is the buckling of the gravity columns (Dimopoulos et al., 2020). A pushdown analysis technique has been used to investigate the robustness of building systems by computing residual capacity and establishing collapse modes of a damaged structure. Simulation results shown that the frame designed for high seismic risk is more robust than the corresponding one designed for moderate seismic risk. It is shown that the dynamic impact factors associated with column removal are significantly lower than the commonly used value of 2 and are in line with lower values in the guidelines recently proposed by the US Department of Defence (Khandelwal and El-Tawil 2011; Alashker et al., 2010; Khandelwal et al., 2009).

A reinforced concrete frame structure is one of the widely used structural system. A localized damage caused by extreme events may lead to progressive collapse of entire structure. A progressive collapse test of three 1/3-scaled reinforced concrete frames has been reported. Test results show that the progressive collapse process of frame structures consisted of five stages: an elastic stage, yield stage, beam mechanism stage, transient stage and catenary stage. The simulation results indicated that the collapse resistance of RC structures was substantially improved with the increased of the slab thickness and seismic design intensity (Zhang and Li 2020). A probabilistic approach has been presented to determine the risk of collapse and reliability of building with special moment frames. The resistance capacity of the damaged building has been evaluated under moderate earthquake followed by explosion against progressive collapse (Abdollahzadeh et al., 2020). A quantitative method of robustness index of diagrid structure based on the mechanical properties of the components and the vertical bearing capacity of the structure has been established to investigate the vertical resistance to progressive collapse and the evolution of its robustness in the process of loading (Liu and Fang 2020). A state of the art on current trends and the research required have been addressed to understand the progressive collapse of steel frame buildings. The assessment methods such as computational and probabilistic models for structural robustness and progressive collapse risk, methodologies for enhancement of system collapse resistance have been highlighted (El-Tawil et al., 2014; El-Tawil and Li 2013).

When a progressive collapse occurs due to sudden column removal, the moment connections must have adequate strength and be able to bridge over the damaged element (Barmaki et al., 2020; Qian et al. 2020; Di Trapani et al., 2020; Shan and Li 2020; Kiakojouri et al., 2020). A comprehensive experimental apparatus has been developed for the progressive collapse testing of reinforced concrete frames. The loading apparatus has been studied for the testing of the 3D frame of progressive collapse resistance of the RC structure under a corner

column removal scenario. The test results showed that the infill walls can provide a suitable path of load transfer and improve the gradual collapse resistance of the RC frames (Prakash and Satyanarayanan 2020). The collapse distribution and propagation has been investigated in the structural elements by tracking down the collapsed locations among the beam and column structural elements in moment-resisting reinforced concrete short buildings, and the effect of the column removal on the expansion and development of the progressive collapse due to the earthquake loads. A collapse distribution pattern has been introduced to predict the progressive collapse propagation scenario due to the earthquake loads and the internal column removal (Karimiyan 2020).

A progressive collapse analysis has been carried out to investigate the influence of strain rate effects on collapse-resistant capacity, collapse mode, and collapse path of the reinforced concrete buildings. It has been concluded that the strain rate effects influence the structure's collapse mode and collapse path (Wang 2020). The experimental studies on the progressive collapse of RC buildings have been summarized to study the numerous aspects such as progressive collapse resistance mechanisms, alternate load path method, testing procedure, boundary conditions and seismic detailing etc. The behaviour of different structural systems and new mitigation schemes utilized in literature to develop progressive collapse resistance have been summarized (Alshaikh et al., 2020). The various column removal methods due to blast loads have been compared in the progressive collapse analysis of RC rigid frame structures and presented a simplified model to evaluate the progressive collapse response of beam-column structures (Naji 2019). A macro-model-based approach has been used to simulate the potential for progressive collapse of a typical reinforced concrete moment frame structure initiated through the loss of one or more first-storey columns. The characterization of nonlinear behaviour associated with the transfer of forces through the joint is critical to predict the large deformation response associated with progressive collapse. A simplified model of a

beam-column joint has been used to represent essential and critical actions in the floor beams and the transfer of these forces through the joint region to the vertical elements. It is demonstrated that the proposed approach using a validated macro-model is a viable methodology for progressive collapse analysis. The study also found that special RC moment frames detailed and designed in zones of high seismicity perform better and are less vulnerable to progressive collapse than the RC frame structures designed for low to moderate seismic risk (Bao et al., 2008).

An analytical approach has been carried out to study the progressive collapse using the Alternate Path Method (APM) from the General Service Administration (GSA) guidelines. Location of the removed column, number of floors, vertical irregularity and their influence have been studied (Agrawal et al., 2019). The effect of available structural capacity on dynamic increase factor (DIF) value in the RC structures has been investigated to the study proposed new DIF formulae to predict the stress and deformations in the RC buildings after column removal (Amiri et al., 2018). A modified sensitive analysis has been applied using the GSA, UFC 4-023-0 and ASCE guidelines to find the critical element of the multi-storey buildings (Farahani et al., 2018). The fragility curves have been used to assess the seismic and progressive collapse resistance of multi-storey rigid frame structures. The study concluded that the progressive collapse design of the RC frame might lead to an undesirable failure mode (i.e., strong-beam-weak-column) under earthquakes, which indicates that a seismic redesign is necessarily after the progressive collapse design (Lin et al., 2017).

The code-based alternate load path method has been applied to assess the threat-independent dynamic column removal responses. The study established the importance of initial damage location and building's size (Kiakojouri et al., 2021). The progressive collapse mechanisms have been investigated in RC beam-column assembly and results stated that the four mechanisms such as flexural action, compressive arch action, plastic hinge formation, and

catenary action, have a significant effect on structural behaviour (Paripour et al., 2021). The effects of opening in the volume of low and mid-rise irregular voided structures with low to high seismic resistance on the progressive collapse vulnerability have been investigated. The results show that moment connections that govern the robustness of the structure are the most critical components in the structure. However, in the scenarios of removing the internal column away from the opening, the progressive collapse mechanism of the structures with or without opening does not differ (Ghobadi and Yavari 2020). A reduced-order computational model has been introduced for delayed collapse behaviour of RC structures. The deformation and failure mechanisms have been observed with the experimental results (Mello et al., 2020).

ASCE/SEI (7-05) Standard defines progressive collapse as the spread of an initial local failure from element to element, resulting in the collapse of an entire structure or a disproportionately large part of it. In general, US building codes do not address progressive collapse prevention design directly. General recommendations for structural integrity are introduced in the commentary of ASCE/SEI 7-05. In recent years two federal agencies, the General Services Administration (GSA) and the Department of Defence (DoD) developed two approaches to address progressive collapse prevention. Both approaches are threat independent methods to reduce the potential for progressive collapse. The application of either method should not be considered to provide blast-resistant design and is limited to buildings without unusual structural configurations (Jayasooriya et al., 2011; Mishra and Netula 2021).

Current methods and practices for modelling and numerical simulation of progressive collapse of RC frame buildings primarily focused on the alternate path method, in which collapse resistance has been assessed by the ability of systems to find alternate load paths following the sudden loss of a structural member. The mechanistic approach to identify the weakest collapse mechanism in building frames has been developed based on virtual work principles. The tie force approach has been used for providing a basic degree of robustness

against progressive collapse in low-risk structures. For structures of significant complexity, scale, or importance, alternative methods that may or may not be threat specific are required by local building codes.

The chapters that follow in this thesis establish a framework for overcoming the limitations and gaps in the current state of the art.

CHAPTER 3 QUANTIFICATION OF BLAST LOADING

3.1 General

A bomb explosion ruins the building's structural frame and causes walls to collapse, flying debris and broken glassware, posing a hazard to human life. Blast loading quantification is critical for defence, transportation security, and structural engineering. The blast loads due to spherical or hemispherical charges have been anticipated using conventional blast resistant design guidelines such as TM 5-1300, DoD, GSA, and empirical equations from the available literature. Instead of the idealised spherical/hemispherical explosives considered in commonly used semi-empirical techniques, realistic explosion scenarios frequently entail detonating non-spherical high explosive charges. As a result, simplified engineering-level tools must integrate the impacts of charge shape and the associated loading distribution. This chapter quantifies the influence of explosive charge shape on structural response. This chapter also develops the equivalent factors of pressure and deformation due to explosive charges shapes such as spherical, cylindrical, rectangular, cubical, and conical charge shapes.

Due to the blast scenario, specific trials cannot be replicated by laboratory testing, despite the explosive shapes, dimensions, and weights being altered. An essential conclusion is that laboratory studies require a meticulous experimental setup and a thorough understanding of the experimental model to prevent incorrect findings. Because technical publications and official standards assume simple conditions, the accuracy of blast load calculation in complicated scenarios is inadequate. Little information on the design parameters and performance of reinforced concrete buildings subjected to blast loads is available due to the unpredictability and difficulty of anticipating accidental explosions.

Empirical (or analytical) approaches, semi-empirical methods, and numerical methods are the methodologies available for predicting blast impacts on building structures. In recent years, computer-assisted research on reinforced concrete member behaviour has progressed from analytical to numerical analysis. In recent years, there has been a surge in interest in creating hydrocodes to aid experimental testing.

3.2 Effect of Charge Shape on Structural Response

3.2.1 Finite Element Simulations

LS-DYNA is a finite element transient dynamic code. Explicit time integration is widely utilised to analyse structures that have substantial deformations. It is exceptionally effective at addressing highly nonlinear dynamic problems and has a lot of material resources. LS-Prepost has different material resources, including material libraries and user-defined material models, allowing users to precisely define element attributes and structural behaviour. Other functions for model simulation include contacts for addressing interactions between separate pieces, boundary conditions, and load implementation. It aids users in understanding and visualising the generated data. Structural deformation, stress contours, strain contours, and displacement contours are some of the outcomes that may be seen (Rajkumar et al., 2020). Users may then forecast the structural response of the actual system when it is subject to a certain static/dynamic loading based on the results.

A numerical simulation approach known as the Multi-Material Arbitrary Lagrange Euler (MM-ALE) method has widely been utilised to anticipate blast loads; this method necessitates a model that includes the explosive charge, the target building of interest, and the whole surrounding air domain. When the TNT equivalency is small, the MM-ALE approach has been routinely utilised to model blast wave propagation and interaction with building structures. The MM-ALE method's numerical model includes the explosive charge and the air

between the target structure and the detonation point (Zhang et al., 2021). A considerable air domain will be present in the far-field situation. As a result, the procedure takes a long time to complete since a small mesh size is required to attain acceptable precision.

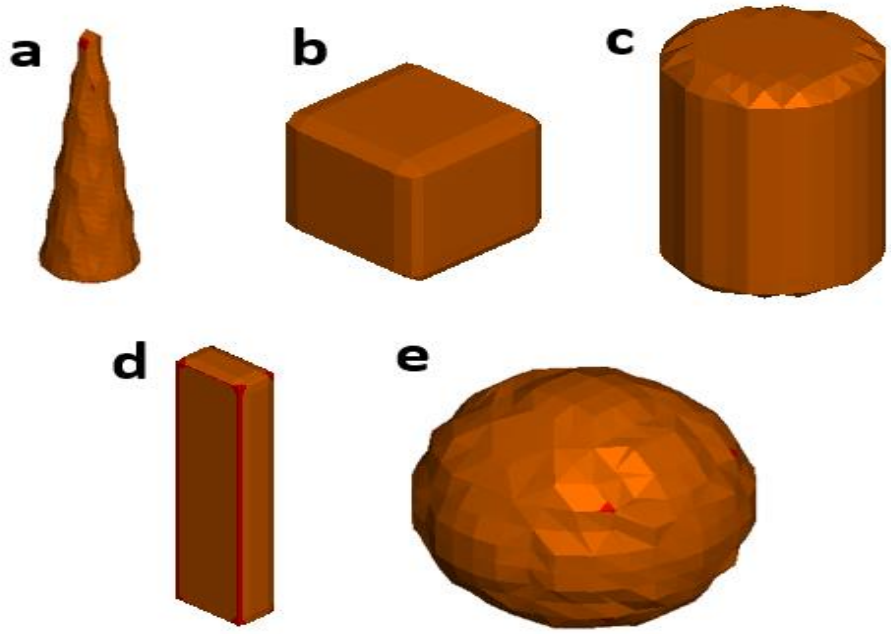

Fig. 3.1. Explosive charge shapes: a) Conical b) Cubical c) Cylindrical d) Rectangular e) Spherical.

Fig. 3.1 illustrates the explosive charge shapes used in the study to achieve spherical equivalent quantities for pressure and deformation responses. This study investigates a single-storey RC rigid frame subject to blast loading and analyses the rigid frame by utilising the MM-ALE technique. The RC frame model is schematically shown in Fig. 3.2, and the specifics of structural components and material attributes are listed in Tables 3.1 and 3.2. As shown in Fig. 3.1, numerical simulations of RC frame structures subject to blast loads are carried out for various explosive charge shapes. The responses are estimated at different locations, such as the top, middle, and bottom parts of the front column of the RC frame, respectively. The spherical

equivalent quantities are also employed in an interior blast study of an RC frame structure that exposed to blast loading.

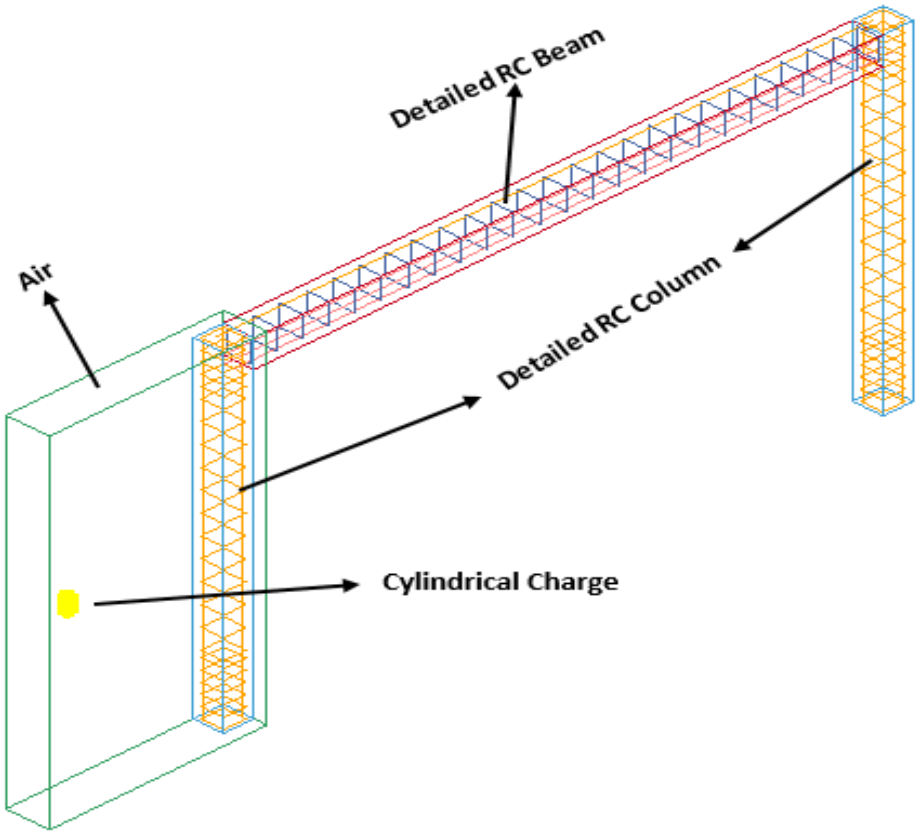

Fig. 3.2. ALE modelling of RC frame.

Table 3.1 Details of the structural member of the RC frame numerical model.

Structural member	Length (mm)	Width (mm)	Depth (mm)	ρ	f_{ck} (MPa)	f_y (MPa)
Column	3000	230	230	0.008	25	255
Beam	5000	230	250	0.013	25	255

Table 3.2. Concrete and reinforcement rebar data used in numerical simulation.

Material	Parameters	Value
Concrete	Concrete strength	25 MPa
	Mass density	2500 kg/m^3
	Poisson's ratio	0.2
	Tensile stress at failure	6 MPa
Steel	Young's modulus	200 GPa
	Longitudinal steel strength	255 MPa
	Transverse steel strength	255 MPa
	Mass density	7850 kg/m^3
	Poisson's ratio	0.3
	Plastic strain at failure	0.18

3.2.2 Numerical Validation

The numerical approach must be validated to ensure the accuracy of the modelling and outcomes. This study considers a quarter scale field experiments of RC two-storey buildings to validate the FEM modelling. The concrete material model employed in the current non-linear study, structural response, and outcome compared to the experimental results were all key aspects that needed to be confirmed. A series of blast tests have been conducted on five different two-story quarter-scale building models to determine the response and damage to the external columns when subjected to explosive generated blast loads (Baylot and Bevins 2007). The current study has chosen experiment No. 2 for comparison. The behaviour of the centre column, which is directly exposed to blast load, is analysed, with data presented in Table 3.3. The pre- and post-experimental configurations of the three-dimensional RC quarter-scale structural model are shown in Fig. 3.3.

Table 3.3 Average values used in test 2 (Baylot and Bevins 2007).

Concrete strength	42 MPa
Modulus of elasticity	28.7 GPa
Concrete density	2068 kg/m^3
Yield strength of longitudinal reinforcement	450 MPa
Yield strength of transverse reinforcement	400 MPa

Ultimate strength of longitudinal reinforcement	510 MPa
Ultimate strength of transverse reinforcement	610 MPa
Elongation of the steel	18%

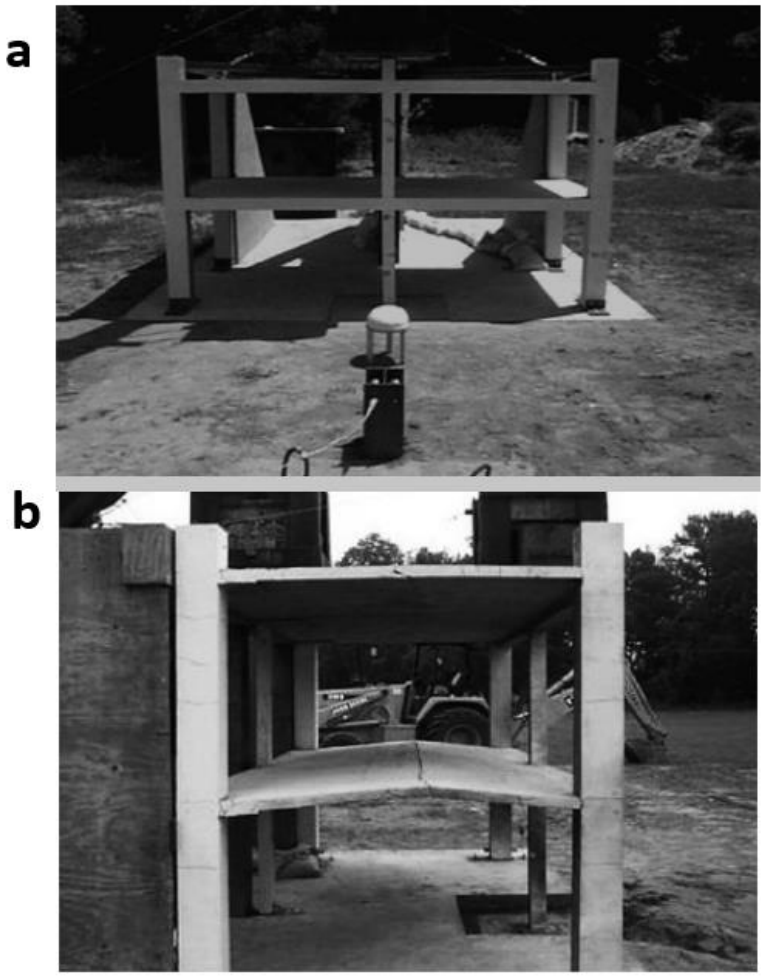

Fig. 3.3. Structure for ¼-scale experiments: (a) no walls and (b) Damage to the intermediate floor (Baylot and Bevins 2007).

As shown in Fig. 3.3a, the requisite blast load parameters for the selected experiment are calculated using 9.71 kg TNT equivalency put with a standoff distance of 1.07 m, 0.2286 m above the ground. The column's cross-section is 85 mm x 85 mm square, with deformed 1.6 steel wire cross ties at 100 mm. It has a longitudinal reinforcement configuration of 8 distorted wires, each with a cross-sectional area of 32.2 mm^2 and a height of 0.9 m. The thickness of the

cover is 8.5 mm. The average strength of unconfined concrete is 42 MPa. For longitudinal and transverse reinforcement, steel wires with yield stresses of 450 MPa and 400 MPa are utilised.

In numerical analysis, both implicit and explicit time integration have been commonly employed. The ALE approach for explosion analysis uses explicit integration in this case. Three components are incorporated in the FE model: explosive and air material as ALE parts and the column as Lagrangian parts. Because there are several ALE materials, the ALE multi-material group is employed. The ALE multi-material formulation is utilised to overcome the issues of substantial mesh distortion encountered in the Lagrangian reference, making it suitable for simulating the detonation of a high explosive and shock wave propagation. To explode the charge in the model, the keyword Initial Detonation is utilised. To avoid wave reflection from the border, use the non-reflection boundary keyword. The keyword Initial Volume Fraction Geometry is utilised to initiate the explosive material inside the air components. Because of the design of the explosive material, this keyword eliminates the need to produce fine mesh for the explosive elements and surrounding air elements. The size of the elements in a FEM analysis affects the findings; therefore, convergence research determined that 25 mm size elements are adequate for both the ALE and Lagrangian portions in the numerical model. Concrete is meshed as 3D eight node solid hexahedron elements while steel reinforcement is meshed as Hughes-Liu beam elements. The steel reinforcement and concrete are linked by shared nodes and they are assumed to be perfectly bonded without any slip (Jayasooriya et al., 2011; Abedini et al., 2020). The keyword Constrained Lagrangian in Solid is used to conduct the coupling method between ALE portions and the Lagrangian part. The Lagrangian component is the slave part, while the ALE portion is the master part. The Lagrangian mesh should cover the ALE mesh, and there should be no shared nodes between the ALE and Lagrangian sections to accomplish an entire fluid-solid interaction (FSI). The validated model is modelled as in Fig. 3.4, and the material models are detailed as in Table 3.4.

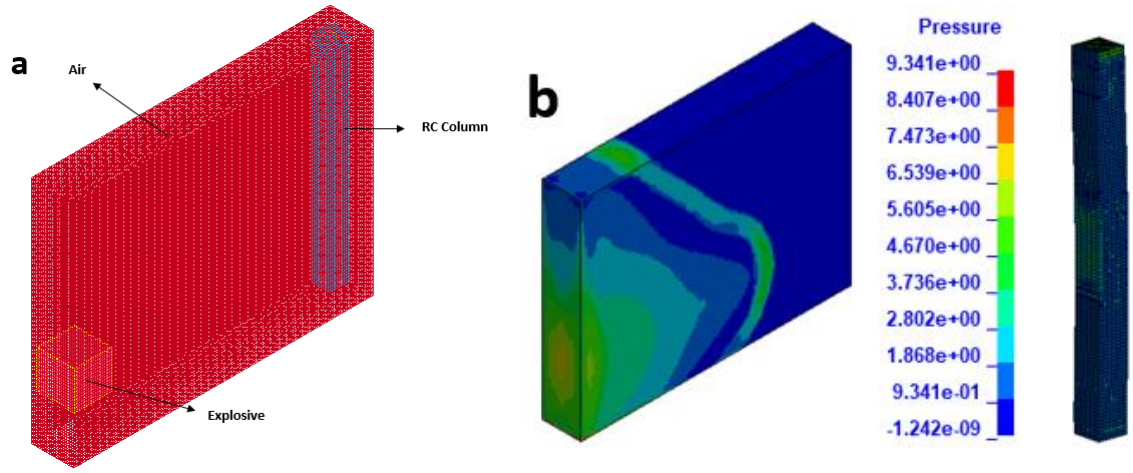

Fig. 3.4. ALE method: a) Modelling b) blast wave propagation and damaged RC column.

Table 3.4. Material properties of concrete, steel, explosive and air.

Units (g, mm, ms, MPa)								
*MAT_CONCRETE_DAMAGE_REL3 (Concrete)								
RO	f_{ck}	PR						
0.0024	25	0.2						
*MAT_PLASTIC_KINEMATIC (Reinforcement)								
RO	f_y	PR	E					
0.0078	255	0.3	2e+5					
*MAT_HIGH_EXPLOSIVE_BURN (Explosive)								
RO	D	PCJ						
0.00163	6930	2.1E+4						
*EOS_JWL (Explosive)								
A	B	R_1	R_2	w	E_0	V_0		
3.712e+5	3231	4.15	0.95	0.3	7000	1		
*MAT_NULL (Air)								
RO	PC	MU						
1.225e-6	-1e-6	8.5e-10						
*EOS_LINEAR_POLYNOMIAL (Air)								
C_0	C_1	C_2	C_3	C_4	C_5	C_6	E_0	V_0
0	0	0	0	0.4	0.4	0	0.25	1

The propagation of shockwaves is investigated during the simulation to evaluate the numerical approach for modelling detonation. The wave propagation of a blast by distance

beyond the explosion's origin is seen in Fig. 3.4b. The blast shock waves move with an immediately rising overpressure front as the explosion occurs. Within moments, the pressure behind the front might plummet below the surrounding atmosphere. It can be observed that high pressure spread fast across the air and then immediately fell. The air pressure abruptly rises to a peak overpressure value over the ambient pressure at a specific location. Over time, the pressure decays to ambient pressure. Further, it decays below ambient pressure to under pressure before eventually restoring to normal ambient pressure levels over a period of time. Depending on the amount of charge weight, height of burst, and standoff distance, the production of ground shock is reduced, and blast waves may contact the building as incident waves rather than reflected blast waves.

The mid-height deflection time history in the experimental test and numerical analysis is shown in Fig. 3.5. The maximum deflection is found to be close to the deflection that has been measured experimentally. Consequently, the present numerical model's results matched the experimental data well. Table 3.5 summarises the validation results for deformation and pressure time histories.

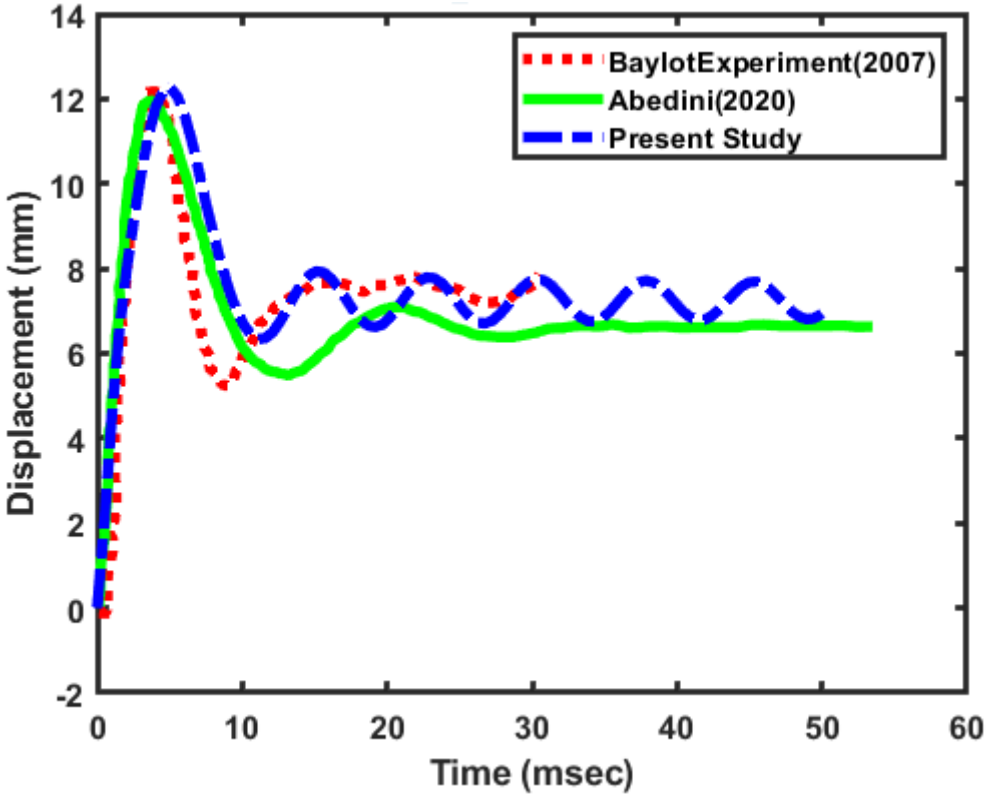

Fig. 3.5. Deformation-time history.

Table 3.5. Summary of numerical validation.

Method	Baylot(2007)		Abedini(2020)		Present study	
	Displacement (mm)	Pressure (MPa)	Displacement (mm)	Pressure (MPa)	Displacement (mm)	Pressure (MPa)
Experiment	12.5	7.5	-	-	-	-
ALE	-	-	12	7.8	12.75	7.557

3.3 RC Frame Subjected to Exterior Blast Loading

A series of simulations are provided in the current study to analyse the non-linear response of RC frames subject to various explosive charge shapes of blast detonations. In this study, the explosive charge weight is 1.5 kg, the standoff distance is 1.07 m, duration of simulation is 3ms and the explosive charge density is 1630 kg/m3, all of which are kept constant for each explosive charge shape. The RC frame's explosive charge shape specifications and results are presented in Table 3.6. The following are the results of numerical simulations conducted to study the impact of charge shape on the structural response at various locations:

Spherical Charge

The RC frame is modelled with a spherical charge, as shown in Fig. 3.2, and numerical analysis is performed using the ALE technique to identify the response at various locations of the front column in the RC frame. Fig. 3.6 and 3.7 depict the deformation and pressure responses of the RC frame, respectively. Due to the spherical charge, the maximum pressure and deformation attained in duration of 3ms are 0.880 MPa and 0.557 mm, respectively.

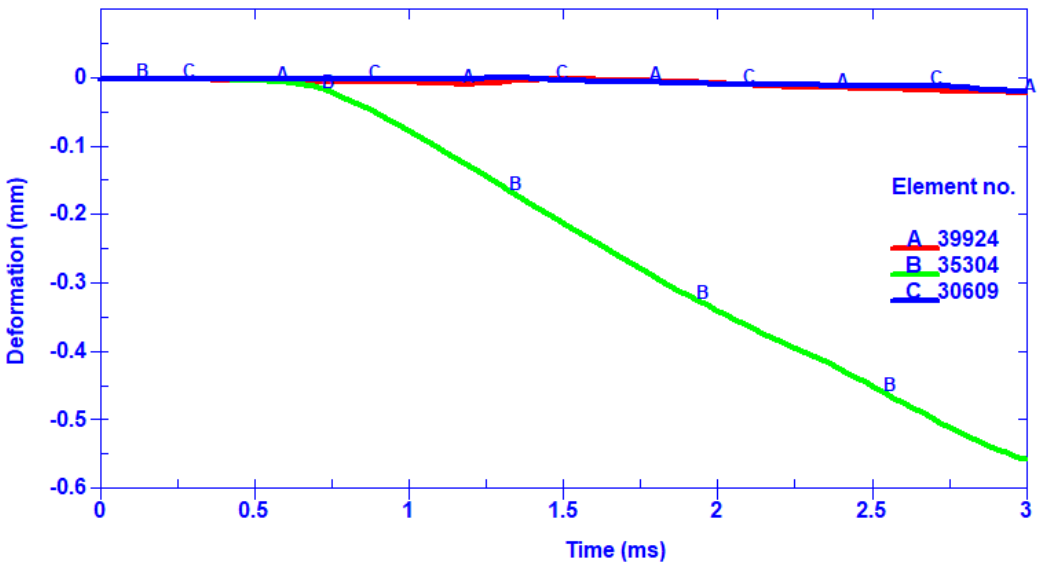

Fig. 3.6. Deformation-time history at different locations (A, B and C represents top, mid, and bottom locations, respectively).

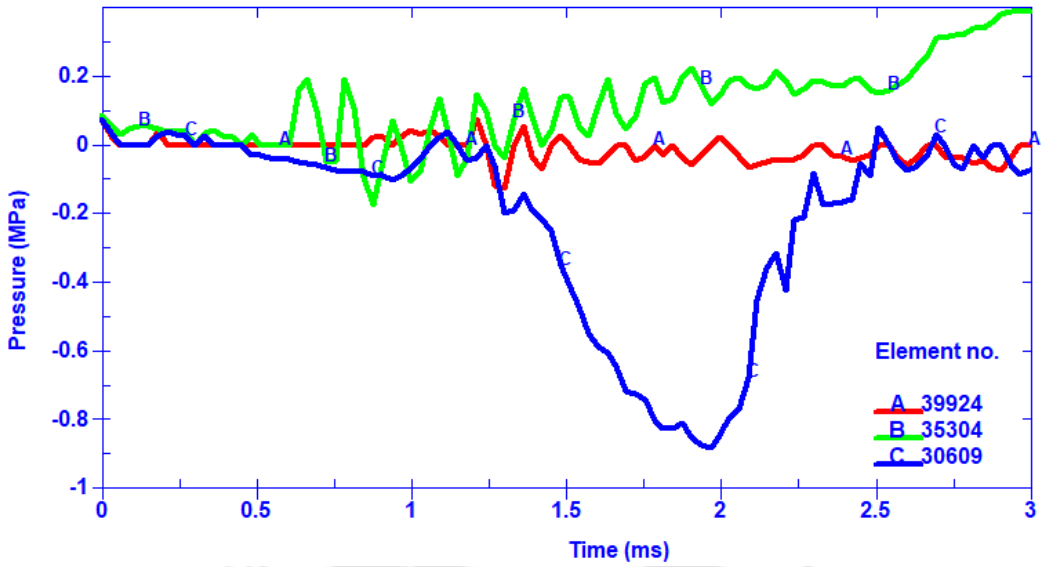

Fig. 3.7. Pressure-time history at different locations (A, B and C represents top, mid, and bottom locations, respectively).

Conical Charge

The RC frame is modelled with conical charge, as shown in Fig. 3.2, and numerical analysis is performed using the ALE technique to identify the response at various locations of the front column in the RC frame. Fig. 3.8 and 3.9 depict the deformation and pressure responses of the RC frame, respectively. Due to the conical charge, the maximum pressure and deformation obtained in the duration of 3ms are 0.835 MPa and 0.725 mm, respectively.

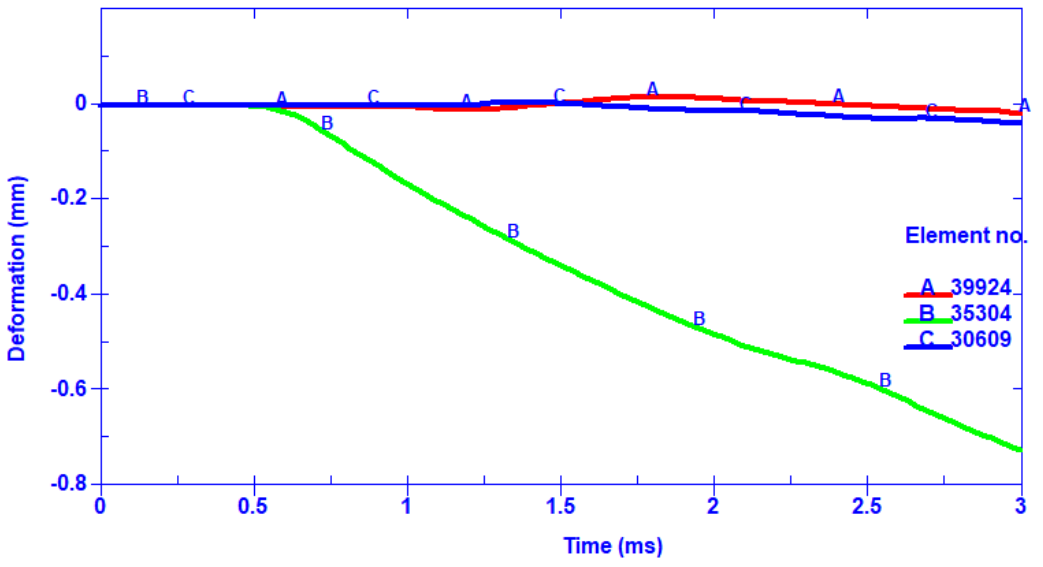

Fig. 3.8. Deformation-time history at different locations (A, B and C represents top, mid, and bottom locations, respectively).

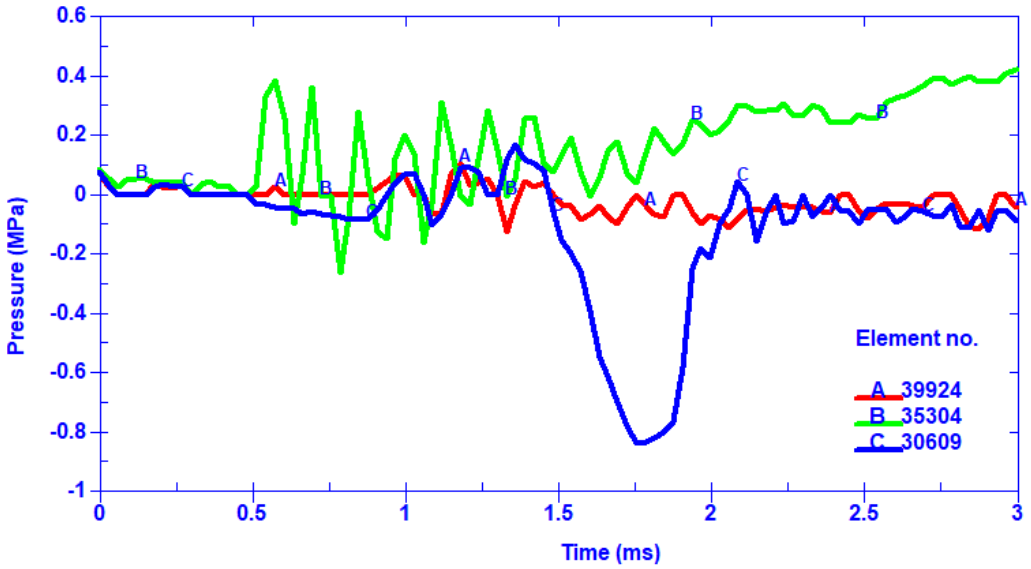

Fig. 3.9. Pressure-time history at different locations (A, B and C represents top, mid, and bottom locations, respectively).

Cubical Charge

The RC frame is modelled with cubical charge, as shown in Fig. 3.2, and numerical analysis is performed using the ALE technique to identify the response at various locations of the front column in the RC frame. Fig. 3.10 and 3.11 demonstrate the deformation and pressure responses of the RC frame, respectively. Due to cubical charge, the maximum pressure and deformation attained in the duration of 3ms are 1.69 MPa and 1.716 mm, respectively.

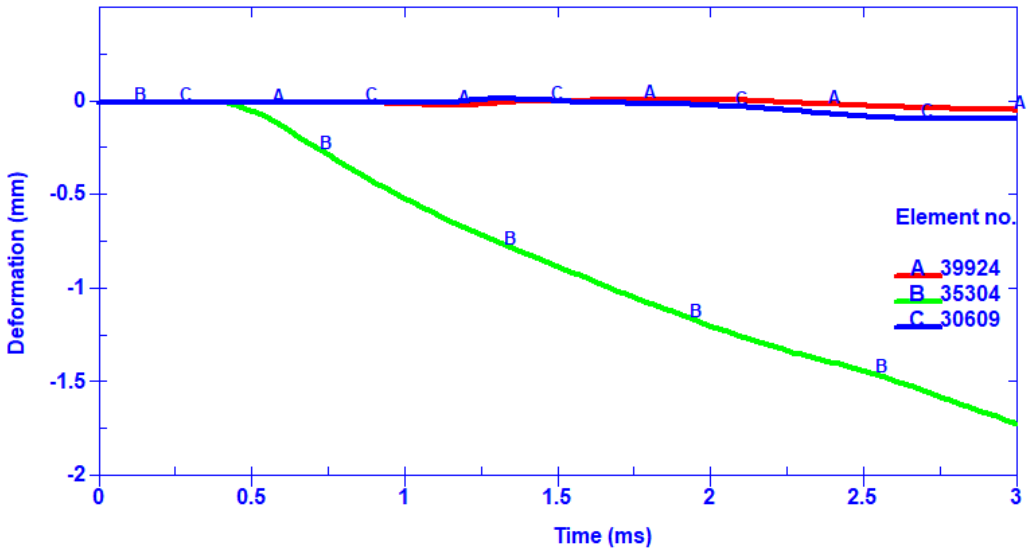

Fig. 3.10. Deformation-time history at different locations (A, B and C represents top, mid, and bottom locations, respectively).

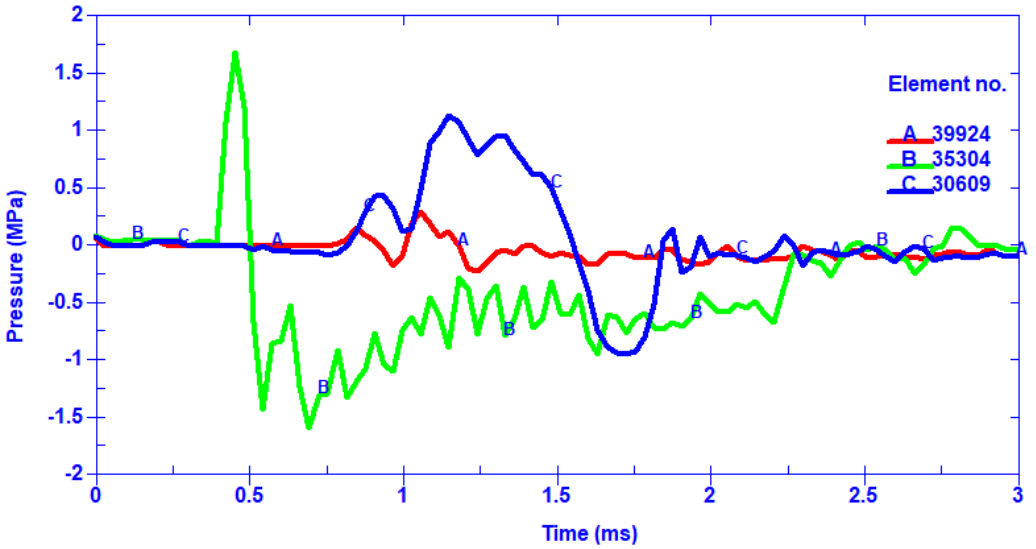

Fig. 3.11. Pressure-time history at different locations (A, B and C represents top, mid, and bottom locations, respectively).

Cylindrical Charge

The RC frame is modelled with a cylindrical charge, as shown in Fig. 3.2, and numerical analysis is performed using the ALE technique to identify the response at various locations of the front column in the RC frame. Fig. 3.12, and 3.13 demonstrate the deformation and pressure responses of the RC frame, respectively. Due to cylindrical charge, the maximum pressure and deformation obtained in the duration of 3ms are 0.869 MPa and 0.686 mm, respectively.

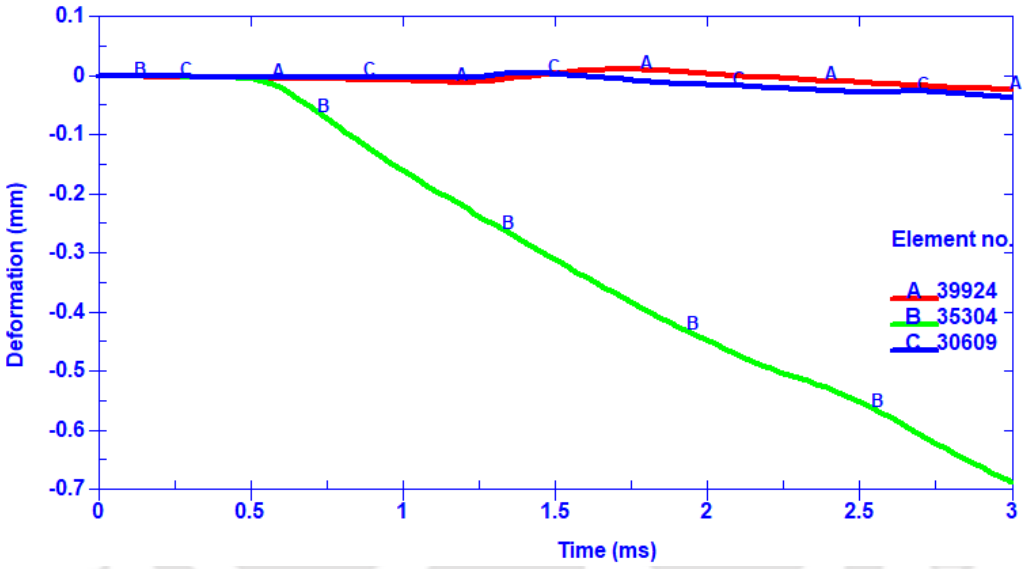

Fig. 3.12. Deformation-time history at different locations (A, B and C represents top, mid, and bottom locations, respectively).

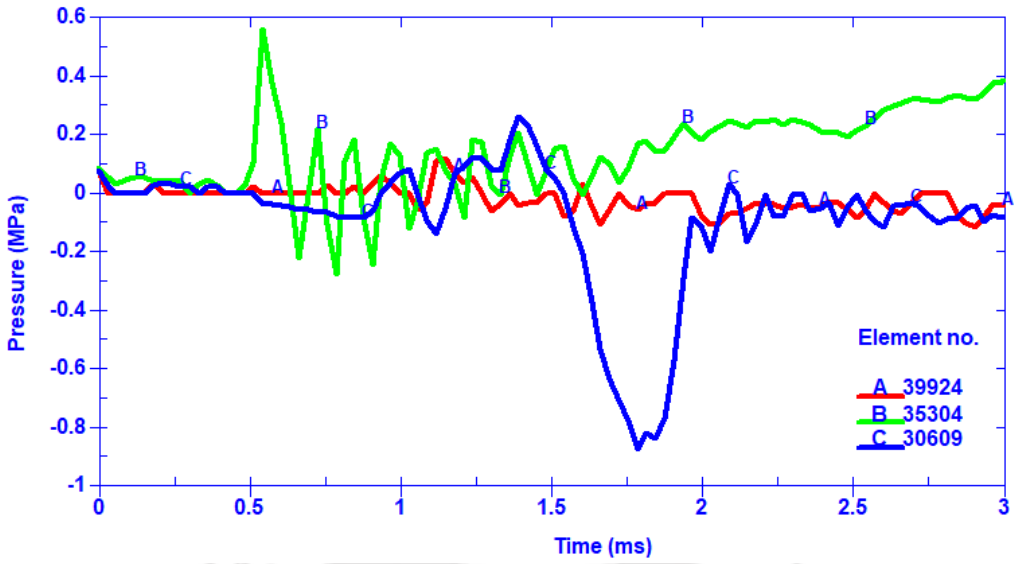

Fig. 3.13. Pressure-time history at different locations (A, B and C represents top, mid, and bottom locations, respectively).

Rectangular Charge

The RC frame is modelled with a rectangular charge shape, as shown in Fig. 3.2, and numerical analysis is performed using the ALE technique to identify the response at various locations of the front column in the RC frame. Fig. 3.14 and 3.15 demonstrate the deformation and pressure responses of the RC frame, respectively. Due to the rectangular charge, the maximum pressure and deformation obtained in the duration of 3ms are 1.498 MPa and 3.052 mm, respectively.

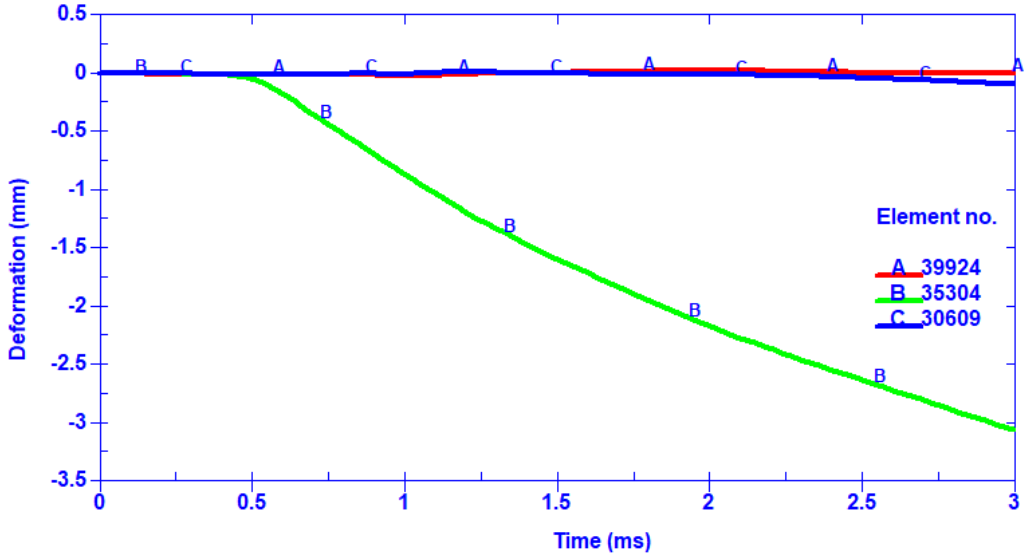

Fig. 3.14. Deformation-time history at different locations (A, B and C represents top, mid, and bottom locations, respectively).

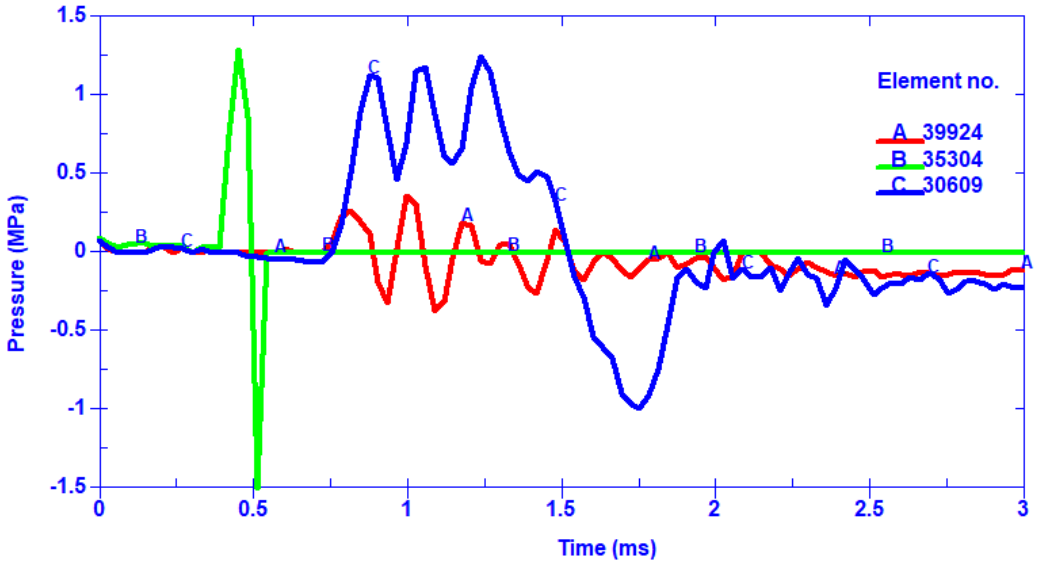

Fig. 3.15. Pressure-time history at different locations (A, B and C represents top, mid, and bottom locations, respectively).

Table 3.6 summarises the pressure and deformation responses of the RC frame for all of the explosive charge shapes obtained at three distinct locations. The pressure and

deformation quantities are normalised with the spherical quantities to produce equivalent spherical values, as shown in Table 3.7.

Table 3.6. Response of RC frame for different explosive charge shapes.

Charge Shape	Weight (g)	Density (kg/m^3)	Height (mm)	Standoff distance (mm)	Location	Element No.	P_{max} (MPa)	δ_{max} (mm)
Spherical 	1500	1630	1500	1070	Top	39924	0.122	0.021
					Middle	35304	0.391	0.557
					Bottom	30609	0.880	0.018
Conical 					Top	39924	0.124	0.017
					Middle	35304	0.423	0.725
					Bottom	30609	0.835	0.039
Cubical 					Top	39924	0.301	0.043
					Middle	35304	1.69	1.716
					Bottom	30609	1.136	0.091
Cylindrical 					Top	39924	0.124	0.022
					Middle	35304	0.561	0.686
					Bottom	30609	0.869	0.035
Rectangular 					Top	39924	0.375	0.028
					Middle	35304	1.498	3.052
					Bottom	30609	1.250	0.091

Table 3.7. Spherical charge equivalent pressure and deformations.

Charge Shape	Weigh t (g)	Density (kg/m^3)	Height (mm)	Standoff distance (mm)	Location	Element No.	$P_{spherical}$ (MPa)	$\delta_{spherical}$ (mm)
Spherical 	1500	1630	1500	1070	Top	39924	1	1
					Middle	35304	1	1
					Bottom	30609	1	1
Conical 					Top	39924	1.016	0.810
					Middle	35304	1.082	1.302
					Bottom	30609	0.945	2.167
Cubical 					Top	39924	2.467	2.048
					Middle	35304	4.322	3.081
					Bottom	30609	1.291	5.056
Cylindrical 					Top	39924	1.016	1.048
					Middle	35304	1.435	1.232
					Bottom	30609	0.988	1.944
Rectangular 					Top	39924	3.074	1.333
					Middle	35304	3.831	5.479
					Bottom	30609	1.420	5.056

For all the explosive charge geometries at the top, middle, and bottom of the column, the pressure and deformation responses are recorded for three elements in the RC frame. For the rectangular explosive charge shape at the mid-point in the RC frame, the maximum deformation is 3.052 mm, and the maximum pressure is 1.498 MPa. The cubical explosive charge shape at the top of the RC frame column has a minimum deformation of 0.017 mm and

a minimum pressure of 0.124 MPa. At the midpoint of the column in the RC frame, the rectangular explosive charge shape causes 5.5 times the deformation caused by the spherical charge shape. At the midpoint of the column, the cubical charge shape creates 4.3 times the pressure generated by the spherical charge shape. Conical, cubical, cylindrical, and rectangular charge shapes contribute 1.08, 4.32, 1.4, and 3.8 times the pressure imposed by the spherical charge shape. Conical, cubical, cylindrical, and rectangular charge shapes give deformations of 1.3, 3.08, 1.23, and 5.5 times that of a spherical charge shape.

3.4 RC Frame Subject to Interior Blast Loading

Interior blast finite element simulations with a spherical explosive charge shape are conducted, and the response of the RC frame to interior blast loads is predicted for other explosive charge shapes. The different explosive charge shapes for the internal bursts are calculated using Table 3.7. According to the clear span of the RC frame, the charge is placed at various points on the ground. The contact blast, quarter-distance blast, and half-distance blast of the clear span are all investigated with finite element simulations.

3.4.1 Interior Contact Blast

The RC frame is modelled with a spherical charge, as illustrated in Fig. 3.16, and numerical analysis is performed using the ALE technique to determine the reaction at various locations of the RC frame exposed to contact interior blast loading. Fig. 3.17 and 3.18 demonstrate the pressure and deformation responses of the RC frame, respectively. Fig. 3.19 depicts a damaged RC frame caused by an inside contact explosion. Table 3.8 shows the pressure and deformation responses for additional explosive charge shapes owing to the RC frame's interior contact explosion. Due to the internal contact blast load, the maximum pressure and deformation obtained in the duration of 3ms are 12.076 MPa and 39.589 mm, respectively.

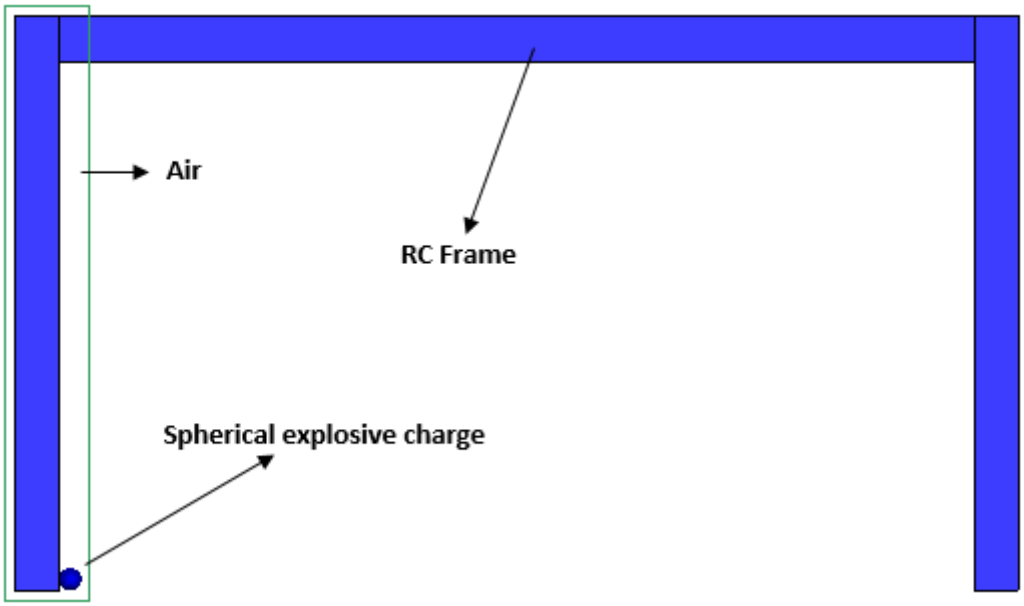

Fig. 3.16. Contact interior blast modelling of RC frame.

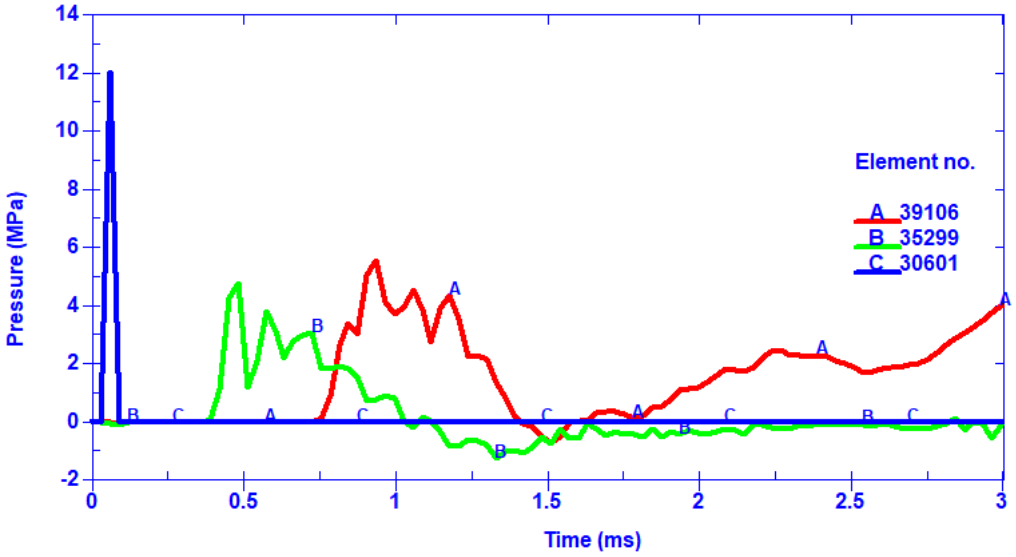

Fig. 3.17. Pressure-time history of elements at different locations (A: Top (just below the beam), B: Middle and C: Bottom) of the targeted column.

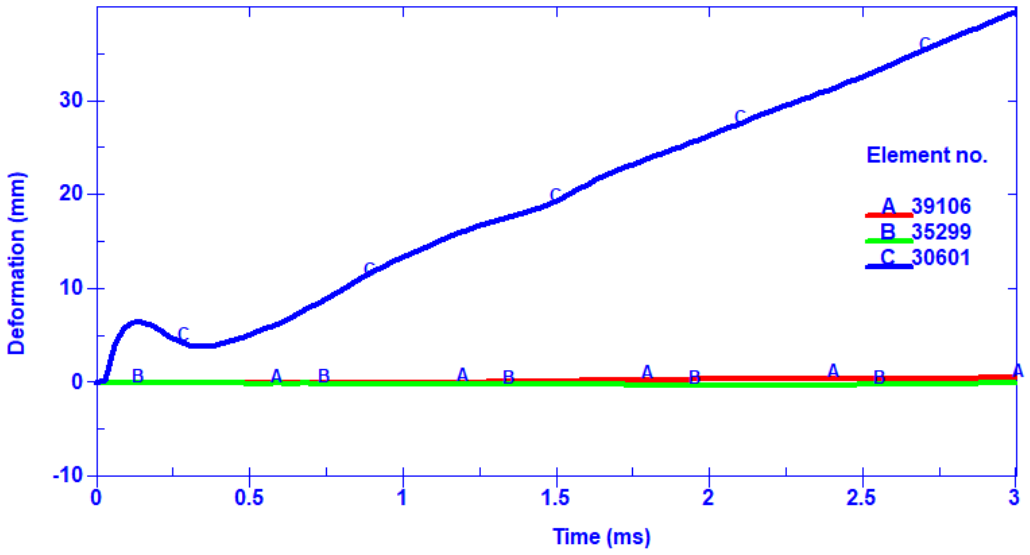

Fig. 3.18. Deformation-time history of elements at different locations (A: Top (just below the beam), B: Middle and C: Bottom) of the targeted column.

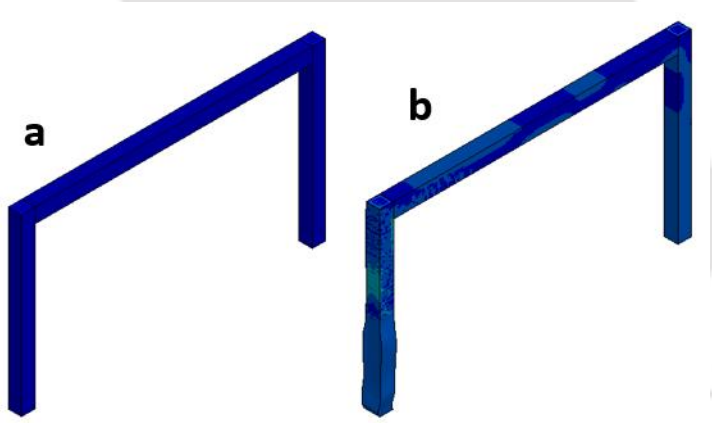

Fig. 3.19. Contact interior RC frame: a) Before blast and b) After blast.

Table 3.8. Response of RC frame due to interior contact blast

Charge Shape	Weight (g)	Density (kg/m^3)	Location	Element No.	P_{max} (MPa)	δ_{max} (mm)
Spherical 	1500	1630	Top	39106	5.574	0.576
			Middle	35299	4.802	0.214
			Bottom	30601	12.076	39.589
Conical 			Top	39106	5.663	0.467
			Middle	35299	5.196	0.279
			Bottom	30601	11.412	85.789
Cubical 			Top	39106	13.751	1.180
			Middle	35299	20.754	0.659
			Bottom	30601	15.590	200.162
Cylindrical 			Top	39106	5.663	0.604
			Middle	35299	6.891	0.264
			Bottom	30601	11.931	76.961
Rectangular 			Top	39106	17.134	0.768
			Middle	35299	18.396	1.172
			Bottom	30601	17.148	200.162

3.4.2 Interior Blast at One-Fourth of Clear Span

The RC frame is modelled with a spherical charge shape, and the blast wave propagation due to interior blast at one-fourth of the clear span is shown in Fig. 3.20. The response at different locations of the RC frame subjected to internal blast at one-fourth of the clear span is calculated numerically using the ALE method. Fig. 3.21 and 3.22 demonstrate the

pressure and deformation responses of the RC frame, respectively. Table 3.9 shows the pressure and deformation responses for additional explosive charge shapes caused by an inside blast at a quarter distance from the RC frame's clear span. At one-fourth of the clear span, the maximum pressure and deformation due to internal blast load in the duration of 3ms are 0.513 MPa and 0.175 mm, respectively.

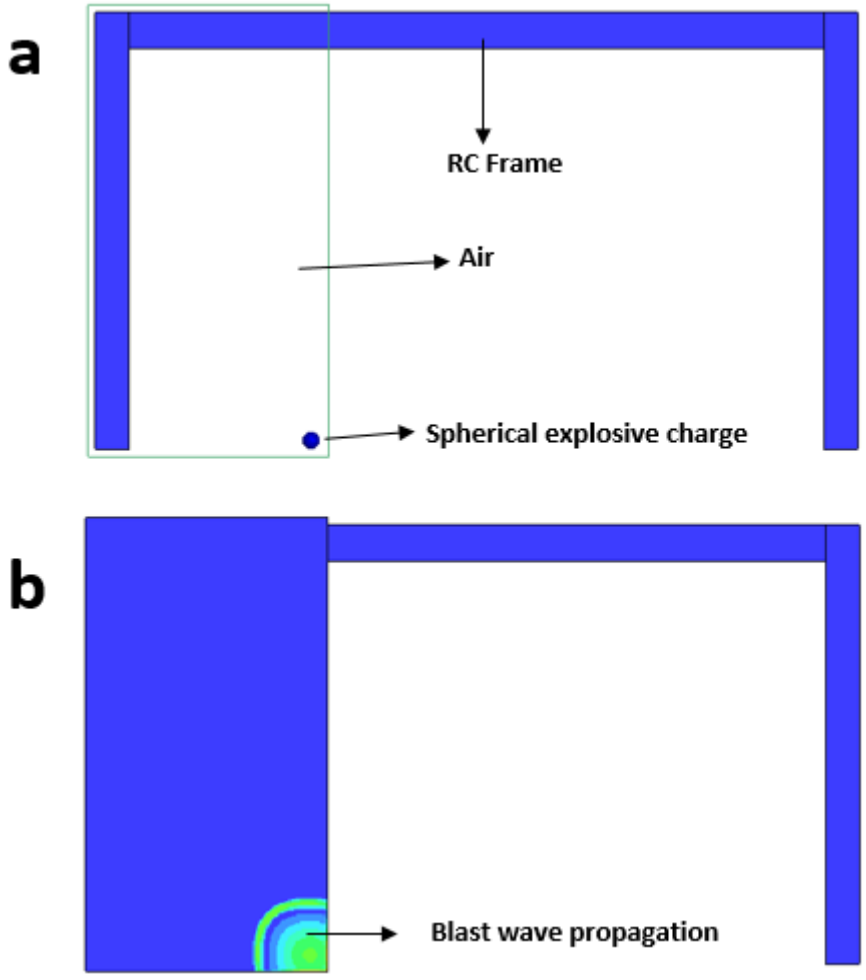

Fig. 3.20. Interior blast: a) Modelling and b) Blast wave propagation.

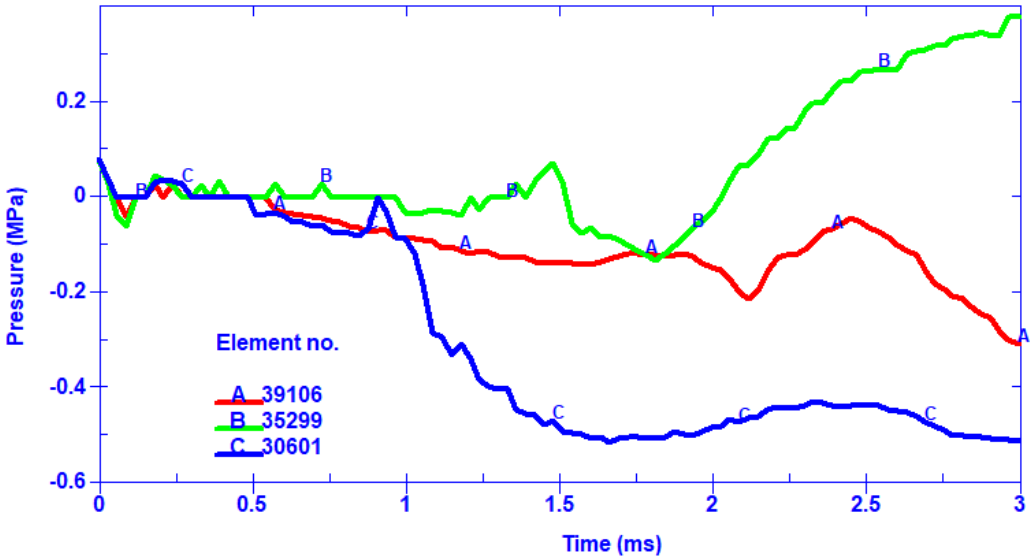

Fig. 3.21. Pressure-time history of elements at different locations (A: Top (just below the beam), B: Middle and C: Bottom) of the targeted column.

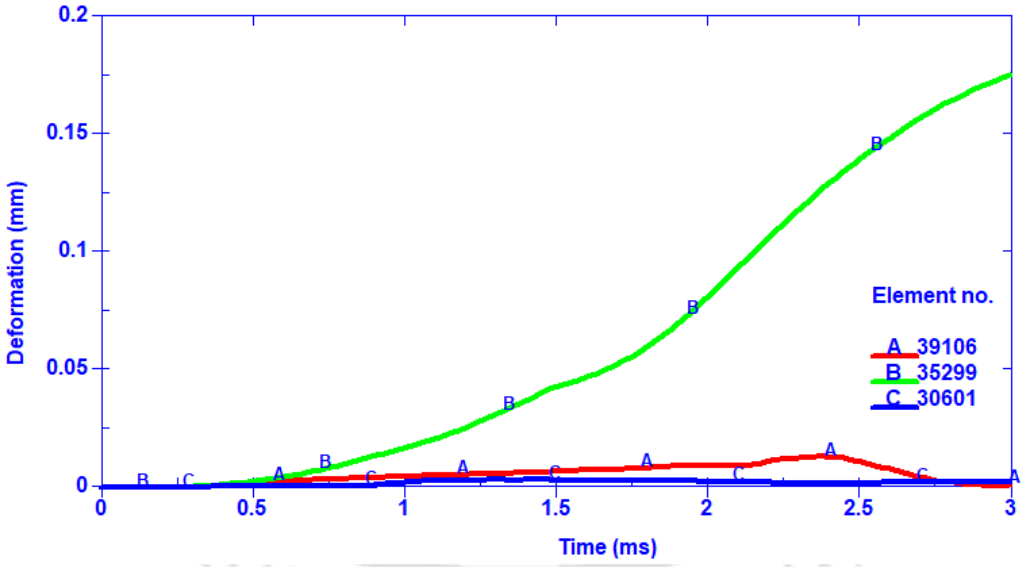

Fig. 3.22. Deformation-time history of elements at different locations (A: Top (just below the beam), B: Middle and C: Bottom) of the targeted column.

Table 3.9. Response of RC frame due to interior blast at one-fourth of the clear span.

Charge Shape	Weight (g)	Density (kg/m^3)	Standoff distance (mm)	Location	Element No.	P_{max} (MPa)	δ_{max} (mm)
Spherical 	1500	1630	1250	Top	39106	0.306	0.013
				Middle	35299	0.379	0.175
				Bottom	30601	0.513	0.003
Conical 				Top	39106	0.311	0.011
				Middle	35299	0.410	0.228
				Bottom	30601	0.485	0.007
Cubical 				Top	39106	0.755	0.027
				Middle	35299	1.638	0.539
				Bottom	30601	0.662	0.015
Cylindrical 				Top	39106	0.311	0.014
				Middle	35299	0.544	0.216
				Bottom	30601	0.507	0.006
Rectangular 				Top	39106	0.941	0.017
				Middle	35299	1.452	0.958
				Bottom	30601	0.728	0.015

3.4.3 Interior Blast at Half of Clear Span

The RC frame is modelled with a spherical charge, and the blast wave propagation due to interior blast at half of the clear span is shown in Fig. 3.23. The response at different locations of the RC frame subjected to internal blast at half of the clear span is calculated numerically using the ALE method. Fig. 3.24 and 3.25 demonstrate the pressure and deformation responses

of the RC frame, respectively. Table 3.10 shows the pressure and deformation responses for additional explosive charge configurations caused by an internal blast at half the clear span of the RC frame. At half of the clear span, the maximum pressure and deformation due to internal blast load in the duration of 3ms are 0.288 MPa and 0.116 mm, respectively.

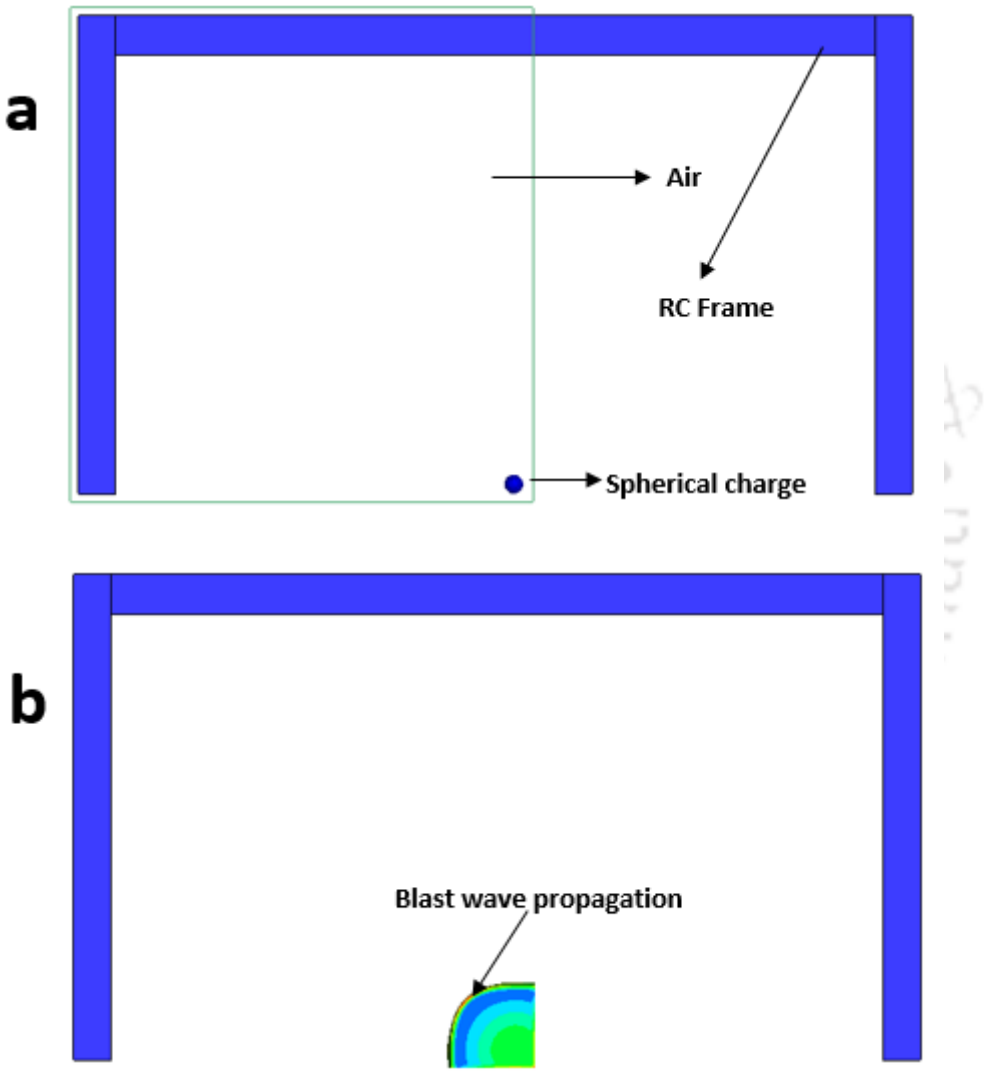

Fig. 3.23. Interior blast: a) Modelling and b) Blast wave propagation.

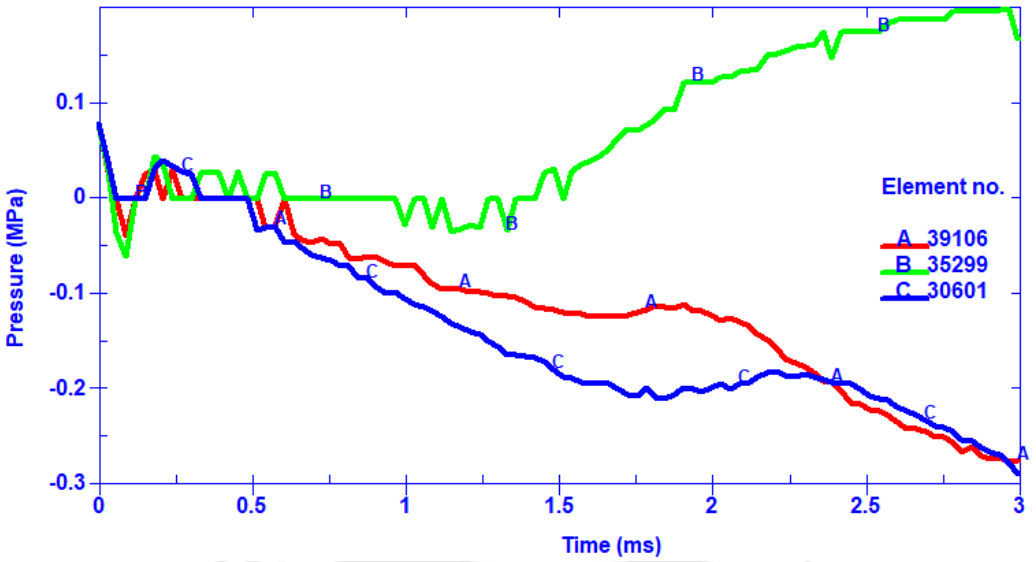

Fig. 3.24. Pressure-time history of elements at different locations (A: Top (just below the beam), B: Middle and C: Bottom, respectively) of the targeted column.

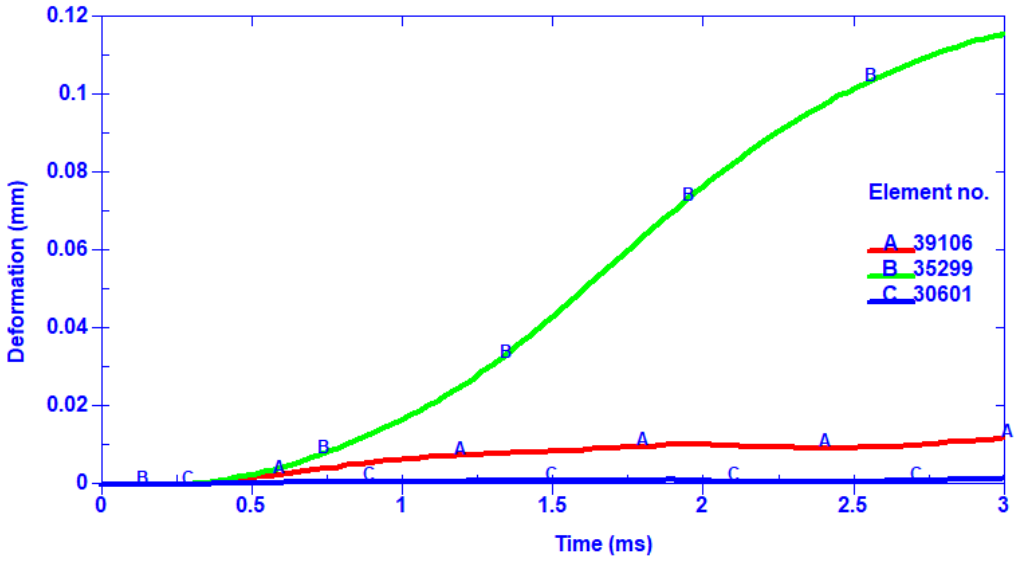

Fig. 3.25. Deformation-time history of elements at different locations (A: Top (just below the beam), B: Middle and C: Bottom, respectively) of the targeted column.

Table 3.10. Response of RC frame due to interior blast at half of the clear span.

Charge Shape	Weight (g)	Density (kg/m^3)	Standoff distance (mm)	Location	Element No.	P_{max} (MPa)	δ_{max} (mm)
Spherical 	1500	1630	2500	Top	39106	0.276	0.012
				Middle	35299	0.199	0.116
				Bottom	30601	0.288	0.002
Conical 				Top	39106	0.280	0.010
				Middle	35299	0.215	0.151
				Bottom	30601	0.272	0.004
Cubical 				Top	39106	0.681	0.025
				Middle	35299	0.860	0.357
				Bottom	30601	0.372	0.010
Cylindrical 				Top	39106	0.280	0.013
				Middle	35299	0.286	0.143
				Bottom	30601	0.285	0.004
Rectangular 				Top	39106	0.848	0.016
				Middle	35299	0.762	0.635
				Bottom	30601	0.409	0.010

3.5 Conclusions

The impact of explosive charge shape on structural response is discovered to be significant. The ALE method of the LS-DYNA hydro-code is used to investigate the responses for five different types of explosive charge shapes, including spherical, cylindrical, rectangular,

cubical, and conical charge shapes, at three different locations of an RC frame structure. Normalization of pressure and deformation parameters with regard to spherical charge shape is performed with respect to the location of element of the column in the RC frame. The corresponding pressure and deformation quantities for the spherical charge shape are determined by the other charge shapes. The spherical equivalent quantities are employed in the RC frame's interior blast analysis. With respect to a spherical charge shape, this study aids in the rapid computation of pressure and deformation of structures subjected to charge shapes such as cubical, conical, rectangular, and cylindrical. The rectangular explosive charge has a more significant structural effect than any other explosive charge. The cubical charge has a lower structural impact than any other explosive charge. The pressure and deformation responses for a given clear span may be interpolated using the interior blast findings for symmetric RC frame constructions.

CHAPTER 4 DEVELOPMENT OF QUADRATIC BLAST PROFILE

4.1 General

Following the positive phase of a blast, the negative phase occurs when the pressure drops below atmospheric pressure. While the positive phase of the explosion has widely been recognised, confirmation of the negative phase is uncommon in the literature. As a result, it has been frequently treated erroneously or ignored entirely. The TM 5-1300/UFC 2005, DoD, GSA, and other blast-resistant design manuals adopted a simplified triangular blast profile and ignored the negative phase effect. The effects of negative phase pressures on the overall motion of an object should also be estimated during the design process. Elastic-plastic response spectra have frequently been used in the design of buildings subject to loads caused by explosions. The triangular shape of blast pressure with respect to time has been used to compute such spectra available in the literature. More blast tests are needed to establish the relationship between positive and negative phase peak overpressures to improve the accuracy of the analytical blast profile. This chapter proposes an alternative simple, reliable, and accurate quadratic blast profile to circumvent the difficulties of Friedlander's profile. This chapter also validates the spectra of an SDOF system subject to exponential and quadratic profiles, and evaluates the analytical solutions of an SDOF system subject to both the profiles.

4.2 Effect of Friedlander's Decay Parameter

4.2.1 Analytical Blast Load Time History Profiles

Friedlander (1940) looked at the findings of various calculations that show how a sound pulse varies when diffracted by an endless screen or a straight-edged wall. The estimates are done for a specific pulse in which the pressure rises instantly and then decays exponentially,

as well as a few other types of incident pulses (Taylor 2006). A pulse's diffraction has been determined by

$$p(z) = (1-z)\,e^{-z} \tag{4.1}$$

where

$$z = \frac{ct}{\lambda} \tag{4.2}$$

λ, is the pulse thickness, c is the velocity of sound, and t is the time, respectively.

As the blast wave passes through the air, the front of the pressure disturbance 'shocks up,' resulting in a near-discontinuous increase in pressure, density, and temperature. Following the shock front, the pressure gradually decreases until it reaches ambient pressure, a period known as the positive phase duration (Fig. 4.1). The semi-empirical 'modified Friedlander equation,' which has been further modified to the linear rise Friedlander equation, can characterise the positive phase of the blast load acting on a structure.

$$p(t) = p_0\left(1-\frac{t}{t_d}\right)e^{-b\frac{t}{t_d}} \tag{4.3}$$

where p_0 is the peak reflected pressure, t_d is the positive phase duration and b is the coefficient that describes the rate of decay of the pressure-time curve, known as the waveform or decay parameter.

$$p(t) = \begin{cases} 0 & 0 \le t \le t_a \\ p_0\left(\dfrac{t-t_a}{t_{rp}-t_a}\right) & t_a < t \le t_{rp} \\ p_0\left(1-\dfrac{(t-t_{rp})}{t_d}\right)e^{-b\frac{(t-t_{rp})}{t_d}} & t_{rp} < t \le t_f \end{cases} \tag{4.4}$$

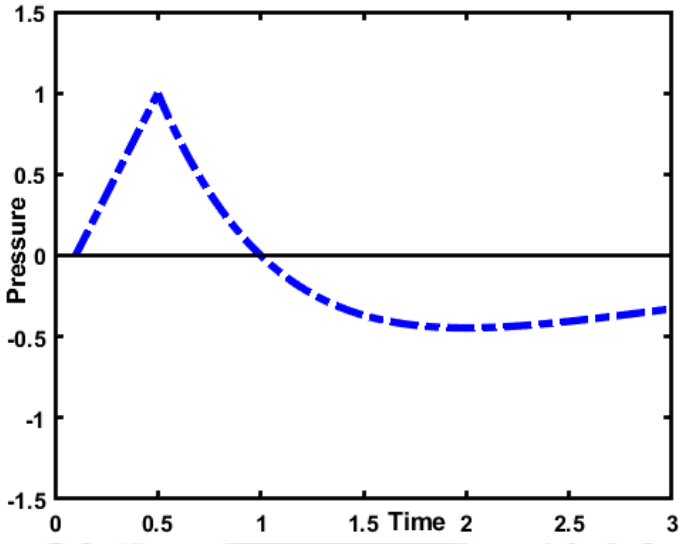

Fig. 4.1. Linear rise – Friedlander blast profile at b=1.

The Friedlander equation's blast pulse profile with a 'b' value of unity has been found to fit several experimental results well. However, the blast pressure can have a negative phase much higher than the phase represented by the 'b' value of one, depending on numerous elements such as changing weight, scaled distance, type of blast, and other considerations. In those cases, 'b' values less than unity are required to idealise the blast pulse profile. Smaller negative pressure corresponds to greater 'b' values, while values above five create essentially no negative phase. The negative phase lasts typically twice as long as the positive phase (Gantes and Pnevmatikos 2004b). In the exponential distribution of Eq. (4.3), the parameter 'b' determines the extent of the negative phase. There is a considerable negative phase when 'b' is less than one, but the negative phase becomes less prominent when 'b' is more than one, as seen in Fig. 4.2. It is demonstrated that 'b' significantly impacts the blast's impulse and negative pressure. According to previous research, the scaled distance, the shape of the blast wave (spherical or hemispherical), and the pressure type (incident or reflected) all influence the decay parameter (Eslami et al., 2020; Syed et al., 2016). The lack of agreement among negative phase expressions emphasises the importance of a well-validated negative phase model.

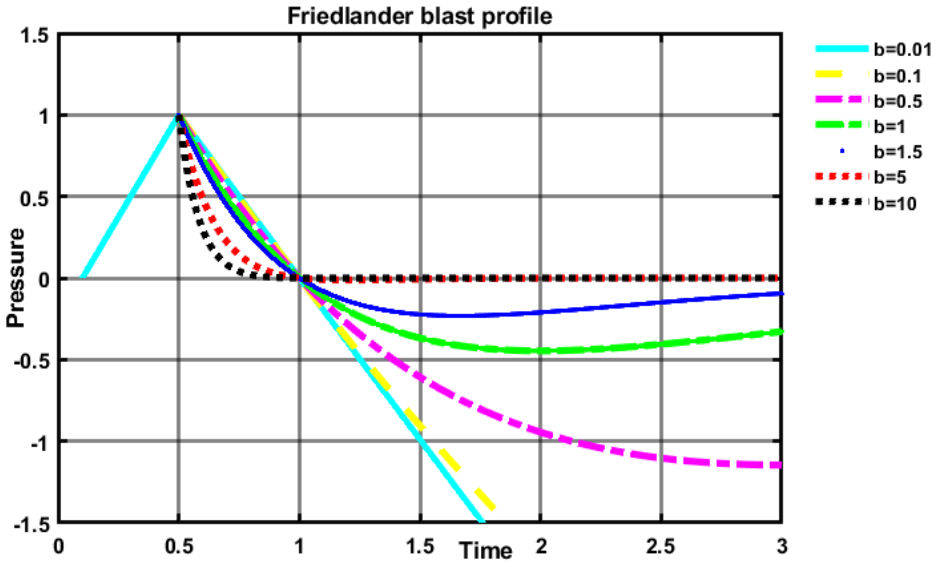

Fig. 4.2. Effect of blast wave decay parameter on Friedlander blast profile.

4.3 Derivation of Quadratic Blast profile

The following assumptions are explored to develop a new simple and accurate blast wave profile:

a) The negative phase rise time (t_{rn}) is 1/4th of the negative phase duration ($t_f - t_d$).

b) The negative phase duration ($t_f - t_d$) doubles the positive phase duration (t_d).

c) The blast duration ratio $n = \frac{t_f}{t_d}$ and peak overpressures ratio $m = \frac{p(t_{rp})}{p(t_{rn})}$ are defined to enhance the accuracy of the blast profile ($p(t_{rp}) = p_0$).

d) At the end of a blast event, the pressure should be zero ($p(t_f) = 0$).

Consider a pressure that varies as a function of time and assume the following basic quadratic form:

$p(t) = At^2 + Bt + C$ ----------(a)

At t = 0, $p(0) = p_0$,

$C = p_0$ ----------(b)

At $t = t_d$, $p(t_d) = 0$

$0 = At_d^2 + Bt_d + p_0$ ----------(c)

At $t = t_f$, $p(t_f) = 0$

$0 = At_f^2 + Bt_f + p_0$ ----------(d)

From assumptions, $nt_d = t_f$ and solve equations (c) & (d)

$$A = \frac{p_0}{nt_d^2}$$

$$B = -\frac{p_0(n+1)}{nt_d}$$

$$p(t) = \begin{cases} p_0\left[\frac{1}{n}\left(\frac{t}{t_d}\right)^2 - \left(\frac{n+1}{n}\right)\left(\frac{t}{t_d}\right) + 1\right] & \text{for } 0 \le t \le t_f \\ 0 & t \ge t_f \end{cases} \quad (4.5)$$

Where t_f = total duration of blast loading, t_d = positive phase duration, and $t_f - t_d$ = negative phase duration, respectively.

From assumption (b), i.e., $2t_d = t_f - t_d \Rightarrow 3t_d = t_f$, n=3.

$$p(t) = \begin{cases} p_0\left[\frac{1}{3}\left(\frac{t}{t_d}\right)^2 - \frac{4}{3}\left(\frac{t}{t_d}\right) + 1\right] & \text{for } 0 \le t \le t_f \\ 0 & t \ge t_f \end{cases} \quad (4.6)$$

The following are the alternative analytical forms of blast profiles with arrival time and positive phase rising time:

Linear rise – Quadratic blast profile

$$p(t)=\begin{cases}0 & 0\le t\le t_a\\ p_0\left(\dfrac{t-t_a}{t_{rp}-t_a}\right) & t_a<t\le t_{rp}\\ B_1\left(t^2-(n+1)t_dt+nt_d^2\right) & t_{rp}<t\le t_f\\ 0 & t>t_f\end{cases} \tag{4.7}$$

Where $B_1=\dfrac{p_0}{nt_d^2-(n+1)t_dt_{rp}+t_{rp}^2}$, t_{rp} = positive phase rise time, t_a = arrival time

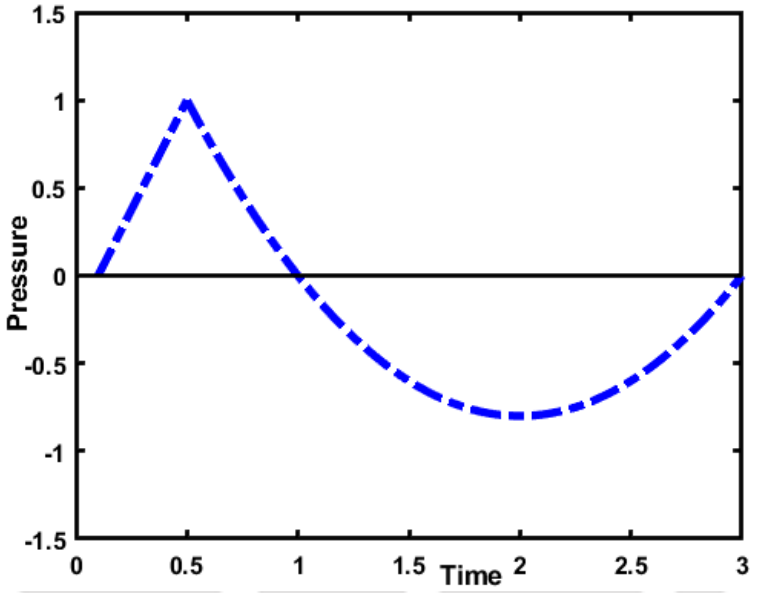

Fig. 4.3. Linear rise – quadratic blast profile

Linear rise – Quadratic – Bilinear blast profile

$$p(t)=\begin{cases}0 & 0\le t\le t_a\\ p_0\left(\dfrac{t-t_a}{t_{rp}-t_a}\right) & t_a<t\le t_{rp}\\ B_1\left(t^2-(n+1)t_dt+nt_d^2\right) & t_{rp}<t\le t_d\\ B_2t+B_3 & t_d<t\le t_{rn}\\ B_4t+B_5 & t_{rn}<t\le t_f\\ 0 & t>t_f\end{cases} \tag{4.8}$$

where

$$B_2 = B_1 \frac{\left(\frac{n+3}{4}\right)^2 - (1+n)\left(\frac{n+3}{4}\right) + n}{\left(\frac{n+3}{4} - 1\right)} t_d$$

$$B_3 = -B_2 t_d$$

$$B_4 = B_1 \frac{\left(\frac{n+3}{4}\right)^2 - (1+n)\left(\frac{n+3}{4}\right) + n}{\left(\frac{n+3}{4} - n\right)} t_d$$

$$B_5 = -B_4 n t_d$$

, $\quad m = \frac{p(t_{rp})}{p(t_{rn})} = \frac{p_0}{p(t_{rn})} \rightarrow p(t_{rn}) = \frac{p_0}{m}$;

t_{rn} = negative phase rise time

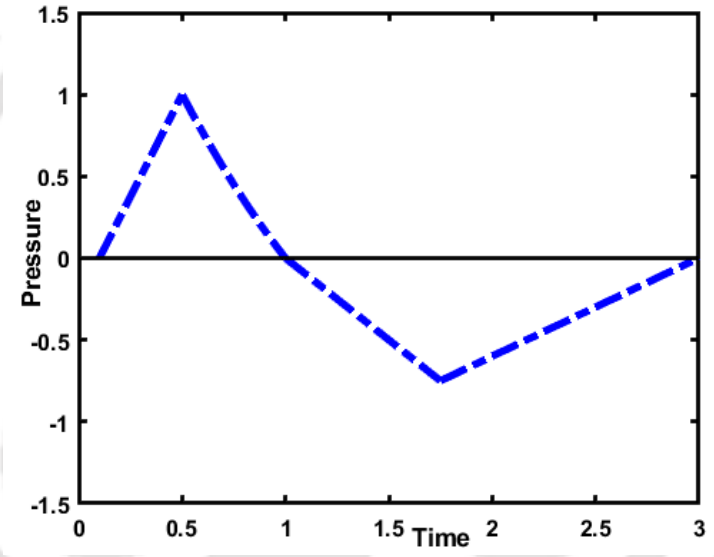

Fig. 4.4. Linear rise – quadratic bilinear blast profile.

Linear rise – Cubic-Bilinear blast profile

$$p(t) = \begin{cases} 0 & 0 \le t \le t_a \\ p_0\left(\frac{t - t_a}{t_{rp} - t_a}\right) & t_a < t \le t_{rp} \\ B_6\left(t^3 - (1+n+n^2)t_d^2 t + (n+n^2)t_d^3\right) & t_{rp} < t \le t_d \\ B_7 t + B_8 & t_d < t \le t_{rn} \\ B_9 t + B_{10} & t_{rn} < t \le t_f \\ 0 & t > t_f \end{cases} \quad (4.9)$$

Where,

$$B_6 = \frac{p_0}{(n+n^2)t_d^3 - (1+n+n^2)t_d^2 t_{rp} + t_{rp}^3}$$

$$B_7 = B_6 \frac{\left(\frac{n+3}{4}\right)^3 - (1+n+n^2)\left(\frac{n+3}{4}\right) + (n+n^2)}{\left(\frac{n+3}{4} - 1\right)} t_d^2$$

$$B_8 = -B_7 t_d$$

$$B_9 = B_6 \frac{\left(\frac{n+3}{4}\right)^3 - (1+n+n^2)\left(\frac{n+3}{4}\right) + (n+n^2)}{\left(\frac{n+3}{4} - n\right)} t_d^2$$

$$B_{10} = -B_9 n t_d$$

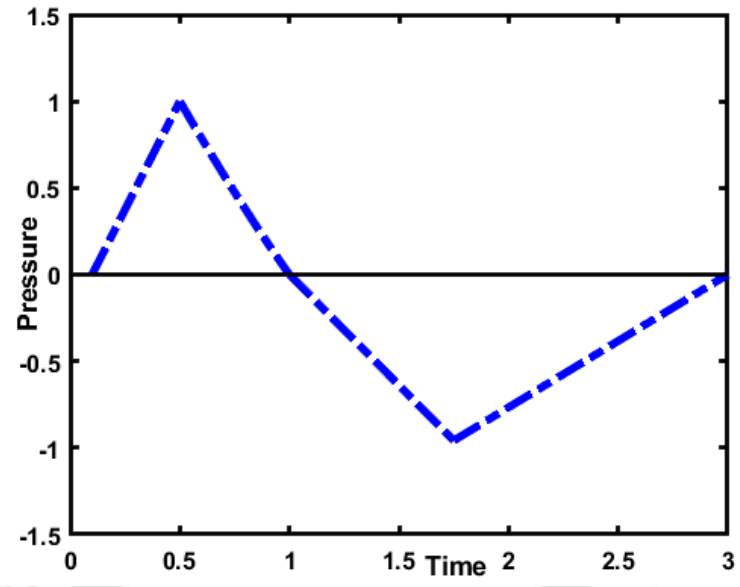

Fig. 4.5. Linear rise – cubic bilinear blast profile.

Linear rise – Quartic – Bilinear blast profile

$$p(t)=\begin{cases}0 & 0\le t\le t_a\\ p_0\left(\dfrac{t-t_a}{t_{rp}-t_a}\right) & t_a<t\le t_{rp}\\ B_{11}\left(t^4-(1+n+n^2+n^3)t_d^3t+(n+n^2+n^3)t_d^4\right) & t_{rp}<t\le t_d\\ B_{12}t+B_{13} & t_d<t\le t_{rn}\\ B_{14}t+B_{15} & t_{rn}<t\le t_f\\ 0 & t>t_f\end{cases} \quad (4.10)$$

Where,

$$B_{11}=\frac{p_0}{(n+n^2+n^3)t_d^4-(1+n+n^2+n^3)t_d^3t_{rp}+t_{rp}^4}$$

$$B_{12}=B_{11}\frac{\left(\frac{n+3}{4}\right)^4-(1+n+n^2+n^3)\left(\frac{n+3}{4}\right)+(n+n^2+n^3)}{\left(\frac{n+3}{4}-1\right)}t_d^3$$

$$B_{13}=-B_{12}t_d$$

$$B_{14}=B_{11}\frac{\left(\frac{n+3}{4}\right)^4-(1+n+n^2+n^3)\left(\frac{n+3}{4}\right)+(n+n^2+n^3)}{\left(\frac{n+3}{4}-n\right)}t_d^3$$

$$B_{15}=-B_{14}nt_d$$

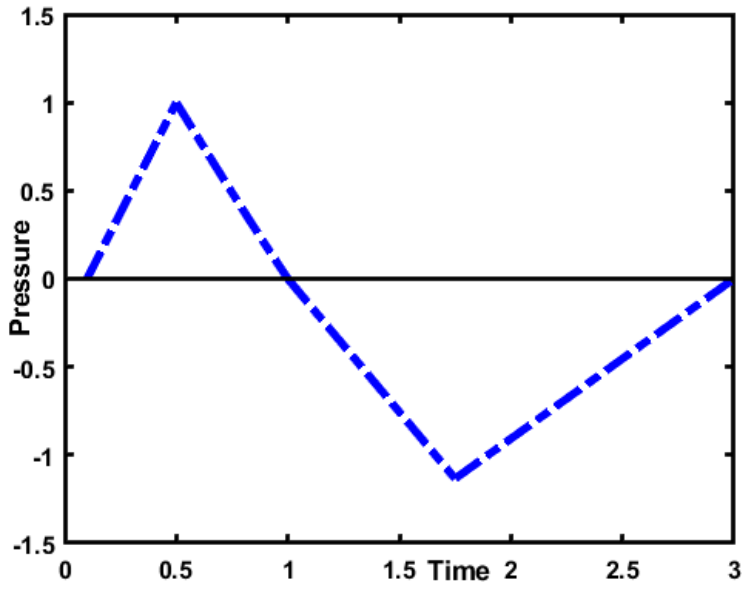

Fig. 4.6. Linear rise – quartic bilinear blast profile.

Linear rise – Biquadratic blast profile

$$p(t)=\begin{cases}0 & 0\le t\le t_a\\ p_0\left(\dfrac{t-t_a}{t_{rp}-t_a}\right) & t_a<t\le t_{rp}\\ B_{17}\left(t^2-(1+n)t_dt+nt_d^2\right) & t_{rp}<t\le t_{rn}\\ B_{18}t+B_{19} & t_{rn}<t\le t_f\\ 0 & t>t_f\end{cases} \tag{4.11}$$

where,

$$B_{17}=\frac{p_0}{nt_d^2-(1+n)t_dt_{rp}+t_{rp}^2}$$

$$B_{18}=B_{17}\frac{\left(\dfrac{n+3}{4}\right)^2-(1+n)\left(\dfrac{n+3}{4}\right)+n}{\left(\dfrac{n+3}{4}-1\right)}$$

$$B_{19}=-B_{18}n^2t_d^2$$

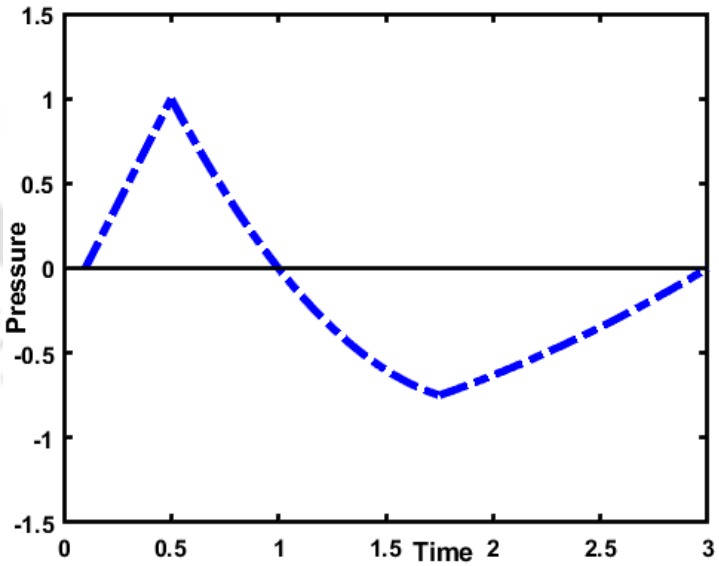

Fig. 4.7. Linear rise – biquadratic blast profile.

Linear rise - Bilinear blast profile

$$p(t)=\begin{cases}0 & 0\le t\le t_a\\ p_0\left(\dfrac{t-t_a}{t_{rp}-t_a}\right) & t_a<t\le t_{rp}\\ p_0\left(\dfrac{t-t_d}{t_{rp}-t_d}\right) & t_{rp}<t\le t_{rn}\\ p_0\left(\dfrac{\frac{n+3}{4}-1}{\frac{n+3}{4}-n}\right)\left(\dfrac{t-nt_d}{t_{rp}-t_d}\right) & t_{rn}<t\le t_f\\ 0 & t>t_f\end{cases} \tag{4.12}$$

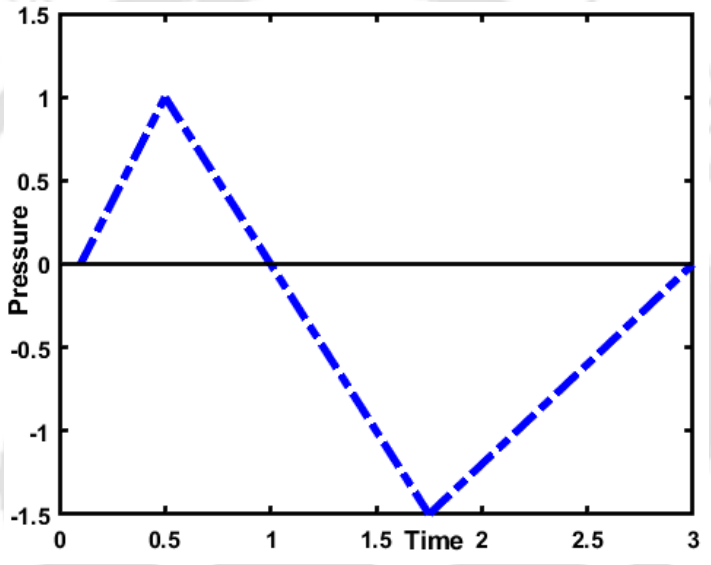

Fig. 4.8. Linear rise - bilinear blast profile.

Linear rise - Trilinear blast profile

$$p(t)=\begin{cases}0 & \\ p_0\left(\dfrac{t-t_a}{t_{rp}-t_a}\right) & 0\le t\le t_a \\ p_0\left(\dfrac{t-t_d}{t_{rp}-t_d}\right) & t_a<t\le t_{rp} \\ p_0\left(\dfrac{t-t_d}{\left(1-\dfrac{n+3}{4}\right)t_d}\right) & t_{rp}<t\le t_d \\ p_0\left(\dfrac{\left(\dfrac{n+3}{4}-1\right)(t-nt_d)}{\left(1-\dfrac{n+3}{4}\right)\left(\dfrac{n+3}{4}-n\right)t_d}\right) & t_d<t\le t_{rn} \\ 0 & t_{rn}<t\le t_f \\ & t>t_f \end{cases} \tag{4.13}$$

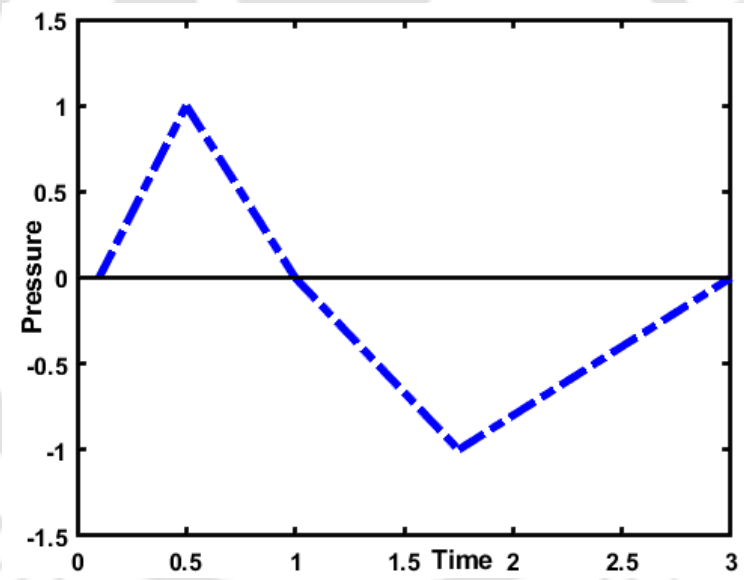

Fig. 4.9. Linear rise – trilinear blast profile.

Linear rise - Cubic blast profile

$$p(t)=\begin{cases}0 & 0\le t\le t_a\\ p_0\left(\dfrac{t-t_a}{t_{rp}-t_a}\right) & t_a<t\le t_{rp}\\ B_{20}\left(t^3-(1+n+n^2)t_d^2t+(n+n^2)t_d^3\right) & t_{rn}<t\le t_f\\ 0 & t>t_f\end{cases} \tag{4.14}$$

Where

$$B_{20}=\frac{P_0}{(n+n^2)t_d^3-(1+n+n^2)t_d^2t_{rp}+t_{rp}^3}$$

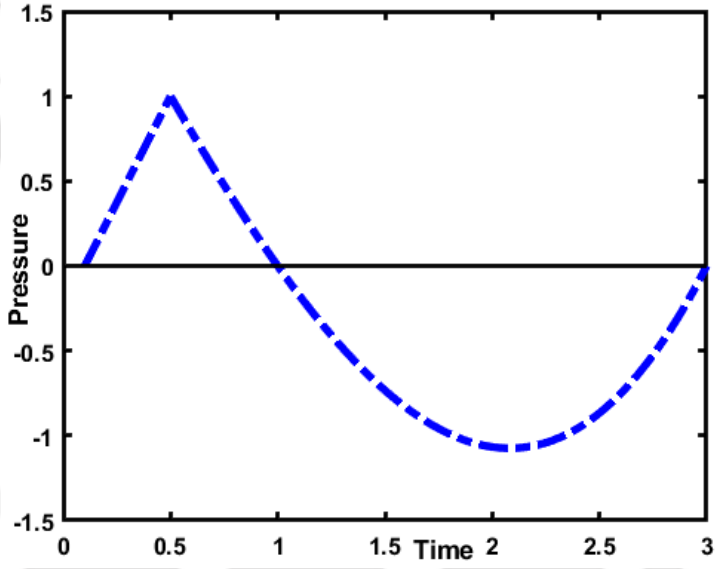

Fig. 4.10. Linear rise – cubic blast profile.

Linear rise – Quartic blast profile

$$p(t)=\begin{cases}0 & 0\le t\le t_a\\ p_0\left(\dfrac{t-t_a}{t_{rp}-t_a}\right) & t_a<t\le t_{rp}\\ B_{21}\left(t^4-(1+n+n^2+n^3)t_d^3t+(n+n^2+n^3)t_d^4\right) & t_{rp}<t\le t_f\\ 0 & t>t_f\end{cases} \tag{4.15}$$

Where,

$$B_{21} = \frac{p_0}{(n+n^2+n^3)t_d^4 - (1+n+n^2+n^3)t_d^3 t_{rp} + t_{rp}^4}$$

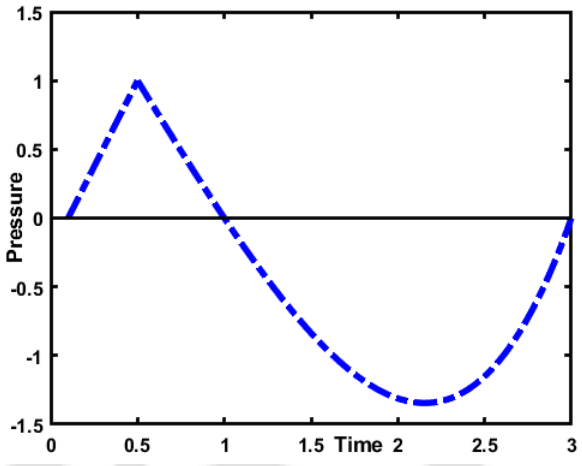

Fig. 4.11. Linear rise – quartic blast profile.

Linear rise – Bicubic blast profile

$$p(t) = \begin{cases} 0 & 0 \le t \le t_a \\ p_0\left(\dfrac{t-t_a}{t_{rp}-t_a}\right) & t_a < t \le t_{rp} \\ B_{22}\left(t^3 - (1+n+n^2)t_d^2 t + (n+n^2)t_d^3\right) & t_{rp} < t \le t_{rn} \\ B_{23}t^3 + B_{24} & t_{rn} < t \le t_f \\ 0 & t > t_f \end{cases} \quad (4.16)$$

Where,

$$B_{22} = \frac{p_0}{(n+n^2)t_d^3 - (1+n+n^2)t_d^2 t_{rp} + t_{rp}^3}$$

$$B_{23} = B_{22}\frac{\left(\dfrac{n+3}{4}\right)^3 - (1+n+n^2)\left(\dfrac{n+3}{4}\right) + (n+n^2)}{\left(\dfrac{n+3}{4}\right)^3 - n^3}$$

$$B_{24} = -B_{23}n^3 t_d^3$$

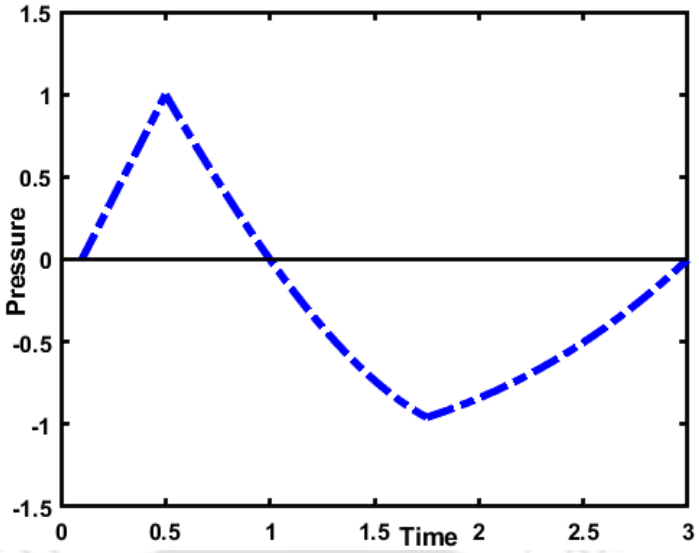

Fig. 4.12. Linear rise – bicubic blast profile.

Linear rise – Bi-quartic blast profile

$$p(t)=\begin{cases}0 & 0\le t\le t_a\\ p_0\left(\dfrac{t-t_a}{t_{rp}-t_a}\right) & t_a<t\le t_{rp}\\ B_{25}\left(t^4-(1+n+n^2+n^3)t_d^3t+(n+n^2+n^3)t_d^4\right) & t_{rp}<t\le t_{rn}\\ B_{26}t^4+B_{27} & t_{rn}<t\le t_f\\ 0 & t>t_f\end{cases} \tag{4.17}$$

Where,

$$B_{25}=\frac{p_0}{(n+n^2+n^3)t_d^4-(1+n+n^2+n^3)t_d^3t_{rp}+t_{rp}^4}$$

$$B_{26}=B_{25}\frac{\left(\dfrac{n+3}{4}\right)^4-(1+n+n^2+n^3)\left(\dfrac{n+3}{4}\right)+(n+n^2+n^3)}{\left(\dfrac{n+3}{4}\right)^4-n^4}$$

$$B_{27}=-B_{26}n^4t_d^4$$

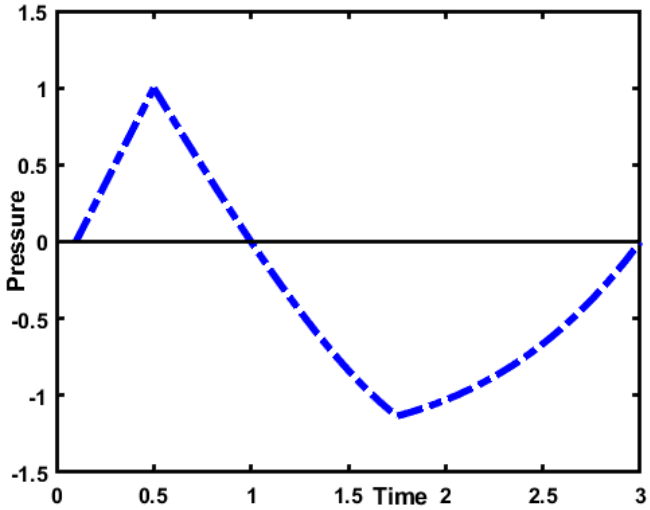

Fig. 4.13. Linear rise – bi-quartic blast profile.

Linear rise – Quadratic linear blast profile

$$p(t)=\begin{cases}0 & 0\le t\le t_a\\ p_0\left(\dfrac{t-t_a}{t_{rp}-t_a}\right) & t_a<t\le t_{rp}\\ B_{28}\left(t^2-(n+1)t_d t+nt_d^2\right) & t_{rp}<t\le t_{rn}\\ B_{29}t+B_{30} & t_{rn}<t\le t_f\\ 0 & t>t_f\end{cases} \tag{4.18}$$

Where,

$$B_{28}=\frac{p_0}{nt_d^2-(n+1)t_d t_{rp}+t_{rp}^2}$$

$$B_{29}=B_{28}\frac{\left(\dfrac{n+3}{4}\right)^2-(1+n)\left(\dfrac{n+3}{4}\right)+n}{\left(\dfrac{n+3}{4}-n\right)}t_d$$

$$B_{30}=-B_{29}nt_d$$

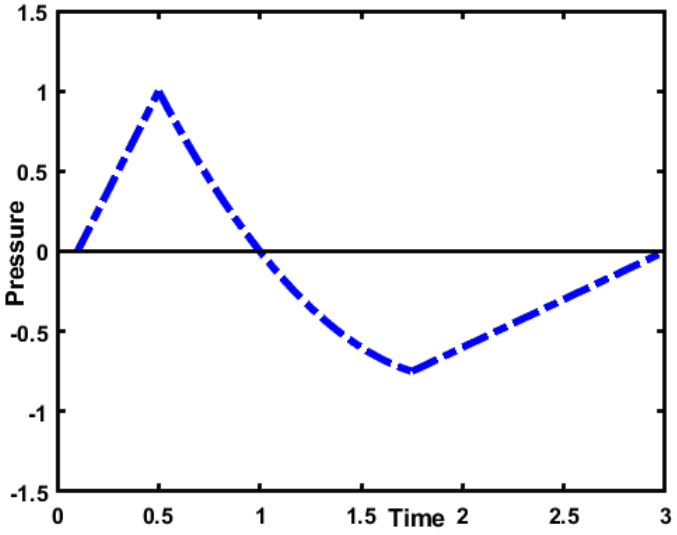

Fig. 4.14. Linear rise – quadratic linear profile.

Linear rise – Cubic linear blast profile

$$p(t)=\begin{cases}0 & 0\le t\le t_a\\ p_0\left(\dfrac{t-t_a}{t_{rp}-t_a}\right) & t_a<t\le t_{rp}\\ B_{31}\left(t^3-(1+n+n^2)t_d^2t+(n+n^2)t_d^3\right) & t_{rp}<t\le t_{rn}\\ B_{32}t+B_{33} & t_{rn}<t\le t_f\\ 0 & t>t_f\end{cases} \tag{4.19}$$

Where,

$$B_{31}=\frac{p_0}{(n+n^2)t_d^3-(1+n+n^2)t_d^2t_{rp}+t_{rp}^3}$$

$$B_{32}=B_{31}\frac{\left(\dfrac{n+3}{4}\right)^3-(1+n+n^2)\left(\dfrac{n+3}{4}\right)+(n+n^2)}{\left(\dfrac{n+3}{4}-n\right)}t_d^2$$

$$B_{33}=-B_{32}nt_d$$

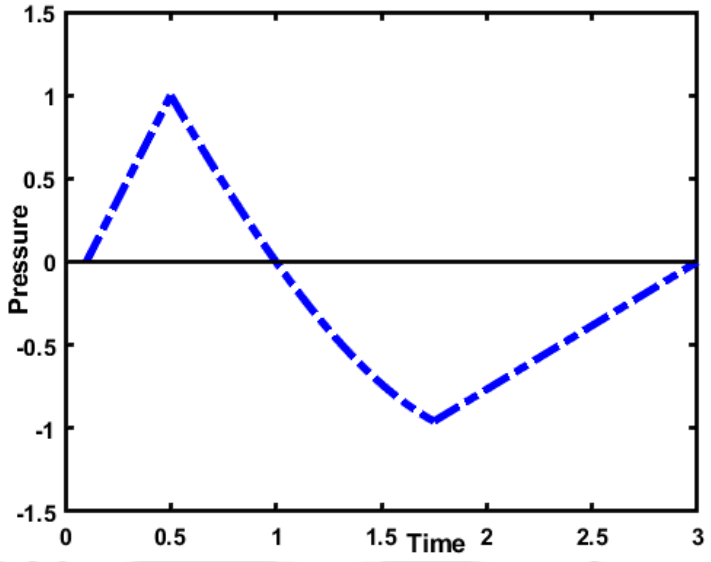

Fig. 4.15. Linear rise – cubic linear blast profile.

Linear rise – Quartic linear blast profile

$$p(t)=\begin{cases}0 & 0\le t\le t_a\\ p_0\left(\dfrac{t-t_a}{t_{rp}-t_a}\right) & t_a<t\le t_{rp}\\ B_{34}\left(t^4-(1+n+n^2+n^3)t_d^3t+(n+n^2+n^3)t_d^4\right) & t_{rp}<t\le t_{rn}\\ B_{35}t+B_{36} & t_{rn}<t\le t_f\\ 0 & t>t_f\end{cases} \tag{4.20}$$

Where,

$$B_{34}=\frac{p_0}{(n+n^2+n^3)t_d^4-(1+n+n^2+n^3)t_d^3t_{rp}+t_{rp}^4}$$

$$B_{35}=B_{34}\frac{\left(\dfrac{n+3}{4}\right)^4-(1+n+n^2+n^3)\left(\dfrac{n+3}{4}\right)+(n+n^2+n^3)}{\left(\dfrac{n+3}{4}-n\right)}t_d^3$$

$$B_{36}=-B_{35}nt_d$$

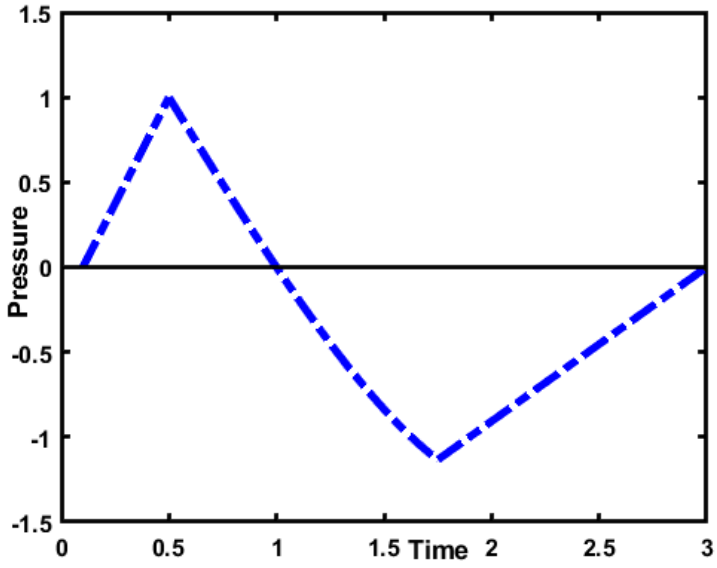

Fig. 4.16. Linear rise – quartic linear blast profile.

4.3.1 Validation of Blast Profiles

The literature's six experimental blast pressure time history profiles are used to validate the calculated linear, quadratic, cubic, and quartic family blast profiles (Fig. 4.17a to 4.17f).

The full-scale field explosion tests on shielded and unprotected concrete slabs are described in Case 1 (Fig. 4.17a). The studies have been carried out by the Ben-Gurion University of the Negev's Protective Technologies Research & Development Centre (BGU-PTR&DC) under contract with the Israeli Ministry of Defence (MoD) and the supervision of the IDF Steering Committee for Protective Structures R&D (Schenker et al., 2008). The tests have been designed to (1) obtain data on the dynamic response of a basic concrete structure to blast loads to verify and validate (V&V) associated computer codes and (2) evaluate the effectiveness of aluminium foams to attenuate blast wave loads. Time-dependent measurements of the concrete slabs' response to blast wave loads have effectively been acquired using a variety of measurement instruments.

The experimental trace from the 6m shot in Case 2 (Fig. 4.17b) confirms the presence of the well-known 'second shock' (Rigby et al., 2014). This phenomenon has not been

accounted for in any empirical forecasts, and its impact has been minimised — it will have a second-order impact compared to the negative phase. The minimum distance between the pressure gauge and the top edge of the bunker wall in the test design was 4m; a clearing wave travelling at 340 m/s from the nearest free edge would take 11.55 ms to reach the gauge site before it could start to alter the pressure measurements.

Overpressure histories at the target point (92-m standoff distance; 5.4-m/kg1/3 scaled distance) are shown in Case 3 (Fig. 4.17c). In Woomera, South Australia, field testing involving the surface detonation of 5,000 kg of trinitrotoluene (TNT) has been conducted (Ngo et al., 2015). The overpressures, impulses, and other data collected in this study have been analysed and compared to existing predictive algorithms and previously published data sets.

Case 4 (Fig. 4.17d), in which three superimposed pressure/time records has been adapted from "identical" experiments in complex urban geometry for statistical analysis, revealing a high level of variability in peak reflected pressure, impulse, and positive phase duration for repeatable tests where variability would be expected to be minimal (Netherton and Stewart 2010). A commonly used predictive blast load model's error (accuracy) has also been evaluated. The variability and/or uncertainty of explosive mass, a net equivalent quantity of an explosive in terms of TNT mass, stand-off distance, air temperature, air pressure, inherent variability, and model error have all been considered in the development of a probabilistic model of blast loading.

Case 5 (Fig. 4.17e) depicts a typically reflected pressure-time history recorded in shot 1 with a 50 kg charge at a stand-off distance of 10.3m (Nassr et al., 2012). The blast wave may be seen to have the normal fast-rising peak pressure, followed by a decline in ambient pressure, all within the positive phase duration and then a negative pressure phase. An equivalent Single-

Degree-of-Freedom (SDOF) model of a beam has been used to assess the experimental results, including material nonlinearity and strain rate effects.

Case 6 (Fig. 4.17f): In the computer study of the plates, the experimental time-history of pressure has been used as an external load. For Test 2, a typical pressure-time history has been provided. In order to generate numerical modelling guides, a comparison of testing and numerical reactions of metallic plates subject to explosive loads has been investigated. Furthermore, a secondary goal was to offer data that could be used to test the accuracy of various computation methods (Jacinto et al., 2001). Two non-stiffened metallic steel plates with different boundary conditions (one clamped in the earth and the other clamped in the four edges) have been subjected to the action of pressure waves generated by the detonation of explosive loads in a series of four natural scale experiments.

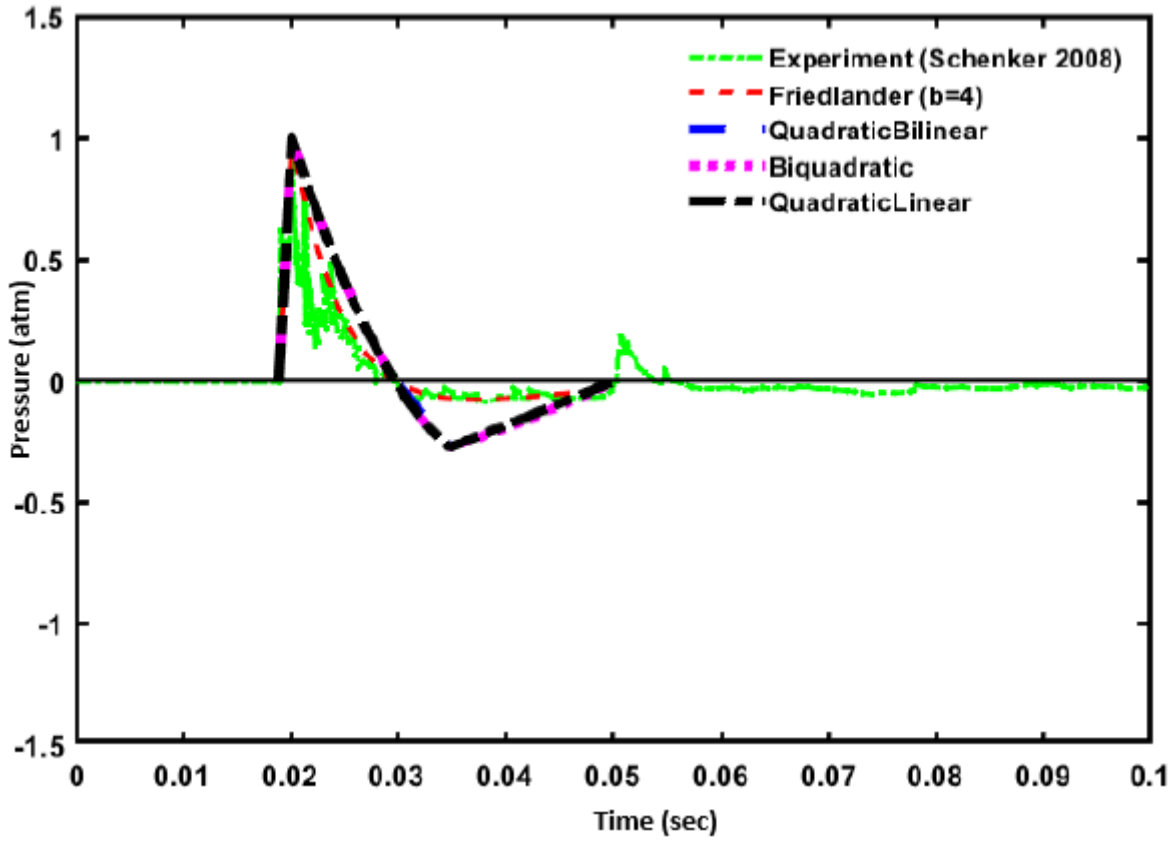

(a) Case 1

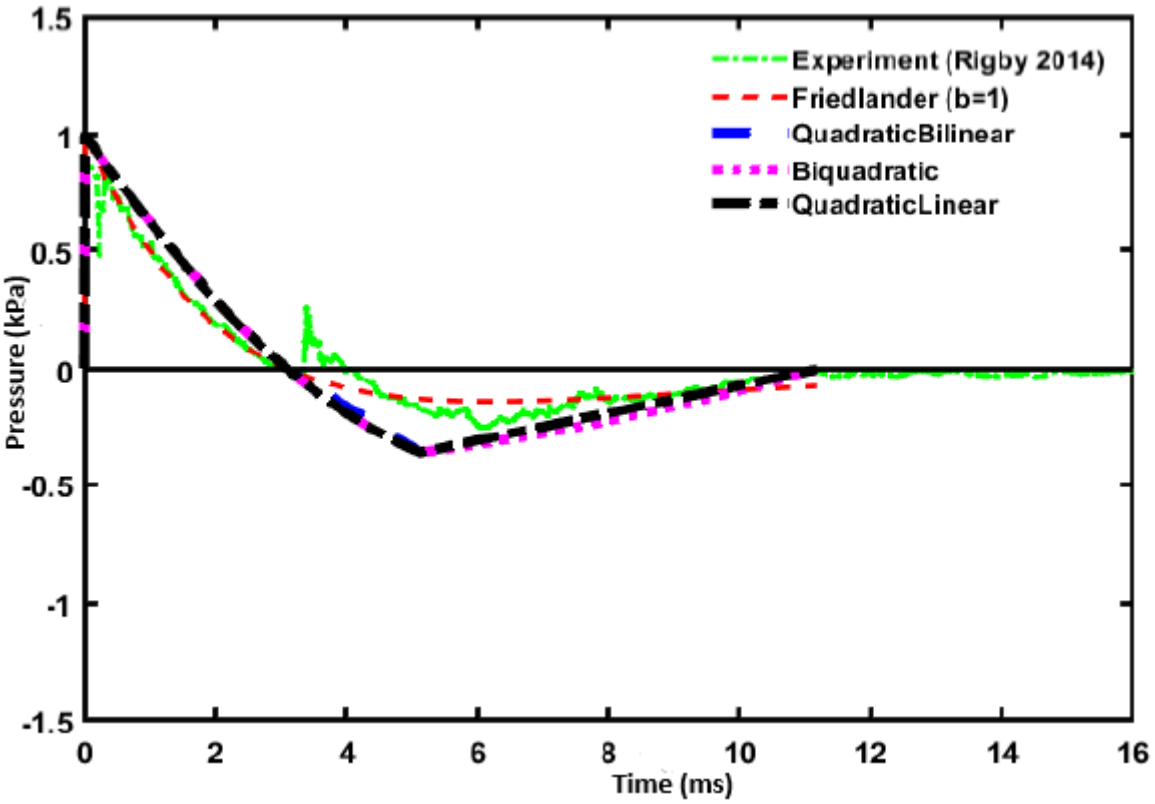
Experiment (Rigby 2014)
Friedlander (b=1)
QuadraticBilinear
Biquadratic
QuadraticLinear
Pressure (kPa)
Time (ms)
1.5
1
0.5
0
-0.5
-1
-1.5
0
2
4
6
8
10
12
14
16

(b) Case 2

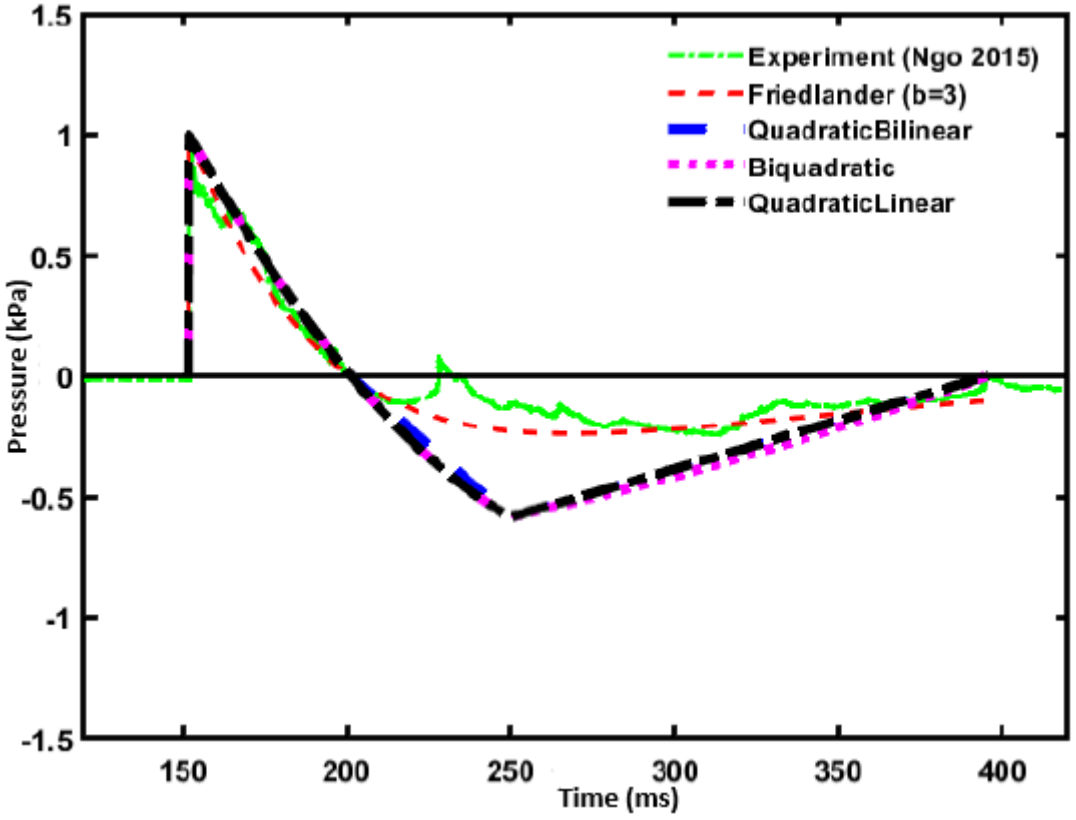
Experiment (Ngo 2015)
Friedlander (b=3)
QuadraticBilinear
Biquadratic
QuadraticLinear
Pressure (kPa)
Time (ms)
1.5
1
0.5
0
-0.5
-1
-1.5
150
200
250
300
350
400

(c) Case 3

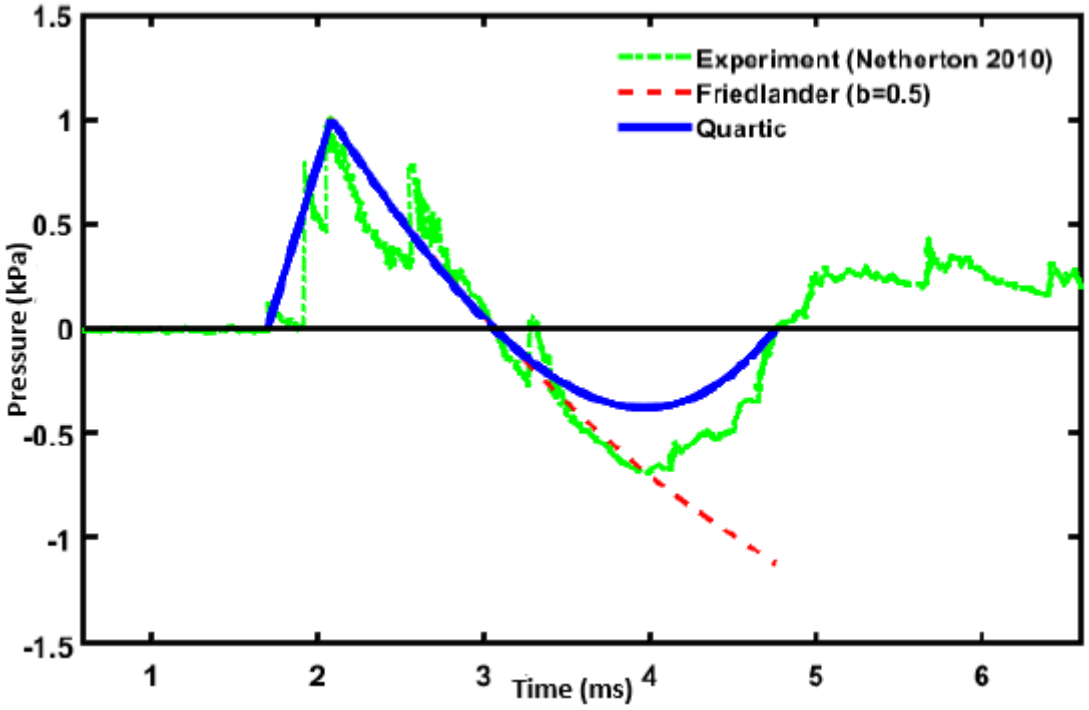

(d) Case 4

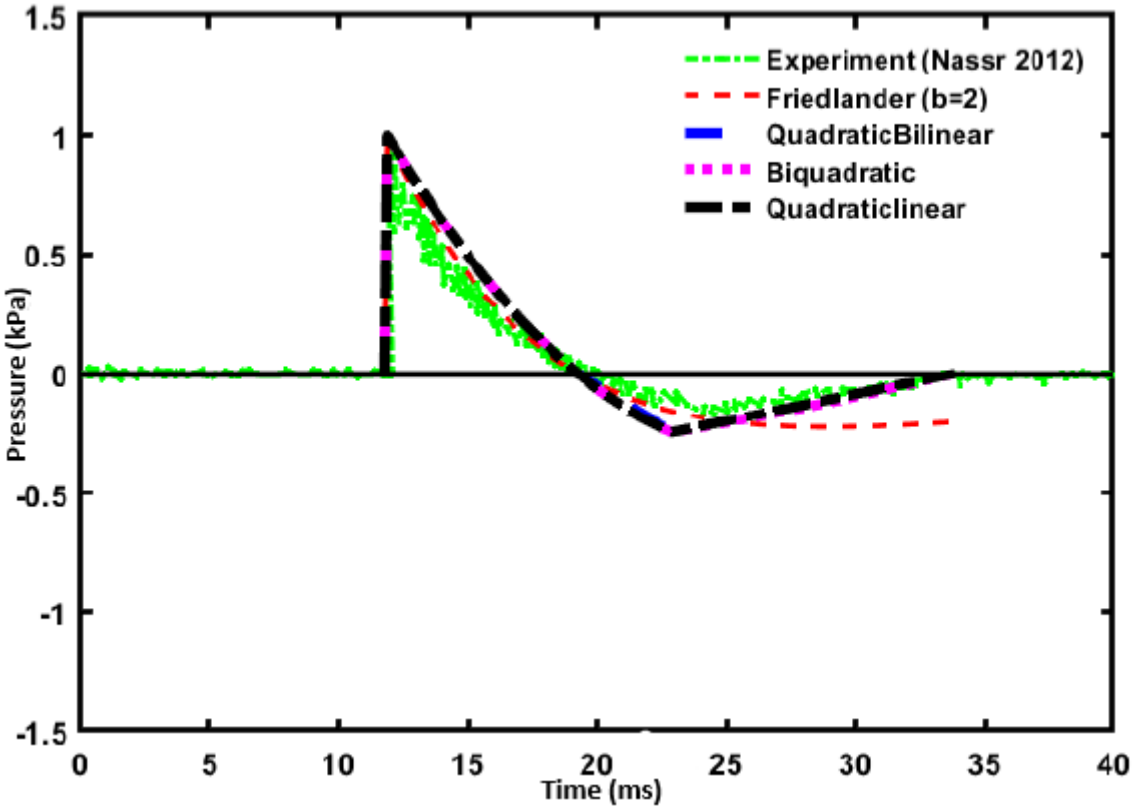

(e) Case 5

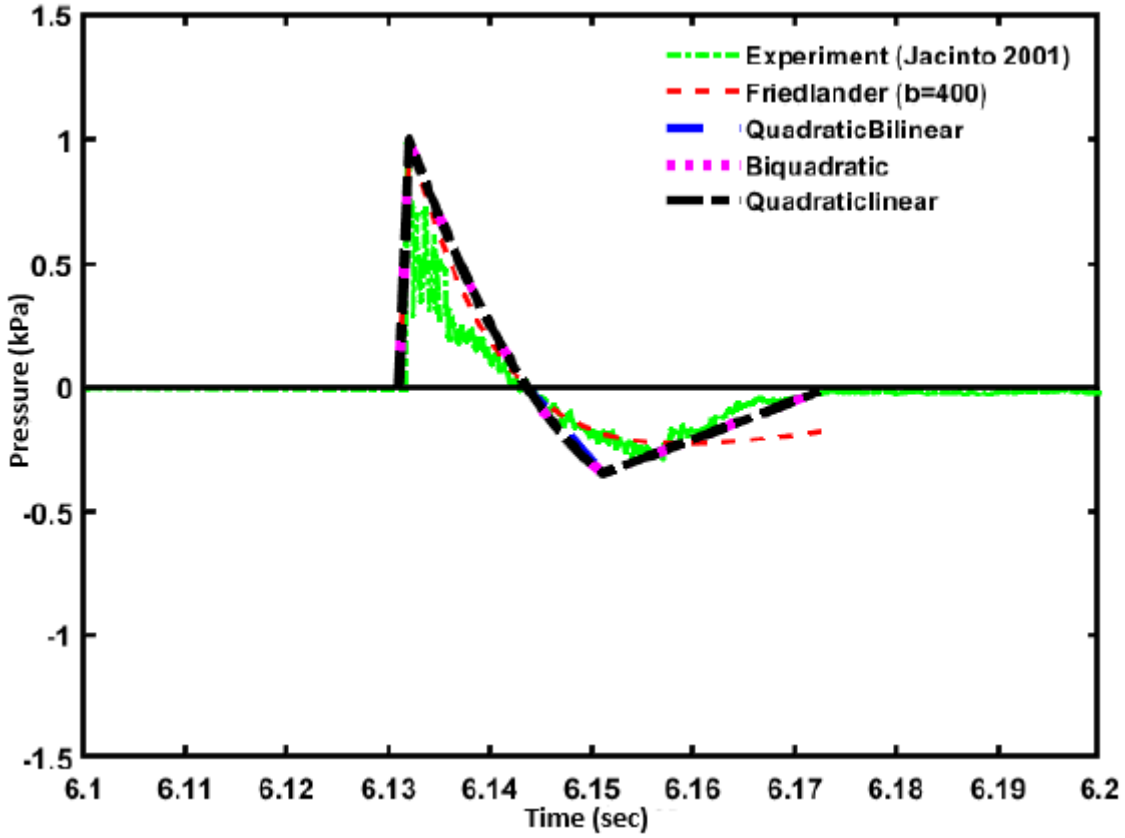

(f) Case 6

Fig. 4.17. Validation of derived blast load profiles with experimental time history.

The developed quadratic family of analytical formulations for blast profile agrees well with the experimental blast time history validations. The blast wave decay parameter is finalised using the trial approach to fit the experimental data. The blast wave decay parameter gives inaccurate and abnormal results in cases 4 (b=0.5) and 6 (b=400). The two scenarios are when the negative peak pressure dominates and the time step is too small. In certain circumstances, analytical formulas from the quartic and quadratic families are best for obtaining the structure's accurate response. By including a relationship between peak positive and negative pressures, the accuracy of these analytical formulations can be improved.

4.3.2 Numerical Validation

Numerical analysis, usually using the finite element method, provides a more accurate way of describing the dynamic response of structures under explosive loads. Several investigators have used such analyses to capture the geometry of the structure, the geographical and temporal distribution of the applied blast pressure, and the impacts of material and geometric nonlinearity, in a suitable manner (Jayasooriya et al., 2011; Domenico et al., 2021). Although some insight into the negative phase of blast pressure has previously been presented based on elastic single-degree-of-freedom (SDOF) analysis, the impact of the negative phase on different types of resistance functions of SDOF models and realistic finite element analysis has not been investigated.

Case 1's time history profiles are validated using a single storey RC frame (Fig. 4.17a). For global analysis, the whole two-dimensional (2D) lateral load resisting structure is created in FEM code SAP2000 (Fig. 4.18) with modelling information given in Table 4.1. Beams and columns are frame elements, and the base of the columns is believed to be fixed. A first-order linear elastic uncoupled time history analysis of the entire building frame with gravity and blast loads is performed to determine the response of the frame structure. The blast loads are applied to the structure as a uniform single load case ($P_0 = \frac{p_0}{A}$ where A= projected area) to evaluate global response. The Hilber–Hughes–Taylor Alpha numerical integration method is used in SAP2000 to analyse the structural response to the blast load time history application. For various reasons, linear elastic analysis is the most suited technique for global analysis (Jayasooriya et al., 2011). The generated blast profiles' deformation, velocity, acceleration, axial force, shear force, and bending moment time history responses are explored and compared to Friedlander's responses for the same parameters (Fig. 4.19 to Fig. 4.24). The results are drawn in MATLAB for a better look.

Table 4.1. The details for numerical modelling of RC frame.

Structural member	Length (mm)	f_{ck} (MPa)	f_y (MPa)	Width, b (mm)	Depth, D (mm)	A_{st} (mm^2)	P_0 (kN/m)
Column	5500	40	415	670	700	3927	100
Beam	11000	40	415	410	710	2945.2	

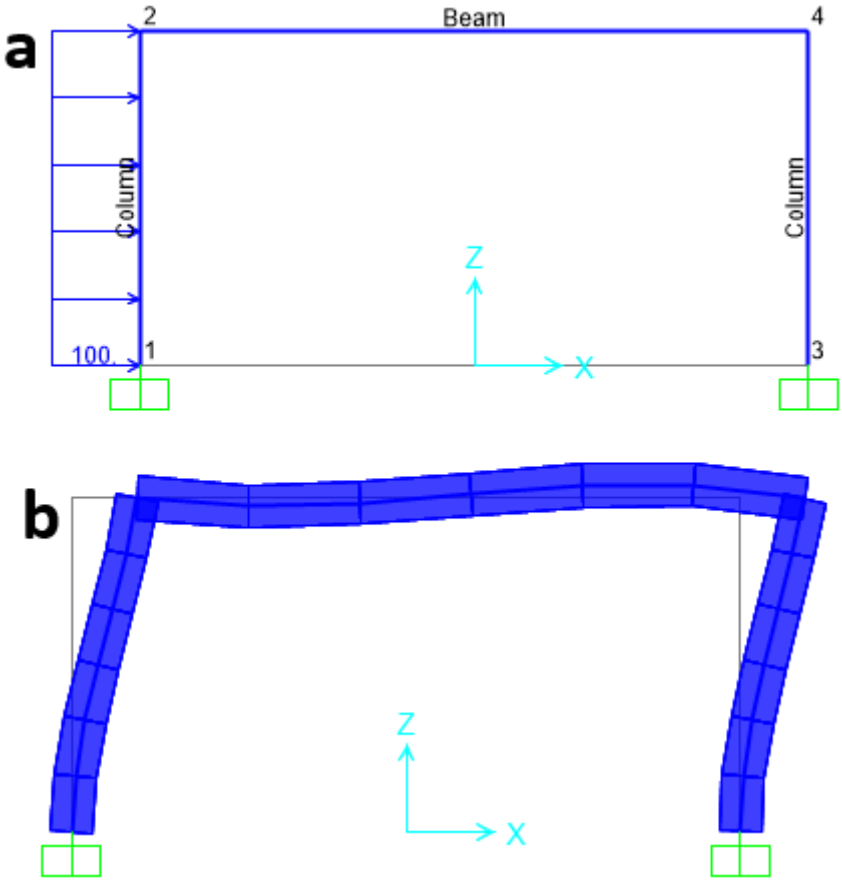

Fig. 4.18. Numerical modelling a) before and b) after the time history blast loading.

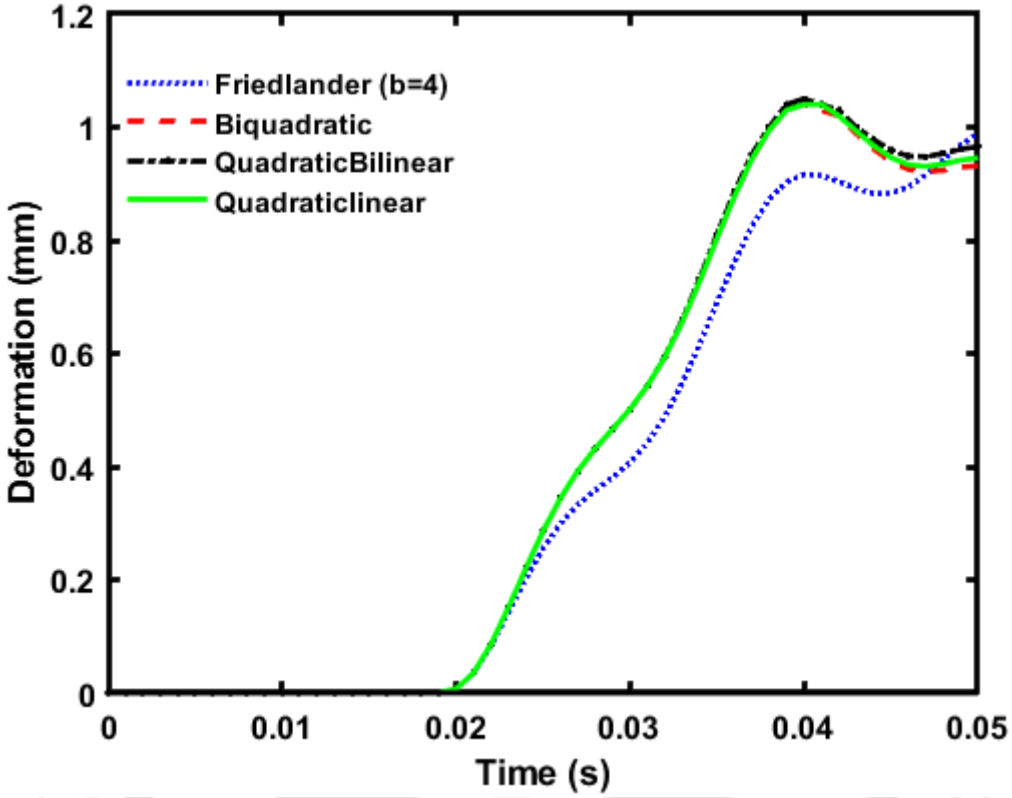

Fig. 4.19. Deformation time history.

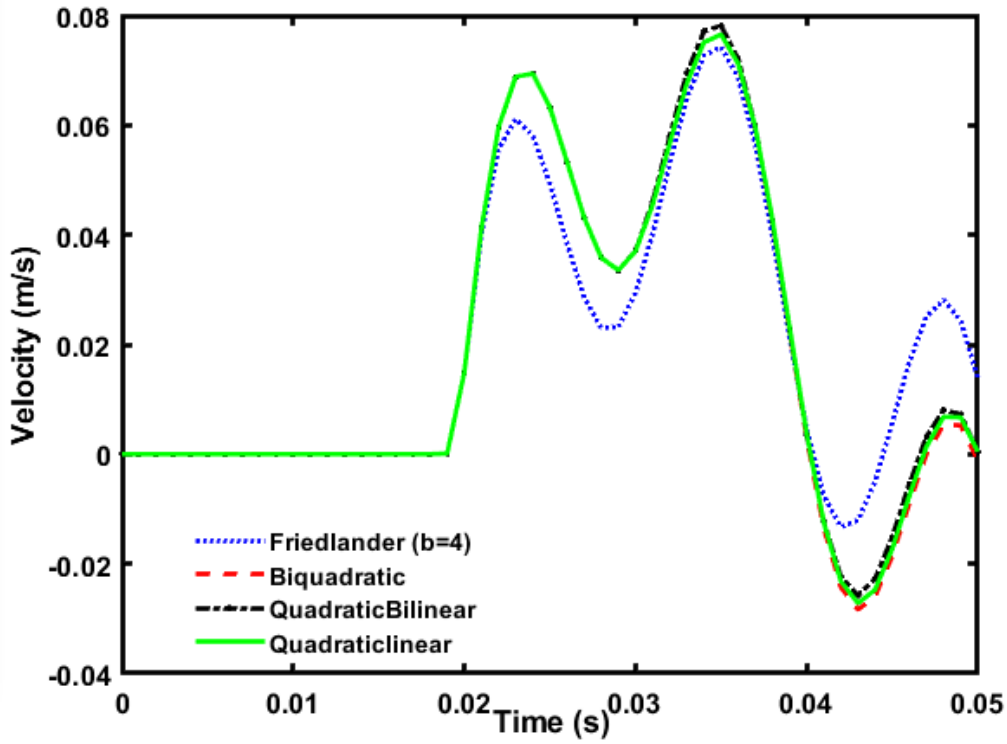

Fig. 4.20. Velocity – time history.

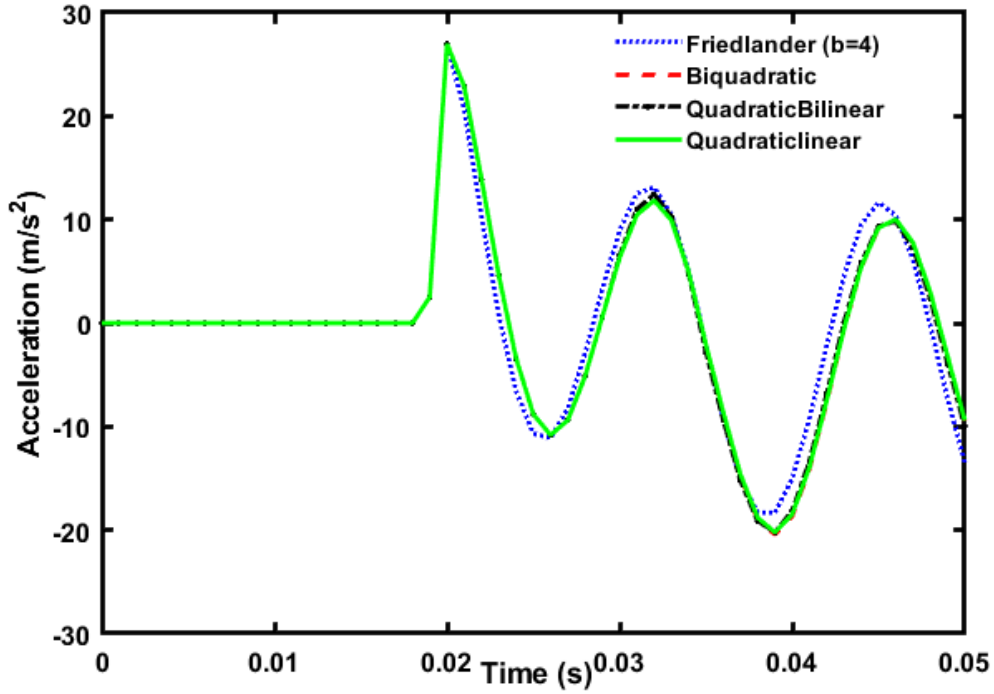

Fig. 4.21. Acceleration – time history.

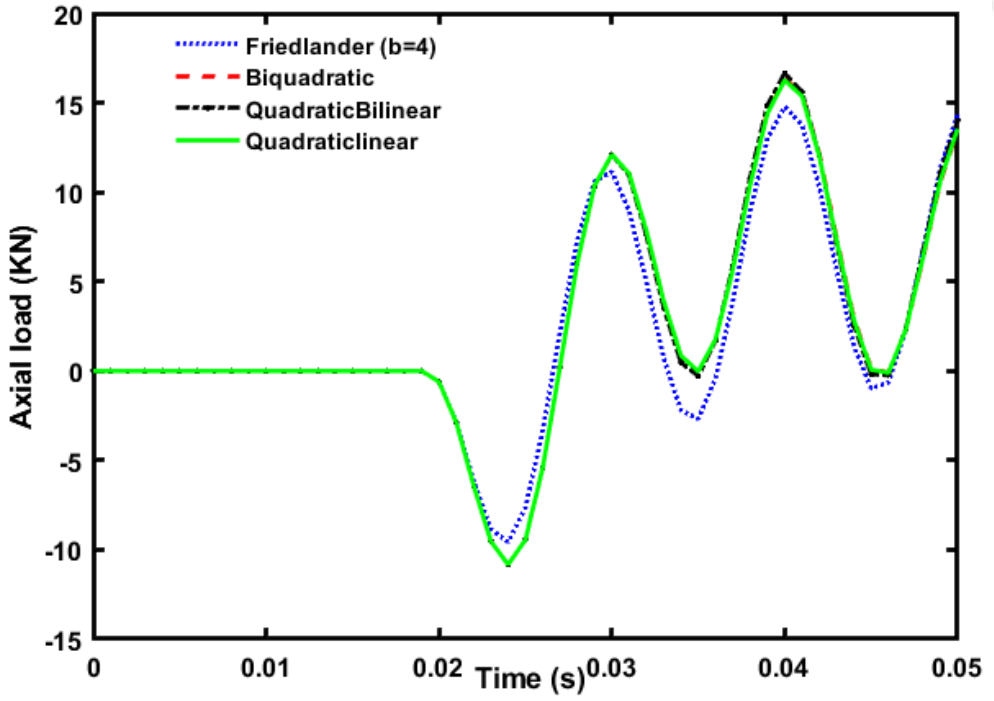

Fig. 4.22. Column axial load-time history.

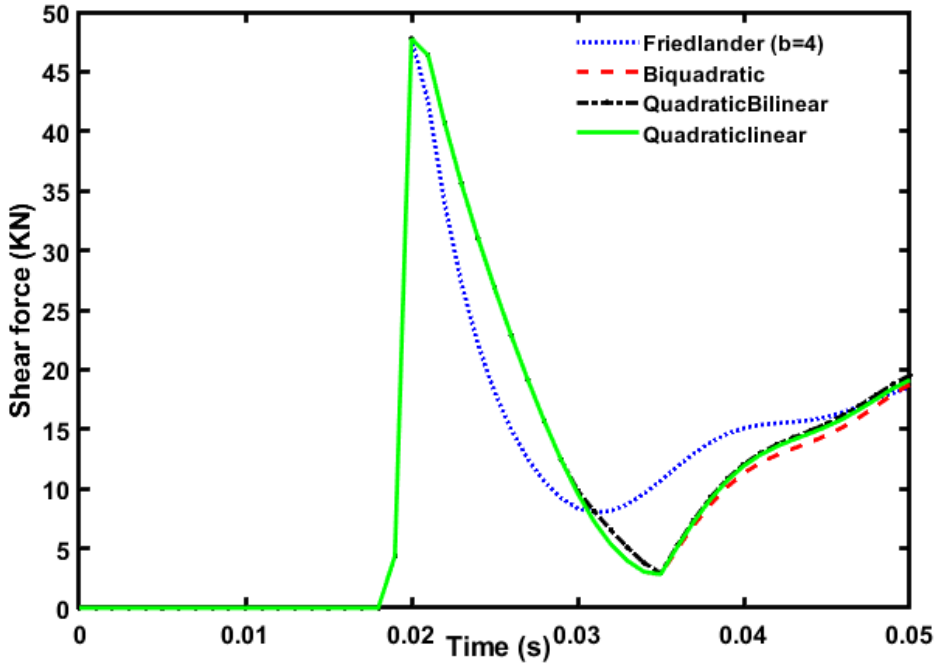

Fig. 4.23. Column shear force-time history.

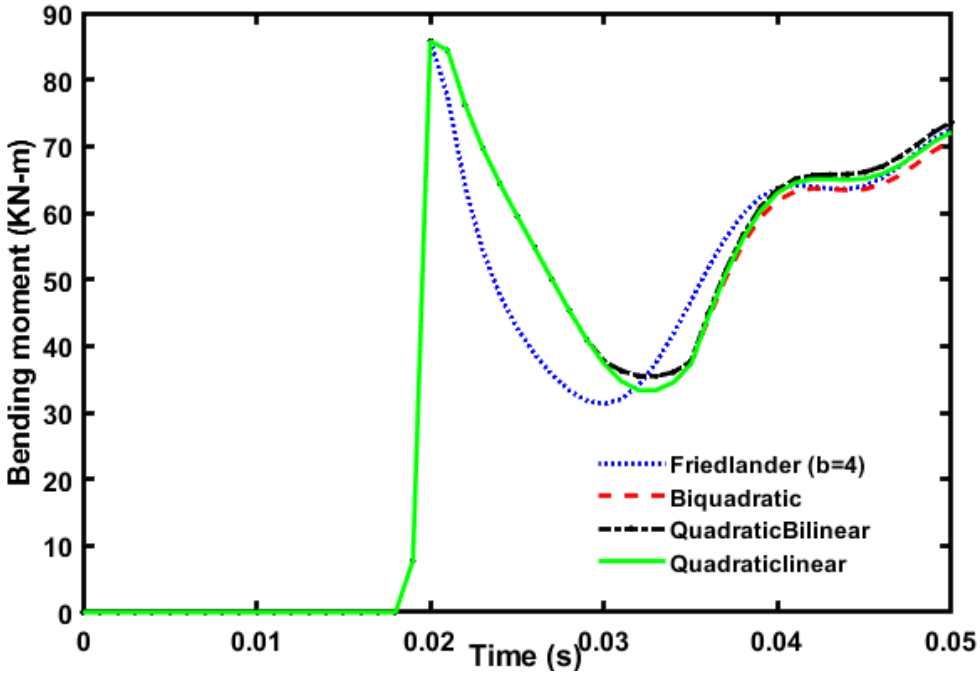

Fig. 4.24. Column bending moment – time history.

The numerical results also suggest that the structural response be investigated using the developed quadratic family profiles which are simple and accurate. The quadratic family

formulas agree with the experimental data, avoiding time demanding blast wave decay parameter calculations and the complexity of the indefinite Friedlander profile.

4.4 Response Spectrum of Quadratic Blast Profile

An impulsive force is an enormous force that acts for a very short time but has a finite time integral. The impulse response function can be used to build the Convolution Integral Method (or Duhamel Integral Method) for determining the response of an SDOF system to broad dynamic stimulation. The applied force is represented as a sequence of infinitesimally brief impulses in the motion solution of an SDOF system. At a certain time, the system's response to an applied force can be calculated by aggregating the responses to all impulses up to that point. Duhamel's integral provides an alternative to the classical solution if the applied force is specified analytically by a simple function that allows analytical assessment of the integral. Air pressures created on a structure resulting from above-ground blasts or explosions are essentially a single pulse that can be idealised using simple shapes. The response to pulse forces will be determined using the classical technique. The first is the excitation's forced vibration phase, which lasts the entire time. The second phase is the free vibration phase, which occurs after the pulse force has ended.

The static resistance function of an elastic-perfectly plastic SDOF system has been investigated without damping (Gantes et al., 2004). The system's response has been separated into four stages, as follows:

1. Response up to the elastic limit x_{el}, corresponding to maximum resistance R_m, characterized by the elastic stiffness k of the system, defined as the ratio of R_m to x_{el}.
2. Plastic response with constant resistance R_m from the elastic limit x_{el} up to a maximum displacement x_m.

3. Rebounding, where the response starts to decrease with the same absolute stiffness as in stage (1) up to a maximum (in absolute terms) negative resistance $-R_m$.

4. Plastic response during rebounding, corresponding to a resistance $-R_m$.

The analytical expressions describing the response in each stage are

$$R = \begin{cases} kx, & 0 < x < x_{el} \quad (\text{stage}\,1), \\ R_m, & x_{el} < x < x_m \quad (\text{stage}\,2), \\ R_m - k(\mathrm{x_m} - \mathrm{x}), & x_m - 2x_{el} < x < x_m \quad (\text{stage}\,3), \\ -\mathrm{R_m}, & x < x_m - 2x_{el} \quad (\text{stage}\,4), \end{cases} \tag{4.21}$$

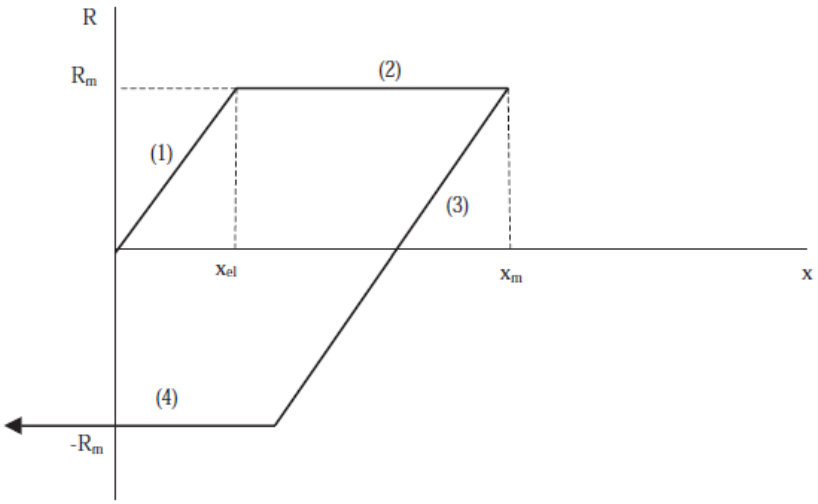

Fig. 4.25. Elastic–perfectly plastic behaviour for SDOF system (Gantes et al., 2004).

A similar technique is used to obtain the response of an SDOF system subjected to exponential and quadratic profiles. The solution derivation and approach process may be found in (Gantes and Pnevmatikos 2004). The solutions in this study are derived using MATLAB.

Exponential Blast Load

The solution of the equation of motion of an SDOF system subject to exponential blast loading is given by

$$p(\mathrm{t}) = \begin{cases} p_0\left(1-\dfrac{t}{t_d}\right)e^{-b\frac{t}{t_d}} & ,0 \le t \le t_f \\ 0 & ,t_f \le t \end{cases} \tag{4.22}$$

For elastic SDOF system;

$$u(\mathrm{t}) = \begin{cases} \dfrac{p_0}{k}\left\{(A-C\,\mathrm{t})\,\mathrm{e}^{-\mathrm{b}\frac{t}{t_d}} - A\cos w_n\,\mathrm{t} + B\sin w_n\,\mathrm{t}\right\} \\ \dfrac{p_0}{k}\left\{A(e^{-b\frac{t_f}{t_d}}\cos w_n(\mathrm{t}-t_f) - \cos w_n\,\mathrm{t}) + B(\sin w_n\,\mathrm{t} - e^{-b\frac{t_f}{t_d}}\sin w_n(\mathrm{t}-t_f)) - C(t_f e^{-b\frac{t_f}{t_d}}\cos w_n(\mathrm{t}-t_f) - \dfrac{b}{w_n^2}e^{-b\frac{t_f}{t_d}}\sin w_n(\mathrm{t}-t_f))\right\} \end{cases}$$

$$\begin{matrix} ,0 \le t \le t_f \\ ,t_f \le t \end{matrix} \tag{4.23}$$

Where b is a wave form coefficient, p_0 is peak load, w_n is the natural frequency and A, B, C, D and E are integration constants, and defined by

$$A = \frac{t_d^2 w_n^2(\mathrm{b}^2 - 2\,\mathrm{b} + t_d w_n^2)}{(\mathrm{b}^2 + t_d^2 w_n^2)^2}$$

$$B = \frac{t_d^3 w_n^3(\mathrm{b}+1) + \mathrm{b}^2\, t_d w_n(\mathrm{b}-1))}{(\mathrm{b}^2 + t_d^2 w_n^2)^2}$$

$$C = \frac{t_d w_n^2}{(\mathrm{b}^2 + t_d^2 w_n^2)}$$

For elastic-plastic SDOF system;

$$u(\mathrm{t}) = \begin{cases} \left\{\dfrac{p_0}{k}\left\{(A-C\,\mathrm{t})\,\mathrm{e}^{-\mathrm{b}\frac{t}{t_d}} - A\cos w_n\,\mathrm{t} + B\sin w_n\,\mathrm{t}\right\}\right\} & ,0 \le t \le t_{el,\max} \\ \left\{\dfrac{p_0}{k}w_n^2\left(-\dfrac{t_d t e^{-b\frac{t}{t_d}}}{b^2} + \dfrac{(b-2)t_d^2 e^{-b\frac{t}{t_d}}}{b^3} - \dfrac{at^2}{2}\right) + Ht + I\right\}; & ,t_{el,\max} \le t_d \end{cases} \tag{4.24}$$

Where $t_{el,\max}$ is the time of maximum response, $u_{el,\max}$ is maximum elastic deformation, $v_{el,\max}$ is maximum elastic velocity, H and I are integration constants and are defined by

$$H = v_{el,\max} + \frac{p_0}{k} w_n^2 \left(\frac{e^{-b\frac{t_{el,\max}}{t_d}}}{b^2} (ab^2 t_{el,\max} e^{b\frac{t_{el,\max}}{t_d}} - bt_{el,\max} + (b-1)t_d \right)$$

$$I = u_{el,\max} + \frac{p_0}{k} w_n^2 \left(-\frac{t_d t_{el,\max} e^{-b\frac{t_{el,\max}}{t_d}}}{b^2} + \frac{(b-2)t_d^2 e^{-b\frac{t_{el,\max}}{t_d}}}{b^3} - \frac{at_{el,\max}^2}{2} \right) - Ht_{el,\max}$$

Quadratic Blast Loading

The solution of the equation of motion of an SDOF system subject to quadratic blast loading is given by

$$p(\mathrm{t}) = \begin{cases} p_0 \left[\frac{1}{n} \left(\frac{t}{t_d} \right)^2 - \left(\frac{n+1}{n} \right) \left(\frac{t}{t_d} \right) + 1 \right]; & 0 \le t \le t_f \\ 0 & t \ge t_f \end{cases} \tag{4.25}$$

For elastic SDOF system;

$$u(\mathrm{t}) = \begin{cases} \frac{p_0}{k} \left(A \sin w_n t + B \cos w_n t + C + \left(\frac{1}{nt_d^2} \right) t^2 - \left(\frac{n+1}{nt_d} \right) t + 1 \right) & 0 \le t \le t_f \\ \frac{p_0}{k} \left(u_{t_f} \cos w_n t + \frac{v_{t_f}}{w_n} \sin w_n t \right) & t \ge t_f \end{cases}; \tag{4.26}$$

Where and A, B, and C are integration constants and defined by

$$A = \frac{n+1}{nw_n t_d}$$

$$B = \frac{2}{n\left(w_n t_d\right)^2} - 1$$

$$C = -\frac{2}{n\left(w_n t_d\right)^2}$$

For elastic-plastic SDOF system;

$$u(\mathrm{t}) = \begin{cases} \frac{p_0}{k}\left(\frac{w_n^2}{12nt_d^2}t^4 - \frac{w_n^2(n+1)}{6nt_d}t^3 + \frac{w_n^2(1-a)}{2}t^2 + Ct + D\right), 0 \le t \le t_{el,\max} \\ \frac{p_0}{k}\left(-\frac{aw_n^2}{2}t^2 + Et + F\right) \qquad\qquad , t_{el,\max} \le t_d \end{cases} \tag{4.27}$$

Where C, D, E and F are integration constants and defined by

$$C = v_{el,\max} - \left(\frac{w_n^2}{3nt_d^2}t_{el,\max}^3 - \frac{w_n^2(n+1)}{2nt_d}t_{el,\max}^2 + w_n^2(1-\mathrm{a})t_{el,\max}\right)$$

$$D = u_{el,\max} - \left(\frac{w_n^2}{12nt_d^2}t_{el,\max}^4 - \frac{w_n^2(n+1)}{6nt_d}t_{el,\max}^3 + \frac{w_n^2(1-a)}{2}t_{el,\max}^2\right) - Ct_{el,\max}$$

$$E = v_{el,\max} + w_n a t_{el,\max}$$

$$F = u_{el,\max} + w_n a t_{el,\max}^2 - Et_{el,\max}$$

4.4.1 Comparison of Response Spectra

A response or shock spectrum is a graph representing an SDOF system's maximum response (e.g., displacement, stress, acceleration) vs a system parameter, usually the un-damped natural frequency. The response ratio, often known as the dynamic load factor (DLF), is valuable for analysing the dynamic response.

$$DLF = \frac{ku(\mathrm{t})}{p_{\max}} \tag{4.28}$$

Thus, the response ratio is the ratio of dynamic response to static deformation. The response-ratio plot $DLF = 1$ corresponds to the static displacement position. The maximum response is defined by the maximum dynamic deflection $u_{\max}$, which occurs at a time t_m. The maximum dynamic deflection $u_{\max}$ can be evaluated by setting $\frac{du(\mathrm{t})}{dt}$ equal to zero, i.e. when the structural

velocity is zero. The structural response to blast loading is significantly influenced by the ratio $\frac{t_d}{T_n}$ or $w_n t_d$ ($\frac{t_d}{T_n} = \frac{w_n t_d}{2\pi}$).

Response spectra for SDOF models may be efficiently utilised to forecast the system's maximum response. UFC 3-304-2 contains widely used response spectra for blast design for elastic-plastic resistance functions and idealised blast loads with positive phase only. The response spectrum for a quadratic blast profile is constructed in this study, and it is compared to the exponential spectrum (Fig. 4.26 & Fig. 4.27). The elastic and inelastic spectra of time and deformation of the structure are analysed for both exponential and quadratic profiles.

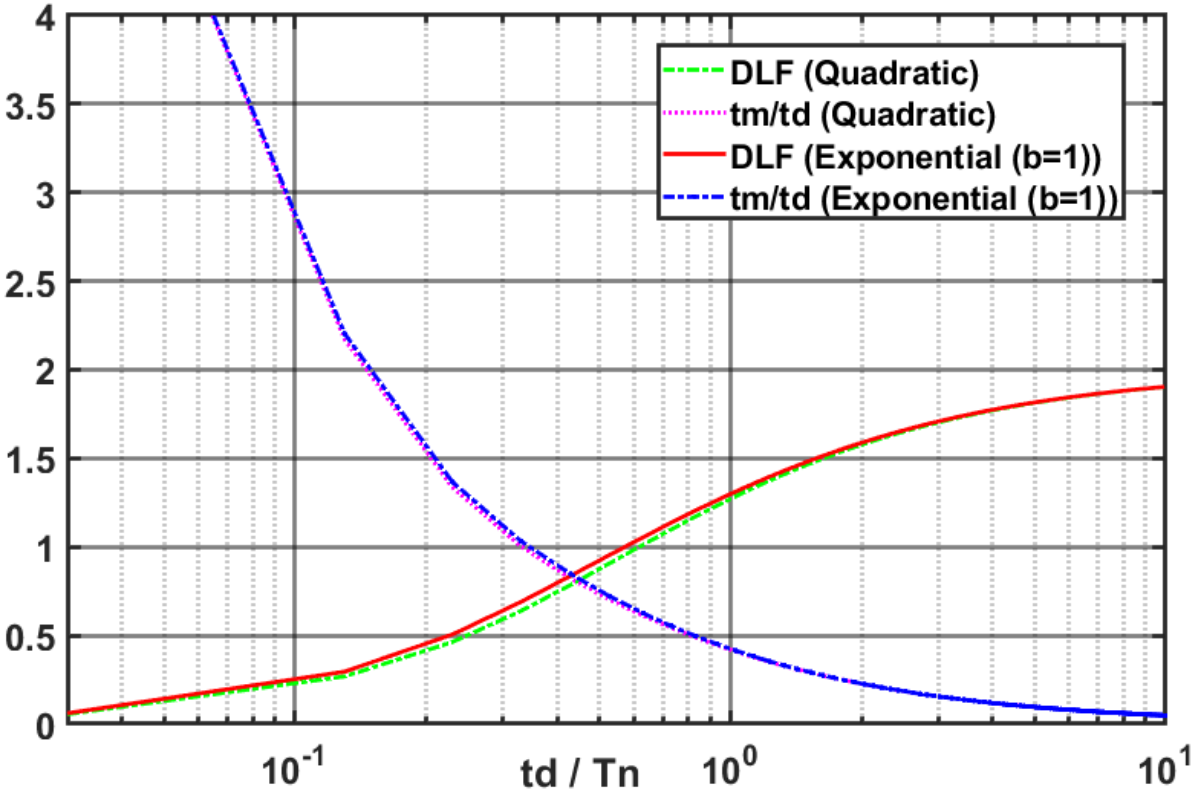

Fig. 4.26. Elastic response spectra - Exponential vs Quadratic blast profiles.

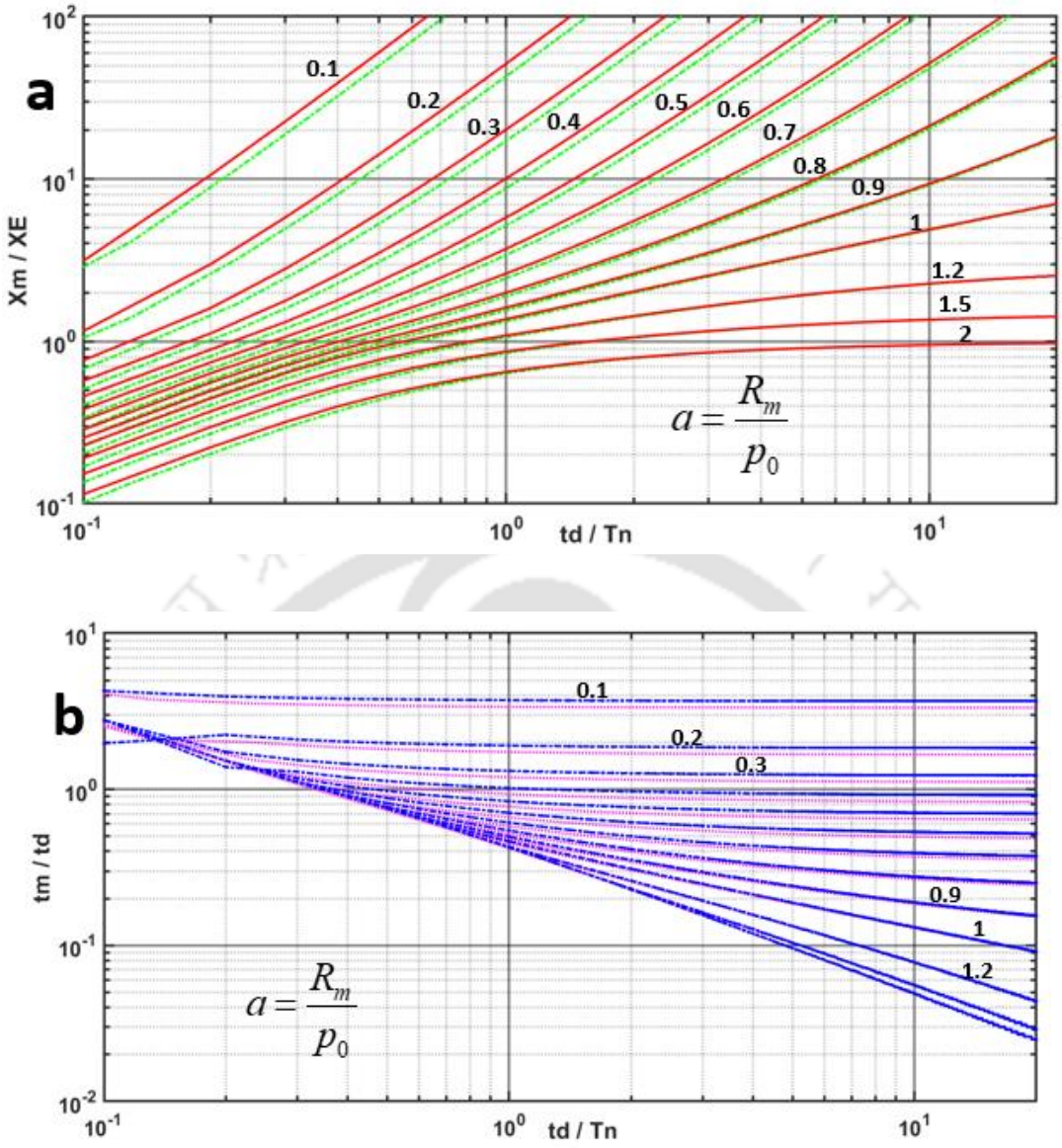

Fig. 4.27. Elastic-plastic response spectra (Exponential vs. Quadratic) - a) Deformation b) Time for different $a = \frac{R_m}{p_0}$.

An elastic-perfectly plastic resistance function has been used to compare response spectra obtained using exponential load (Gantes et al., 2004). Elastic-plastic response spectra have frequently been used in the design of buildings subject to loads caused by explosions. The response spectra based on an exponential and quadratic distribution of blast pressure are validated, as they are more in line with experimental data. In order to compare the proposed

profile, characteristic values of maximum response for different combinations of ratios $\frac{R_m}{p_0}$ and $\frac{t_d}{T_n}$ are considered (Fig. 4.30).

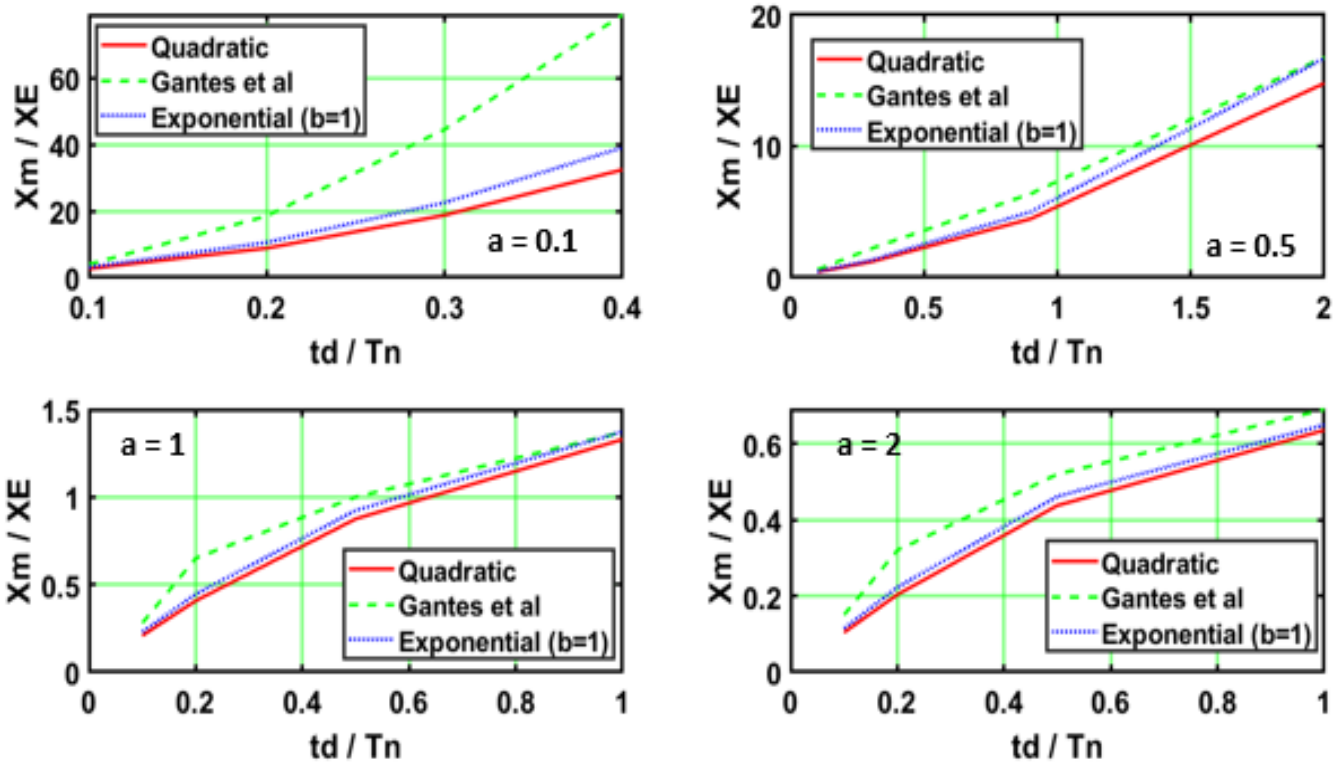

Fig. 4.28. Elastic-plastic behaviour of exponential pulse (b=1) and where $a = \frac{R_m}{p_0}$.

4.4.2 Numerical Example - Multi-Storey Building

The validated experimental time history profile against the quadratic linear analytical blast time history profile (Fig. 4.17a) is used in the numerical analysis of a multi-storey building. A 10-storey, 5-bay multi-storey building subject to quadratic-linear blast time history is modelled in SAP2000 software (Fig. 4.30a) to understand and investigate the response of the structure for a given realistic blast profiles (Tolani et al., 2020). The pressure time history is

converted into uniformly distributed load time history by multiplying with the tributary width of the structural member in the multi-storey building. Modelling details are as follows:

Beam = 0.3m x0.5m x 6m

Column = 0.3m x 0.3m x 3m

Wall = 3m x 6m (Thickness = 0.25m)

Slab = 6m x 6m (Thickness = 0.15m)

Grade of concrete = M30

Grade of steel = Fe415

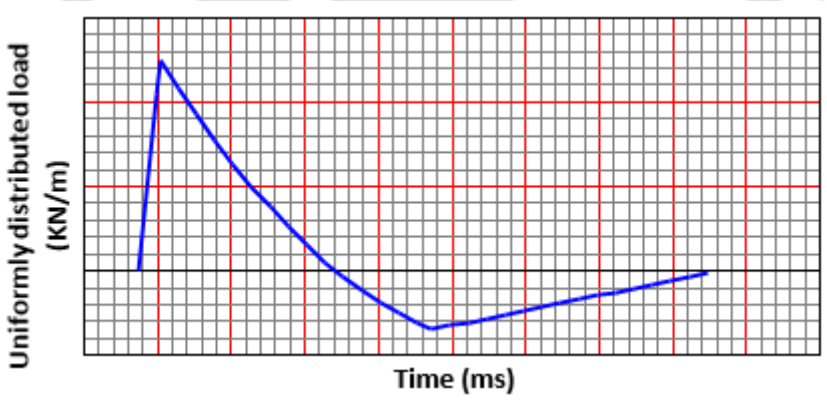

Fig. 4.29. Quadratic-linear time history (SAP2000 software).

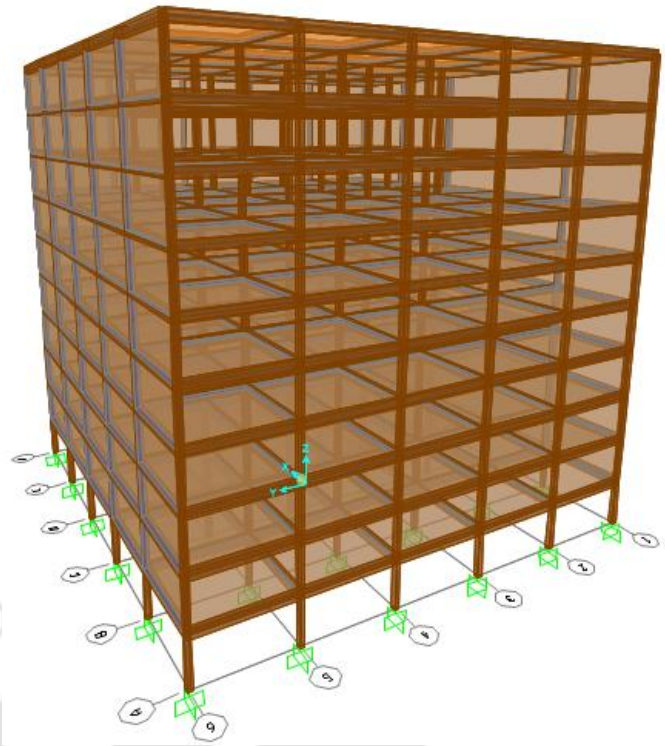

(a) Multi-storey building (3D Model) in SAP2000.

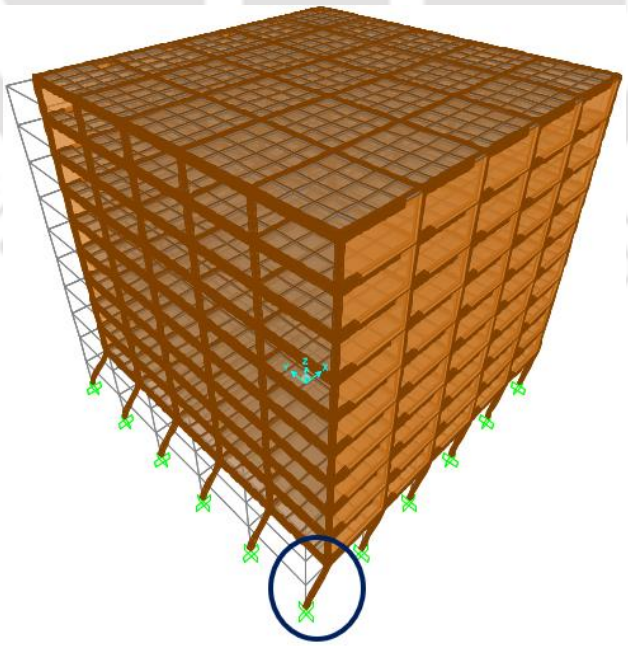

(b) Deformed building due to quadratic linear blast time history.

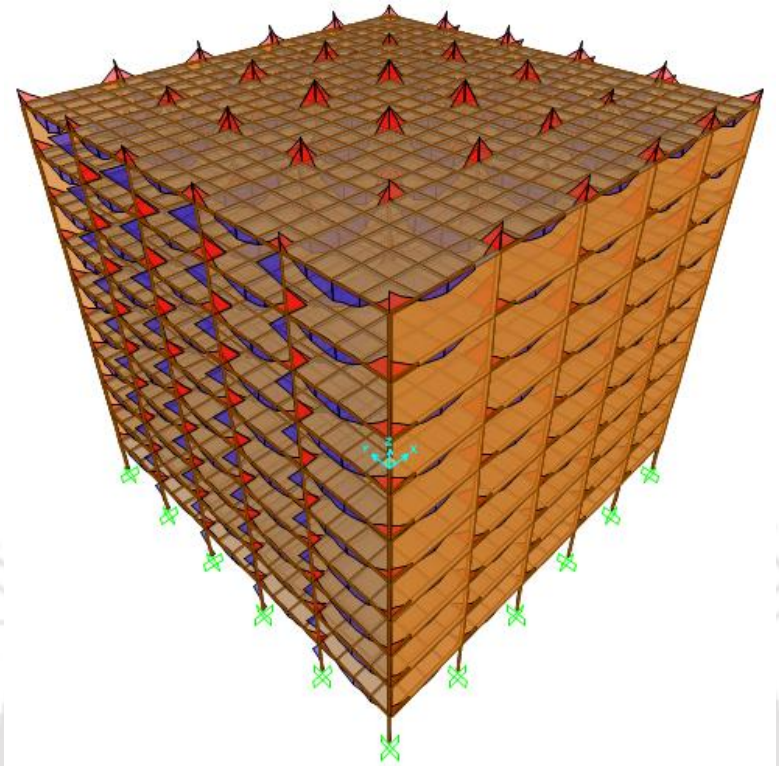

(c) Bending moment diagram of building.

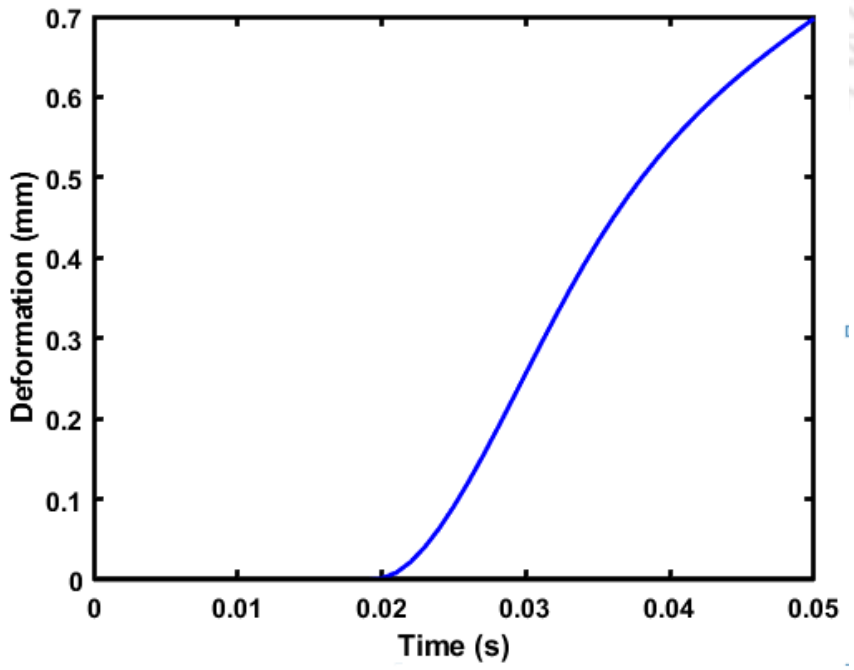

(d) Deformation time history of column (circled in Fig. 4.30b).

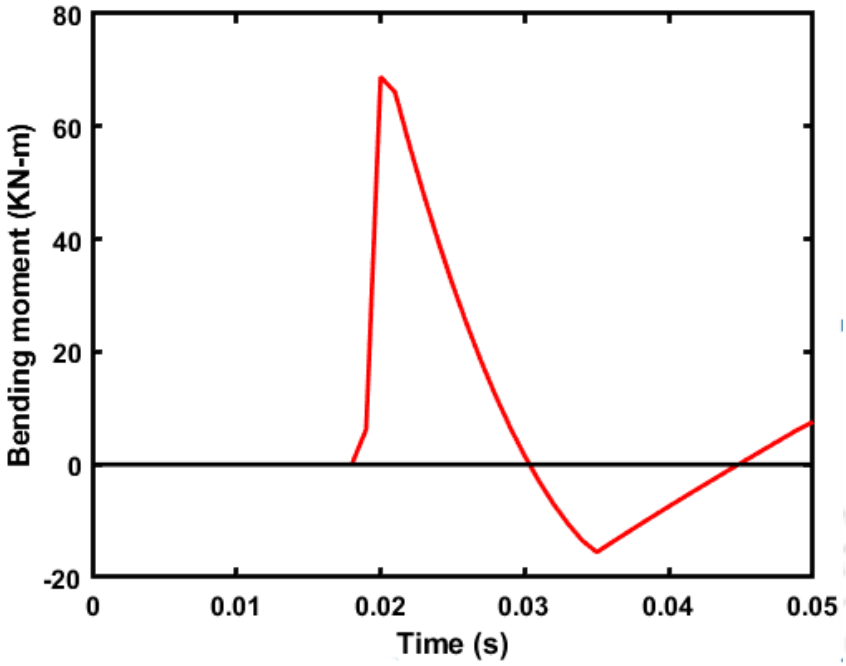

(e) Bending moment time history of column (circled in Fig. 4.30b).

Fig. 4.30. A 10-storey, 5-bay building subject to blast time history loading.

4.5 Conclusion

A new family of linear, quadratic, cubic, and quartic of blast profiles is developed in this study. The developed models overcome the limitations of Friedlander blast profile's that gives erroneous results during the negative phase effect. The extent of the changes in responses that will be apparent when applying the different load models is estimated using single-degree-of-freedom systems under various loading approximations. Finite element evaluations are carried out to highlight the consistency of the results produced by the various loading models. The literature's six experimental blast pressure-time history profiles are used to generate and

validate the newly developed linear, quadratic, cubic, and quartic family of blast profiles. The blast profiles of the quadratic family are found to be accurate. The spectra of an SDOF system subject to exponential and quadratic profiles are compared, and the analytical solutions of an SDOF system are evaluated. There is no discernible difference; however, in the elastic-plastic spectra, it ranges from 0.01 to 0.46. To test the accuracy of the quadratic blast profile, a numerical analysis of a single-story RC frame is performed using SAP2000 for one of the six experiments. More blast tests are needed to establish the relationship between positive and negative peak pressures to improve the accuracy of the analytical blast profile. This study can expand to include other functions, such as trigonometry functions, to improve the results. With so many variables impacting whether the negative phase is conservative, non-conservative, or has no effect, determining when the negative phase may be ignored or not is difficult and impractical. Indeed, it may be argued that the negative phase should not be ignored until the engineer is confident that its implications are comprehended.

CHAPTER 5 DEVELOPMENT OF PROBABILISTIC MODELS FOR CRITICAL LOAD AND COLLAPSE RESISTANCE FACTORS OF MULTI-STOREY BUILDINGS

5.1 General

In the construction of buildings, concrete and steel rigid frame structures are the most commonly used civil engineering structures. Rigid frame buildings are vulnerable to lateral loads (blast loads) during their lifetime. In the design of blast-resistant structures, rigid frame structure construction has been chosen because it enables open internal space while also providing strong resistance to lateral stresses. Furthermore, due to the eventual formation of plastic hinges, this structure has intrinsic energy absorption capabilities up to the structure's ultimate capacity. The TM 5-1300/UFC 2005 blast resistant design manual limits the peak loads of rigid frame constructions to a single storey only. This chapter develops the probabilistic models to predict the critical load and collapse resistance factors of multi-storey rigid frame structures (midrise buildings) subject to uniform lateral blast loads. The uncertainties in these critical load elements, such as the direction and critical location of the frame structures, are inherent. The peak loads of multi-storey rigid frame constructions are calculated using these factors.

When the beam-to-column connections of a frame are sufficiently stiff, the original angles between intersecting members remain practically unchanged. Flexure of beams and columns, as well as rotation at the joints, define a rigid frame. With the rigid frame action, the production of shear forces and bending moments in the frame members and joints resist lateral loads in this system. Minimising positive moments in beam spans allows the continuity at both ends of beams and helps to resist gravity loads more effectively. Because of their versatility in architectural planning, moment frames have several advantages in building applications. Stiffness rather than strength has frequently been used to manage the depths of frame members

to reduce storey drift under lateral loads. The lateral displacement of one level relative to the level below is known as storey drift.

5.2 Development of Database

A numerical modelling is adopted to generate the database for development of the probabilistic models to predict the critical load and collapse resistance factors of multi-storey rigid frame structures (midrise buildings) subject to uniform lateral blast loads. The methodology for collection of data points is outlined which is used in this study. The analysis in this study considers fix ending rigid frame constructions with a unit bay and storey lengths. For this study, the lateral uniform load facing members (beams and columns) are considered exterior members, whereas the following members are considered interior members. The investigation considered elastic behaviour as well as a static load scenario. Initially, a simple two-dimensional portal frame is analysed with SAP2000 software, and the software's accuracy is manually tested against results from traditional methods for the same frame. The results were found to be extremely accurate, and further information may be found in the following sections of this chapter.

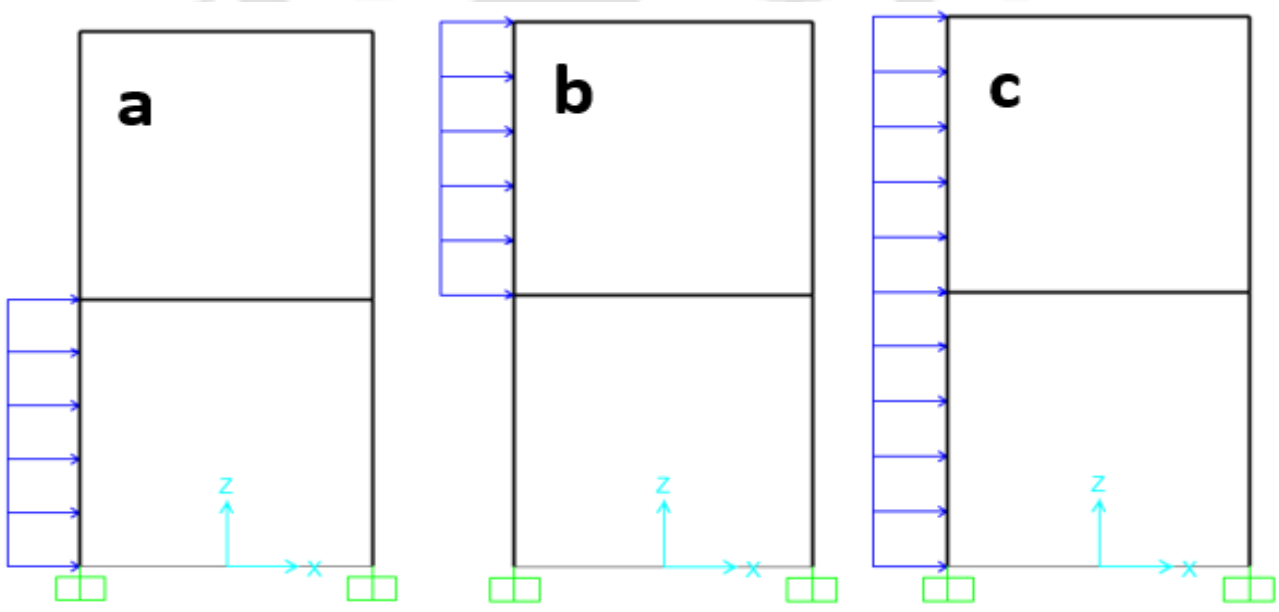

Fig. 5.1 Methodology: a) Case study 1 b) Case study 2 and c) Case study 3.

Data Collection

SAP2000 is a civil-engineering software package that is adopted to analyse and design any type of structural system. Basic and advanced systems, ranging from 2D to 3D and simple to complex geometry, can be modelled, analysed, designed, and optimised, utilising an object-based modelling environment that simplifies and accelerates the engineering process. The following is the data collection methodology for developing probabilistic models of critical load factors:

Step1: The dead weight of structural members is neglected while modelling a 2D rigid frame with unit dimensions in SAP2000 software.

Step2: A unit lateral uniform load is imposed on the different floors of the rigid frame structure as shown in Fig. 5.1 to discover the critical member and location of lateral uniform load, and the member reaction loads (bending, shear, and axial) are obtained for each scenario.

Step3: The critical load factor is considered as the maximum reaction load (bending, shear, and axial) of all possible scenarios of rigid frame structures.

Step4: By increasing the number of bays and storeys, the same procedure is followed up to 25-storey and 25-bay rigid frame structures (mid-rise building frames).

Step5: 12 sets of data are collected for the exterior and interior members (beams and columns) of the rigid frame for each critical case to obtain three load factors (bending, shear, and axial), and a similar method is followed for 625 critical cases to obtain critical load factors.

Step6: The entire data is captured in OriginPro software for data analysis and the development of probabilistic models of critical load factors.

Data Analysis

The OriginPro software is used to create probabilistic models for the critical load factors of rigid frame constructions. Statistical measures such as standard deviation, coefficient of variation, and coefficient of determination are used to confirm the accuracy of each probabilistic model. This method is chosen because it is one of the most practical, realistic, and cost-effective ways to examine structures subject to unexpected lateral loads (blast and wind). It satisfies all of the classic rigid frame preliminary analysis methodologies. This procedure improves on current classical methods (the portal method, the method of virtual work, Castigliano's theorem, the force method, the slope-displacement method, and the stiffness method), which require the assumption of a contra-flexure point to solve indeterminate rigid frames and yield approximate results. In contrast, this approach yields accurate results and saves time for complex rigid frame structures.

5.2.1 Validation

Validation of numerical approaches is required to ensure the accuracy of the modelling and resulting findings. Modelling and analysing structural responses under random environmental pressures, such as blast loads, can be done using computer programmes. Experiments involving such explosions are not possible due to safety concerns and the great danger involved. Computer simulations with finite element modelling and analytical procedures using the computer codes SAP2000 are used in this research. A first-order linear elastic uncouples analysis of the frame structure with unit loads is performed to validate the model. The SAP2000 frame structure model is used to simulate rigid frames to obtain the database for development of the probabilistic models for critical load factors. The proposed methodology is well explained and supported in Table 5.1, Fig. 5.2, and Fig. 5.3. Overall, observations show that the current study's findings are similar to those found in the Unified Facilities Criteria guidelines (UFC 2005). Fig. 5.4 shows various examples of rigid frames subject to limiting

resistance (Ru) with critical load factors utilised to validate the adapted approach. The results provide appropriate confidence in this modelling approach because the current study evaluates critical load factors of rigid frames subject to lateral uniform loads. Furthermore, they provide confidence in the parameter selection and analysis utilised in this study, allowing them to be extended for more extensive analyses of the structural components of interest.

Table 5.1. Critical load factors of the rigid frame structure.

No. of stories (m)	No. of Bays (n)	Axial Load Factor		Shear Load Factor	
		UFC 2005	Study	UFC 2005	Study
1	1	0.2	0.2	0.8	0.8
1	2	0.3	0.27	0.7	0.73

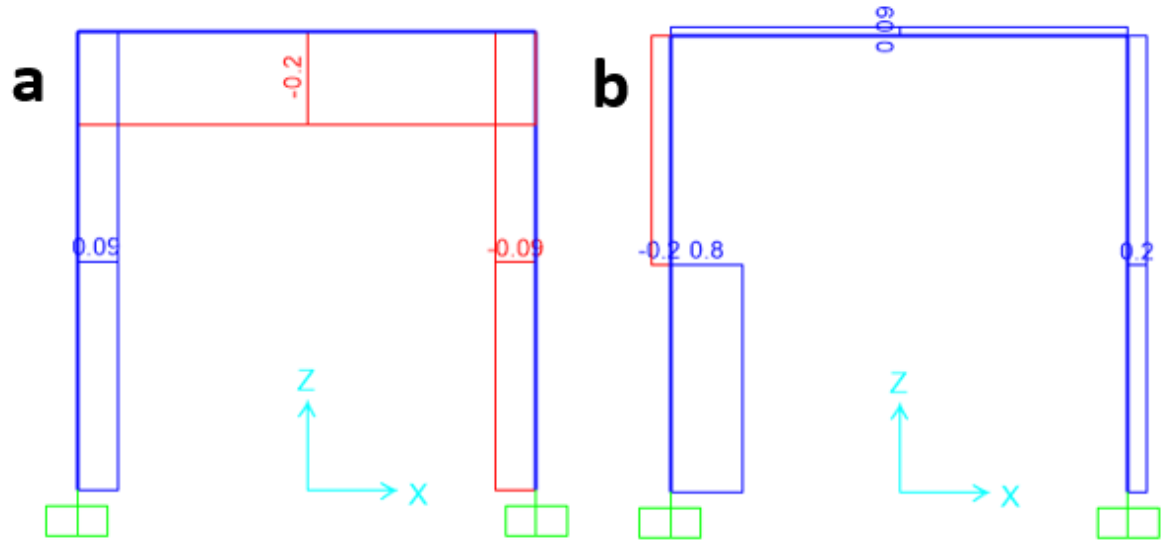

Fig. 5.2. Validation 1: a) Axial critical load factor b) Shear critical load factor of the rigid frame (m=1 and n=1).

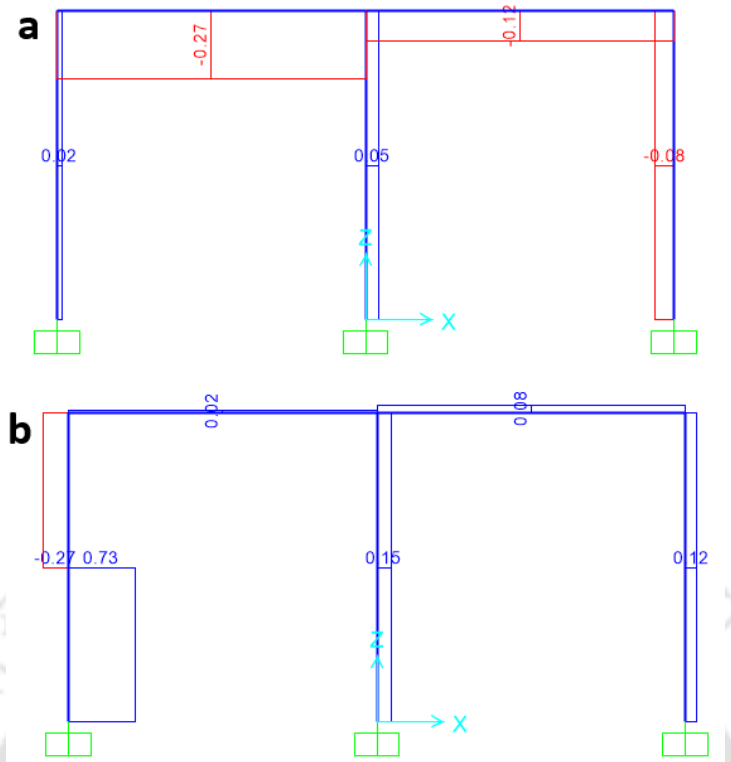

Fig. 5.3. Validation 2: a) Axial critical load factor b) Shear critical load factor of the rigid frame (m=1 and n=2).

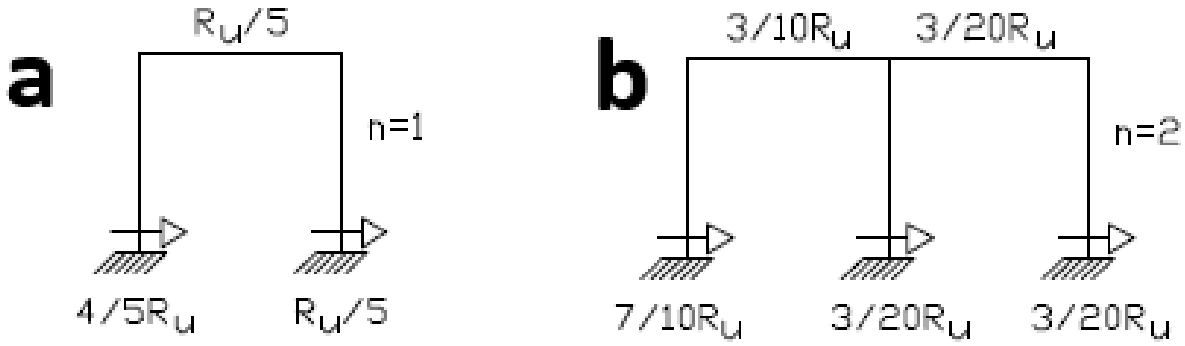

Fig. 5.4. Critical load factors of rigid frame: a) case (m=1 and n=1) b) case (m=1 and n=2) (UFC 2005).

5.3 Probabilistic Models for Critical Load Factors and Peak Loads

Under the action of horizontal and vertical blast loads, each member in a frame has been subjected to a combination of bending moments, shear forces, and axial loads. However,

using a simplified approach, the phasing between critical values of the axial force, shear force, and bending moment cannot be determined (UFC 2005). As a result, the peak axial loads, shear force, and moments obtained should be assumed to act simultaneously for trial beam-column design. As a result, they must be built to withstand lateral loads (blast loads).

Exterior Columns

The probabilistic equation (5.1) is developed in this study to calculate the axial critical load factors for the exterior columns (ECA). As illustrated in Fig. 5.5, a surface plot is created for the recorded data and the probabilistic model's accuracy with SAP2000 data is shown. Tables 5.2 and 5.3 include the regression parameters, constant values, and correlation matrix for the probabilistic model, respectively.

$$ECA = z0 + Bm^{C} + Dn^{E} + Fm^{C}n^{E} \text{ for } n\geq 1 \text{ and } m\geq 1 \quad (5.1)$$

Where ‘m’ is the number of storeys, ‘n’ is the number of bays in the building and z0, B, C, D, E and F are constants listed in Table 5.2.

Table 5.2. Regression parameters of ECA.

Constant	Value	Standard Error	Standard Deviation	Coefficient of Variation
z0	0.17258	0.0061		
B	-1.80891	0.09413		
C	-1.24312	0.00791		
D	-0.01314	8.62081E-4	0.05642	0.037
E	0.96809	0.01128		
F	1.26733	0.04515		

Table 5.3. Correlation Matrix of ECA.

Constant	z0	B	C	D	E	F
z0	1					
B	-0.193	1				
C	0.035	0.076	1			
D	-0.445	0.435	-0.727	1		
E	0.120	0.808	-0.199	0.520	1	
F	-0.082	-0.886	-0.037	-0.399	-0.963	1

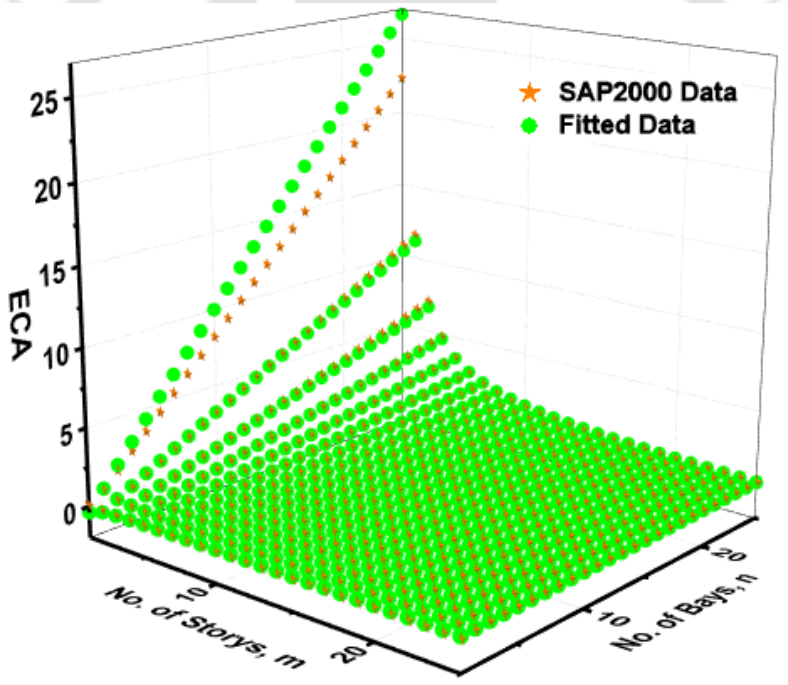

Fig. 5.5. Exterior column axial load factor (ECA).

The peak axial load (A_{EC}) in a multi-storey building's exterior column, when subjected to horizontal uniform loading, is given by

$$A_{EC} = ECA \times R_u \text{ (kN)} \tag{5.2}$$

Where R_u is the limiting resistance.

The probabilistic equation (5.3) is developed in this study to calculate the shear critical load factors for the outer columns (ECS). As illustrated in Fig. 5.6, a surface plot is created for the recorded data and the empirical model's accuracy with SAP2000 data is shown. Tables 5.4 and 5.5 include the regression parameters, constant values, and correlation matrix for the probabilistic model, respectively.

$$ECS = z0 + Bm^C + Dn^E + Fm^C n^E \text{ for n}\geq 1 \text{ and m}\geq 1 \quad (5.3)$$

Where 'm' is the number of storeys, 'n' is the number of bays in the building and z0, B, C, D, E and F are constants listed in Table 5.4.

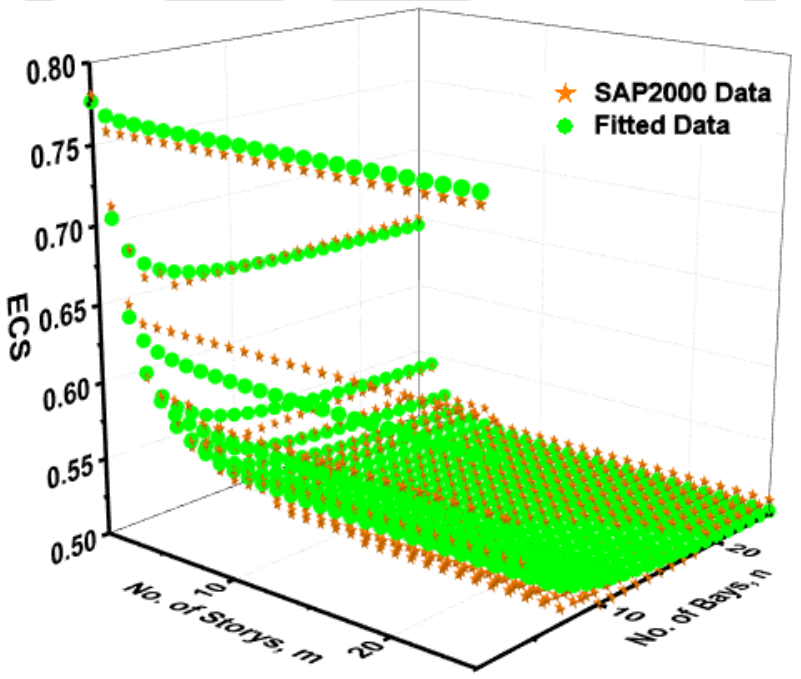

Fig. 5.6. Exterior column shear load factor (ECS).

Table 5.4. Regression parameters of ECS.

Constant	Value	Standard Error	Standard Deviation	Coefficient of Variation
z0	0.49485	8.00599e-4		
B	0.14652	0.00194		
C	-1.78734	0.04958		
D	0.27165	0.00173	0.00782	0.0145
E	-1.14847	0.01563		
F	-0.1366	0.0079		

Table 5.5. Correlation Matrix of ECS.

Constant	z0	B	C	D	E	F
z0	1					
B	-0.248	1				
C	-0.382	-0.107	1			
D	-0.266	0.142	0.164	1		
E	-0.782	0.160	-0.0003	-0.069	1	
F	0.071	-0.521	0.025	-0.334	0.012	1

The peak shear load (V_{EC}) in a multi-storey building's exterior column, when subjected to horizontal uniform loading, is given by

$$V_{EC} = ECS \times R_u \text{ (kN)} \tag{5.4}$$

where R_u is the limiting resistance.

Table 5.6 is developed in this study to calculate the bending critical load factors for the exterior columns (ECB). As illustrated in Fig. 5.7, a surface plot is created for the recorded data and the probabilistic model's accuracy with SAP2000 data is shown. Tables 5.7 and 5.8 include the regression parameters, constant values, and correlation matrix for the probabilistic model, respectively.

Table 5.6. ECB load factors.

ECB	Remarks
$z0 + Bm^C + Dn^E + Fm^C n^E$	for n≥1 and m>1
0.24	for n=1 and m=1
0.19	for n=2 and m=1
0.15	for n>2 and m=1

Table 5.7. Regression parameters of ECB.

Constant	Value	Standard Error	Standard Deviation	Coefficient of Variation
z0	0.08266	0.00106		
B	-0.00149	2.17949E-4		
C	0.8924	0.03845		
D	0.28486	0.01235	0.00977	0.0762
E	-1.50405	0.01031		
F	0.04146	0.00547		

Table 5.8. Correlation Matrix of ECB.

Constant	z0	B	C	D	E	F
z0	1					
B	-0.647	1				
C	-0.365	0.897	1			
D	-0.489	0.879	0.905	1		
E	-0.189	-0.147	-0.0287	-0.024	1	
F	0.398	-0.908	-0.994	-0.937	0.010	1

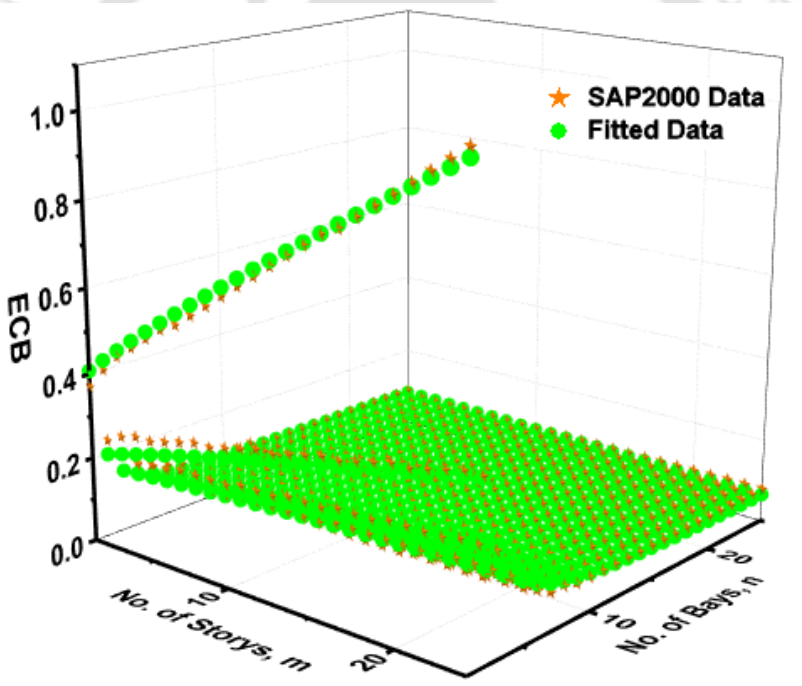

Fig. 5.7. Exterior column bending load factor (ECB).

The peak bending moment (M_{EC}) in a multi-storey building's exterior column when subjected to horizontal uniform loading is given by

$$M_{EC} = ECB \times R_u \text{ (kN-m)} \tag{5.5}$$

Where R_u is the limiting resistance.

Interior Columns

Table 5.9 is developed in this study to calculate the axial critical load factors for interior columns (ICA). As illustrated in Figs. 5.8 and 5.9, a surface plot is created for the recorded data, and the accuracy of the developed probabilistic models with SAP2000 data is shown. Tables 5.10, 5.11, and 5.12, Table 5.13, respectively, list the regression parameters, constant values, and correlation matrices for the probabilistic models.

Table 5.9. Regression parameters of ICA (For n=3 to 12 and m≥13).

Constant	Value	Standard Error	Standard Deviation	Coefficient of Variation
z0	-0.01211	0.00481		
A	-0.20611	0.08058		
B	-97.91283	41.43501		
C	8.25196	27.46353		
D	1.23116	0.01678	0.01907	0.03
E	-8.18393	27.46343		
F	0.00253	0.00846		
G	1.23147	0.01681		

Table 5.10. Correlation Matrix of ICA (For n=3 to 12 and m≥13).

Constant	z0	A	B	C	D	E	F	G
z0	1							
A	-0.031	1						
B	0.077	-0.076	1					
C	0.028	-0.031	0.002	1				
D	0.138	0.068	-0.076	0.042	1			
E	-0.028	0.031	-0.002	-1	-0.042	1		
F	-0.029	0.029	-0.0004	-0.999	-0.056	0.999	1	
G	0.134	0.069	-0.076	-0.018	0.998	0.018	0.004	1

Table 5.11. ICA load factors.

ICA	Remarks
0.02	For n≥3 and m=1
0.03	For n=2 and m≥2
0.04	For n≥3 and m=2
0.05	For n=2 and m≥2
0.05	For n≥13 and m=3
0.06	For n≥13 and m=4 to 6
$z0 + Am^B + Cn^D + Em^F n^G$	For n=3 to 12 and m≥13
$z0 + Am^B + Cn^D + Em^F n^G$	For n≥13 and m≥7

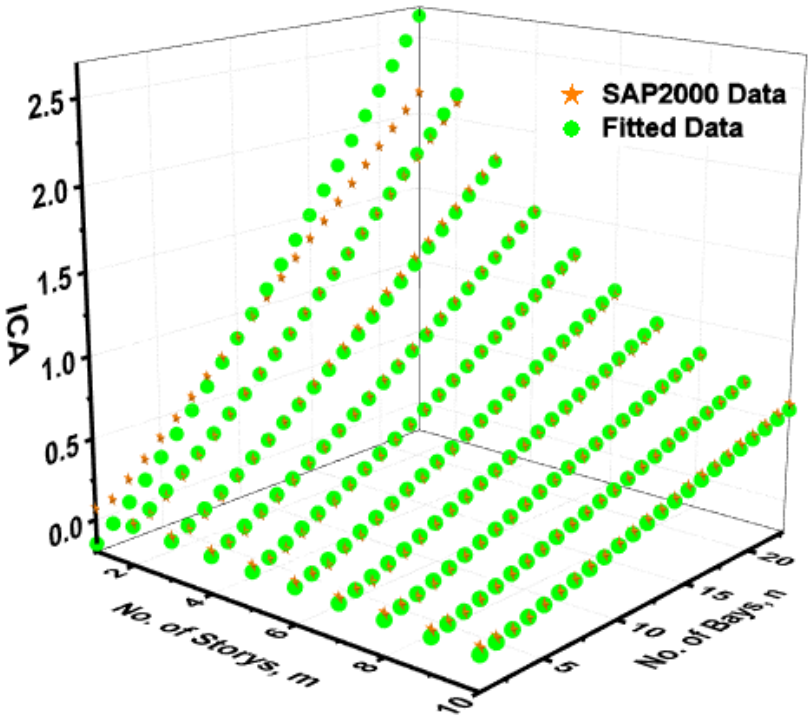

Fig. 5.8. Interior column axial load factor (ICA).

Table 5.12. Regression parameters of ICA (For n≥13 and m≥7).

Constant	Value	Standard Error	Standard Deviation	Coefficient of Variation
z0	0.0924	0.01729		
A	0.03787	0.00247		
B	0.99617	0.01844		
C	-0.01631	0.01571		
D	0.31959	0.20285	0.00355	0.0158
E	-0.00971	0.00148		
F	1.09259	0.02034		
G	0.30831	0.0246		

Table 5.13. Correlation Matrix of ICA (For n≥13 and m≥7).

Constant	z0	A	B	C	D	E	F	G
z0	1							
A	-0.641	1						
B	0.095	-0.756	1					
C	-0.988	0.534	0.042	1				
D	-0.953	0.413	0.179	0.986	1			
E	0.818	-0.908	0.426	-0.760	-0.677	1		
F	0.281	-0.864	0.953	-0.155	-0.012	0.629	1	
G	0.820	-0.469	-0.216	-0.851	-0.863	0.778	0.005	1

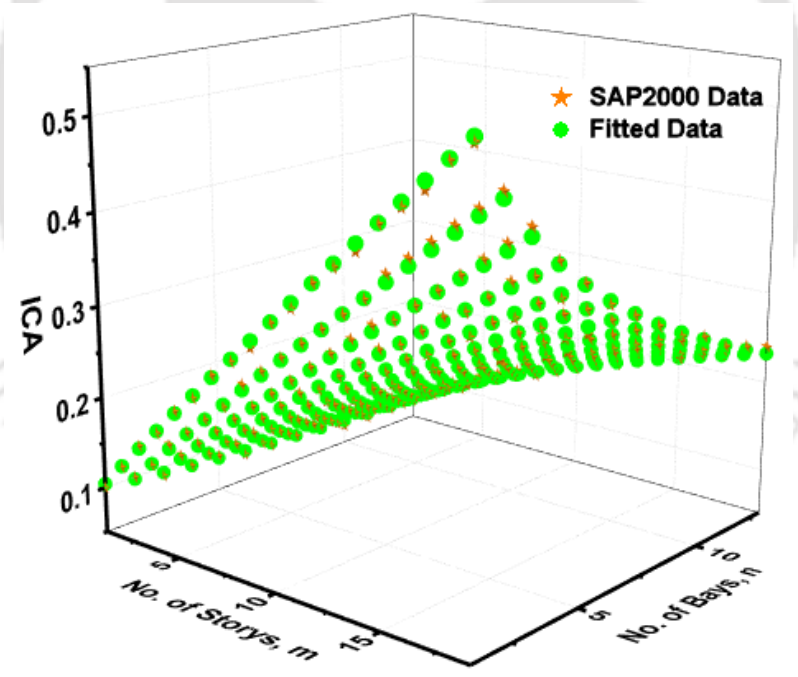

Fig. 5.9. Interior column axial load factor (ICA).

The peak axial load (A_{IC}) in a multi-storey building's interior column, when subjected to horizontal uniform loading, is given by

$$A_{IC} = ICA \times R_u \text{ (kN)} \tag{5.6}$$

Where R_u is the limiting resistance.

Table 5.14 is developed in this study to calculate the shear critical load factors for the interior columns (ICS). As illustrated in Fig. 5.10, a surface plot is created for the recorded data, and the developed probabilistic model's accuracy with SAP2000 data is shown. Tables 5.15 and 5.16 provide the regression parameters, constant values, and correlation matrix for the probabilistic models.

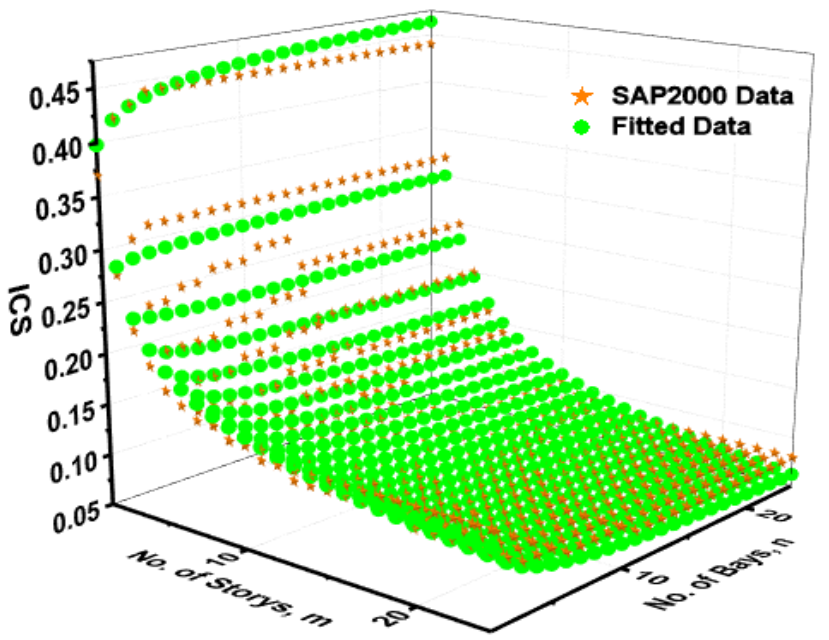

Fig. 5.10. Interior column shear load factor (ICS).

Table 5.14. ICS load factors.

ICS	Remarks
0.16	For n=2 and m=1
0.12	For n=3 to 6 and m=1
0.08	For n≥6 and m=1

$z0 + Bm^C + Dn^E + Fm^C n^E$ For n≥2 and m≥2

Table 5.15. Regression parameters of ICS.

Constant	Value	Standard Error	Standard Deviation	Coefficient of Variation
z0	-0.04864	0.01972		
B	0.54755	0.03504		
C	-0.62031	0.01265		
D	0.12988	0.01769	0.01204	0.0872
E	-0.32785	0.08382		
F	-0.23046	0.0341		

Table 5.16. Correlation Matrix of ICS.

Constant	z0	B	C	D	E	F
z0	1					
B	-0.978	1				
C	-0.205	0.062	1			
D	-0.975	0.978	0.094	1		
E	-0.966	0.965	-0.001	0.940	1	
F	-0.957	-0.957	-0.024	-0.951	-0.866	1

The peak shear load (V_{IC}) in a multi-storey building's interior column, when subjected to horizontal uniform loading, is given by

$$V_{IC} = ICS \times R_u \text{ (kN)} \tag{5.7}$$

Where R_u is the limiting resistance.

Table 5.17 is developed in this study to calculate the bending critical load factors for interior columns (ICB). As illustrated in Fig. 5.11, a surface plot is created for the recorded data, and the developed probabilistic model's accuracy with SAP2000 data is shown. Tables 5.18 and 5.19 provide the regression parameters, constant values, and correlation matrix for the probabilistic models.

Table 5.17. Load factors of ICB.

ICB	Remarks
0.09	For n=2 and m=1
0.07	For n=3 and m=1
0.05	For n≥4 and m=1
$z0 + Bm^C + Dn^E + Fm^C n^E$	For n≥2 and m≥2

Table 5.18. Regression parameters of ICB.

Constant	Value	Standard Error	Standard Deviation	Coefficient of Variation
z0	0.05963	0.00524		
B	0.12113	0.02239		
C	-0.78069	0.00986		
D	-0.01595	0.004	0.00728	0.0875
E	0.465	0.05799		
F	0.06958	0.01737		

Table 5.19. Correlation Matrix of ICB.

Constant	z0	B	C	D	E	F
z0	1					
B	-0.977	1				
C	-0.086	0.009	1			
D	-0.972	0.982	-0.062	1		
E	-0.953	0.972	0.0005	0.991	1	
F	0.967	-0.989	0.004	-0.995	-0.995	1

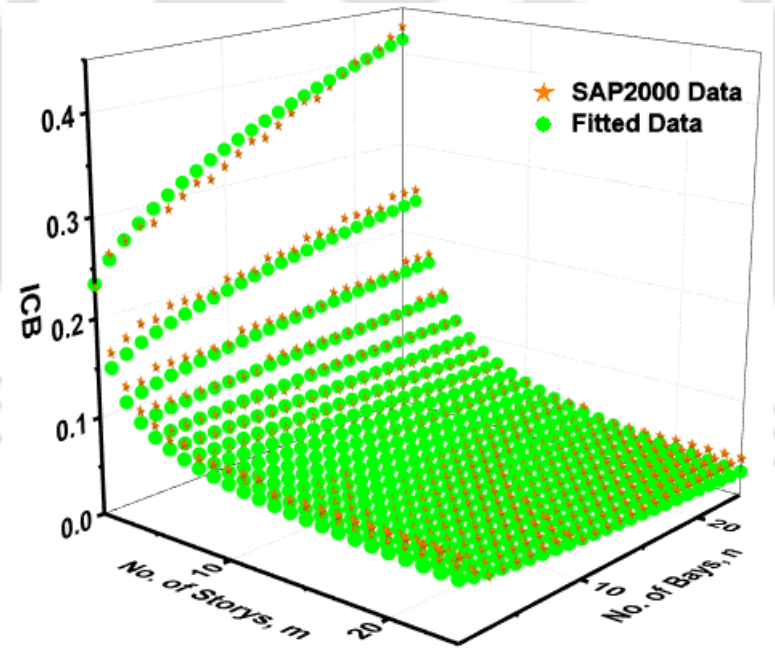

Fig. 5.11. Interior column bending load factor (ICB).

The peak bending moment (M_{IC}) in a multi-storey building's interior column when subjected to horizontal uniform loading is given by

$$M_{IC} = ICB \times R_u \text{ (kN-m)} \tag{5.8}$$

Where R_u is the limiting resistance.

Exterior Beams

Table 5.20 is developed in this study to calculate the axial critical load factors for the exterior beams (EBA). These factors are constant for the rigid frame structure's chosen storeys and bays.

Table 5.20. EBA load factors.

EBA	Remarks
0.27	For n=1 and m≥2
0.35	For n=2 and m≥2
0.42	for n=3 and m≥2
0.5	For n≥4 and m≥2
0.22	For n=1 and m=1
0.29	For n=2 and m=1
0.32	For n=3 and m=1

The peak axial load (A_{EB}) in a multi-storey building's exterior beam, when subjected to horizontal uniform loading, is given by

$$A_{EB} = EBA \times R_u \text{ (kN)} \tag{5.9}$$

Where R_u is the limiting resistance.

Table 5.21 is developed in this study to calculate the shear critical load factors for the exterior beams (EBS). As illustrated in Fig. 5.12, a surface plot is created for the recorded data, and the developed probabilistic model's accuracy with SAP2000 data is shown. Tables

5.22 and 5.23 include the regression parameters, constant values, and correlation matrix for the probabilistic model, respectively.

Table 5.21. EBS load factors.

EBS	Remarks
$-0.055m^2 + 0.517m - 0.326$	For n=1 and m=1 to 5
$z0 + Am^B + Cn^D + Em^F n^G$	For n=2 to 9 and m=1 to 5
0.94	For n=1 and m≥6
0.49	For n=2 and m≥6
0.31	For n=3 and m≥6
0.22	For n=4 and m≥6
0.17	For n=5 and m≥6
0.14	For n=6 and m≥6
0.12	For n=7 and m≥6
0.1	For n≥8 and m≥3
0.13	For n≥10 and m=2
0.01	For n≥10 and m=1

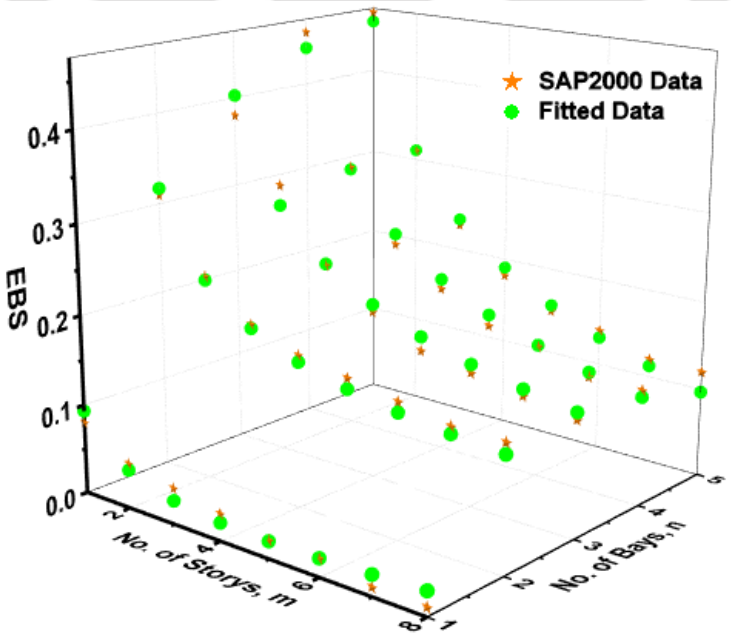

Fig. 5.12. Exterior beam shear load factor (EBS).

Table 5.22. Regression parameters of EBS.

Constant	Value	Standard Error	Standard Deviation	Coefficient of Variation
z0	-82.14144	492.86966		
A	14.01594	89.77991		
B	0.06946	0.24635		
C	152.625	907.03818		
D	0.04512	0.26707	0.01232	0.0712
E	-84.40671	919.99554		
F	0.01262	0.11722		
G	0.07696	0.19549		

Table 5.23. Correlation Matrix of EBS.

Constant	z0	A	B	C	D	E	F	G
z0	1							
A	-0.470	1						
B	0.279	-0.978	1					
C	-0.388	0.995	-0.992	1				
D	0.857	0.049	-0.253	0.139	1			
E	-0.106	-0.826	0.924	-0.874	-0.602	1		
F	-0.323	-0.681	0.817	-0.745	-0.763	0.975	1	
G	0.700	-0.959	0.880	-0.929	0.234	0.635	0.448	1

The peak shear load (V_{EB}) in a multi-storey building's exterior beam, when subjected to horizontal uniform loading, is given by

$$V_{EB} = EBS \times R_u \text{ (kN)} \tag{5.10}$$

Where R_u is the limiting resistance.

Table 5.24 is developed in this study to calculate the bending critical load factors for the exterior beams (EBB). As illustrated in Fig. 5.13, a surface plot is created for the recorded data, and the developed probabilistic model's accuracy with SAP2000 data is shown. Tables 5.25 and 5.26 include the regression parameters, constant values, and correlation matrix for the probabilistic model, respectively.

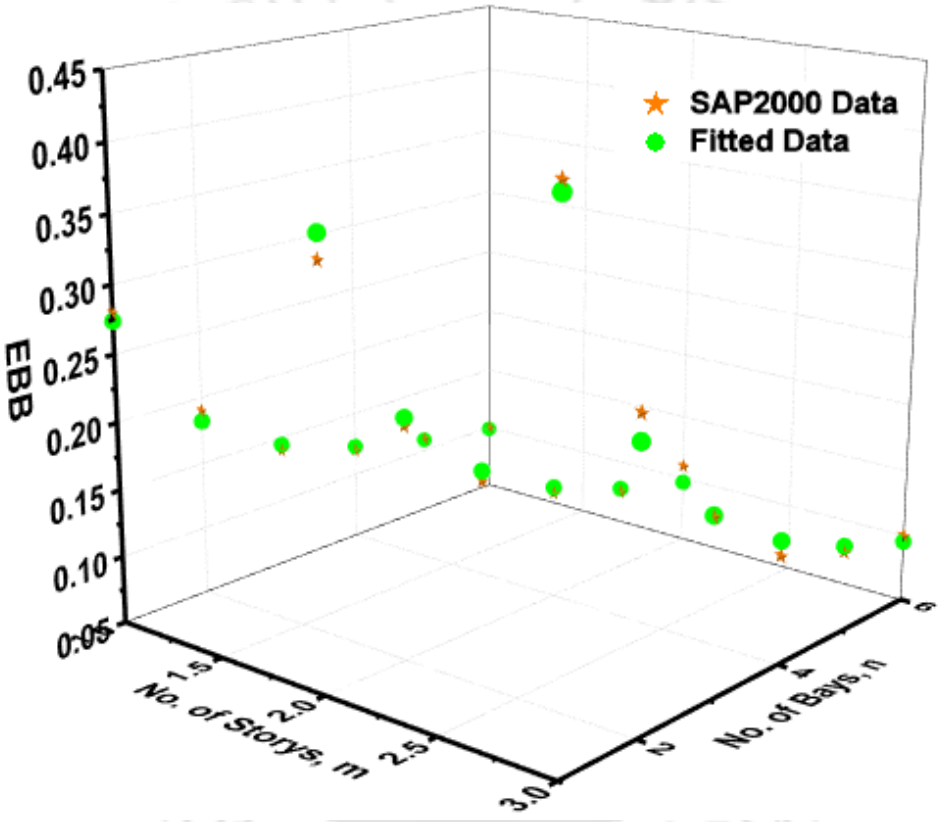

Fig. 5.13. Exterior beam bending load factor (EBB).

Table 5.24. EBB load factors.

EBB	Remarks
0.08	For n=1 and m=1
0.05	For n=2 and m=1
0.02	For n≥3 and m=1
0.47	For n=1 and m≥5
0.27	For n=2 and m≥5
0.18	For n=3 and m≥5
0.13	For n=4 and m≥5
0.1	For n=5 and m≥5
0.08	For n≥6 and m≥5
0.09	For n≥7 and m=2 to 4
$z0 + Bm^C + Dn^E + Fm^C n^E$	For n=1 to 6 and m=2 to 4

Table 5.25. Regression parameters of EBB.

Constant	Value	Standard Error	Standard Deviation	Coefficient of Variation
z0	-17.5976	1014.79994		
B	17.61379	1014.79017		
C	-0.00389	0.2243		
D	52.71269	3017.09604	0.01029	0.0572
E	-0.63496	0.12212		
F	-52.455	3017.0872		

Table 5.26. Correlation Matrix of EBB.

Constant	z0	B	C	D	E	F
z0	1					
B	-1	1				
C	-0.999	0.999	1			
D	-0.999	0.999	1	1		
E	-0.411	0.411	0.407	0.408	1	
F	0.999	-0.999	-1	-1	-0.408	1

The peak bending moment (M_{EB}) in a multi-storey building's exterior beam when subjected to horizontal uniform loading is given by

$$M_{EB} = EBB \times R_u \text{ (kN-m)} \tag{5.11}$$

Where R_u is the limiting resistance.

Interior Beams

Table 5.27 is developed in this study to calculate the axial critical load factors for the interior beams (IBA). As illustrated in Fig. 5.14, a surface plot is created for the recorded data, and the developed probabilistic model's accuracy with SAP2000 data is shown. Tables 5.28 and 5.29 show the regression parameters, constant values, and correlation matrix for the probabilistic model.

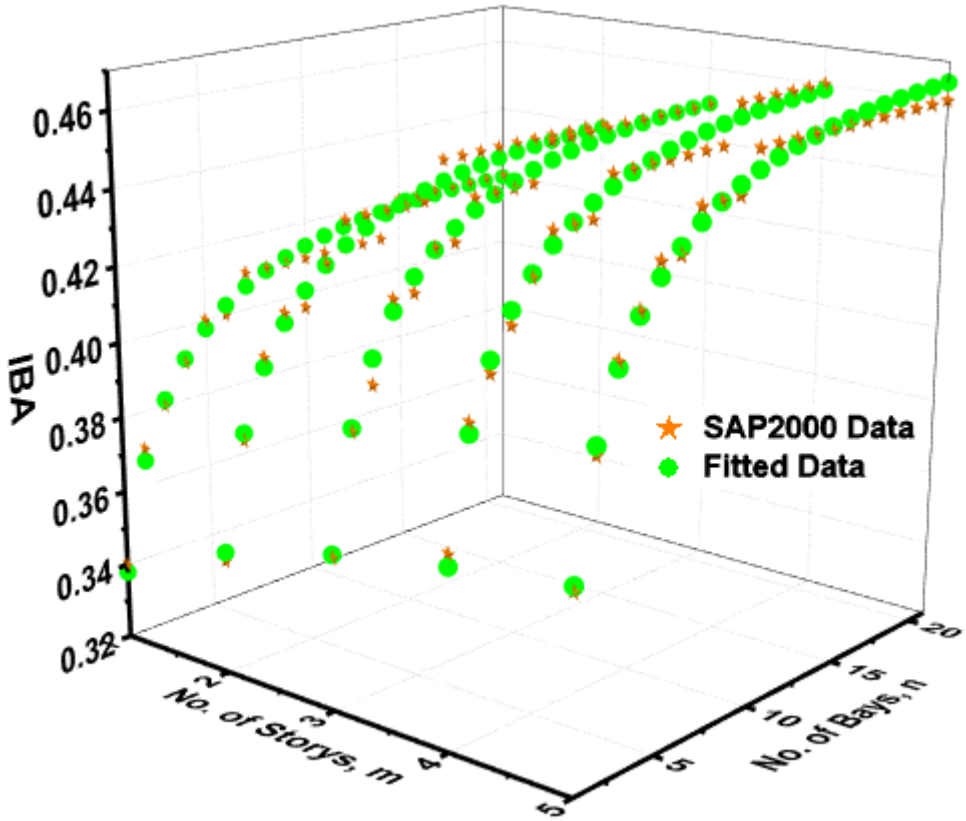

Fig. 5.14. Interior beam axial load factor (IBA).

Table 5.27. IBA load factors.

IBA	Remarks
0.23	For n=3 to 5 and m=1
0.45	For n≥6 and m≥7
0.27	For n≥6 and m=1
0.25	For n=3 and m≥2
0.33	For n=4 and m≥2
0.39	For n=5 and m≥7
$z0 + Am^B + Cn^D + Em^F n^G$	For n≥4 and m=2 to 6

Table 5.28. Regression parameters of IBA.

Constant	Value	Standard Error	Standard Deviation	Coefficient of Variation
z0	-4.55171	216.8006		
A	4.29264	217.13032		
B	0.00327	0.16819		
C	1.37727	16.17199		
D	0.16585	0.58759	0.00317	0.0074
E	-0.78039	16.79134		
F	-0.00876	0.15617		
G	0.23651	0.6294		

Table 5.29. Correlation Matrix of IBA

Constant	z0	A	B	C	D	E	F	G
z0	1							
A	-0.999	1						
B	0.999	-0.999	1					
C	-0.486	0.488	-0.516	1				
D	-0.490	0.493	-0.520	0.983	1			
E	0.487	-0.489	0.518	-0.999	-0.988	1		
F	-0.488	0.490	-0.519	0.998	-0.991	-0.999	1	
G	0.478	-0.480	0.509	-0.996	-0.965	0.993	-0.990	1

The peak axial load (A_{IB}) in a multi-storey building's interior beam, when subjected to horizontal uniform loading, is given by

$$A_{IB} = IBA \times R_u \text{ (kN)} \tag{5.12}$$

Where R_u is the limiting resistance.

Table 5.30 is developed in this study to calculate the shear critical load factors for the interior beams (IBS). As illustrated in Fig. 5.15, a surface plot is created for the recorded data, and the developed probabilistic model's accuracy with SAP2000 data is shown. Tables 5.31 and 5.32 include the regression parameters, constant values, and correlation matrix for the probabilistic model, respectively.

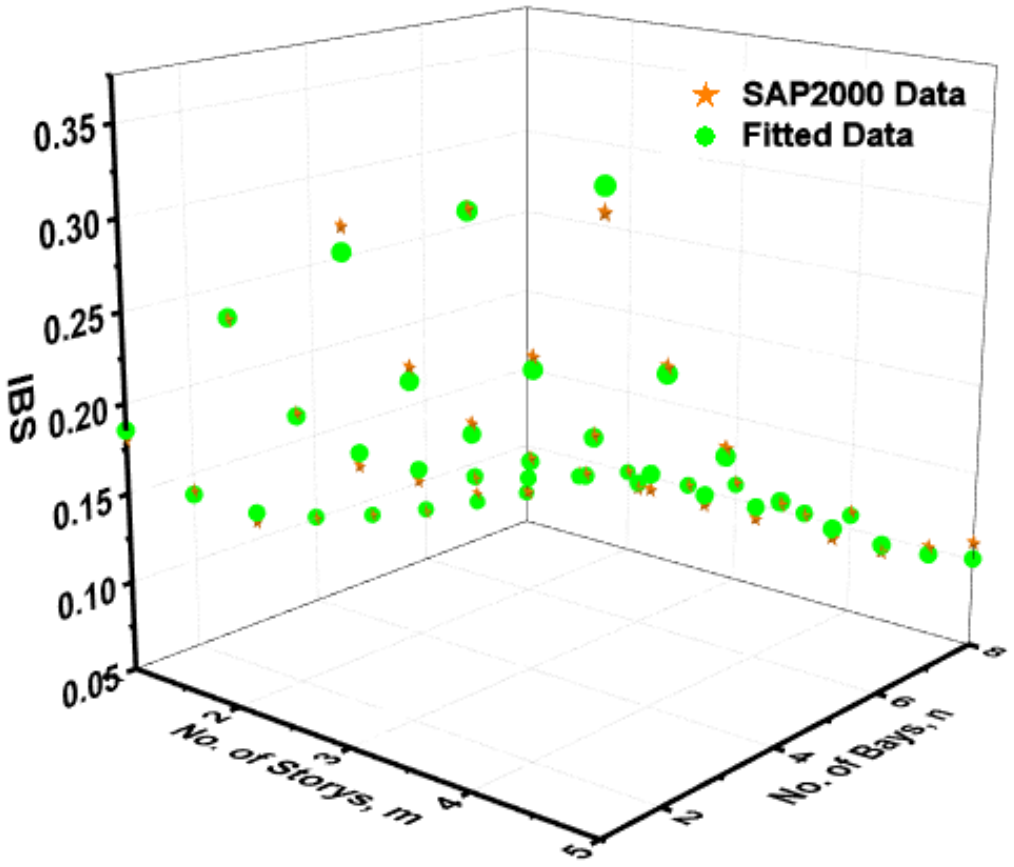

Fig. 5.15. Interior beam shear load factor (IBS).

Table 5.30. IBS load factors.

IBS	Remarks
0.05	For n=3 and m=1
0.03	For n≥4 and m=1
0.09	For n≥12 and m≥2
0.39	For n=4 and m≥7
0.28	For n=5 and m≥7
0.23	For n=6 and m≥7
0.15	For n=7 to 11 and m≥7
$z0 + Am^B + Cn^D + Em^F n^G$	For n=4 to 11 and m=2 to 6

Table 5.31. Regression parameters of IBS.

Constant	Value	Standard Error	Standard Deviation	Coefficient of Variation
z0	-0.11817	0.06906		
A	5.85449	120.21075		
B	0.63771	0.22414		
C	0.04377	0.06588		
D	-0.95948	1.1398	0.006202	0.0369
E	-5.59474	120.20007		
F	0.64908	0.21198		
G	0.00672	0.14149		

Table 5.32. Correlation Matrix of IBS

Constant	z0	A	B	C	D	E	F	G
z0	1							
A	0.213	1						
B	0.888	0.568	1					
C	0.687	-0.430	0.472	1				
D	0.820	-0.005	0.766	0.885	1			
E	-0.214	-1	-0.569	0.430	0.004	1		
F	0.682	-0.521	0.405	0.969	0.801	0.520	1	
G	-0.233	-0.999	-0.586	0.411	-0.015	0.999	0.502	1

The peak shear load (V_{IB}) in a multi-storey building's interior beam, when subjected to horizontal uniform loading, is given by

$$V_{IB} = IBS \times R_u \text{ (kN)} \tag{5.13}$$

Where R_u is the limiting resistance.

Table 5.33 is developed in this study to calculate the bending critical load factors for the interior beams (IBB). As illustrated in Fig. 5.16, a surface plot is created for the recorded data, and the developed probabilistic model's accuracy with SAP2000 data is shown. Tables 5.34 and 5.35 include the regression parameters, constant values, and correlation matrix for the probabilistic model, respectively.

Table 5.33. IBB load factors.

IBB	Remarks
0.02	For n≥3 and m=1
0.05	For n≥9 and m≥2
0.2	For n=3 and m≥7
0.15	For n=4 to 6 and m≥7
0.08	For n=7 to 8 and m≥7
$z0 + Am^B + Cn^D + Em^F n^G$	For n=3 to 8 and m=2 to 6

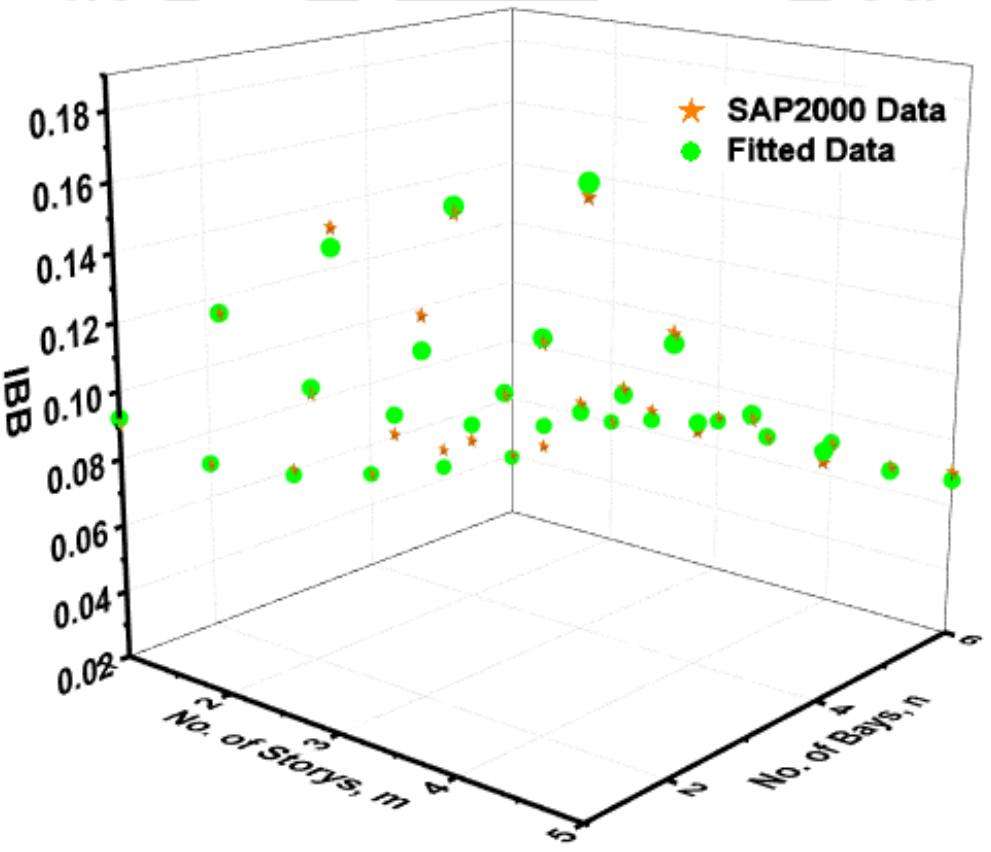

Fig. 5.16. Interior beam bending load factor (IBB).

Table 5.34. Regression parameters of IBB.

Constant	Value	Standard Error	Standard Deviation	Coefficient of Variation
z0	-0.1008	0.18046		
A	2.19648	104.05034		
B	0.84653	0.54089		
C	0.10425	0.21179		
D	-0.20389	0.4983	0.00394	0.0421
E	-2.10776	104.06634		
F	0.85898	0.3522		
G	0.00554	0.27032		

Table 5.35. Correlation Matrix of IBB.

Constant	z0	A	B	C	D	E	F	G
z0	1							
A	-0.742	1						
B	-0.742	0.810	1					
C	-0.966	0.701	0.846	1				
D	-0.986	0.826	0.802	0.957	1			
E	0.742	-1	-0.810	-0.701	-0.826	1		
F	0.132	-0.466	0.140	0.093	-0.184	0.465	1	
G	0.745	-0.999	-0.818	-0.7	-0.829	0.999	0.453	1

The peak bending moment (M_{IB}) in a multi-storey building's interior beam when subjected to horizontal uniform loading is given by

$$M_{IB} = IBB \times R_u \text{ (kN-m)} \tag{5.14}$$

Where R_u is the limiting resistance.

The ultimate strength of the members operating as beam-columns determines the frame's overall resistance. The preliminary sizing of the members can be done using the criteria described in Chapter 7 for beams and columns after the peak values of the forces and moments have been computed throughout the frame.

5.4 Discussion

By considering software-based case studies utilising SAP2000 software, this chapter explored the critical load factors of rigid frame structures subject to lateral uniform loads (blast and wind). Probabilistic models are developed for the critical load factors. The significant standard deviation (σ), coefficient of variation (CV), and coefficient of determination (R^2) all indicate the accuracy of the developed probabilistic models. These probabilistic models can be used to calculate the critical loads applied to the members in a rigid frame (beams and columns). The rigid frame members' peak loads are calculated using critical load factors. Peak loads are utilised to design key load-bearing elements in multi-storey rigid frame constructions. These peak loads can also be employed to prevent multi-story rigid frame structures from collapsing. These peak loads are helpful in keeping the DCR (Demand-Capacity Ratio) values within unity, preventing progressive collapse. This research develops the easy to use and accurate probabilistic models to calculate the peak loads acting on the members in a rigid frame.

CHAPTER 6 DEVELOPMENT OF SHAPE FUNCTION FOR SDOF ANALYSIS OF MULTI-STOREY BUILDINGS

6.1 General

Standard blast resistant design guidelines such as DoD, TM5-1300, and UFC 2005, among others, established a solid analytical framework for equivalent SDOF systems subject to blast loads and limited to single-storey frame structures. The mode shape function has been used to create an equivalent single degree of freedom system for a multi-storey building. In the literature, the mode shape function of multi-story buildings has only been limited to the first mode. This chapter develops a modified shape function of multi-storey buildings using the shape function of an existing cantilever beam. The developed modified mode shape function can be used to accurately predict the response of a multi-story building subject to blast loading. The mode shape function of the building is formulated as a function of the mode number.

Any arbitrary function that meets the boundary criteria can be used to describe the deformed structure. However, the success of this technique in practice will be determined by how closely the assumed shape function approximates the dynamic system's real displacements. For mid-rise buildings, most seismic building codes employ the straight-line shape function. After obtaining the dynamic response in terms of the generalised coordinate, the displacements in the structure have been determined. The system can vibrate in any mode or a mixture of modes depending on the initial conditions or external forcing stimulation. Each mode has its frequency, referred to as a natural frequency. Natural frequencies are as many as natural modes.

6.2 Dynamic Analysis of MDOF Systems

A finite number of displacement coordinates determine the displacement configuration in MDOF systems. Because structures are continuous systems with an endless number of

degrees of freedom, the true response of a multi-degree of freedom system can only be determined by analysing the inertia effects at each mass particle.

Eigen Modal Analysis

The number of modes in an idealised MDOF system equals the number of masses. Each mode has its natural period of vibration, which is moulded by a line connecting the deflected masses into a distinct mode. In general, six to ten modes in each direction are considered sufficient for conventional buildings (Paz and Halperson 1980). The undamped system's inherent frequencies and modes fulfil the algebraic eigen problem and are given by

$$[\mathrm{K} - w_r^2 M]\phi_r = 0 \tag{6.1}$$

giving the eigenpairs (w_r^2, ϕ_r), r = 1, 2, …, n. The modes ϕ_r are assumed to have been normalized, and the modal masses M_r and modal stiffnesses K_r calculated using

$$\begin{aligned} M_r &= \phi_r^T M \phi_r \\ K_r &= \phi_r^T K \phi_r = w_r^2 M_r \end{aligned} \tag{6.2}$$

Where M, and K are system mass and stiffness matrices, respectively. For each mode of vibration, the polynomial's solution yields one real root. As a result, n natural frequencies are derived for a system with n degrees of freedom. The fundamental frequency is the least obtained value, and the matching mode is the fundamental or initial mode. These formulas apply to both rigid-body and flexible modes, assuming any exist. Any standard structural dynamic book will have more information on this method (Paz and Halperson 1980).

Equivalent SDOF Analysis Using Shape Function

The building's mass is considered to be concentrated at several levels (floors and roof), each of which is rigid in its plane; consequently, only horizontal displacements are feasible in

such a structure (Paz and Halperson 1980). The lateral displacement shape y (x, t) is specified in terms of a single generalised coordinate (u(t)) to model the structure as a single degree of freedom (Fig. 6.1) by

$$y(x,t) = \phi(x)u(t) \tag{6.3}$$

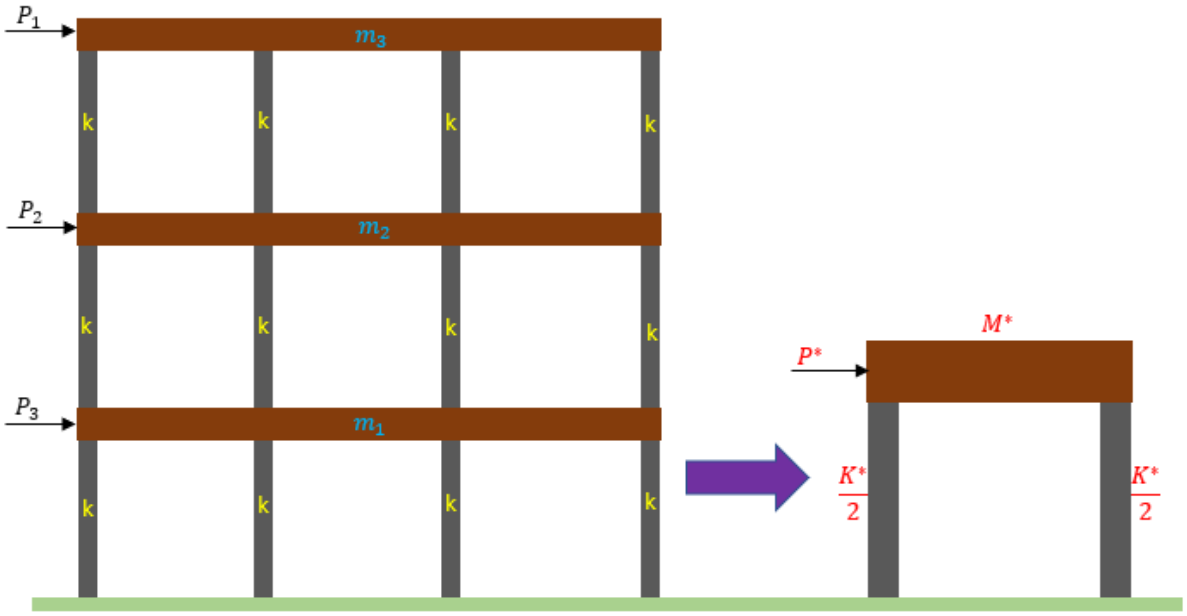

Fig. 6.1. Equivalent SDOF system of the multi-storey building.

The generalized coordinate u(t) is selected as the lateral displacement at the building's top level, which requires that the shape function be assigned a unit value at that level; that is, $\phi(H)$ = 1.0, where H is the height of the building. The equation of motion for the generalized undamped single-degree-of-freedom system is obtained by

$$M^*\ddot{u}(t) + K^*u(t) = P^*(t) \tag{6.4}$$

where M^*, K^*, and $P^*(t)$ are, respectively, the generalized mass, generalized stiffness, and generalized force, and are given for a discrete system, by

$$M^* = \sum_{i=1}^{N} m_i \Phi_i^2$$

$$K^* = \sum_{i=1}^{N} k_i \Delta\Phi_i^2$$

$$P^*(t) = \sum_{i=1}^{N} P_i(t)\Phi_i \tag{6.5}$$

$$H^* = \frac{\sum_{i=1}^{N} m_i \Phi_i h_i}{\sum_{i=1}^{N} m_i \Phi_i}$$

The natural frequency for the generalized system is given as follows;

$$w_n = \sqrt{\frac{K^*}{M^*}} \tag{6.6}$$

where the upper index N in the summations is equal to the number of storeys or levels in the building. m_i, k_i and $P_i(t)$ are, respectively, the mass, stiffness and the external force at the ith level of the building. The various expressions for the equivalent parameters are obtained by equating the kinetic energy, potential energy, and the virtual work done by the damping forces and external forces in the actual structure with the corresponding expressions for the generalized single-degree-of-freedom system. The relative displacement $\Delta\Phi_i$ between two consecutive levels of the building is given by

$$\Delta\Phi_i = \Phi_i - \Phi_{i-1} \tag{6.7}$$

with $\Delta\Phi_0 = 0$ at the ground level, and the shape function of multi-story buildings is limited to the first mode only. Any standard structural dynamics book will have more information on this method (Paz and Halperson 1980).

6.3 Modified Shape Function

A cantilever beam system can deflect in an endless number of shapes; hence it must be regarded as an infinite-degree-of-freedom system for precise analysis. However, by constraining the deflections of the beam to a single shape function that approximates the fundamental vibration mode, it is possible to achieve approximate findings that are accurate to a useful degree for the lowest (also known as fundamental) natural frequency. The mode shape will be bending, shear, or bending and shear, depending on the structural system. Eq. (6.8) shows the bending mode of a cantilever beam as follows:

$$\phi(x) = (\cosh(a_n x) - \cos(a_n x)) - k_n(\sinh(a_n x) - \sin(a_n x)) \tag{6.8}$$

Where $k_n = \frac{\cosh(a_n L) + \cos(a_n L)}{\sinh(a_n L) + \sin(a_n L)}$, L is the length of the cantilever beam, and the constant "$a_n L$" can be solved from the frequency equation $\cosh(a_n L) + \cos(a_n L) + 1 = 0$. The constant values for the first six modes are given in Table 6.1. See the cantilever shape function page for further information (Chopra 2012).

The substantial bending stiffness of the horizontal elements in multi-storey shear buildings prevents significant rotations in the beam-column connections. As a result, the structure's horizontal strength is only characterised by lateral displacements. The structures with the aforementioned features are referred to as shear type systems in dynamic analysis because their global behaviour is dictated by shear deformation. In order to adapt the cantilever shape function for the shear buildings, $\phi(x)$ and the constant "$a_n L$" are redefined.

Replace the terms $\phi(x)$, k_n and "$a_n L$" with $\phi(z)$, B_n and "$S_n H$" to define the shape function for the shear building. The generalized coordinate is selected as the lateral displacement at the top level of the building, which requires that the shape function be assigned

a unit value at that level; that is, $\phi(H)$ = 1.0, where H is the height of the building. To achieve this, divide the equation (6.8) by $\phi(H)$ (since $\phi(\mathrm{L}) > 1$ for cantilever beam), and represent the modified equation with $\Phi(\mathrm{z})$ as follows:

$$\phi(\mathrm{z}) = (\cosh(\mathrm{S}_n\mathrm{z}) - \cos(\mathrm{S}_n\mathrm{z})) - B_n(\sinh(\mathrm{S}_n\mathrm{z}) - \sin(\mathrm{S}_n\mathrm{z})) \tag{6.9}$$

$$\Phi(\mathrm{z}) = \frac{\phi(\mathrm{z})}{\phi(\mathrm{H})} = \frac{(\cosh(\mathrm{S}_n\mathrm{z}) - \cos(\mathrm{S}_n\mathrm{z})) - B_n(\sinh(\mathrm{S}_n\mathrm{z}) - \sin(\mathrm{S}_n\mathrm{z}))}{\phi(\mathrm{H})} \tag{6.10}$$

Where $B_{\mathrm{n}} = \frac{\cosh(\mathrm{S}_n H) + \cos(\mathrm{S}_n H)}{\sinh(\mathrm{S}_n H) + \sin(\mathrm{S}_n H)}$ and S_n is the mode shape factor defined by the equation (6.11). The values of the constant "$\mathrm{S}_n\mathrm{H}$" for the first six modes are given in Table 6.1. The first six modes generated from the modified shape function are shown in Fig. 6.2.

$$S_n = \frac{(2.836 \times \text{Mode Number} + 0.2594)}{Height\ of\ building(H)} \tag{6.11}$$

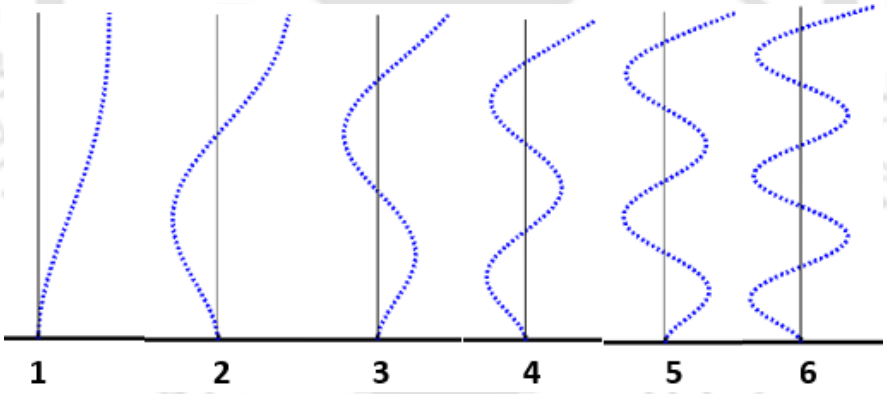

Fig. 6.2. Free vibration modes generated from the modified mode shape function.

Table 6.1. Cantilever shape function vs modified shape function

Mode Number	Cantilever beam ($a_n L$)	Shear building ($S_n H$)
1	1.8751	3.115
2	4.6941	6.081
3	7.8548	8.617
4	10.996	11.496
5	14.137	14.425
6	17.279	17.388
n	$\cosh(a_n L) + \cos(a_n L) = -1$	$(2.836 \times n + 0.2594)$

6.3.1 Validation

SAP2000 software has frequently been used by practising engineers because of its user-friendly graphical user interface, quick modelling choices, and post-processing features (Li et al. 2019). A 10-storey, 5-bay RC building is modelled with tied joints to ensure rigidity at the joints to test the modified mode shape function, and the model details are presented in Fig. 6.3. According to Indian requirements, all support conditions are fixed as they would be in actual construction. The software estimated self-weight manually (Parthasarathi et al., 2019). A two-dimensional finite element is a planar frame element. Both local and global coordinates are used to express it. Bending moment, shear force, and axial force are the internal stress resultants at a cross-section of a planar frame member (Baylot and Bevins, 2007; Jayasooriya et al., 2011; Shi Yanchao et al., 2010). The validation method is derived and evaluated statistically using Eigen modal analysis. Fig. 6.4 depicts the numerical results. Table 6.2 contains the validated results.

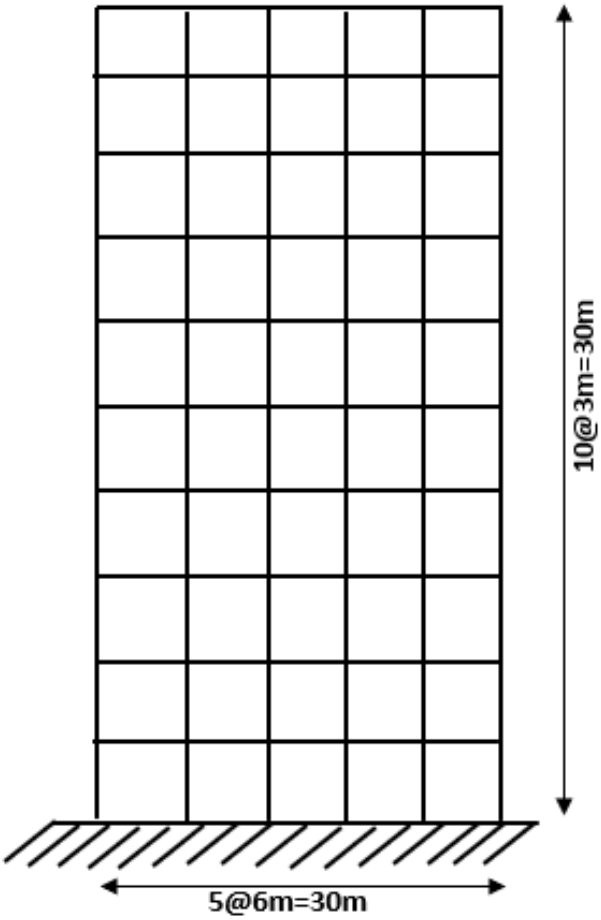

Dimensions of model

Beams = 0.4m x 0.7m

Columns = 0.4m x 0.4m

Story height = 3m

Story width = 6m

I_c = 0.00213m^4

I_b = 0.0114m^4

E = 31.62x10^{6}kN/m^2

No. stories (m) = 10

No. bays (n) = 5

Fig. 6.3. A 10-storey, 5-bays RC rigid frame building.

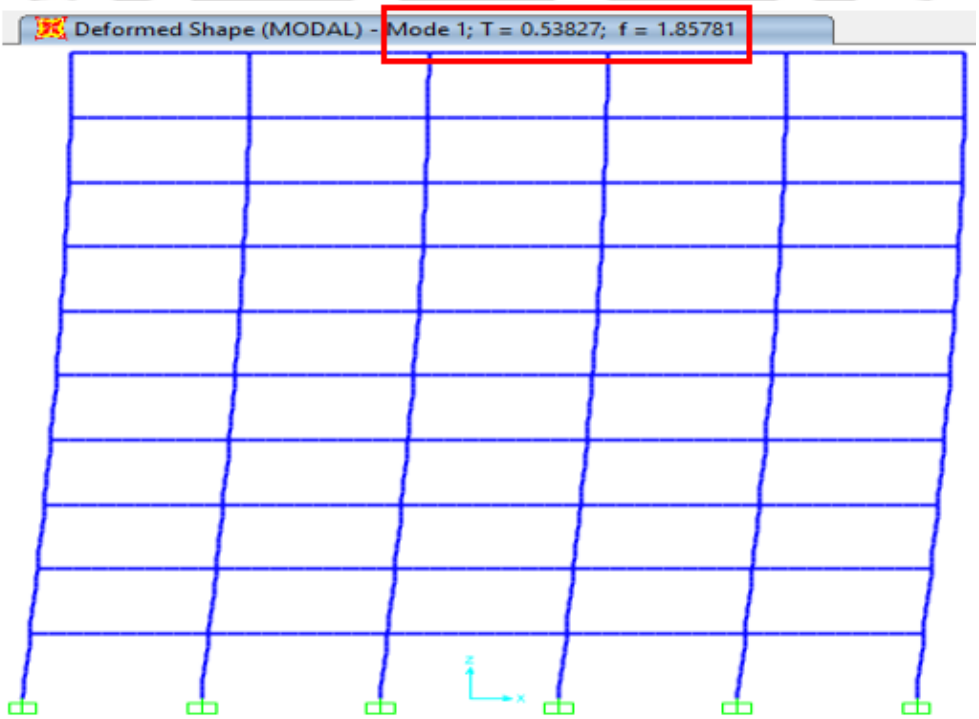

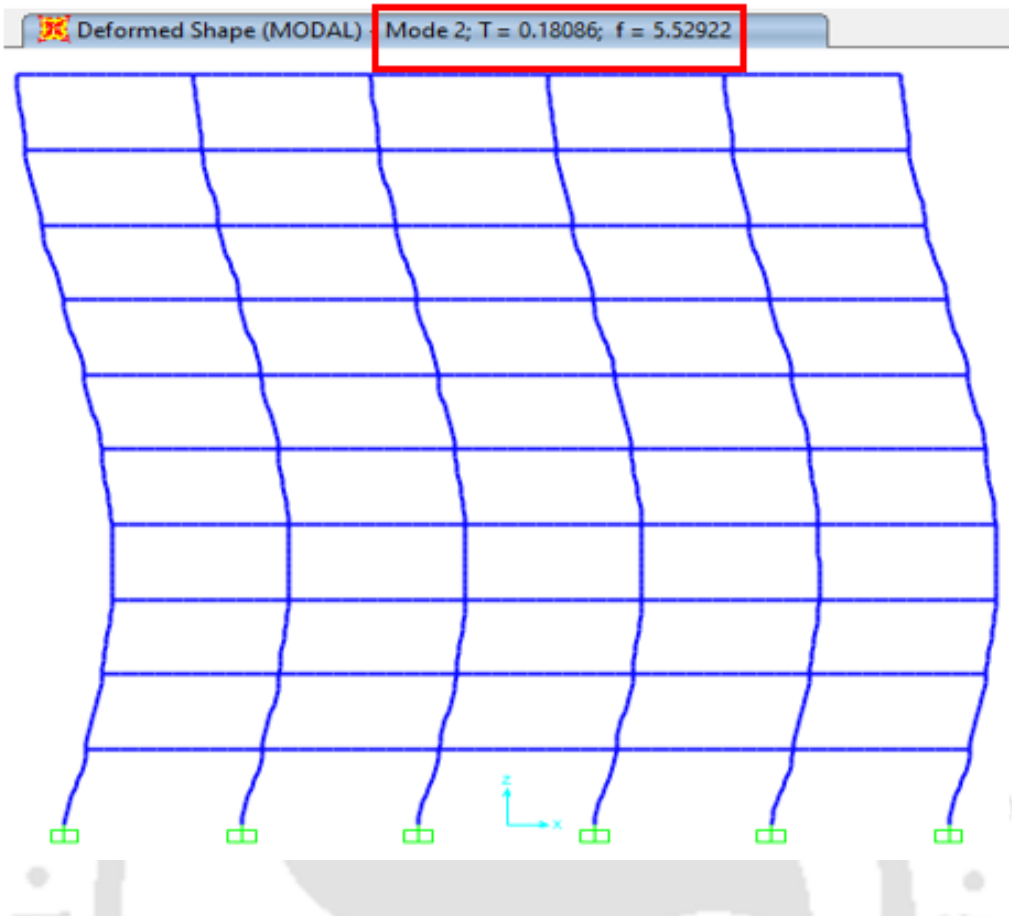
Deformed Shape (MODAL)
Mode 2; T = 0.18086; f = 5.52922

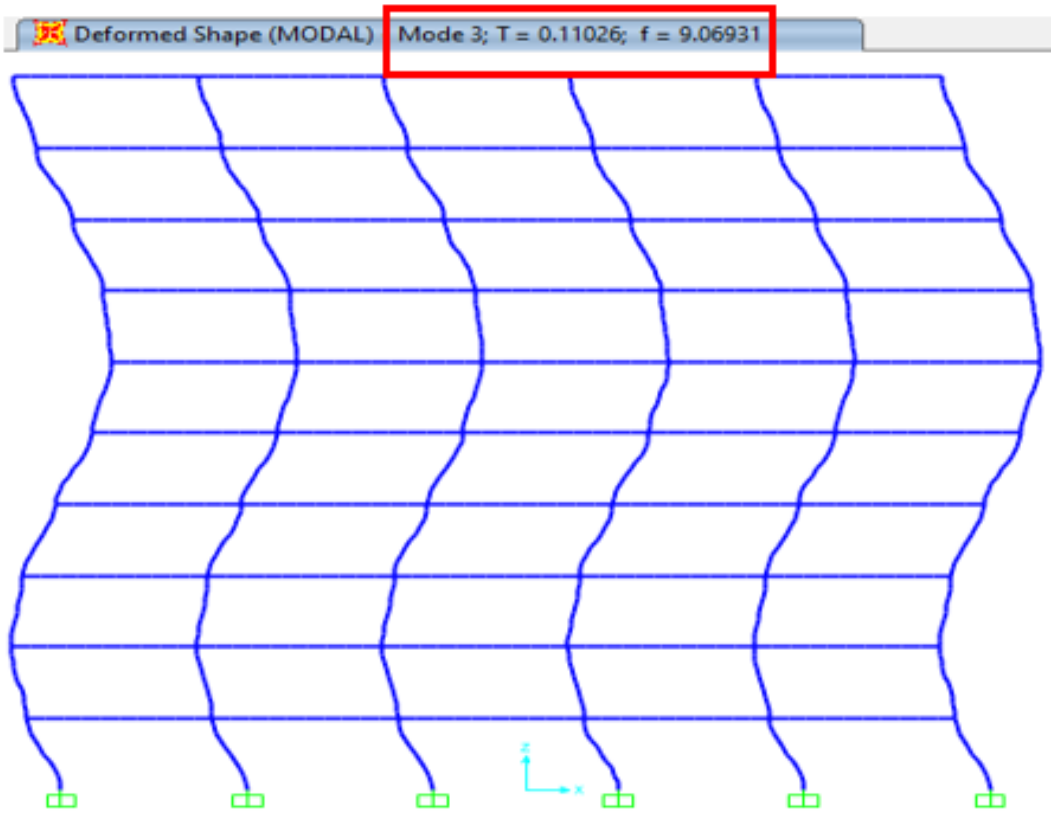
Deformed Shape (MODAL)
Mode 3; T = 0.11026; f = 9.06931

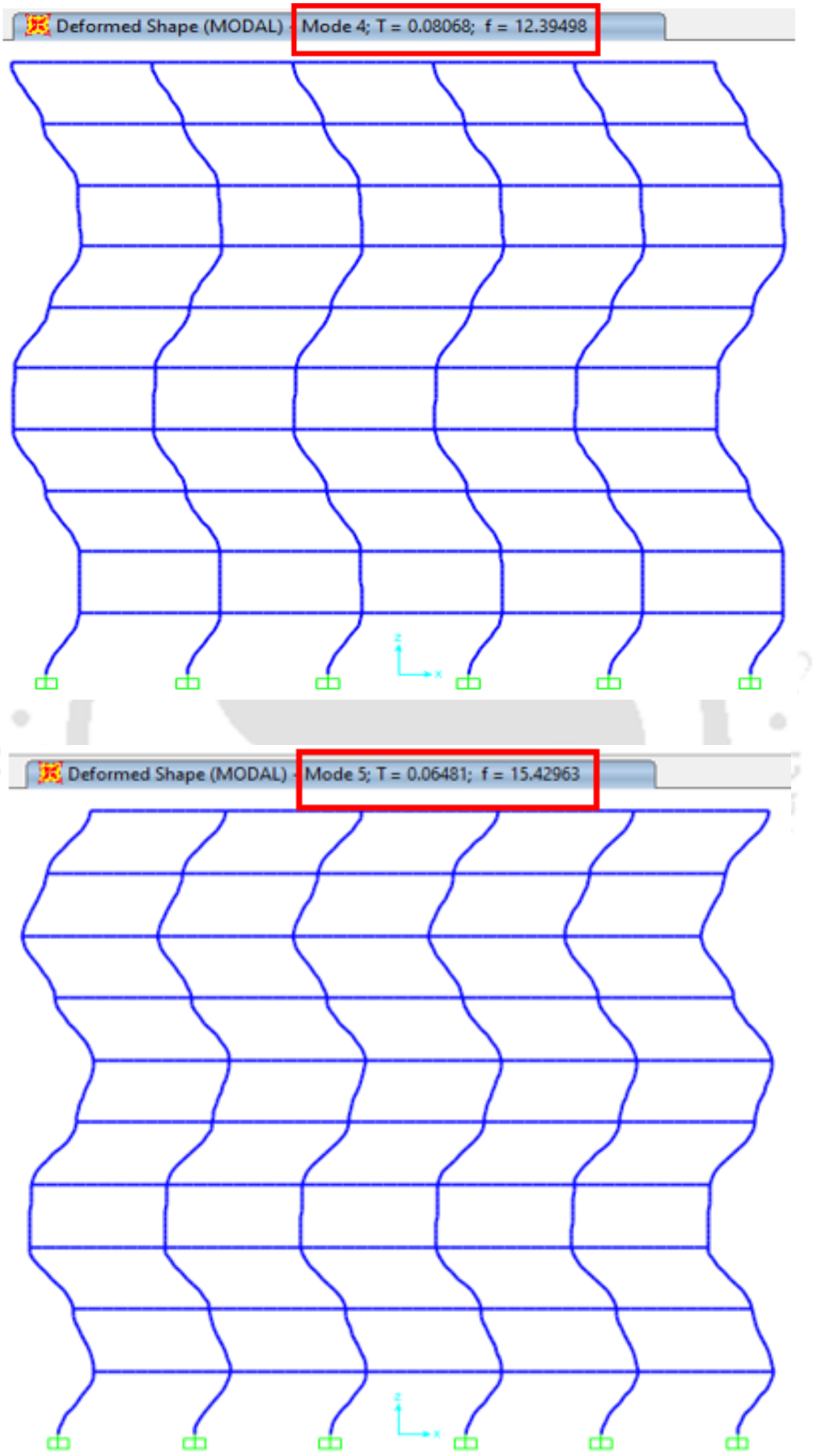
Deformed Shape (MODAL) - Mode 4; T = 0.08068; f = 12.39498
Deformed Shape (MODAL) - Mode 5; T = 0.06481; f = 15.42963

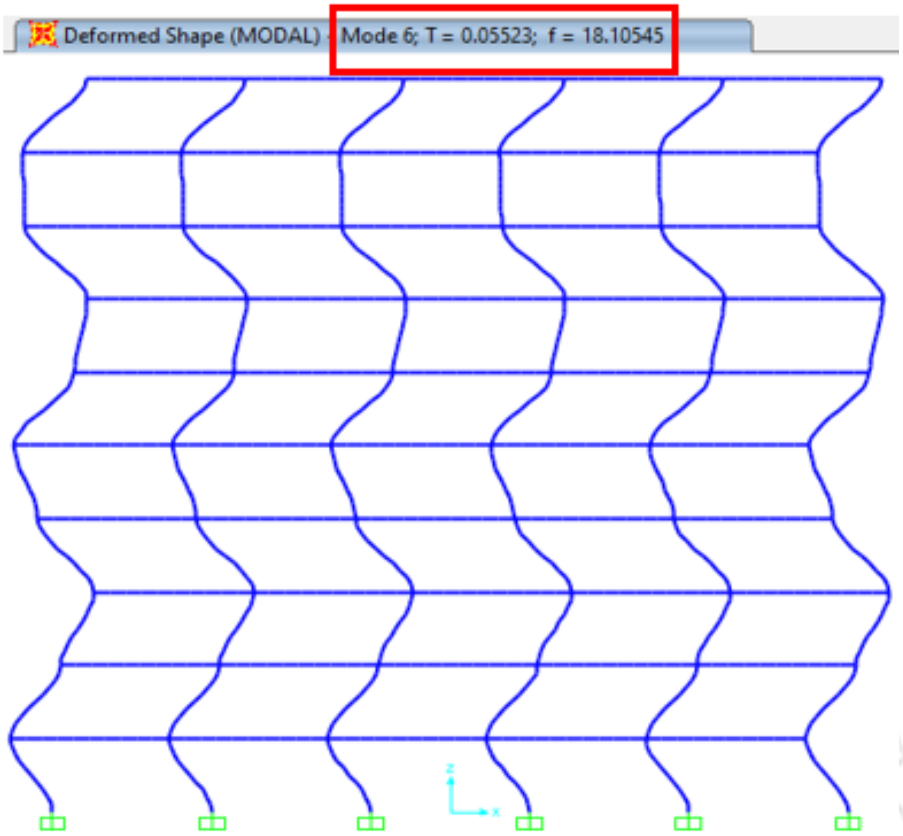

Fig. 6.4. The first 6 modes of the 10-story, 5-bays RC rigid frame.

Table 6.2. The validation results of the modified shape function

Analysis Method	Time period (T) of the building model (sec)					
	Mode 1	Mode 2	Mode 3	Mode 4	Mode 5	Mode 6
Modified Shape Function	0.48849	0.18054	0.11026	0.08086	0.06481	0.05523
Eigen Modal Analysis	0.53160	0.17820	0.10820	0.07880	0.06300	0.05350
SAP2000 Software	0.53827	0.18086	0.11026	0.08068	0.06481	0.05523

Table 6.2 shows that the results of the modified shape function, the Eigen technique and SAP2000 are very similar. In the first mode, the modified shape function has a relative inaccuracy of 9.25 percent, and all subsequent modal values are closer to existing approaches. As a result, the modified shape function can be utilised to convert multi-storey buildings into

equivalent SDOF shear buildings and perform modal analysis. In the following section, numerical problems are solved using the modified mode shape function, which is utilised to find the maximum response of buildings subject to blast loading in the following example.

6.3.2 Numerical Examples

For the first six modes of the shear buildings, the following are analysed 1) modified mode shape function and 2) normalised Eigen modal analysis for a 10-storey and 5-bays RC structure subject to blast loading, as illustrated in Fig. 6.3. Using the modified mode shape function, the shear building's maximum elastic response is calculated when subjected to blast time history loading. The values for $P_o = 100kN$ ($P_o = p_o$ x tributary area) and $t_d = 0.0029\sec$ are considered.

1. *Modified Mode Shape Function*

   Stiffness of each story;

$$k = 6\times\frac{12EI}{L^3} = 6\times\frac{12\times 31.62\times 10^6\times 0.00213}{3^3} = 179898.46\left(kN/m\right)$$

   Weight and mass of each story level and roof;

$$W = (DL)_{beams} + (DL)_{columns}$$
$$W = (5\times 0.4\times 0.7\times 6\times 25) + (6\times 0.4\times 0.4\times 3\times 25) = 282kN$$
$$W_{roof} = (5\times 0.4\times 0.7\times 6\times 25) + (6\times 0.4\times 0.4\times 1.5\times 25) = 246kN$$
$$m_1 = m_2 = m_3 = ... = m_9 = \frac{W}{9.8} = \frac{282}{9.8} = 28.78(\text{kN}.s^2/m)$$
$$\text{m}_{10} = \frac{W_{roof}}{9.8} = \frac{246}{9.8} = 25.10(\text{kN}.s^2/m)$$

Where $(DL)_{beams}$, and $(DL)_{columns}$ are dead loads of beams and columns, respectively.

The generalized stiffness, mass, and force of the shear buildings are calculated as follows:

Table 6.3. For mode 1: S_n =0.10383 and B_n =0.91289.

Height (H)(m)	Stiffness (k)(kN/m)	Mass (m) (kN-s^2)	Φ_i	$\Delta\Phi_i$	$P_o \times \Phi_i$	$m \times \Phi_i^2$	$k \times \Delta\Phi_i^2$
30	179898.46	25.10	1	0.012168	100	25.10204082	26.63522
27	179898.46	28.78	0.987832133	0.033637	98.783213	28.07949747	203.5453
24	179898.46	28.78	0.95419517	0.068093	95.419517	26.1997689	834.1245
21	179898.46	28.78	0.886102288	0.106606	88.610229	22.59387638	2044.51
18	179898.46	28.78	0.77949647	0.140893	77.949647	17.48442434	3571.157
15	179898.46	28.78	0.638603038	0.16367	63.860304	11.73505131	4819.124
12	179898.46	28.78	0.474932571	0.16896	47.493257	6.490631343	5135.656
9	179898.46	28.78	0.305972442	0.152299	30.597244	2.693938389	4172.751
6	179898.46	28.78	0.153673276	0.110781	15.367328	0.679547361	2207.778
3	179898.46	28.78	0.042892612	0.042893	4.2892612	0.052940499	330.9729

$$P_0^* = \sum P_o \times \Phi_i = 622.37kN$$
$$M^* = \sum m \times \Phi_i^2 = 141.11kN.s^2/m$$
$$K^* = \sum k \times \Delta\Phi_i^2 = 23346.25kN/m$$
$$w_n = \sqrt{\frac{K^*}{M^*}}$$
$$w_1 = \sqrt{\frac{K^*}{M^*}} = \sqrt{\frac{23346.25}{141.11}} = 12.8626rad/\sec$$
$$T_n = \frac{2\pi}{w_n}$$
$$T_1 = \frac{2\pi}{w_1} = \frac{2 \times 3.14}{12.8626} = 0.4885\sec$$

Similarly, calculated for the following five modes and the time period values are given in Table 6.2.

2. *Normalized Eigen Modal Analysis*

$$M = \begin{pmatrix} 25.10 & 0 & 0 & 0 & 0 & 0 & 0 & 0 & 0 & 0 \\ 0 & 28.78 & 0 & 0 & 0 & 0 & 0 & 0 & 0 & 0 \\ 0 & 0 & 28.78 & 0 & 0 & 0 & 0 & 0 & 0 & 0 \\ 0 & 0 & 0 & 28.78 & 0 & 0 & 0 & 0 & 0 & 0 \\ 0 & 0 & 0 & 0 & 28.78 & 0 & 0 & 0 & 0 & 0 \\ 0 & 0 & 0 & 0 & 0 & 28.78 & 0 & 0 & 0 & 0 \\ 0 & 0 & 0 & 0 & 0 & 0 & 28.78 & 0 & 0 & 0 \\ 0 & 0 & 0 & 0 & 0 & 0 & 0 & 28.78 & 0 & 0 \\ 0 & 0 & 0 & 0 & 0 & 0 & 0 & 0 & 28.78 & 0 \\ 0 & 0 & 0 & 0 & 0 & 0 & 0 & 0 & 0 & 28.78 \end{pmatrix}$$

$$K = 10^5 \times \begin{pmatrix} 3.5980 & -1.7990 & 0 & 0 & 0 & 0 & 0 & 0 & 0 & 0 \\ -1.7990 & 3.5980 & -1.7990 & 0 & 0 & 0 & 0 & 0 & 0 & 0 \\ 0 & -1.7990 & 3.5980 & -1.7990 & 0 & 0 & 0 & 0 & 0 & 0 \\ 0 & 0 & -1.7990 & 3.5980 & -1.7990 & 0 & 0 & 0 & 0 & 0 \\ 0 & 0 & 0 & -1.7990 & 3.5980 & -1.7990 & 0 & 0 & 0 & 0 \\ 0 & 0 & 0 & 0 & -1.7990 & 3.5980 & -1.7990 & 0 & 0 & 0 \\ 0 & 0 & 0 & 0 & 0 & -1.7990 & 3.5980 & -1.7990 & 0 & 0 \\ 0 & 0 & 0 & 0 & 0 & 0 & -1.7990 & 3.5980 & -1.7990 & 0 \\ 0 & 0 & 0 & 0 & 0 & 0 & 0 & -1.7990 & 3.5980 & -1.7990 \\ 0 & 0 & 0 & 0 & 0 & 0 & 0 & 0 & -1.7990 & 1.7990 \end{pmatrix}$$

The natural frequencies and normalized mode shapes of the model;

$$[\mathrm{K} - w_r^2 M] = 0 \qquad (6.40)$$

$$w_n = \begin{pmatrix} 11.81 & 0 & 0 & 0 & 0 & 0 \\ 0 & 35.26 & 0 & 0 & 0 & 0 \\ 0 & 0 & 58.08 & 0 & 0 & 0 \\ 0 & 0 & 0 & 79.75 & 0 & 0 \\ 0 & 0 & 0 & 0 & 99.69 & 0 \\ 0 & 0 & 0 & 0 & 0 & 117.34 \end{pmatrix}$$

The normalized modes are given by

$$\Phi = \begin{pmatrix} 1.0000 & 1.0000 & 1.0000 & 1.0000 & 1.0000 & 1.0000 \\ 1.9805 & 1.8265 & 1.5293 & 1.1126 & 0.6132 & 0.0789 \\ 2.9167 & 2.2896 & 1.2332 & 0.0930 & -0.7486 & -1.0160 \\ 3.7878 & 2.2971 & 0.2715 & -1.0212 & -0.9201 & 0.1271 \\ 4.5742 & 1.8477 & -0.8367 & -1.0963 & 0.3715 & 0.9902 \\ 5.2584 & 1.0306 & -1.4933 & -0.0558 & 1.0724 & -0.3278 \\ 5.8250 & 0.0085 & -1.3440 & 1.0414 & 0.0681 & -0.9238 \\ 6.2614 & -1.0153 & -0.4692 & 1.0790 & -1.0444 & 0.5151 \\ 6.5579 & -1.8371 & 0.6588 & 0.0186 & -0.4963 & 0.8193 \\ 6.7078 & -2.2934 & 1.4312 & -1.0607 & 0.8410 & -0.6812 \end{pmatrix}$$

The modal time periods are given by

$$T_n = \frac{2\pi}{w_n}$$

$$T_1 = \frac{2\pi}{w_1} = \frac{2 \times 3.14}{11.81} = 0.5316 \sec$$

Similarly, the following five time periods for the first six modes of the RC rigid frame shear building are;

$$T_n = [0.5316 \quad 0.1782 \quad 0.1082 \quad 0.0788 \quad 0.0630 \quad 0.0535]$$

Now, calculate the maximum response of RC shear building using modified mode shape function results as follows;

For mode 1:

The equivalent static deformation is, $X_E = \frac{P_0^*}{K^*} = \frac{622.37}{23346.25} = 0.0267m = 26.7mm$

From the elastic response spectrum given in chapter 4 from Fig. 4.26;

$$\frac{t_d}{T_n} = \frac{0.0029}{0.4885} = 0.0059; \frac{X_m}{X_E} = 1.22 \Rightarrow X_m = 0.0267 \times 1.22 = 0.03257 \text{ m} = 32.57 \text{ mm}$$

The maximum dynamic deformation of the RC shear building subject to blast loading is 32.57mm. Similarly, other modes can also be calculated and find the critical failure mode of the shear building.

6.4 Discussion

The developed shape function and generalised coordinates can be used to create the equivalent SDOF system of a multi-storey building. In the extant literature, the shape function for multi-storey buildings is only available in the first mode. The modified shape function is developed in this research so that it can be utilised for the modal analysis of multi-storey buildings. The developed mode shape function is presented as a function of the mode number. For a particular mode number, this factor determines the mode shape. The developed mode shape function is validated using a 10-storey, 5-bay RC rigid frame shear building. For the first six modes of the construction, the natural time period is estimated. The results are in good agreement with the existing methodologies and numerical model in SAP2000 software. The first mode has a relative inaccuracy of 9.25 percent, but the remaining modes are closer to known approaches. The equivalent SDOF system of a multi-storey building subject to harmonic, seismic, transient, blast, and impact loads can be created using this modified shape function. A numerical example for buildings subject to blast load employing modified shape function and blast response spectrum is provided to emphasise the developed framework. The critical failure mode of the building structures can be determined using this equivalent SDOF multi-modal analysis.

CHAPTER 7 DESIGN OF MULTI-STOREY BUILDINGS BASED ON DEVELOPED MODELS

7.1 General

In blast-resistant structures, the rigid frame construction has been preferred because it enables open internal space while also providing strong resistance to lateral loads. Furthermore, due to the gradual development of plastic hinges up to the structure's ultimate capacity, this style of design has intrinsic energy absorption capabilities. The dynamic plastic design of frames for blast resistant buildings has been geared at industrial building uses, such as single-story, multi-bay structures, frequent in ammunition manufacture and storage facilities. This treatment is mostly for acceptor constructions subject to modest blast overpressure (UFC 2005). This chapter presents a detailed methodology for analysis and design of multi-storey building based on the developed models for blast load profile, probabilistic models to predict the critical load and collapse resistance factors and modified shape function.

Blast resistant frames are defined by (a) the simultaneous application of vertical and horizontal pressure-time loadings with peak pressures significantly higher than conventional loads, (b) design criteria allowing inelastic local and overall dynamic structural deformations (deflections and rotations), and (c) design requirements dictated by the facility's operational needs and the need for reusability with minor repair work after an incident.

7.2 Approximate Member Design Methods

7.2.1 Equivalent SDOF Method

Equivalent stiffness and mass parameters must be calculated when modelling a structural member with distributed mass and stiffness as an equivalent SDOF system. The parameters of the SDOF are described as "equivalent" since they are determined to ensure energy equivalence with the real structure. This is accomplished by matching the displacement (and velocity) of a single point of interest or degree of freedom on the real structure with the displacement (and

velocity) of the equivalent mass, hence ensuring kinematic similarity. The applied load must also be idealised to match the external work done. The column/beam's resistance function is depicted in Fig. 7.1, where Mn and Mp are the section's negative and positive plastic moments at the indicated positions, and EI is the member's bending stiffness. The equivalent SDOF's displacement response may then be utilised to calculate the beam's internal shear and bending moments and estimate stresses.

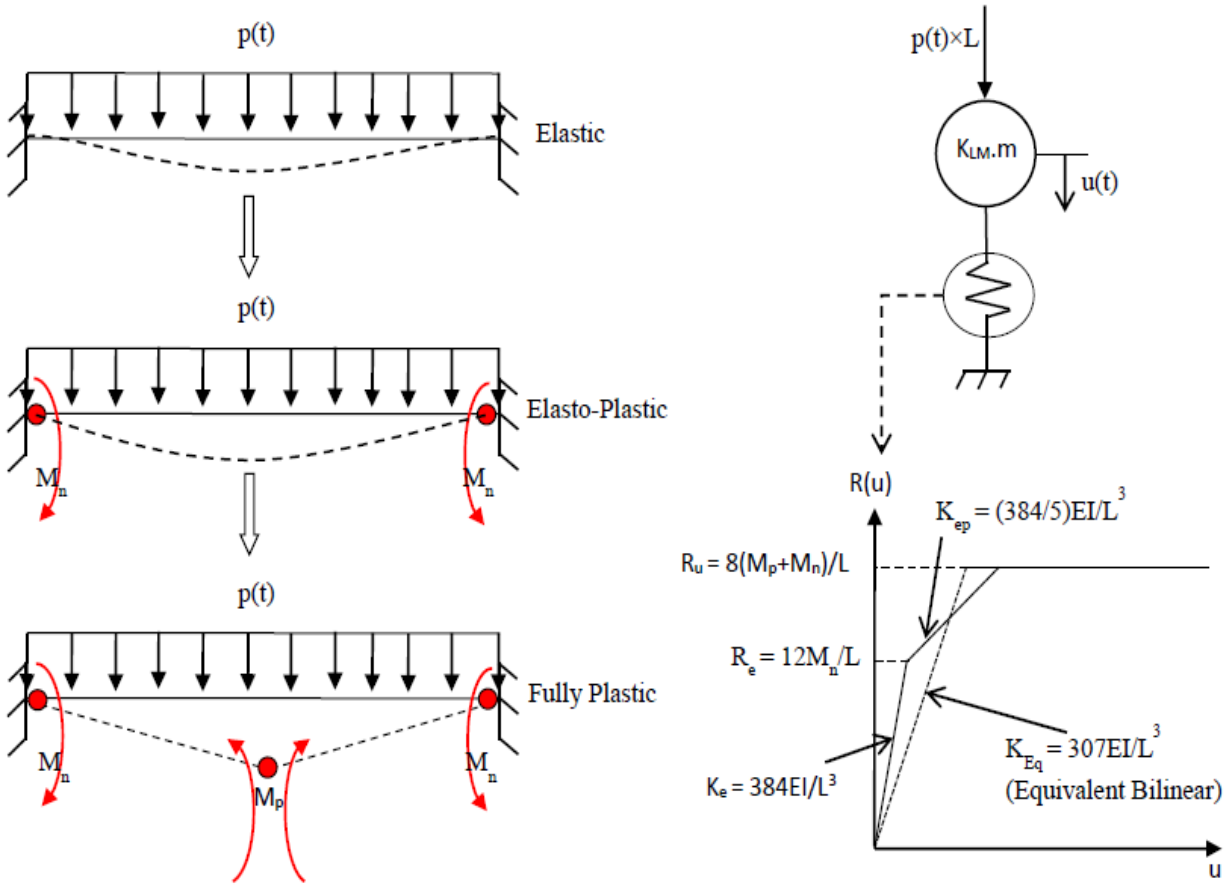

Fig. 7.1. Definition of SDOF model and the resistance function (Danesh Nourzadeh 2017).

The parameters of the equivalent SDOF are determined by the real structure's expected deformed shape under the applied load. The corresponding system's stiffness, for example, is defined as the total load (as distributed on the real structure) that would induce a unit deflection at the degree of freedom of interest on the actual structure. According to this definition, the

equivalent stiffness of a beam/column with a point load at mid-span will differ from that of the same beam/column with a uniform load. The expected deformed shape, or the amount of dispersed mass that "participates" in the deformation, also influences the equivalent mass.

Transformation factors have been proposed to make the formulation of similar SDOF models easier. The transformation factors have been calculated by matching the equivalent SDOF system's work, strain energy, and kinetic energy with the actual distributed structure (UFC 2005).

Table 7.1. Transformation factors for selected one-way elements.

Parameter	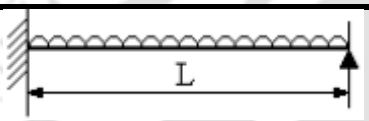 Simply supported and fixed			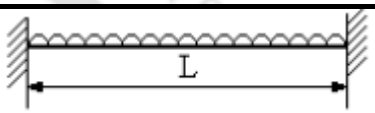 Fixed ends		
Strain Range	Elastic	Elastic-Plastic	Plastic	Elastic	Elastic-Plastic	Plastic
K_L	0.58	0.64	0.50	0.53	0.64	0.50
K_M	0.45	0.50	0.33	0.41	0.50	0.33
K_{LM}	0.78	0.78	0.66	0.77	0.78	0.66
k	$\frac{185EI}{L^4}$	$\frac{384EI}{5L^4}$	0	$\frac{384EI}{L^4}$	$\frac{384EI}{5L^4}$	0
R_m	$\frac{8\,M_N}{L^2}$	$\frac{4(M_N+2M_P)}{L^2}$	$\frac{4(M_N+2M_P)}{L^2}$	$\frac{12\,M_N}{L^2}$	$\frac{8(M_N+M_P)}{L^2}$	$\frac{8(M_N+M_P)}{L^2}$
K_E	$\frac{160EI^*}{L^4}$			$\frac{307EI^*}{L^4}$		

Where, M_P is span moment, and M_N is support moment;

E is the modulus of elasticity of Concrete;

I is Moment of Inertia;

I^* (average cracked Moment of Inertia) = $\frac{1}{5}I_g + \frac{4}{5}I_c$;

I_g is the gross moment of inertia and;

I_c is crack moment of inertia;

K_E is equivalent stiffness.

7.2.2 Newmark's Mechanical Model

For an RC column under ultimate performance level, Newmark's analytical model for deformation is used in this research (Brooks and Newmark 1953).

$$\frac{X_m}{X_E} \cong 1 + \left(\frac{\omega_n t_d}{\beta}\right)^2 \left(\frac{1}{2} - \frac{\beta}{3}\right) \tag{7.1}$$

β is explained as the ratio of yield strength to the average applied load,

$\beta = \frac{R_u}{P_o}$ and P_o = $p_{spherical}$ x tributary width of the structural member

X_E is the equivalent maximum elastic-plastic deformation and can be calculated using the following relation:

$$X_E = \frac{R_u}{K_E} \tag{7.2}$$

For calculating the maximum deformation (X_m) from the Newmark equation, β is kept 1, as capacity is independent of the applied load. Hence, the Newmark equation can be reduced to:

$$\frac{X_m}{X_E} = 1 + \frac{(\omega_n t_d)^2}{6} \tag{7.3}$$

7.3 Member Design Approach

Structures are frequently split into many constituent elements or substructures to make analysis and design easier. This allows simple structural members or elements to be considered under simply applied forces. As individual structural members are investigated, the reaction forces generated by those parts can be used for their supporting elements, and so on, until the structure as a whole has been investigated. This member-by-member technique is common in conventional design, and it may also be used in blast design with equivalent single-degree-of-freedom models. However, successful use of this strategy frequently necessitates a degree of artistry in structural behaviour separation.

7.3.1 Using Peak Loads

Using an equivalent SDOF model, the following approach is adopted to design for the blast resistance of structural members:

Step 1 - Determine Peak Loads

The peak loads such as axial force, shear force and bending moment of multi-storey buildings can be calculated from Chapter 5.

Peak Load = (Critical Load Factor) x (Applied Load or Limiting Resistance) (7.4)

Step 2 - Compute the Member Resistance

The member's resistance is computed to construct the resistance-displacement function. Flexural resistance governs most of the time; therefore, flexure is designed first, and shear is checked. The dynamic strengths of the materials in flexure are computed by multiplying the

reinforcing steel yield strength and concrete compressive strength by the relevant SIF (Strength increase factor) and DIF (Dynamic increase factor) values:

$$(f_y)_{\text{dynamic}} = SIF.DIF.f_y$$
$$(f_c^{'})_{\text{dynamic}} = SIF.DIF.f_c^{'} \quad \text{for bending} \tag{7.5}$$

Where f_y is the yield strength of steel, and $f_c^{'}$ is the compressive strength of concrete.

These quantities are then used to calculate the nominal resistive moment. To do so, the depth of the compressive stress block is calculated in the same way as in traditional design but with dynamic strength values instead of static strength values.

$$a = \frac{A_s(f_y)_{\text{dynamic}}}{0.85b(f_c^{'})_{\text{dynamic}}} \tag{7.6}$$

Where $(f_y)_{\text{dynamic}}$ is the dynamic yield strength of steel, $(f_c^{'})_{\text{dynamic}}$ is the dynamic compressive strength of concrete, A_s is the area of steel, and b is the width of the member.

The effective depth of the cross-section is taken as:

$$d = D - \frac{1}{2}\phi_{bar} - (\text{cover}) \tag{7.7}$$

Where D is the total depth and ϕ_{bar} is the diameter of the rebar.

The nominal resisting moment is then calculated by multiplying the force in the steel with the internal couple moment arm based on dynamic reinforcing steel yield strength.

$$M_n = A_s(f_y)_{\text{dynamic}}\left(d - \frac{a}{2}\right) \tag{7.8}$$

In flexure, the resistance of a simply supported and fixed-ended unit width cross-section is calculated as

$$R_p = \frac{12M_p}{L^2} \tag{7.9}$$

The term M_p is the plastic bending moment of the unit strip and is equal to M_n the nominal moment capacity computed above.

The shear resistance of the trial section is conservatively calculated using only the concrete's shear resistance (disregarding the additional shear resistance provided by reinforcing steel, which can be included in the calculation at the discretion of the designer). A method similar to the one described above is used for bending resistance.

$$(f_c^{'})_{\text{dynamic}} = SIF.DIF.f_c^{'} \qquad \text{for shear} \tag{7.10}$$

The nominal shear strength of the concrete is computed using ACI 318:

$$V_n = 2bd\sqrt{(f_c^{'})_{\text{dynamic}}} \tag{7.11}$$

The shear resistance at the critical section, which is located at a distance from the support, is calculated as follows:

$$R_s = V_n \frac{L}{L/2 - d} \tag{7.12}$$

If the estimated shear resistance is greater than the bending resistance ($R_p < R_s$), the bending resistance will dominate the trial section's design, the desired failure mode.

Step 3 - Define the Equivalent SDOF System

The equivalent stiffness and mass of a structural member are determined by the structural member's force and displacement boundary conditions, as previously stated. A

proportion of mass from components of the structure supported by the member under consideration must be added to achieve the correct dynamic response. Conventional loads, such as gravity loads, must be determined for the member as part of developing the corresponding SDOF system.

The deflection at midspan determines the equivalent stiffness of a simply supported and fix-ended column under a uniform load. As a result, the following equation can be used to calculate the equivalent stiffness of the trial section:

$$K_E = \frac{160EI^*}{L^4} \tag{7.13}$$

The stiffness is a function of the unit width trial section's moment of inertia. Because both elastic and plastic deformation is expected, the moment of inertia of the unit width trial section can be calculated as the average of the gross and cracked moments of inertia. The trial section's gross moment of inertia is calculated as follows:

$$I_g = \frac{bD^3}{12} \tag{7.14}$$

The following formulae determine the cracked moment of inertia:

$$C = \frac{-nA_s + \sqrt{nA_s(nA_s + 2bd)}}{b}$$
$$I_{cr} = \frac{bC^3}{3} + nAs(d - C)^2 \tag{7.15}$$

The average moment of inertia, which will be used in the stiffness calculation, is calculated as follows:

$$I_{avg} = \frac{I_g + I_{cr}}{2} \tag{7.16}$$

After that, the yield or elastic limit deflection can be calculated as follows:

$$X_E = \frac{R_m}{K_E} \tag{7.17}$$

The column's unit width strip's corresponding (or participating) mass is then calculated. To do so, first determine the actual mass of the unit strip.

$$m = \frac{\gamma_c DbL}{g} \tag{7.18}$$

The equivalent mass of the simply supported and fix-ended unit width trial section is calculated by multiplying the actual mass by a load-mass transformation factor. Because the reaction is predicted in both the elastic and plastic regimes, calculating the average load-mass factor by the actual mass yields a single value for the equivalent mass.

$$m_e = K_{LM}.m \tag{7.19}$$

After calculating the equivalent stiffness and mass of the unit width trial section, the equivalent SDOF system's natural period of vibration is calculated as follows:

$$T_n = 2\pi\sqrt{\frac{m_e}{K_E}} \tag{7.20}$$

Step 4-Apply Loads and Solve the Equivalent SDOF

The member is subjected to blast and conventional loads using load combinations. The corresponding SDOF system's peak deflection is determined by the maximum support rotation and ductility ratio. Dynamic support reactions are also computed and applied to supporting members as applied loads. If the natural period of the equivalent SDOF is longer than the positive phase duration of the blast wave, the natural period is compared. If the $\frac{t_d}{T_n}$ ratio is less

than 0.4, the response of the equivalent SDOF will be in the impulsive regime. This allows the SDOF response to be solved by simply equating the kinetic energy given by the blast wave with the system's internal strain energy.

$$x_m = \pi \frac{p_0 t_d}{K_E T_n} \tag{7.21}$$

Step 5 - Check Response Limits

The response limits are compared to the maximum support rotation and ductility ratio. The design is complete when the member response meets the response limits for the intended level of protection. Otherwise, actions are performed to harden the member design, and the design is re-checked.

$$x_p = x_m - X_E \tag{7.22}$$

The ductility ratio is then calculated by multiplying the maximal and pre-yield elastic deformation ratios:

$$\mu = \frac{x_m}{X_E} \tag{7.23}$$

$\mu > \mu_{\max}$ for superficial damage

The following formula is used to calculate the rotation at the supports:

$$\theta = \tan^{-1}\left(\frac{x_m}{L/2}\right) \tag{7.24}$$

$$\theta < \theta_{\max}$$

Member-by-member analysis with SDOF models is a typical and robust method for blast-resistant design. It's vital to note that this method may not capture all of the complexity

of a structural system's dynamic reaction. Inherently, the SDOF technique assumes stiff supports, but in reality, structural elements may interact, and dynamic responses may be coupled. If the natural frequencies of coupled components are near each other, ignoring dynamic coupling may result in unconservative outcomes.

7.3.2 Using Capacity Based Design Software (CBDS)

A user-friendly Capacity Based Design Software (CBDS) is developed indigenously with a graphical interface for designing a structural member subject to blast loading, as shown in Fig. 7.2. It is an in-house programme that calculates the capacity of critical components that are subject to blast loading. The length of the member, blast intensity, and performance level are the three inputs required to design a member. Figs. 7.3 and 7.4 show the sample RC beam and column designs, respectively.

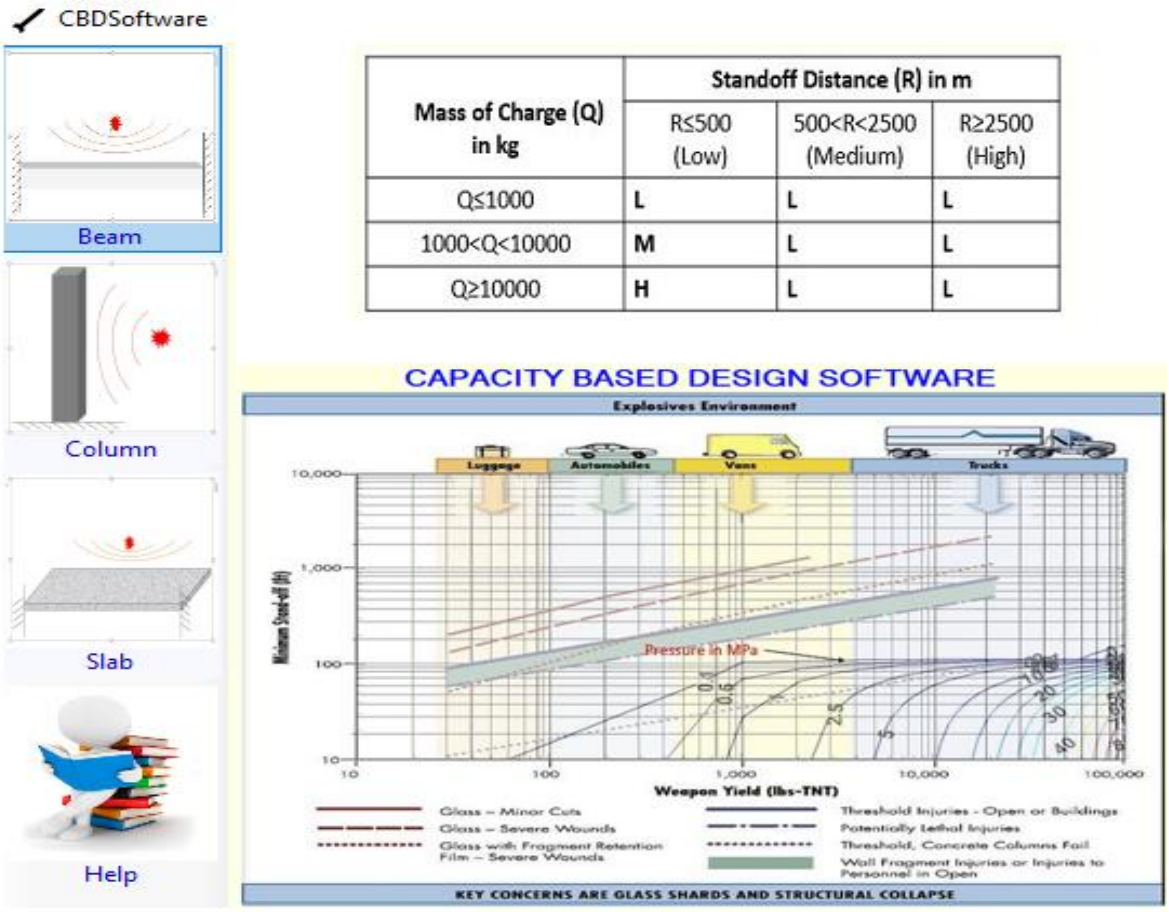

Fig. 7.2 User interface of CBDS.

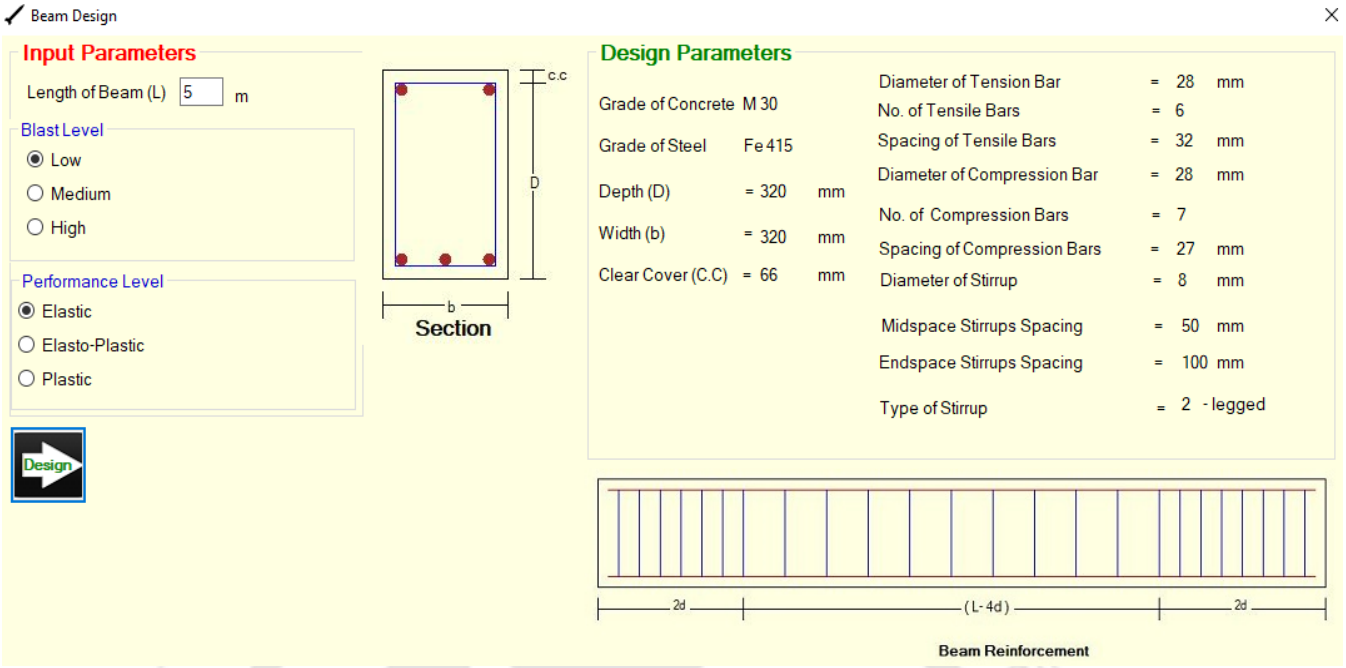

Fig. 7.3. RC beam design in CBDS.

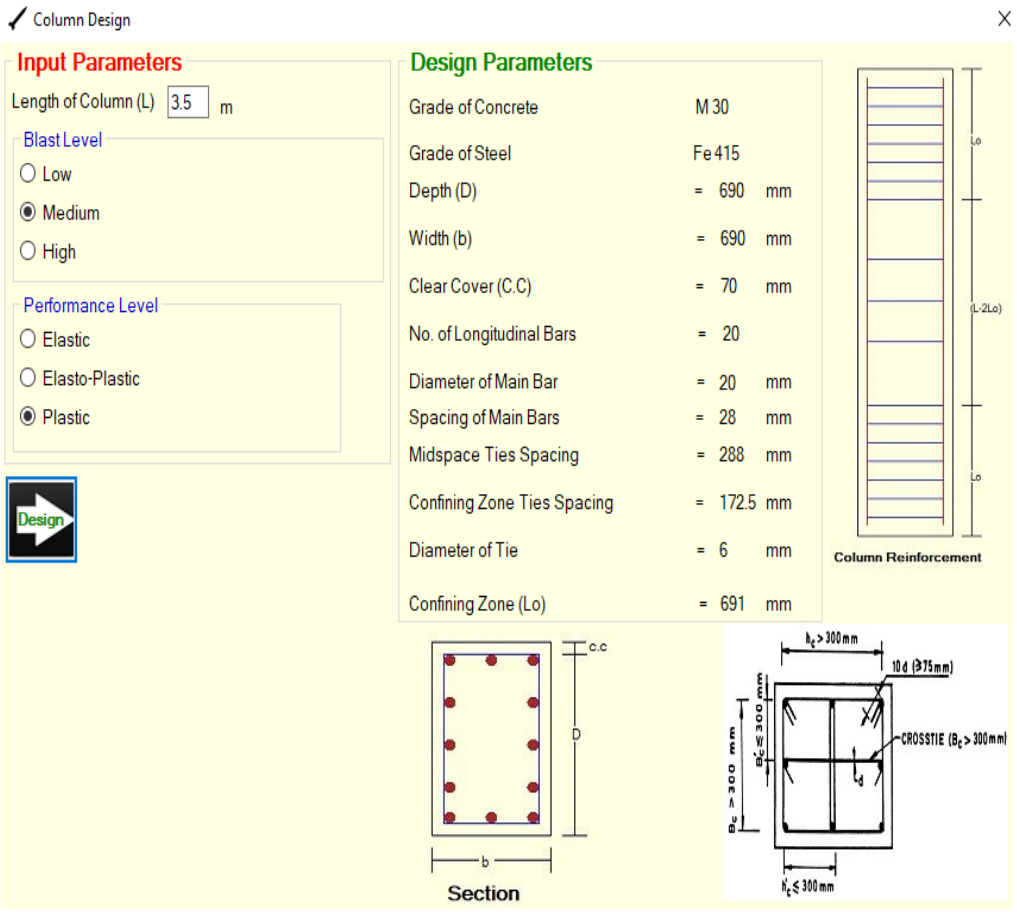

Fig. 7.4. RC Column design in CBDS.

7.4 Design of Rigid Frame Structures

The structural members will deflect and fail over time if the structure is not ductile enough to withstand the deflections generated by the explosion impact. An explosive engineer must be aware of all types of collapse mechanisms to arrange for an implosion that is appropriate for the design's situation. Fig. 7.5 depicts the roof purlins' alignment concerning the blast load directions. This design technique aims to proportion the frame members so that the peak loads shown in Chapter 5 are an affordable option.

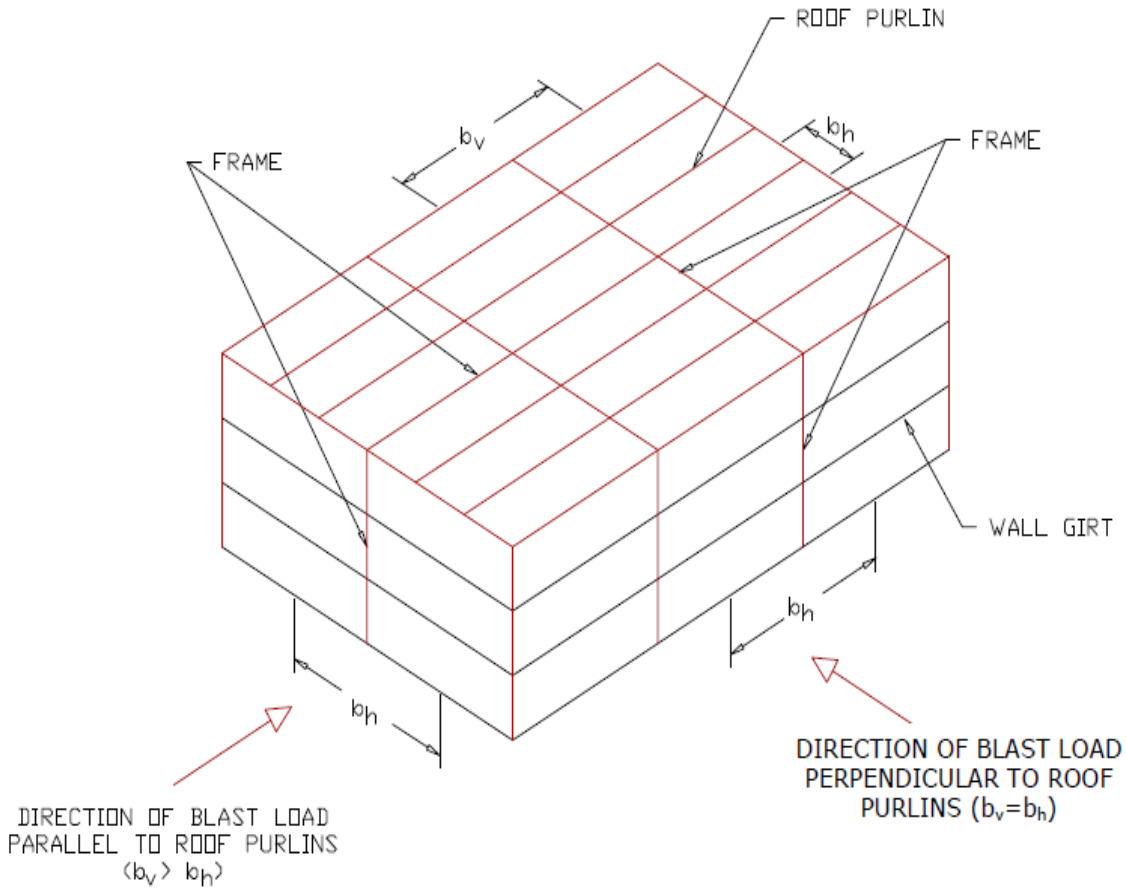

Fig. 7.5. Orientation of Roof Purlins with respect to Blast load direction for Frame Blast Loading (UFC 2005).

The horizontal to vertical peak loading ratio, represented by α for a given frame, is impacted by the structure's horizontal frame plan and is calculated as follows:

$$\alpha = \frac{q_h}{q_v} \tag{7.25}$$

Where

$q_v = p_v b_v$ = peak vertical load on the rigid frame

$q_h = p_h b_h$ = peak horizontal load on the rigid frame

p_v = blast overpressure on roof

p_h = reflected blast pressure on the front wall

b_v = tributary width for vertical loading

b_h = tributary width for horizontal loading

The roof purlins' orientation in relation to the blast load directions is depicted in Fig.7.5. When the direction of the blast load is perpendicular to the roof purlins, the value of α will typically be in the range of 1.8 to 2.5. The frame in this scenario supports the roof purlins, and the tributary width for the horizontal and vertical loads is the same. When the direction of the blast load is parallel to the roof purlins, the α value is substantially higher. In this situation, the frame's girder does not support the roof purlins, and the vertical loading's tributary width is significantly smaller than the horizontal loading's tributary width.

UFC (2005) presents rational approaches for accomplishing the preliminary design of blast resistant frames quickly and efficiently. A DLF of 1.25 is recommended for a beam collapse mechanism, while 0.625 is recommended for a panel or mixed collapse mechanism. Because the natural period of vibration in the side-sway mode is generally significantly longer than the natural period of vibration in the individual elements, the DLF for

a frame is smaller than that for a beam mechanism. Comprehensive frame analysis is performed to check that a trial design fits the specified deformation criteria and verify the sufficiency of the member sizes established based on estimated dynamic forces and moments. Peak loads generated by the analysis are considered when establishing the sizes of individual elements. After the trial member sizes have been determined, the frame's natural period and deflection may be calculated. The maximum deflections and rotations do not exceed the specified maximum values, as shown in Table 7.2.

Table 7.2. Deformation criteria for frame structures.

Element	Deformation Type	Maximum Deformation
Frame structures	δ	$\frac{H^*}{25}$
	Θ	2^o

Θ = Maximum member end rotation (degrees) measured from chord joining the member ends

δ = Relative side-sway deflection between stories

H* = Storey height of the equivalent SDOF system

Considering an equivalent single degree of freedom system, the side-sway natural period and stiffness (K^*) of the multi-storey rigid frame for desired mode shape is calculated from the procedure presented in chapter 6. The limiting resistance R_u is given by

$$R_u = \alpha w H^* \tag{7.26}$$

Where w is equal to the equivalent static uniform load based on the dynamic load factor. The equivalent elastic deflection X_E corresponding to R_u is

$$X_E = \frac{R_u}{K^*} \tag{7.27}$$

Knowing the side-sway resistance and the side-sway natural period of vibration T_n, the ductility ratio (μ) for the side-sway deflection of the frame can be computed using the dynamic response. The maximum deflection X_m is then calculated from

$$X_m = \mu X_E \tag{7.28}$$

Where μ = ductility ratio in side-sway.

7.4.1 Design Procedure

The design methodology for a multi-storey building subject to blast pressure-time loading using the developed approach is as follows:

Step 1: Calculate the peak loads in the multi-storey rigid frame from Chapter 5, such as axial, shear, and bending moments.

Step 2: Use the final design criteria and member design technique given in Section 7.3 to design each member.

Step 3: Calculate the natural period of the multi-storey building using the moments of inertia from Step 2 and the stiffness for the specified mode shape from Chapter 5.

Step 4: Using $\frac{t_d}{T_n}$ and $\frac{P_o}{R_u}$ quantities, extract the $\frac{X_m}{X_E}$ values from the response spectrum given in chapter 4.

Step 5: If the deflection conditions for both side-sway and beam mechanisms are met, the preliminary design's outputs are the member sizes from Step 2. If the side-sway mechanism's

deflection criteria are exceeded, the resistance of all or most of the members should be increased.

The following design example problem succinctly explains the aforesaid procedure.

Illustrative Problem

Design a 5-bay, 10-story, RC fix-ended rigid frame subjected to horizontal pressure-time loading in its plane shown in Fig. 7.6. The positive phase loading duration is 0.0029 seconds, and the peak overpressure is 166.67 kN/m^2. It is required to design the frame structure for more than one incident. The deformation limits shall be half that permitted for personnel protection: $\delta = \frac{H^*}{50}$ and $\Theta_{max} = 1°$ for individual members.

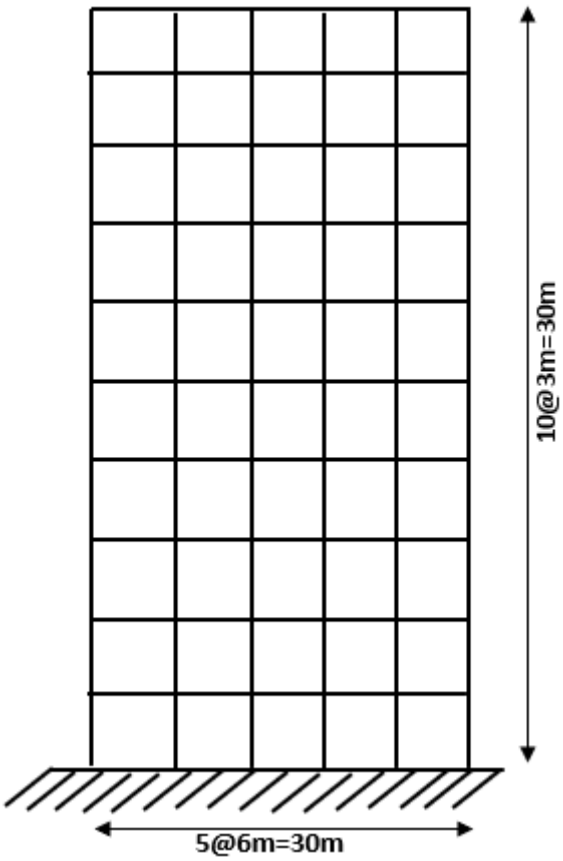

Fig. 7.6. RC 10-storey, 5-bay multi-storey building.

Step 1: Calculate the peak loads such as axial, shear and bending moments in the rigid frame structure from Chapter 5 as follows (Assume $R_u = P_o$, i.e., Capacity = Demand);

The static load acting on the structure $P_o = p \times$ tributary width

$$R_u = P_o = 166.67 \times 6 = 1000kN/m$$

Exterior column:

$$A_{EC} = ECA \times R_u = 1.42 \times 1000 = 1420kN$$

$$V_{EC} = ECS \times R_u = 0.53 \times 1000 = 530kN$$

$$M_{EC} = ECB \times R_u = 0.12 \times 1000 = 120kN - m$$

Interior column:

$$A_{IC} = ICA \times R_u = 0.51 \times 1000 = 510kN$$

$$V_{IC} = ICS \times R_u = 0.23 \times 1000 = 230kN$$

$$M_{IC} = ICB \times R_u = 0.12 \times 1000 = 120kN.m$$

Exterior beam:

$$A_{EB} = EBA \times R_u = 0.47 \times 1000 = 470kN$$

$$V_{EB} = EBS \times R_u = 0.17 \times 1000 = 170kN$$

$$M_{EB} = EBB \times R_u = 0.10 \times 1000 = 100kN - m$$

Interior beam:

$$A_{IB} = IBA \times R_u = 0.38 \times 1000 = 380kN$$

$$V_{IB} = IBS \times R_u = 0.24 \times 1000 = 240kN$$

$$M_{IB} = IBB \times R_u = 0.12 \times 1000 = 120kN - m$$

Step 2: Using the approximation member design approach from section 7.3, design rigid frame structure members with the following results:

Table 7.3. Estimated member sizes from peak loads.

Member	Bending Moment (kN-m)	Shear Force (kN)	Axial Load (kN)	Section	Moment of Inertia Ix (m^4)
Exterior column	120	530	1420	0.4mx0.4m	0.00213
Interior column	120	230	510	0.4mx0.4m	0.00213
Exterior beam	100	170	470	0.4mx0.7m	0.0114
Interior beam	120	240	380	0.4mx0.7m	0.0114

Step 3: Determine the stiffness and sway deflection of the RC rigid frame as follows:

E = 31.62×10^6 kN/m^2;

Stiffness of each story;

$$k = 6 \times \frac{12EI}{L^3} = 6 \times \frac{12 \times 31.62 \times 10^6 \times 0.00213}{3^3} = 179898.46\left(kN/m\right)$$

Weight and mass of each story level and roof;

$$W = (DL)_{beams} + (DL)_{columns}$$
$$W = (5\times0.4\times0.7\times6\times25) + (6\times0.4\times0.4\times3\times25) = 282kN$$
$$W_{roof} = (5\times0.4\times0.7\times6\times25) + (6\times0.4\times0.4\times1.5\times25) = 246kN$$
$$m_1 = m_2 = m_3 = ... = m_9 = \frac{W}{9.8} = \frac{282}{9.8} = 28.78(\text{kN}.s^2/m)$$
$$\text{m}_{10} = \frac{W_{roof}}{9.8} = \frac{246}{9.8} = 25.10(\text{kN}.s^2/m)$$

Where $(DL)_{beams}$, and $(DL)_{columns}$ are dead loads of beams and columns, respectively.

The shear buildings' generalised stiffness, mass, and force are determined in Table 7.4.

Table 7.4. For mode 1: S_n =0.10383 and B_n =0.91289.

Height (H)(m)	Stiffness (k)(kN/m)	Mass (m) (kN.s^2)	Φ_i	$\Delta\Phi_i$	$P_o\times\Phi_i$	$m\times\Phi_i^2$	$k\times\Delta\Phi_i^2$
30	179898.46	25.10	1	0.012168	100	25.10204082	26.63522
27	179898.46	28.78	0.987832133	0.033637	98.783213	28.07949747	203.5453
24	179898.46	28.78	0.95419517	0.068093	95.419517	26.1997689	834.1245
21	179898.46	28.78	0.886102288	0.106606	88.610229	22.59387638	2044.51
18	179898.46	28.78	0.77949647	0.140893	77.949647	17.48442434	3571.157
15	179898.46	28.78	0.638603038	0.16367	63.860304	11.73505131	4819.124
12	179898.46	28.78	0.474932571	0.16896	47.493257	6.490631343	5135.656
9	179898.46	28.78	0.305972442	0.152299	30.597244	2.693938389	4172.751
6	179898.46	28.78	0.153673276	0.110781	15.367328	0.679547361	2207.778
3	179898.46	28.78	0.042892612	0.042893	4.2892612	0.052940499	330.9729

$$P_0^* = \sum P_o \times \Phi_i = 622.37kN$$

$$M^* = \sum m \times \Phi_i^{\,2} = 141.11kN.s^2 / m$$

$$K^* = \sum k \times \Delta\Phi_i^{\,2} = 23346.25kN / m$$

$$w_n = \sqrt{\frac{K^*}{M^*}}$$

$$w_1 = \sqrt{\frac{K^*}{M^*}} = \sqrt{\frac{23346.25}{141.11}} = 12.8626rad / \sec$$

$$T_n = \frac{2\pi}{w_n}$$

$$T_1 = \frac{2\pi}{w_1} = \frac{2 \times 3.14}{12.8626} = 0.4885\sec$$

Now, for the first mode shape, calculate the maximum response of RC shear-type multi-storey building as follows:

For Mode 1:

The equivalent static deformation is, $X_E = \frac{P_0^*}{K^*} = \frac{622.37}{23346.25} = 0.0267m = 26.7mm$

From the elastic response spectrum given in chapter 4 from Fig. 4.26;

$$\frac{t_d}{T_n} = \frac{0.0029}{0.4885} = 0.0059; \frac{X_m}{X_E} = 1.22 \Rightarrow X_m = 0.0267 \times 1.22 = 0.03257\,\text{m} = 32.57\,\text{mm}$$

The maximum dynamic deformation of the RC shear building subjected to blast loading is 32.57mm.

$$\delta = \frac{H^*}{50} = \frac{20.91}{50} = 0.4182m = 418.2mm > 32.57mm \text{ (OK)}$$

Step 4: Check the deflection of members in the rigid frame as follows;

Exterior beam:

For an elastic-plastic response, take the average load-mass factor for the plastic and elastic response:

$$K_{LM} = (0.77 + 0.66)/2 = 0.715$$

$$m_e = K_{LM}.m = 0.715 \times 4.2857 = 3.064 kN.\sec^2/m$$

$$K_E = \frac{307EI}{L^4} = \frac{307 \times 31.62 \times 10^6 \times 0.0114}{6^4} = 0.085388 \times 10^6 kN/m$$

$$T_n = 2\pi\sqrt{\frac{m_e}{K_E}} = 2 \times 3.1416 \times \sqrt{\frac{3.064}{0.085388 \times 10^6}} = 0.0376$$

$\frac{t_d}{T_n} = \frac{0.0029}{0.0376} = 0.077$ and $\frac{P_o}{R_u} = 1$, from the response spectrum of chapter 4 from Fig. 4.27.

$\frac{X_m}{X_E} = 0.2389$ and $X_E = \frac{R_u}{K_E} = \frac{1000 \times 3}{(85388)} = 0.03513m = 35.13mm$

$$X_m = 0.03513 \times 0.2389 = 0.00839\,\text{m} = 8.39\,\text{mm}$$

$$\tan\Theta = \frac{X_m}{(L/2)} = \frac{0.00839}{(6/2)} = 0.00279$$

$$\Theta = \tan^{-1}(0.00279) = 0.16° < 1° \text{ (OK)}$$

Exterior column:

For an elastic-plastic response, take the average load-mass factor for the plastic and elastic response:

$$K_{LM} = (0.78 + 0.66)/2 = 0.72$$

$$m_e = K_{LM}.m = 0.72 \times 1.2244 = 0.8816 kN.\sec^2/m$$

$$K_E = \frac{160EI}{L^4} = \frac{160 \times 31.62 \times 10^6 \times 0.00213}{3^4} = 0.133038 \times 10^6 kN/m$$

$$T_n = 2\pi\sqrt{\frac{m_e}{K_E}} = 2 \times 3.1416 \times \sqrt{\frac{0.8816}{0.133038 \times 10^6}} = 0.01617$$

$\frac{t_d}{T_n} = \frac{0.0029}{0.01617} = 0.179$ and $\frac{P_o}{R_u} = 1$, from the response spectrum of chapter 4 from Fig. 4.27.

$\frac{X_m}{X_E} = 0.5411$ and $X_E = \frac{R_u}{K_E} = \frac{1000 \times 3}{(133038)} = 0.02254m = 22.54mm$

$X_m = 0.02254 \times 0.5411 = 0.0122\,\text{m} = 12.2\,\text{mm}$

$\tan\Theta = \frac{X_m}{(L/2)} = \frac{0.0122}{(3/2)} = 0.00813$

$\Theta = \tan^{-1}(0.00813) = 0.47° < 1°$ (OK)

Step 5: The deflections of the local mechanisms are within the criteria. The side-sway deflection is acceptable. The assumed sections can be used for the analysis.

7.4.2 Controlled Progressive Collapse

A demand-capacity ratio (DCR) is used to assess the risk of progressive collapse. For each scenario, DCR is defined as the ratio of the force (bending moment, axial force, shear force, or torsional moment) in the structural member after the instantaneous removal of a column to the design strength of the member (Cai et al., 2012).

$$DCR = \frac{Q_{UD}}{Q_{CE}} \tag{7.29}$$

where

Q_{UD} = force in the structural member

Q_{CE} = ultimate un-factored capacity of the structural member

If the DCR of a structural member surpasses 2.0 for conventional structural configurations and 1.5 for unusual structural configurations, it is regarded to have failed. Facilities with a relatively straightforward layout are classified as traditional structural configurations. If the DCR value is higher than the allowed, the member must be strengthened.

According to this report's proposed analysis and designed framework, the DCR value is always limited to less than or equal to unity. Since the peak loads contain the inherent nature of uncertainties, such as the direction and location of blast loading, the Q_{UD} value is always less than or equal to Q_{CE} the value.

7.5 Conclusions

The equivalent SDOF approach with multi-modal analysis has been developed to overcome design constraints in the literature and blast-resistant design manuals where rigid frame structures have been limited to the single storey only. The stiffness and natural period for the desired mode of the multi-storey building are calculated using the modified mode shape function introduced in Chapter 6. The member sizes are calculated based on peak loads, including inherent uncertainties such as blast direction and position, as discussed in Chapter 5. The member design technique and deformation criteria for the equivalent SDOF method are based on well-known blast resistant design documents such as TM 5-1300/UFC 2005, DoD, etc. The suggested analytical and design methodology intrinsically controls progressive collapse by limiting the DCR value to less than or equal to unity. Only midrise buildings with up to 25 storeys and 25 bays are allowed to have peak loads. A user-friendly Capacity Based Design Software (CBDS) is developed with a graphical interface for designing a structural member subject to blast loading.

CHAPTER 8 PROGRESSIVE COLLAPSE RESISTANCE

8.1 General

Structures have been built to endure certain extreme forces and stresses. However, the member fails when the load operating on an element exceeds its ultimate capacity. When a load-bearing structural member in a building falls, it causes the failure of adjacent members, and the failure of adjacent members causes the failure of additional neighbouring or higher-storey members, and so on, resulting in the failure of the entire structure. This occurrence is called progressive collapse or progressive failure. In a nutshell, it's the process by which a local failure becomes a global failure. When a structure is subject to unusual loads, the structural elements are the first to be damaged. Vertical structural member damage is more dangerous than horizontal structural member damage. When a vertical member, such as a column, is destroyed due to a sudden load impact, the load is distributed to other adjacent or neighbouring elements. There will be no failure if the neighbouring members have the capacity to withstand the additional load, but if they do not, the member will fail. When that component fails again, the adjacent member must be able to tolerate the failure, or else the failure will continue to escalate, resulting in a chain reaction of failure and structural collapse.

The TM 5-1300/UFC 2005, GSA, and ASCE 7-05 design manual limits progressive collapse methods (column removal methods) to direct and indirect methods. These manuals quantified the DCR (Demand-Capacity-Ratio) values to control the progressive collapse of the building frame structures. This chapter develops probabilistic collapse resistance factors for multi-storey building. The developed probabilistic collapse resistances factors (axial, shear and bending) of multi-storey rigid frame constructions can be used to design and mitigate the progressive collapse of the multi-storey buildings.

8.2 Methodology for Collapse Resistance Factors

A numerical simulation methodology is adapted to evaluate the collapse resistance factors of rigid frame structures. The analysis in this study considers fix ending rigid frame constructions with a unit bay and storey lengths. This study considers the unit gravity loads of horizontal members, as shown in Fig. 8.1a. The investigation considers the elastic behaviour as well as a static load scenario. Initially, a simple two-dimensional portal frame is analysed with SAP2000 software, and the software's accuracy is manually tested against results from traditional methods for the same frame. The results are found to be extremely accurate, and further information provided in the following sections of this Chapter.

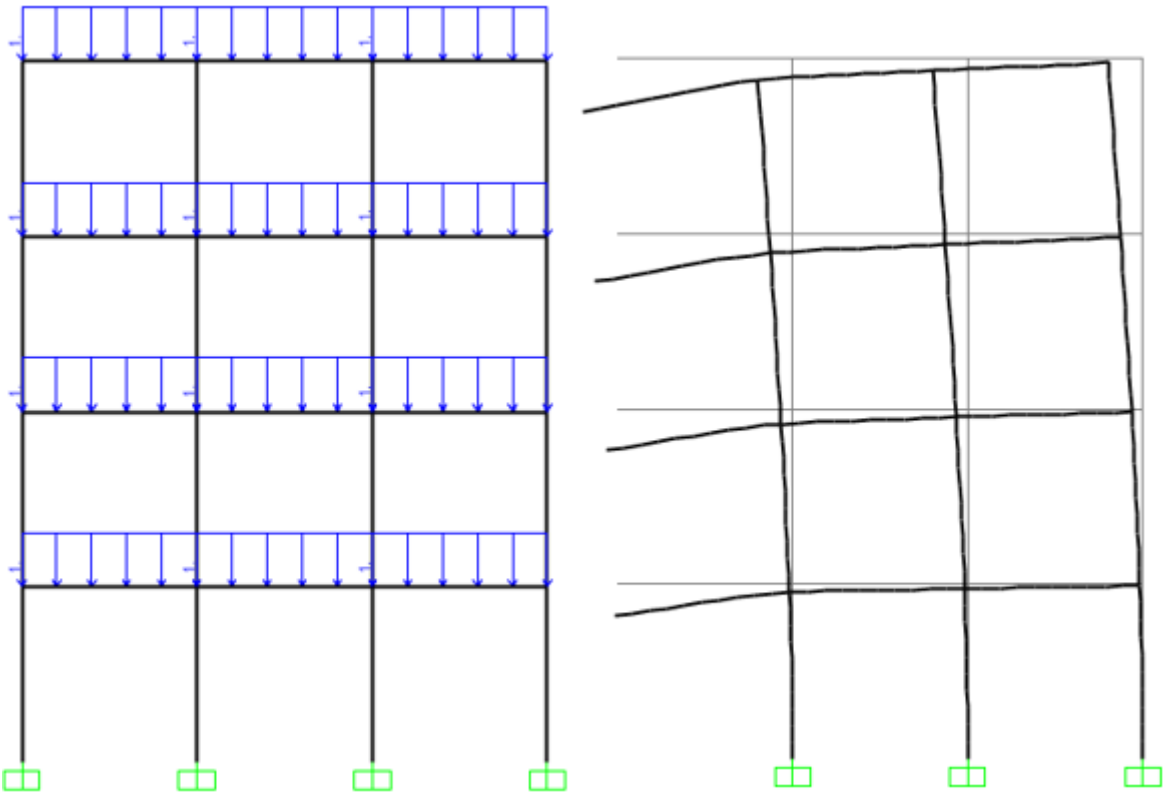

(a) Before and after collapse

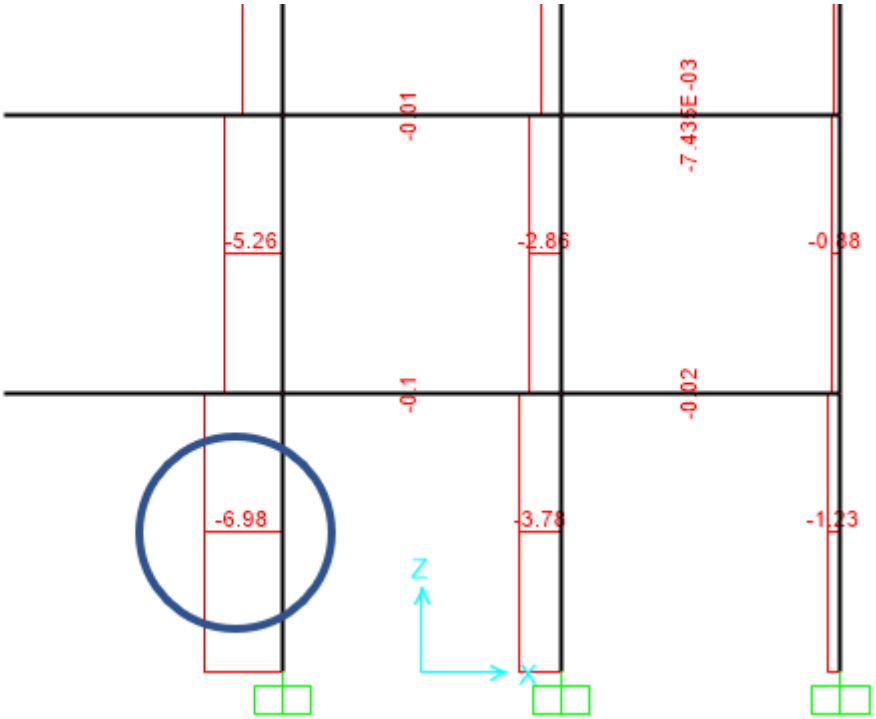

(b) Obtained Column Axial Resistance Factor (CAR)

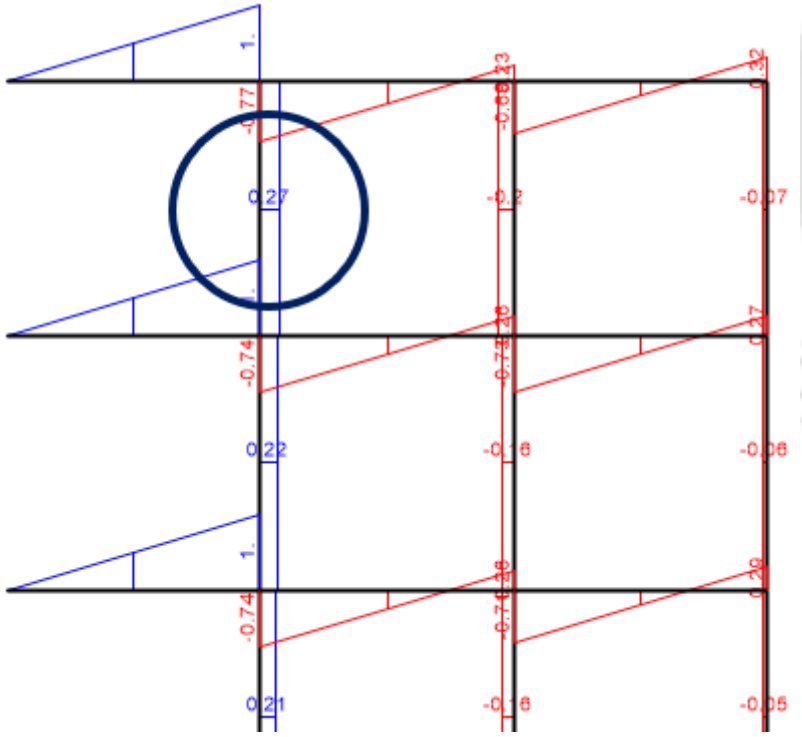

(c) Obtained Column Shear Resistance Factor (CSR)

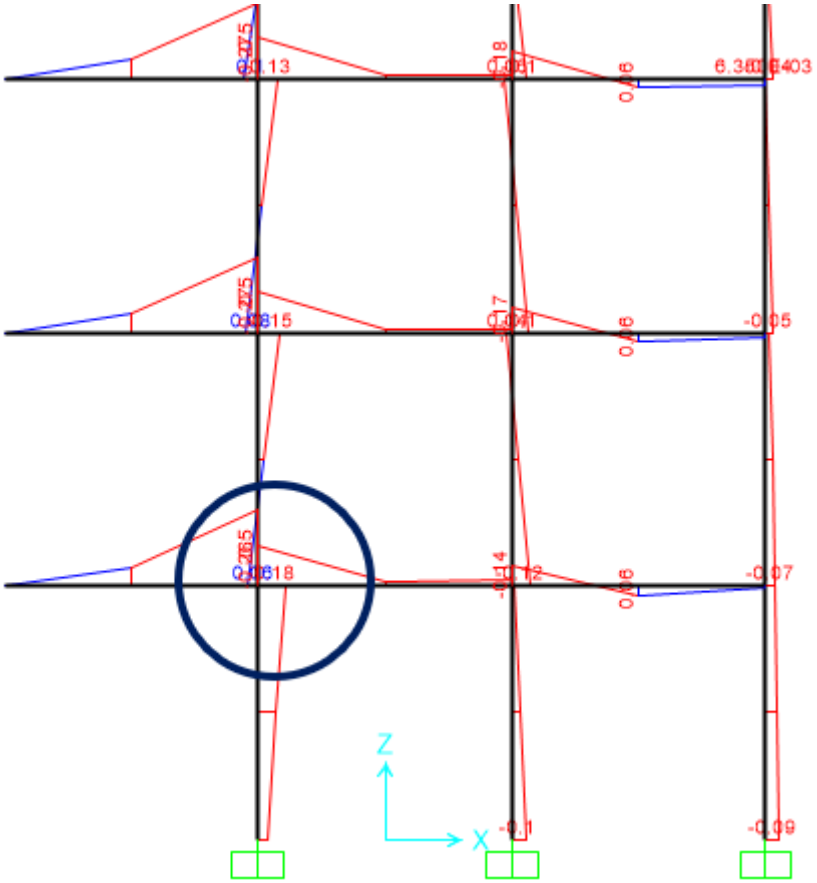

(d) Obtained Column Bending Resistance Factor (CBR)

Fig. 8.1. Methodology: Collapse resistance factors of 3-bay, 4-storey building.

Data Collection

The following is the data collection methodology for developing probabilistic models of collapse resistance factors:

Step1: The unit dead weight of horizontal structural members is considered while modelling a 2D rigid frame with unit dimensions in SAP2000 software.

Step2: A unit gravity load is imposed at the floor levels of the rigid frame structure as shown in Fig. 8.1a to discover the critical member, and the member reaction loads (bending, shear, and axial) are obtained for each collapse scenario as shown in Fig. 8.1b to 8.1d.

Step3: The collapse resistance factor is the maximum reaction load (bending, shear, and axial) of all possible collapse scenarios of rigid frame structures. Fig. 8.1 type is the most critical case.

Step4: By increasing the number of bays and storeys, the same procedure is followed up to 25-storey and 25-bay rigid frame structures (mid-rise building frames).

Step5: Six sets of data are gathered for the beams and columns of the rigid frame for each collapsed case to obtain three load factors (bending, shear, and axial), and a similar method is followed for 600 critical cases to obtain collapse resistance factors.

Step6: The entire data is captured in OriginPro software for data analysis and the development of empirical models of collapse resistance factors.

Data Analysis

OriginPro software is used to develop probabilistic models for the collapse resistance factors of rigid frame constructions. Statistical measures such as standard deviation, coefficient of variation, and coefficient of determination are used to confirm the accuracy of each probabilistic model.

8.3 Quantification of Collapse Resistance

To obtain the probabilistic models of the collapse resistance factors (bending, shear and axial) of the multi-story rigid frames, 600 rigid frame models are analysed using SAP2000 software. Origin software is used for data management and fitting SAP2000 data. The results are categorized for column and beams of rigid frame structures, and six empirical models, i.e., 3 for columns and 3 for beams, are developed, respectively.

Collapse Resistance of Columns

The axial collapse resistance factors for the columns (CAR) is obtained from the developed probabilistic equation (8.1). A surface plot is drawn for the recorded data, as shown in Fig. 8.2, and it describes the accuracy of the probabilistic model with SAP2000 data. The regression parameters, values for constants, and correlation matrix for the probabilistic model are listed in Table 8.1 and 8.2.

$$CAR = z0 + Bm^{C} + Dn^{E} + Fm^{C}n^{E} \text{ for } n \geq 3 \text{ and } m \geq 1 \quad (8.1)$$

Where ‘m’ is the number of storeys, ‘n’ is the number of bays in the building and z0, B, C, D, E and F are constants listed in Table 8.1.

Table 8.1. Regression parameters of CAR.

Constant	Value	Standard Error	Standard Deviation	Coefficient of Variation
z0	1.20136	0.04746		
B	-2.69984	0.09721		
C	-0.49904	0.01246		
D	1.24823	0.01355	0.09016	0.0050
E	0.93694	0.00221		
F	1.01359	0.01155		

Table 8.2. Correlation Matrix of CAR.

Constant	z0	B	C	D	E	F
z0	1					
B	-0.563	1				
C	0.444	0.040	1			
D	-0.813	0.053	-0.650	1		
E	0.514	0.133	-0.038	-0.701	1	
F	0.159	-0.729	0.143	0.200	-0.626	1

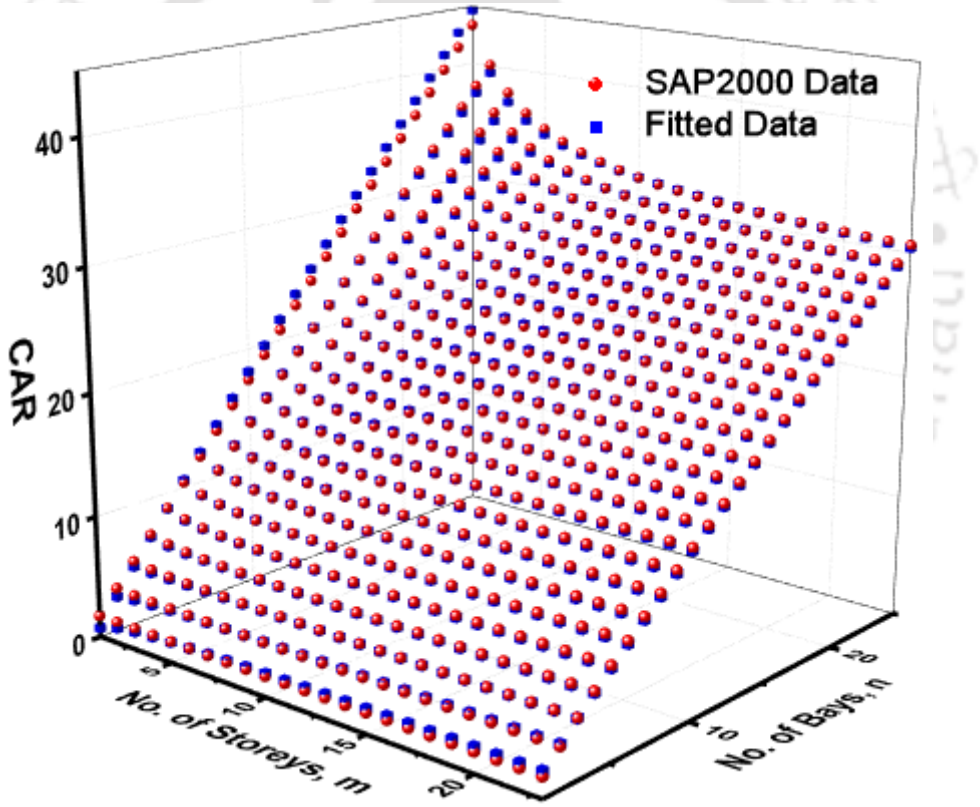

Fig. 8.2. Column Axial Resistance factor (CAR).

The minimum axial resistance (A_{RC}) required in the column to mitigate the progressive collapse of multi-storey buildings is given by

$$A_{RC} = CAR \times R_{u,beam} \text{ (kN)} \tag{8.2}$$

Where $R_{u,beam}$ is the limiting resistance of intact beam.

The shear collapse resistance factors for the columns (CSR) is obtained from the developed probabilistic equation (8.3) and Table 8.3. A surface plot is drawn for the recorded data, as shown in Fig. 8.3, and it describes the accuracy of the probabilistic model with SAP2000 data. The regression parameters, values for constants and correlation matrix for the probabilistic model, are listed in Table 8.4 and Table 8.5, respectively.

$$CSR = z0 + Bm^C + Dn^E + Fm^C n^E \text{ for n≥3 and m≥2} \tag{8.3}$$

Where 'm' is the number of storeys, 'n' is the number of bays in the building and z0, B, C, D, E and F are constants listed in Table 8.4.

Table 8.3. CSR factors.

CSR	Remarks
$z0 + Bm^C + Dn^E + Fm^C n^E$	for n≥3 and m≥2
0.21	for n≥6 and m=1
0.17	for n=3 to 5 and m=1

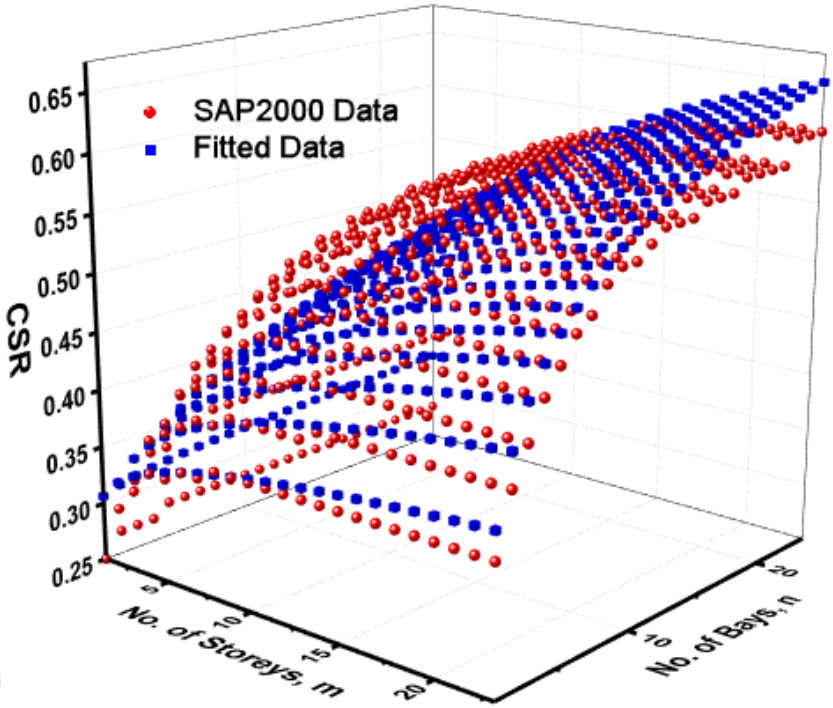

Fig. 8.3. Column Shear Resistance factor (CSR).

Table 8.4. Regression parameters of CSR.

Constant	Value	Standard Error	Standard Deviation	Coefficient of Variation
z0	36.61018	98.84651		
B	-36.46134	98.87925		
C	0.01221	0.03056		
D	-38.28959	103.56738	0.02376	0.0473
E	0.04707	0.04006		
F	38.44725	103.5969		

Table 8.5. Correlation Matrix of CSR.

Constant	z0	B	C	D	E	F
z0	1					
B	-1	1				
C	-0.932	0.932	1			
D	-0.999	0.999	0.939	1		
E	-0.331	0.332	-0.029	0.313	1	
F	0.999	-0.999	-0.939	-1	-0.315	1

The minimum shear resistance (V_{RC}) required in the column to mitigate the progressive collapse of multi-storey buildings is given by

$$V_{RC} = CSR \times R_{u,beam} \text{ (kN)} \tag{8.4}$$

Where $R_{u,beam}$ is the limiting resistance of intact beam.

The bending collapse resistance factors for the columns (CBR) is obtained from the developed probabilistic equation (8.5) and (8.6). A surface plot is drawn for the recorded data, as shown in Fig. 8.4 and 8.5, respectively, and they describe the accuracy of the probabilistic model with SAP2000 data. The regression parameters, values for constants and correlation matrix for the probabilistic model are listed in Tables 8.6, 8.7, 8.8 and 8.9, respectively.

$$CBR = z0 + Bm^{C} + Dn^{E} + Fm^{C}n^{E} \text{ for n=3 to 4 and m}\geq 1 \tag{8.5}$$

Where ‘m’ is the number of storeys, ‘n’ is the number of bays in the building and z0, B, C, D, E and F are constants listed in Table 8.6.

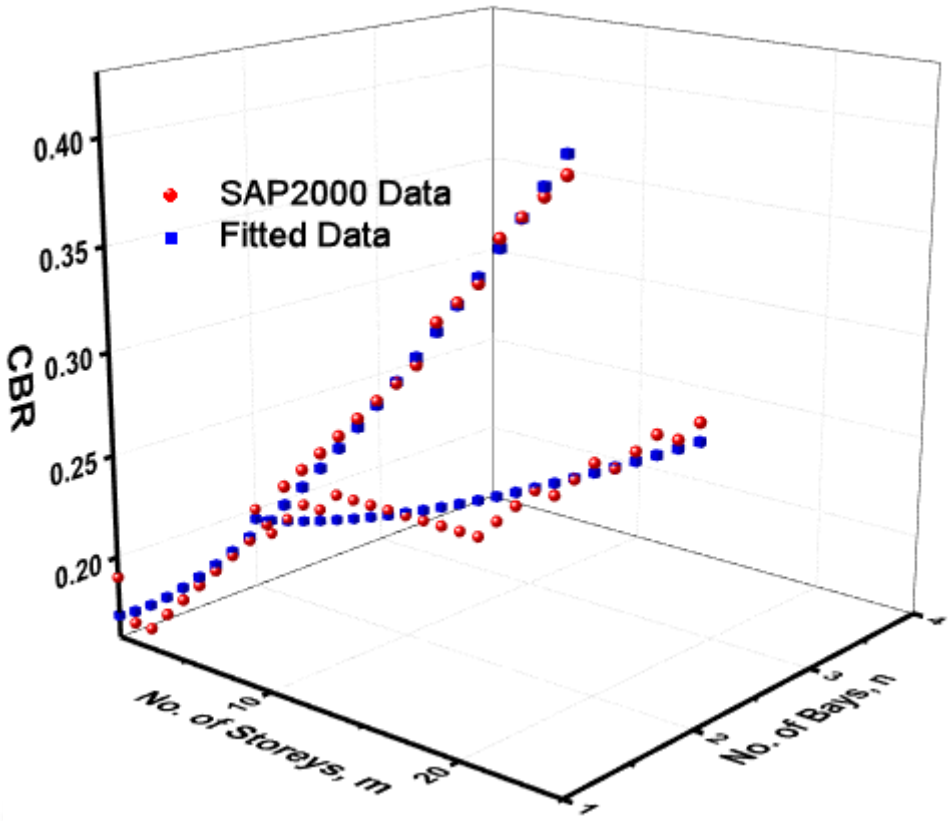

Fig. 8.4. Column Bending Resistance factor (CBR) for n= 3 to 4 and m≥1.

Table 8.6. Regression parameters of CBR for n= 3 to 4 and m≥1.

Constant	Value	Standard Error	Standard Deviation	Coefficient of Variation
z0	0.7638	166.44999		
B	-0.0404	12.13063		
C	1.38423	0.07086		
D	-0.59585	166.45	0.00757	0.0292
E	-0.06421	18.34317		
F	0.04342	12.13066		

Table 8.7. Correlation Matrix of CBR for n= 3 to 4 and m≥1.

Constant	z0	B	C	D	E	F
z0	1					
B	-1	1				
C	-0.066	0.666	1			
D	-1	1	0.066	1		
E	1	-1	-0.065	-1	1	
F	1	-1	-0.066	-1	1	1

$$CBR = z0 + Bm^{C} + Dn^{E} + Fm^{C}n^{E} \text{ for n≥5 and m≥1} \quad (8.6)$$

Where ‘m’ is the number of storeys, ‘n’ is the number of bays in the building and z0, B, C, D, E and F are constants listed in Table 8.8.

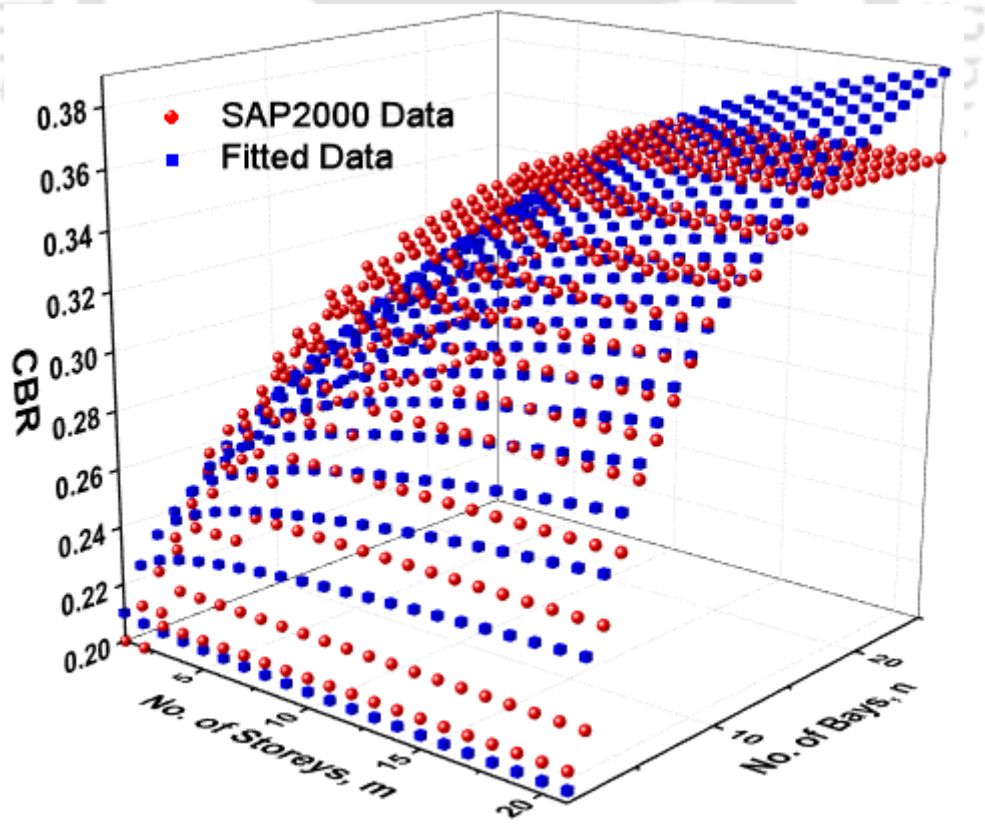

Fig. 8.5. Column Bending Resistance factors (CBR) for n≥5 and m≥1.

Table 8.8. Regression parameters of CBR for n≥5 and m≥1.

Constant	Value	Standard Error	Standard Deviation	Coefficient of Variation
z0	30.61666	74.86956		
B	-31.72551	75.97969		
C	0.02203	0.04192		
D	-30.3191	74.72522	0.0105	0.0335
E	0.01588	0.02371		
F	31.63794	75.83739		

Table 8.9. Correlation Matrix of CBR for n≥5 and m≥1.

Constant	z0	B	C	D	E	F
z0	1					
B	-0.999	1				
C	-0.784	0.769	1			
D	-1	0.999	0.783	1		
E	-0.550	0.569	-0.085	0.551	1	
F	0.999	-1	-0.769	-0.999	-0.570	1

The minimum bending resistance (M_{RC}) required in the column to mitigate the progressive collapse of multi-storey buildings is given by

$$M_{RC} = CBR \times R_{u,beam} \text{ (kN-m)} \tag{8.7}$$

Where $R_{u,beam}$ is the limiting resistance of intact beam.

Collapse Resistance of Beams

The axial collapse resistance factors for the beams (BAR) is obtained from the developed probabilistic equation (8.8) and Table 8.10. A surface plot is drawn for the recorded data, as shown in Fig. 8.6, and it describes the accuracy of the probabilistic model with SAP2000 data. The regression parameters, values for constants, and correlation matrix for the probabilistic model are listed in Table 8.11 and 8.12.

$$BAR = z0 + Bm^{C} + Dn^{E} + Fm^{C}n^{E} \text{ for } n\geq 3 \text{ and } m\geq 2 \quad (8.8)$$

Where 'm' is the number of storeys, 'n' is the number of bays in the building and z0, B, C, D, E and F are constants listed in Table 8.11.

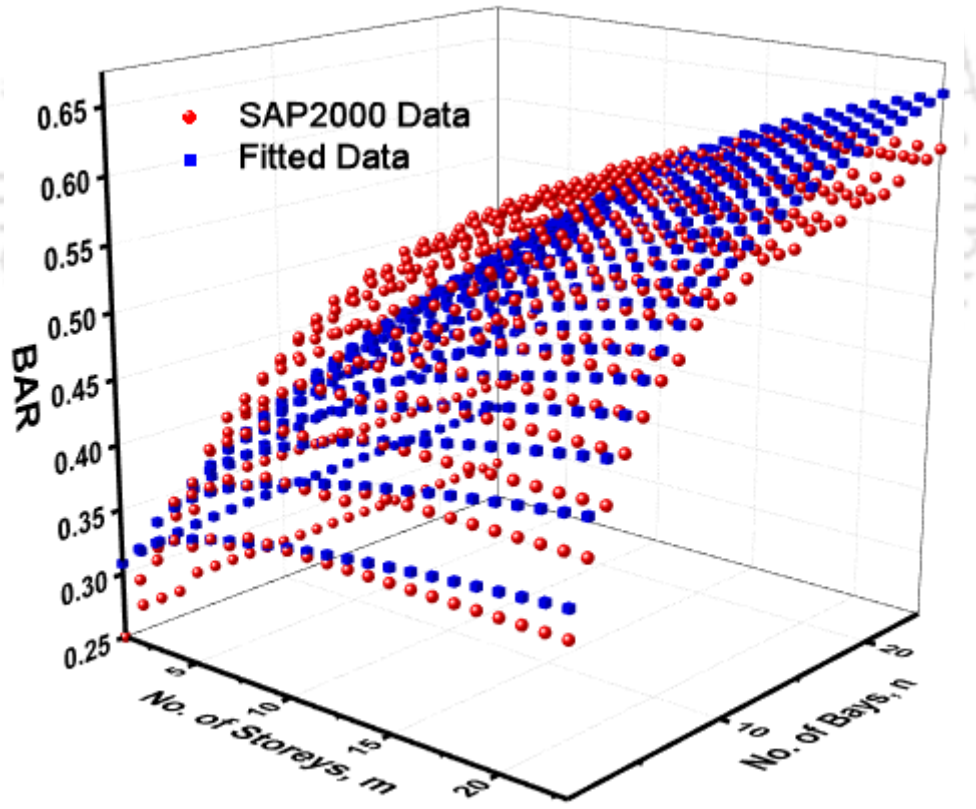

Fig. 8.6. Beam Axial Resistance factor (BAR).

Table 8.10. BAR factors.

BAR	Remarks
$z0 + Bm^C + Dn^E + Fm^C n^E$	for n≥3 and m≥2
0.21	for n≥6 and m=1
0.17	for n=3 to 5 and m=1

Table 8.11. Regression parameters of BAR.

Constant	Value	Standard Error	Standard Deviation	Coefficient of Variation
z0	65.02174	179.19378		
B	-64.88998	179.2373		
C	0.00928	0.02414		
D	-67.18941	185.13165	0.02336	0.0465
E	0.03709	0.03827		
F	67.36583	185.17181		

Table 8.12. Correlation Matrix of BAR.

Constant	z0	B	C	D	E	F
z0	1					
B	-1	1				
C	-0.911	0.910	1			
D	-0.999	0.999	0.917	1		
E	-0.307	0.308	-0.111	0.293	1	
F	0.999	-0.999	-0.916	-1	-0.294	1

The minimum axial resistance (A_{RB}) required in beam to mitigate the progressive collapse of multi-storey buildings is given by

$$A_{RB} = BAR \times R_{u,\text{beam}} \text{ (kN)} \tag{8.9}$$

Where $R_{u,beam}$ is the limiting resistance of intact beam.

The shear collapse resistance factors for the beams (BSR) is obtained from the developed probabilistic equation (8.10). A surface plot is drawn for the recorded data, as shown in Fig. 8.7, and it describes the accuracy of the probabilistic model with the SAP2000 data. The regression parameters, values for constants, and correlation matrix for the probabilistic model are listed in Table 8.13 and Table 8.14.

$$BSR = z0 + Bm^C + Dn^E + Fm^C n^E \text{ for n≥3 and m≥1} \tag{8.10}$$

Where 'm' is the number of storeys, 'n' is the number of bays in the building and z0, B, C, D, E and F are constants listed in Table 8.13.

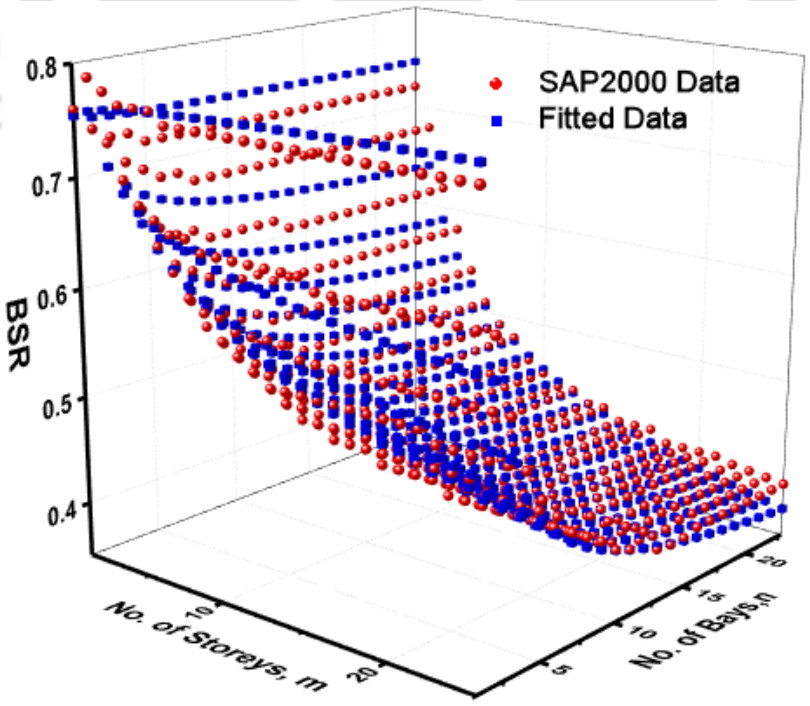

Fig. 8.7. Beam Shear Resistance factors (BSR).

Table 8.13. Regression parameters of BSR.

Constant	Value	Standard Error	Standard Deviation	Coefficient of Variation
z0	-0.05098	0.04001		
B	0.79525	0.03796		
C	-0.23343	0.01718		
D	0.84804	0.04405	0.01572	0.0308
E	-0.69319	0.01973		
F	-0.83792	0.04624		

Table 8.14. Correlation Matrix of BSR.

Constant	z0	B	C	D	E	F
z0	1					
B	-0.994	1				
C	-0.971	0.952	1			
D	-0.956	0.964	0.929	1		
E	-0.200	0.208	-0.0003	0.087	1	
F	0.871	-0.899	-0.823	-0.969	-0.080	1

The minimum shear resistance (V_{RB}) required in beam to mitigate the progressive collapse of multi-storey buildings is given by

$$V_{RB} = BSR \times R_{u,beam} \text{ (kN)} \tag{8.11}$$

Where $R_{u,beam}$ is the limiting resistance of intact beam.

The bending collapse resistance factors for the beams (BBR) is obtained from the developed probabilistic equation (8.12), (8.13) and Table 8.19. A surface plot is drawn for the recorded data, as shown in Fig. 8.8 and 8.9, respectively, and they describe the accuracy of the probabilistic model with the SAP2000 data. The regression parameters, values for constants and correlation matrix for the probabilistic model are listed in Tables 8.15, 8.16, 8.17 and Table 8.18, respectively.

$$BBR = z0 + Bm^{C} + Dn^{E} + Fm^{C}n^{E} \text{ for n= 3 to 5 and m≥1} \qquad (8.12)$$

Where 'm' is the number of storeys, 'n' is the number of bays in the building and z0, B, C, D, E and F are constants listed in Table 8.15.

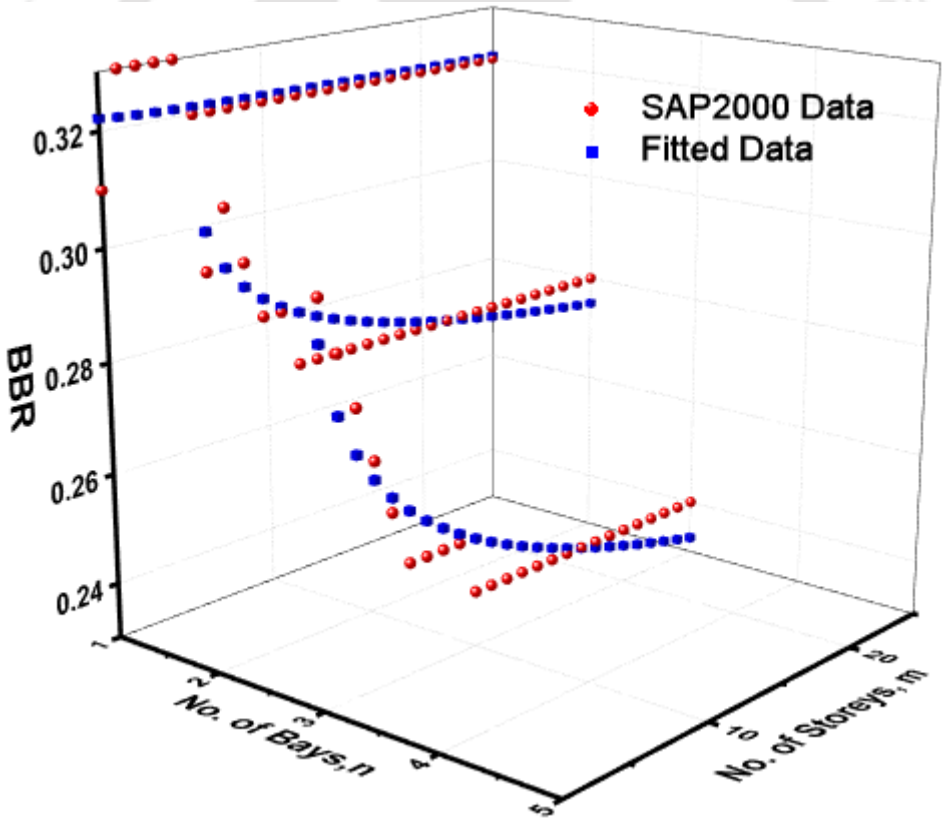

Fig. 8.8. Beam Bending Resistance factors (BBR) for n= 3 to 5 and m≥1.

Table 8.15. Regression parameters of BBR for n= 3 to 5 and m≥1.

Constant	Value	Standard Error	Standard Deviation	Coefficient of Variation
z0	-10.70628	454.02462		
B	-11.51677	474.09514		
C	0.85544	0.13034		
D	11.04757	454.02488	0.00508	0.0178
E	0.001	0.04103		
F	-11.53558	474.09525		

Table 8.16. Correlation Matrix of BBR for n= 3 to 5 and m≥1.

Constant	z0	B	C	D	E	F
z0	1					
B	-1	1				
C	-0.116	-0.116	1			
D	-1	1	-0.116	1		
E	-0.999	-0.999	0.110	-0.999	1	
F	1	-1	0.116	-1	0.999	1

$$BBR = z0 + Bm^{C} + Dn^{E} + Fm^{C}n^{E} \quad \text{for n= 3 to 5 and m≥1} \tag{8.13}$$

Where ‘m’ is the number of storeys, ‘n’ is the number of bays in the building and z0, B, C, D, E and F are constants listed in Table 8.17.

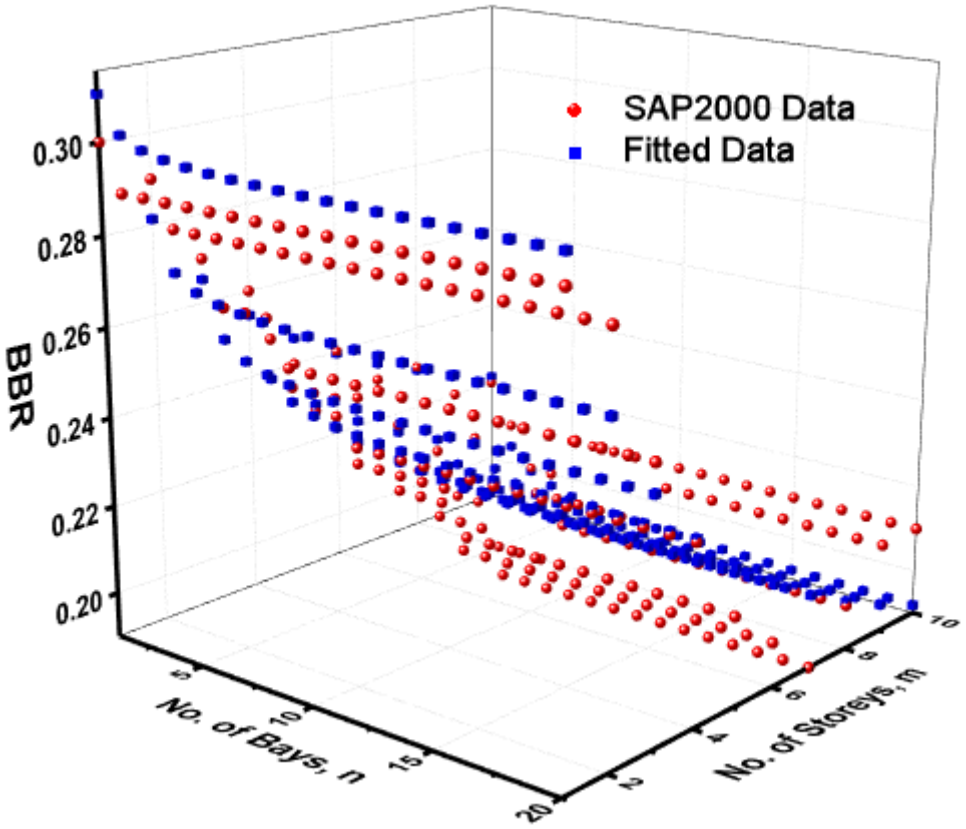

Fig. 8.9. Beam Bending Resistance factors (BBR) for m= 1 to 10 and n≥6.

Table 8.17. Regression parameters of BBR for m= 1 to 10 and n≥6.

Constant	Value	Standard Error	Standard Deviation	Coefficient of Variation
z0	-0.21355	0.32952		
B	0.09474	0.07199		
C	-1.17732	0.3974		
D	0.5097	0.32817	0.01105	0.0482
E	-0.10041	0.07307		
F	-0.08073	0.07745		

Table 8.18. Correlation Matrix of BBR for m= 1 to 10 and n≥6.

Constant	z0	B	C	D	E	F
z0	1					
B	-0.738	1				
C	-0.018	0.011	1			
D	-0.999	0.741	0.015	1		
E	-0.999	0.724	-0.00002	0.998	1	
F	0.686	-0.995	-0.008	-0.688	-0.670	1

Table 8.19. BBR load factors.

BBR	Remarks
0.23	For n≥6 and m≥10
$z0 + Bm^C + Dn^E + Fm^C n^E$	For n=3 to 5 and m≥1
$z0 + Bm^C + Dn^E + Fm^C n^E$	For n≥6 and m=1 to 10

The minimum bending resistance (M_{RB}) required in beam to mitigate the progressive collapse of multi-storey buildings is given by

$$M_{RB} = BBR \times R_{u,beam} \text{ (kN-m)} \tag{8.14}$$

Where $R_{u,beam}$ is the limiting resistance of intact beam.

The developed probabilistic Collapse resistance factors can be used to quantify the required resistance to mitigate the progressive collapse of multi-storey buildings.

8.4 Validated Numerical Example

A 10-storey and 5-bays RC structure, as illustrated in Fig. 6.3, is considered to validate the proposed procedure with the gravity loads. The numerical model details are given in section 6.3.1 of chapter 6.

Numerical Method (SAP2000)

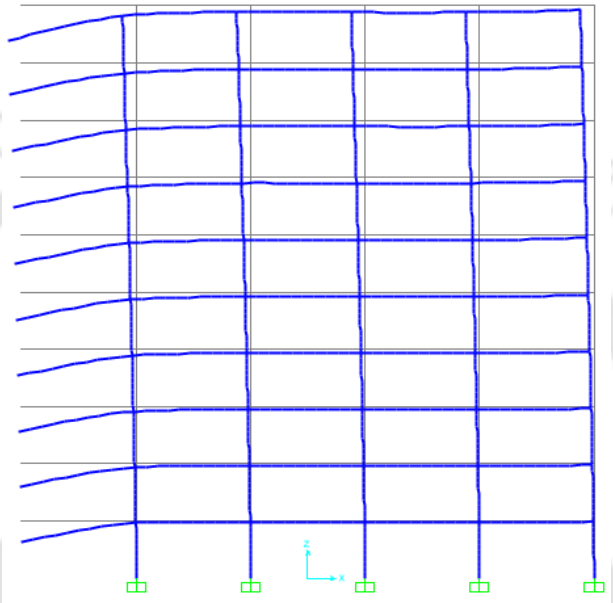

(a) Collapsed building or series of columns removed.

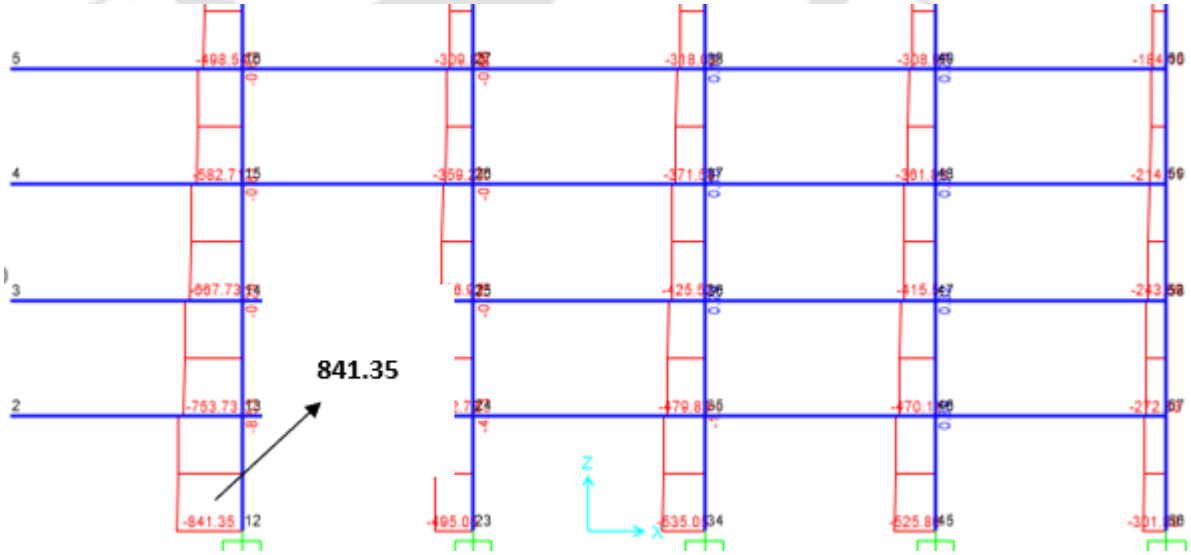

(b) Axial Resistance Results (kN).

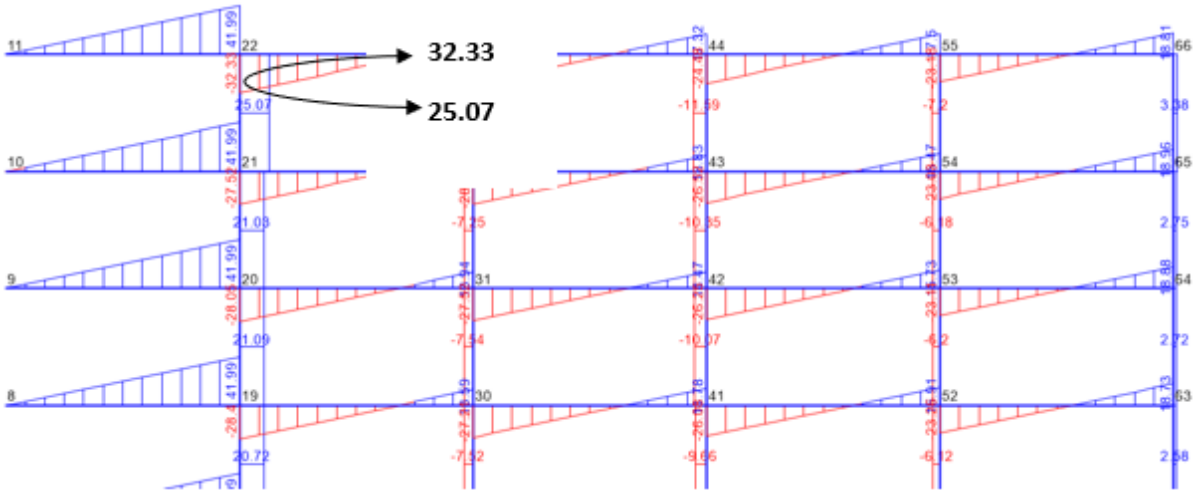

(c) Shear Resistance Results (kN).

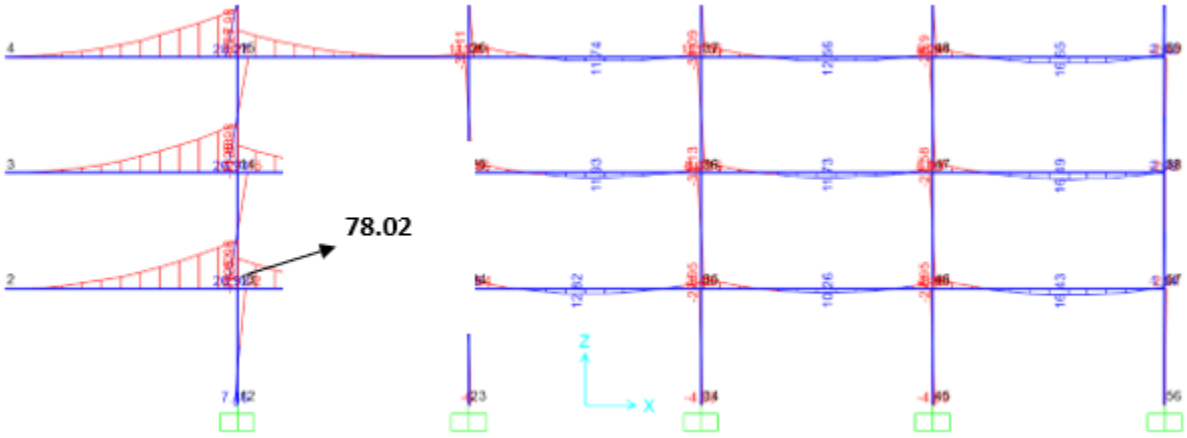

(d) Bending Moment Resistance Results (kN-m).

Fig. 8.10. Numerical results from SAP2000 Software.

Proposed Method (Collapse Resistance Factors)

Number of bays (n) = 5

Number of storeys (m) = 10

From section 8.3, the collapse resistance factors are

CAR = 15.43; CSR = 0.42; CBR = 0.26;

BAR = 0.42; BSR = 0.58; BBR = 0.24;

The resistance of intact beam from the gravity loads;

$$R_{u,beam} = (DL)_{beams} + (DL)_{columns}$$
$$R_{u,beam} = (0.4 \times 0.7 \times 6 \times 25) + (0.4 \times 0.4 \times 3 \times 25) = 54KN$$

Where $(DL)_{beams}$, and $(DL)_{columns}$ are dead loads of beams and columns, respectively.

The minimum resistances required in the collapsed building to mitigate the progressive collapse of the multi-storey building are given by

$$A_{RC} = CAR \times R_{u,\text{beam}}$$
$$A_{RC} = 15.43 \times 54 = 833.22KN$$
$$A_{RB} = BAR \times R_{u,\text{beam}}$$
$$A_{RB} = 0.42 \times 54 = 22.68KN$$

$$V_{RC} = CSR \times R_{u,beam}$$
$$V_{RC} = 0.42 \times 54 = 22.68KN$$
$$V_{RB} = BSR \times R_{u,beam}$$
$$V_{RB} = 0.58 \times 54 = 31.32KN$$

$$M_{RC} = CBR \times R_{u,beam}$$
$$M_{RC} = 0.26 \times 3 \times 54 = 42.12KN.m$$
$$M_{RB} = BBR \times R_{u,beam}$$
$$M_{RB} = 0.24 \times 6 \times 54 = 77.76KN.m$$

Table 8.20. Summary of validation results

Analysis Method	Required Resistance					
	A_{RC}(kN)	V_{RC}(kN)	M_{RC}(kN.m)	A_{RB}(kN)	V_{RB}(kN)	M_{RB}(kN.m)
Proposed Method	833.22	22.68	42.12	22.68	31.32	77.76
SAP2000 Software	841.25	25.07	40.65	25.07	33.64	78.02
Relative Error (%)	0.954	9.53	3.49	9.53	6.89	0.333

Table 8.20 shows that the results of the proposed method and SAP2000 are very similar. Both the methods have a relative inaccuracy ranging from 0.33 to 9.53 percent. As a result, the proposed method can be utilised to calculate the minimum required resistances of multi-storey buildings to mitigate the progressive collapse of the buildings. A similar procedure is adopted to quantify the collapse resistance factors for other two cases such as 1) For top column removal and 2) For bottom column removal, respectively. The following sections quantify the resistance factors for the aforesaid cases.

8.5 Collapse Resistance for Top Column Removal

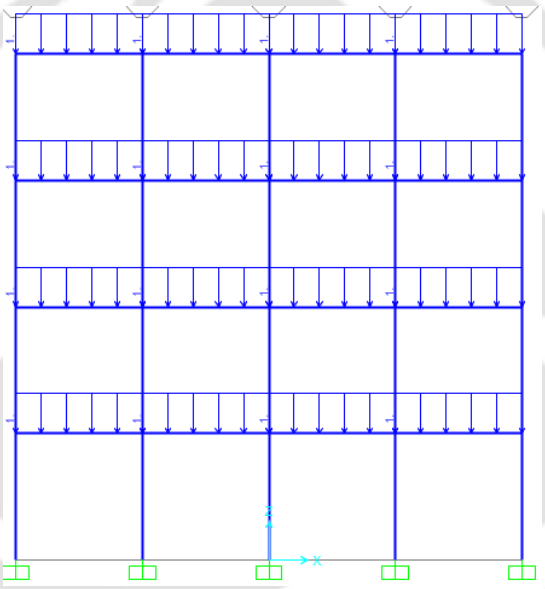

(a)

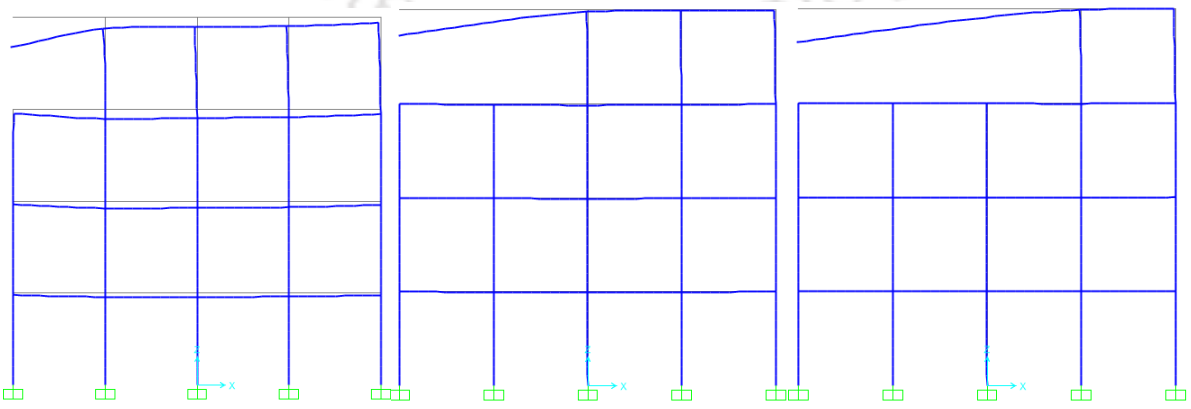

(b)

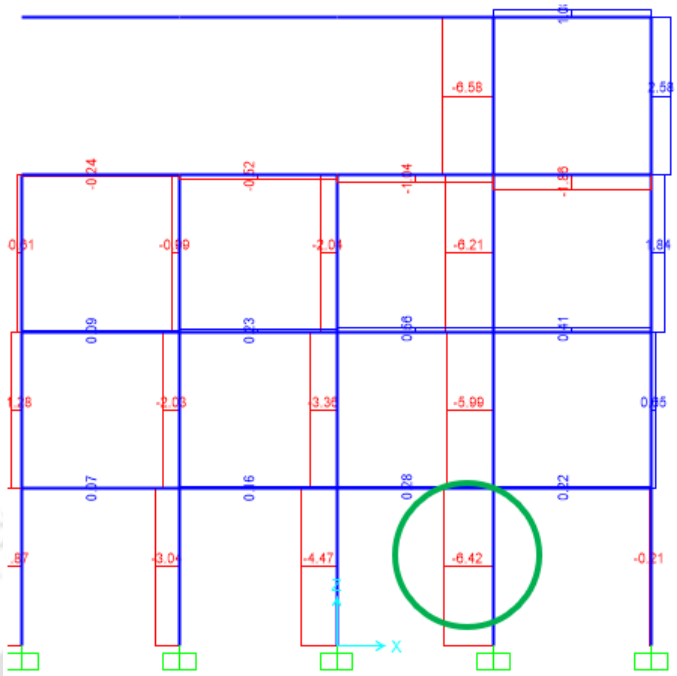

(c)

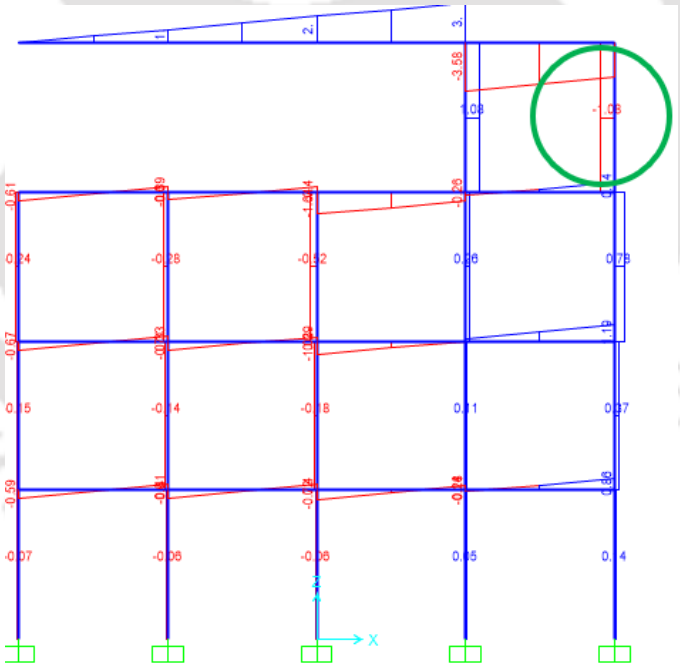

(d)

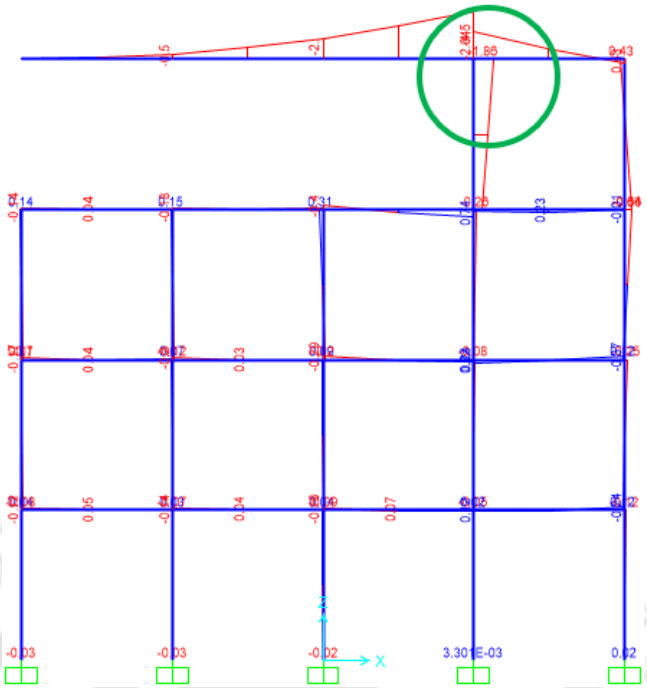

(e)

Fig. 8.11. Multi-storey building: a) Unit gravity load b) Collapse mechanism c) Collapse Axial Resistance factor (CAR) d) Collapse Shear Resistance factor (CSR) e) Collapse Bending Resistance factor (CBR).

The axial collapse resistance factors (CAR) for the top column removal is obtained from the developed probabilistic equation (8.15). A surface plot is drawn for the recorded data, as shown in Fig. 8.12, and it describes the accuracy of the probabilistic model with SAP2000 data. The regression parameters, values for constants, and correlation matrix for the probabilistic model are listed in Table 8.21 and 8.22.

$$CAR = z0 + Bm^{C} + Dn^{E} + Fm^{C}n^{E} \quad \text{for n}\geq 2 \text{ and m}\geq 2 \tag{8.15}$$

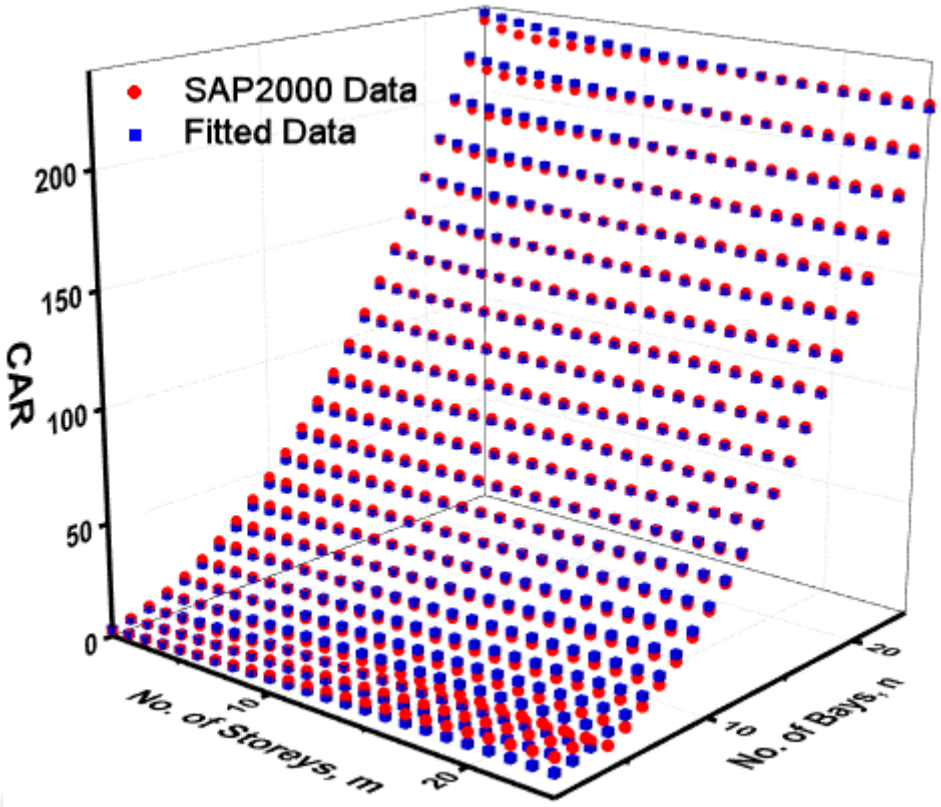

Fig. 8.12. Collapse Axial Resistance factor (CAR).

Table 8.21. Regression parameters of CAR.

Constant	Value	Standard Error	Standard Deviation	Coefficient of Variation
z0	1.24494	1.15142		
B	1.30392	0.77357		
C	0.58832	0.1517		
D	0.41728	0.01848	0.05673	0.0067
E	1.9982	0.01378		
F	-0.00755	0.00456		

Table 8.22. Correlation Matrix of CAR.

Constant	z0	B	C	D	E	F
z0	1					
B	-0.979	1				
C	0.960	-0.995	1			
D	-0.419	0.364	-0.376	1		
E	0.071	-0.014	0.033	-0.912	1	
F	0.961	-0.981	0.979	-0.451	0.079	1

The minimum axial resistance (A_{RC}) required in the column to mitigate the progressive collapse of multi-storey buildings is given by

$$A_{RC} = CAR \times R_{u,beam} \text{ (kN)} \tag{8.16}$$

Where $R_{u,beam}$ is the limiting resistance of intact beam.

The shear collapse resistance factors (CSR) for the top column removal is obtained from the developed probabilistic equation (8.17). A surface plot is drawn for the recorded data, as shown in Fig. 8.13, and it describes the accuracy of the probabilistic model with SAP2000 data. The regression parameters, values for constants and correlation matrix for the probabilistic model, are listed in Table 8.23 and Table 8.24, respectively.

$$CSR = z0 + Bm^{C} + Dn^{E} + Fm^{C}n^{E} \text{ for } n \geq 2 \text{ and } m \geq 2 \tag{8.17}$$

Where ‘m’ is the number of storeys, ‘n’ is the number of bays in the building and z0, B, C, D, E and F are constants listed in Table 8.23.

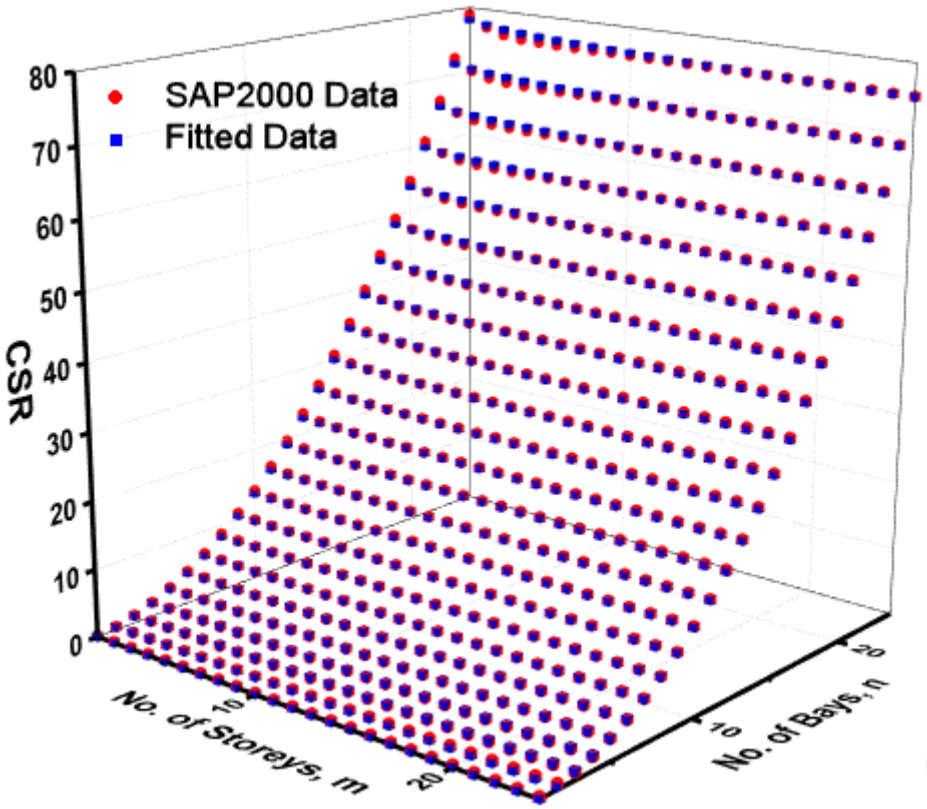

Fig. 8.13. Collapse Shear Resistance factor (CSR).

Table 8.23. Regression parameters of CSR.

Constant	Value	Standard Error	Standard Deviation	Coefficient of Variation
z0	-46.58775	637.6628		
B	46.57882	637.66166		
C	8.17493E-4	0.01118		
D	1.94326	24.9103	0.0604	0.0023
E	2.02744	0.00161		
F	-1.81885	24.91025		

Table 8.24. Correlation Matrix of CSR.

Constant	z0	B	C	D	E	F
z0	1					
B	-1	1				
C	0.999	0.999	1			
D	-0.999	0.999	-1	1		
E	0.042	-0.042	-0.042	-0.042	1	
F	0.999	-0.999	-0.939	1	-1	1

The minimum shear resistance (V_{RC}) required in the column to mitigate the progressive collapse of multi-storey buildings is given by

$$V_{RC} = CSR \times R_{u,beam} \text{ (kN)} \tag{8.18}$$

Where $R_{u,beam}$ is the limiting resistance of intact beam.

The bending collapse resistance factors (CBR) for the top column removal is obtained from the developed probabilistic equation (8.19). A surface plot is drawn for the recorded data, as shown in Fig. 8.14, and it describes the accuracy of the probabilistic model with SAP2000 data. The regression parameters, values for constants and correlation matrix for the probabilistic model are listed in Tables 8.25 and 8.26, respectively.

$$CBR = z0 + Bm^{C} + Dn^{E} + Fm^{C}n^{E} \text{ for } n \geq 2 \text{ and } m \geq 2 \tag{8.19}$$

Where ‘m’ is the number of storeys, ‘n’ is the number of bays in the building and z0, B, C, D, E and F are constants listed in Table 8.25.

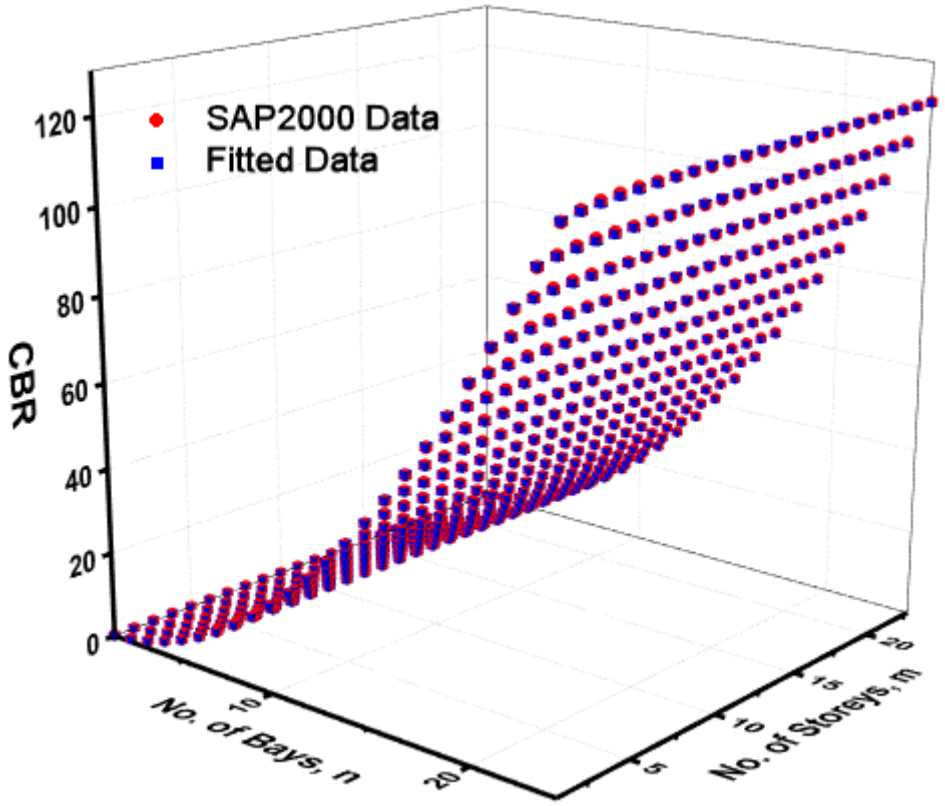

Fig. 8.14. Collapse Bending Resistance factor (CBR).

Table 8.25. Regression parameters of CBR.

Constant	Value	Standard Error	Standard Deviation	Coefficient of Variation
z0	-0.11454	0.19187		
B	3.23118E-5	0.00424		
C	1.99356	3.44713E-4		
D	0.09129	0.18668	0.01435	0.00034
E	0.01225	2.81477E-4		
F	0.20618	0.00425		

Table 8.26. Correlation Matrix of CBR.

Constant	z0	B	C	D	E	F
z0	1					
B	0.041	1				
C	0.006	0.040	1			
D	-0.999	-0.041	0.0004	1		
E	0.215	0.908	0.037	-0.215	1	
F	-0.047	-0.998	-0.089	0.046	-0.912	1

The minimum bending resistance (M_{RC}) required in the column to mitigate the progressive collapse of multi-storey buildings is given by

$$M_{RC} = CBR \times R_{u,beam} \text{ (kN-m)} \quad (8.20)$$

Where $R_{u,beam}$ is the limiting resistance of intact beam.

8.6 Collapse Resistance for Bottom Column Removal

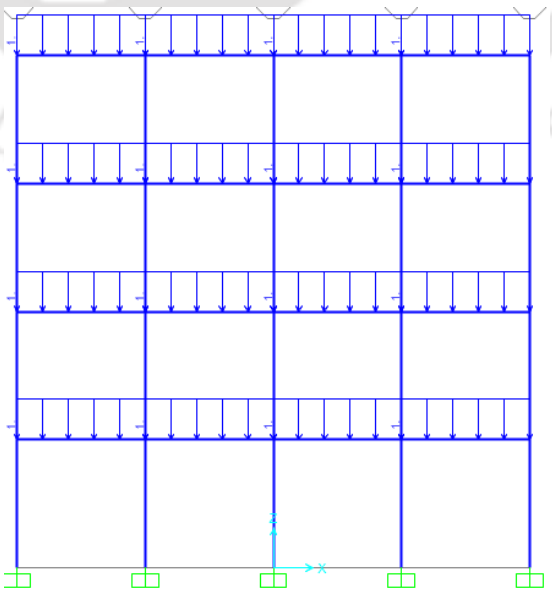

(a)

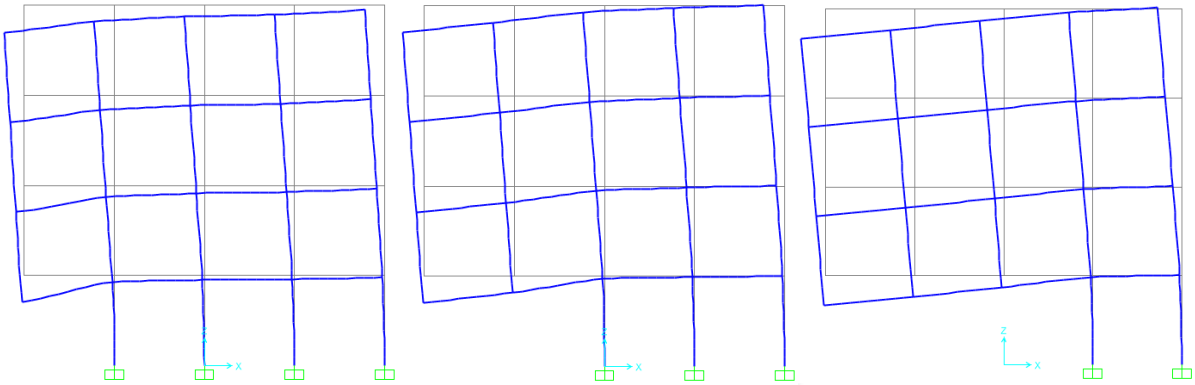

(b)

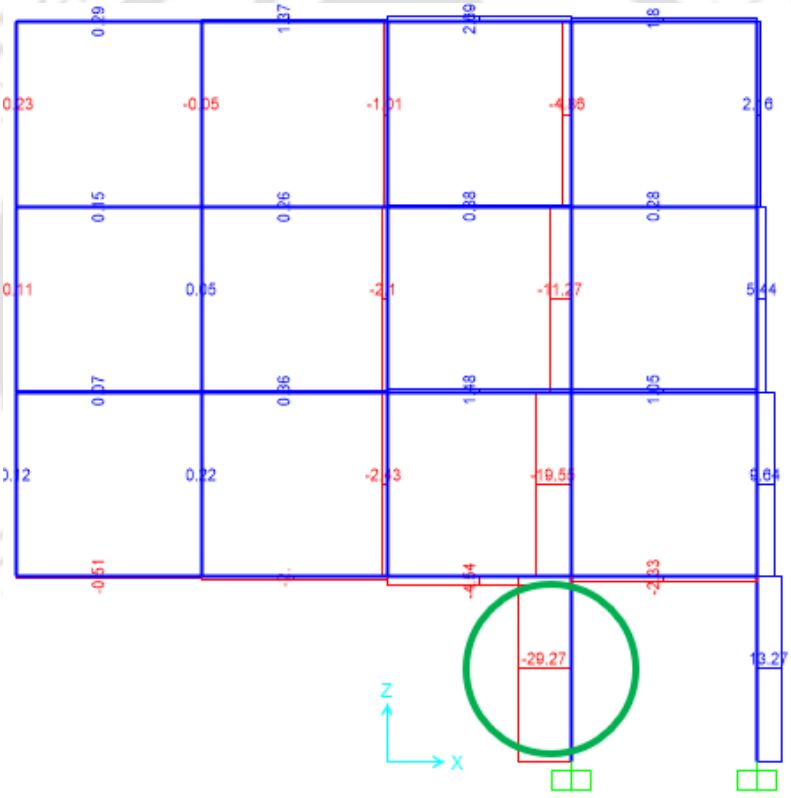

(c)

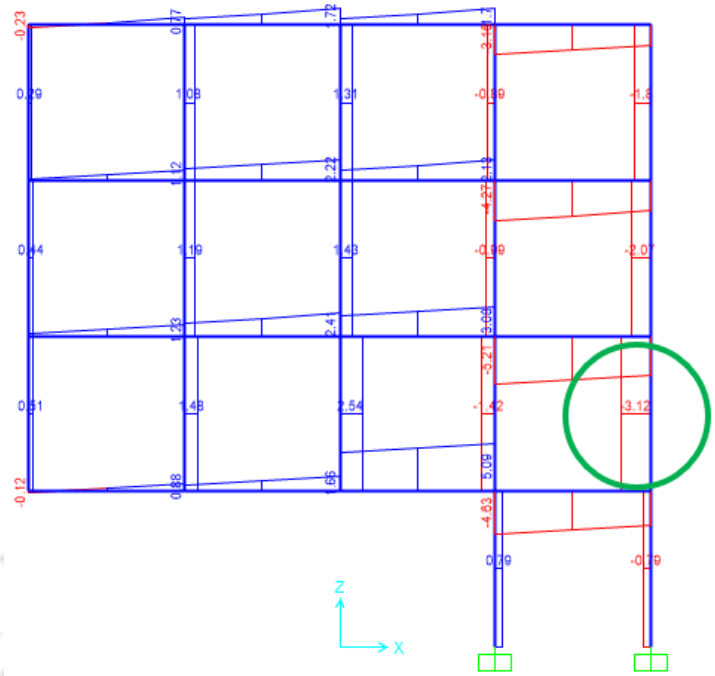

(d)

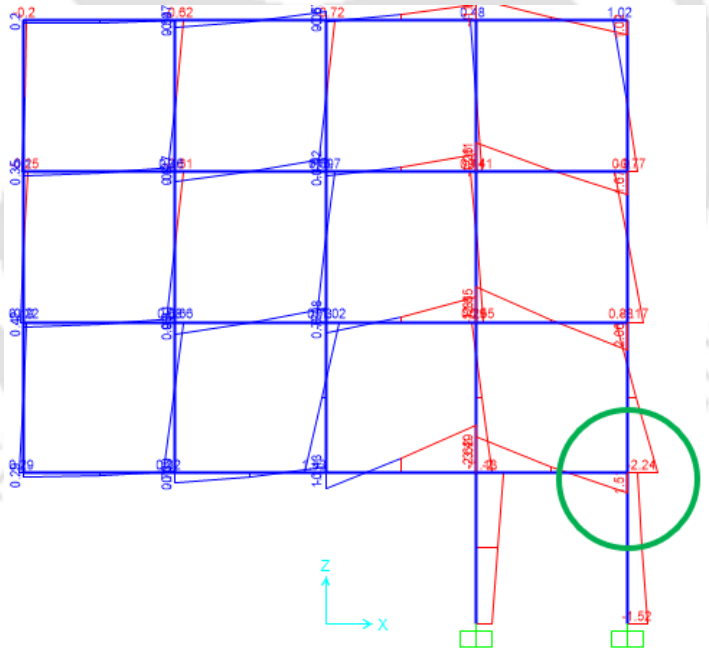

(e)

Fig. 8.15. Multi-storey building: a) Unit gravity load b) Collapse mechanism c) Collapse Axial Resistance factor (CAR) d) Collapse Shear Resistance factor (CSR) e) Collapse Bending Resistance factor (CBR).

The axial collapse resistance factors (CAR) for the bottom column removal is obtained from the developed probabilistic equation (8.21). A surface plot is drawn for the recorded data, as shown in Fig. 8.16, and it describes the accuracy of the probabilistic model with SAP2000 data. The regression parameters, values for constants, and correlation matrix for the probabilistic model are listed in Table 8.27 and 8.28.

$$CAR = z0 + Bm^{C} + Dn^{E} + Fm^{C}n^{E} \text{ for } n \geq 2 \text{ and } m \geq 2 \quad (8.21)$$

Where 'm' is the number of storeys, 'n' is the number of bays in the building and z0, B, C, D, E and F are constants listed in Table 8.27.

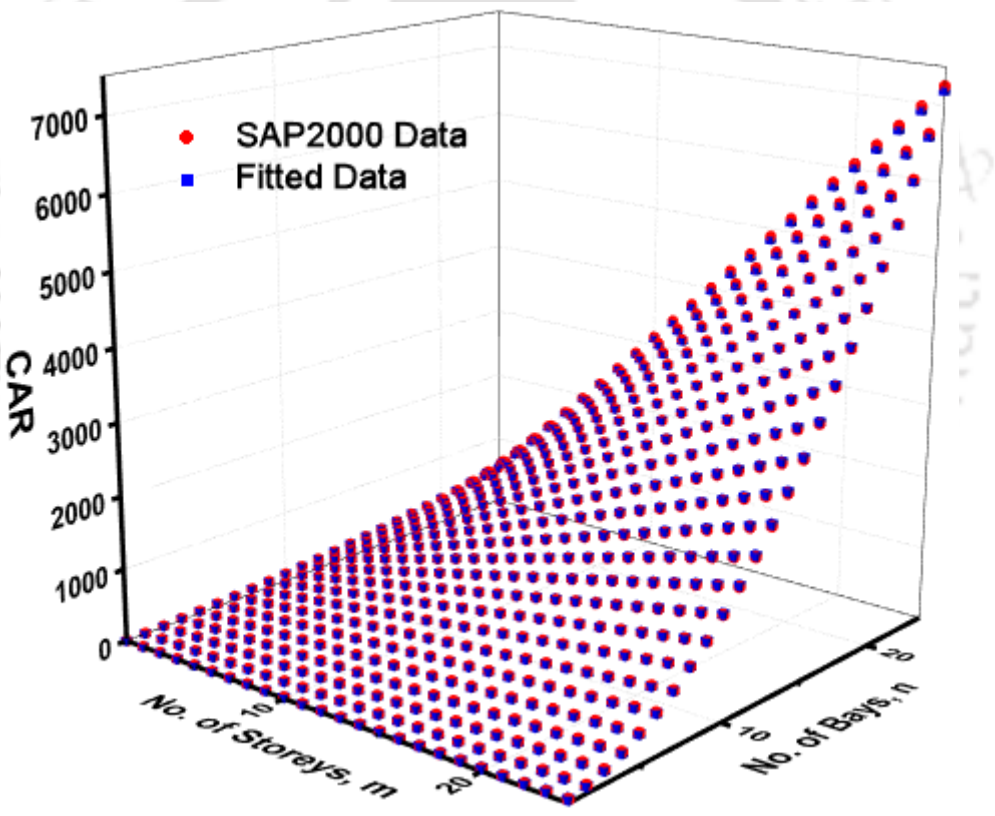

Fig. 8.16. Collapse Axial Resistance factor (CAR).

Table 8.27. Regression parameters of CAR.

Constant	Value	Standard Error	Standard Deviation	Coefficient of Variation
z0	1.57331	0.11913		
B	1.23077	0.02097		
C	1.01821	0.00203		
D	0.65076	0.01146	0.05836	0.000041
E	1.87393	0.00134		
F	0.70383	0.0053		

Table 8.28. Correlation Matrix of CAR.

Constant	z0	B	C	D	E	F
z0	1					
B	-0.586	1				
C	0.017	-0.311	1			
D	-0.119	-0.266	0.858	1		
E	-0.008	0.407	-0.026	-0.182	1	
F	0.014	0.030	-0.847	-0.682	-0.498	1

The minimum axial resistance (A_{RC}) required in the column to mitigate the progressive collapse of multi-storey buildings is given by

$$A_{RC} = CAR \times R_{u,beam} \text{ (kN)} \tag{8.22}$$

Where $R_{u,beam}$ is the limiting resistance of intact beam.

The shear collapse resistance factors (CSR) for the bottom column removal can be obtained from the empirical equation (8.23). A surface plot is drawn for the recorded data, as shown in Fig. 8.17, and it describes the accuracy of the probabilistic model with SAP2000 data. The regression parameters, values for constants and correlation matrix for the probabilistic model, are listed in Table 8.29 and Table 8.30, respectively.

$$CSR = z0 + Bm^{C} + Dn^{E} + Fm^{C}n^{E} \text{ for n}\geq 2 \text{ and m}\geq 2 \quad (8.23)$$

Where 'm' is the number of storeys, 'n' is the number of bays in the building and z0, B, C, D, E and F are constants listed in Table 8.29.

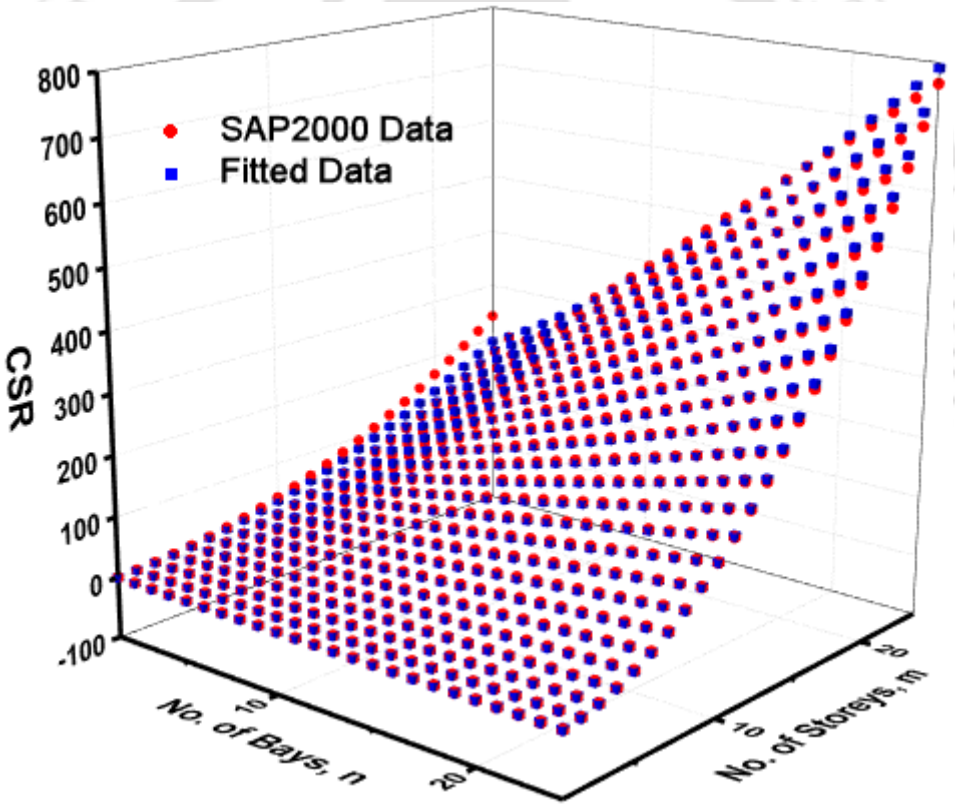

Fig. 8.17. Collapse Shear Resistance factor (CSR).

Table 8.29. Regression parameters of CSR.

Constant	Value	Standard Error	Standard Deviation	Coefficient of Variation
z0	-0.53331	0.13966		
B	0.04227	0.00665		
C	1.25375	0.01695		
D	0.3667	0.00854	0.03148	0.0019
E	1.95842	0.00696		
F	0.02229	0.00127		

Table 8.30. Correlation Matrix of CSR.

Constant	z0	B	C	D	E	F
z0	1					
B	-0.638	1				
C	0.041	-0.329	1			
D	-0.319	-0.193	0.417	1		
E	0.282	0.140	0.002	-0.864	1	
F	-0.117	0.229	-0.930	-0.102	-0.355	1

The minimum shear resistance (V_{RC}) required in the column to mitigate the progressive collapse of multi-storey buildings is given by

$$V_{RC} = CSR \times R_{u,beam} \text{ (kN)} \tag{8.24}$$

Where $R_{u,beam}$ is the limiting resistance of intact beam.

The bending collapse resistance factors (CBR) for the bottom column removal can be obtained from the equations (8.25). A surface plot is drawn for the recorded data, as shown in Fig. 8.18, and it describes the accuracy of the probabilistic model with SAP2000 data. The regression parameters, values for constants and correlation matrix for the probabilistic model are listed in Tables 8.31 and Table 8.32, respectively.

$$CBR = z0 + Bm^{C} + Dn^{E} + Fm^{C}n^{E} \text{ for n}\geq 2 \text{ and m}\geq 2 \quad (8.25)$$

Where ‘m’ is the number of storeys, ‘n’ is the number of bays in the building and z0, B, C, D, E and F are constants listed in Table 8.31.

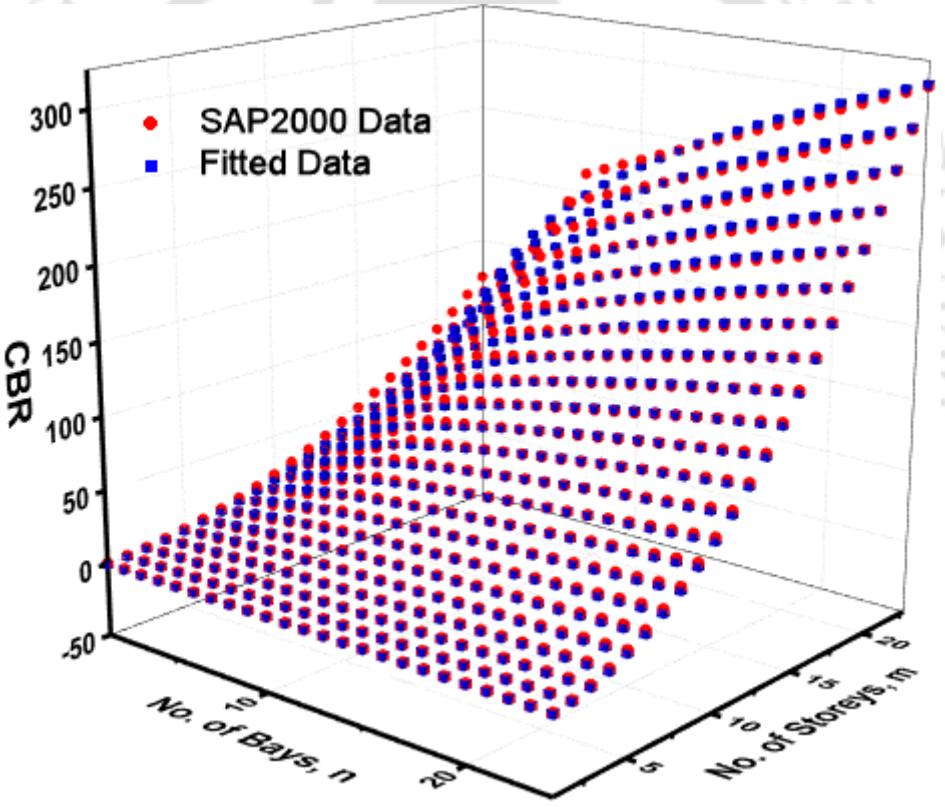

Fig. 8.18. Collapse Bending Resistance factor (CBR).

Table 8.31. Regression parameters of CBR.

Constant	Value	Standard Error	Standard Deviation	Coefficient of Variation
z0	-1.3637	0.17464		
B	0.75548	0.0912		
C	0.35446	0.01569		
D	-0.00741	0.02083	0.02193	0.0026
E	1.94209	0.00522		
F	0.22915	0.01819		

Table 8.32. Correlation Matrix of CBR.

Constant	z0	B	C	D	E	F
z0	1					
B	-0.914	1				
C	0.293	-0.561	1			
D	0.232	-0.505	0.986	1		
E	0.047	0.098	0.033	0.045	1	
F	-0.266	0.501	-0.977	-0.980	-0.225	1

The minimum bending resistance (M_{RC}) required in the column to mitigate the progressive collapse of multi-storey buildings is given by

$$M_{RC} = CBR \times R_{u,beam} \text{ (kN-m)} \tag{8.26}$$

Where $R_{u,beam}$ is the limiting resistance of intact beam.

8.7 Discussion

By adopting numerical simulation to generate database for the development of probabilistic models, this chapter develops probabilistic models for collapse resistance factors for multi-storey building subject to gravity loads. Using OriginPro software, probabilistic models are created for the collapse resistance factors based on the regression analysis. The significant standard deviation (σ), coefficient of variation (CV), and coefficient of determination (R^2) all indicate the accuracy of the probabilistic models. These empirical models can be used to generate collapse resistance factors for rigid frame members (beams and columns). The rigid frame members' minimum required resistances are calculated using collapse resistance factors. To mitigate the progressive collapse, the minimum required resistance can be utilised to design key load-bearing elements in multi-storey rigid frame constructions.

CHAPTER 9 CONCLUSIONS AND FUTURE SCOPE

9.1 Summary

Instead of the idealised spherical or hemispherical explosives considered in commonly used semi-empirical techniques, realistic explosion scenarios frequently include detonating non-spherical high explosive charges. The spherical equivalent quantities for pressure and deformation of explosive charge geometries such cylindrical, conical, rectangular, and cubical shapes are developed in this study. The blast load due to spherical or hemispherical explosions has been predicted or quantified using empirical equations or graphs in the literature. The blast loads caused by researched explosions such as cylindrical, conical, rectangular, and cubical can be anticipated or measured using spherical equivalent factors. These equivalent factors are used to analyse RC frame structures that have been subjected to internal explosions caused by explosives like cylindrical, cubical, rectangular, and conical charges. The quantifiable blast loads caused by the above-mentioned explosions are now ready to be used in the time history study of blast-damaged structures.

While the positive phase of the explosion is widely recognised, confirmation of the negative phase is uncommon in the literature. As a result, it is frequently treated erroneously or ignored entirely. The effects of negative phase pressures on the overall motion of an object should also be estimated during the design process. The limits of Friedlander's time history profile are investigated, and a new simple, dependable, and accurate quadratic blast time history profile is devised. Friedlander's profile and the quadratic profile's elastic response spectra are compared. The response spectra of the quadratic blast profile are quite similar to Friedlander's spectra. Generalised relationships between peak overpressures and durations in the positive and negative phases are introduced to build the other types of time history profiles. The derived blast time history profiles are validated using numerical time history analysis. The derived profiles match Friedlander's profile very well.

In the design of blast-resistant structures, rigid frame structure construction was chosen because it enables open internal space while also providing strong resistance to lateral loads. Furthermore, due to the eventual invention of plastic hinges, this structure has intrinsic energy absorption capabilities up to the structure's ultimate capacity. The TM 5-1300 design handbook outlines rational techniques for undertaking the preliminary design of blast-resistant single-storey rigid frames quickly and efficiently. The probabilistic models for critical load and collapse resistance factors of multi-storey rigid frames are developed in this study. These load factors account for the inherent uncertainties in blast loadings, such as blast direction and critical position. The peak loads of multi-storey buildings, such as axial, shear, and bending moments, are calculated. In the design of multi-storey buildings, these peak loads are utilised to estimate the size of the structural element. This study also explored the progressive collapse resistance factors of multi-storey buildings to quantify the required resistance to mitigate the progressive collapse of the buildings.

The framework for equivalent SDOF systems subject to blast loading is thoroughly established. The modified mode shape function is used to create an equivalent single degree of freedom system for multi-storey buildings or skyscrapers. In the literature, the mode shape function of multi-storey buildings is only limited to the first mode. The existing cantilever shape function is used to create this modified mode shape function. An empirical model is developed to determine the mode shape factor as a function of the mode number to improve the accuracy of the modified shape function. The natural time periods for the first six modes created by the modified mode shape function are compared to existing literature and the numerical model in SAP2000 software. Existing approaches agree well with the results. Finally, multi-storey buildings subject to blast loading are designed using peak loads and modified shape functions. In the design of midrise multi-storey buildings, the equivalent SDOF approach of desired mode shape is applied. A user-friendly Capacity Based Design Software

(CBDS) is developed with a graphical interface for designing a structural member subject to blast loading. Probabilistic models for collapse resistance factors for multi-storey building is developed. The developed probabilistic collapse resistances factors (axial, shear and bending) of multi-storey rigid frame constructions can be used to design and mitigate the progressive collapse of the multi-storey buildings.

9.2 Conclusions

Using the finite element ALE approach, this study looked at the impact of explosive charge shapes on structure response. This research looks at five different explosive charge shapes: spherical, conical, cubical, cylindrical, and rectangular. The values for spherical equivalent pressure and deformations are determined. For the rectangular explosive charge shape at the mid location in the RC frame, the maximum deformation is 3.052 mm, and the maximum pressure is 1.498 MPa. The cubical explosive charge shape at the top of the RC frame column has a minimum deformation of 0.017 mm and a minimum pressure of 0.124 MPa. At the midpoint of the column in the RC frame, the rectangular explosive charge shape causes 5.5 times the deformation caused by the spherical charge shape. At the midpoint of the column, the cubical charge shape generates 4.3 times the pressure generated by the spherical charge shape. Conical, cubical, cylindrical, and rectangular charge shapes contribute 1.08, 4.32, 1.4, and 3.8 times the pressure imposed by the spherical charge shape. Conical, cubical, cylindrical, and rectangular charge shapes give deformations of 1.3, 3.08, 1.23, and 5.5 times that of a spherical charge shape. Compared to other explosive charge shapes, the rectangular explosive charge has a more significant impact on the structure. Compared to other explosive charges, the cubical charge has a lower influence on the structure. The blast loads in multi-storey buildings subject to internal explosions can be interpolated and quantified using the interior blast load results. The spherical equivalent factors can be used to calculate the blast load caused by cubical, conical, rectangular, and cylindrical charges.

To solve the shortcomings of Friedlander's profile, this study developed an alternative simple and accurate quadratic blast profile. Analytical solutions for an SDOF system with exponential and quadratic profiles are examined. Both the exponential and quadratic profiles' response spectra are compared. The difference between their elastic spectra is very small or non-existent, whereas their inelastic spectra range from 0.01 to 0.46. The proposed and exponential profiles are used to validate the experimental blast pressure-time history profiles found in the literature. The suggested profiles are very similar to Friedlander's profile. These profiles can be employed in the blast time history study of structures as an alternative to Friedlander's profile. To improve the accuracy of the analytical blast profile, more blast tests are needed to establish the relationship between positive and negative phase peak overpressures. This study might be expanded to include other functions such as trigonometry functions, to improve the results. With so many variables impacting whether the negative phase is conservative, non-conservative, or has no effect, determining when the negative phase may be ignored or not is difficult and impractical. Indeed, it may be argued that the negative phase should not be ignored until the engineer is confident that its implications are comprehended.

Using a numerical simulation approach, this research develops probabilistic models for the critical load factors of multi-storey rigid frame buildings subject to lateral uniform loads. The derived load factors matched the existing standard blast-resistant design manual, TM 5-1300. These critical load factors demonstrate the inherent nature of uncertainties, such as blast loading direction and critical location. These load factors' probabilistic models are being developed. Future studies can use these probabilistic models to design essential load-bearing elements of reinforced concrete and steel rigid frame structures. The peak loads in multi-storey rigid frame constructions are calculated using these probabilistic models for critical load factors. In the design of multi-storey buildings, the computed peak loads are utilised to determine the size of the structural member. The progressive collapse resistance factors are

also developed to quantify the required resistance to mitigate the progressive collapse of the buildings. Only fixed-ended rigid frame constructions subject to lateral uniform loads are considered in this study. These findings contribute to a growing body of knowledge about the importance of critical load factors. This research is the initial step in improving our computer-based case study models' knowledge.

The modified shape function of multi-storey buildings is developed in this study. Existing finite element methods agree well with the natural time periods created by the modified shape function. The first mode has a relative inaccuracy of 9.25 percent, but the remaining modes are closer to known approaches. The equivalent SDOF system of a multi-storey building subject to harmonic, seismic, transient, blast, and impact loads can be created using this modified shape function. For the required mode shape, the modified shape function is useful in designing multi-storey buildings.

The multi-storey building is designed using peak loads and a modified shape function with an equivalent SDOF approach. The suggested analysis and design approach fundamentally control the progressive collapse of multi-storey buildings subject to blast loading. The findings of this work contribute to our understanding of structural response to blast loads and improve finite element models for assessing the performance of concrete and steel structures under extreme loads.

Probabilistic models of collapse resistance factors for multi-storey building are developed. The developed probabilistic collapse resistances factors (axial, shear and bending) of multi-storey rigid frame constructions can be used to design and mitigate the progressive collapse of the multi-storey buildings.

9.3 Future Research Scope

The future effort might be focused on improving the currently proposed methods based on this set foundation:

- This study considers the vertical and parallel orientation of the conical, cylindrical, and rectangular charge shapes. The outcomes may differ if the explosive charge shapes are oriented differently.
- The variables include stand-off distance, explosive density, burst height, and charge weight, which can all be employed in a parametric analysis.
- This study could be expanded to include irregular or other explosive charge shapes.
- The linear, quadratic, cubic, and quartic family blast profiles are derived in this study, and they can be extended to trigonometric and exponential functions to improve analytical blast profile accuracy.
- To improve the accuracy of the analytical blast profile, more blast tests are needed to establish the relationship between positive and negative peak overpressures.
- To improve the negative phase effect in the study, the individual response spectrum for both the positive phase and negative phase of blast loading is advised.
- The critical load factors are limited to fix-ended rigid frames. The study can further be extended to pin-ended rigid frames.
- For horizontal uniform loads, critical load factors are determined. The research can be expanded to include point loads.
- The modified shape function is limited to shear type multi-storey buildings only. The study can further be extended to bending type multi-storey buildings.

LIST OF PUBLICATIONS

1. **Chinna Seethayya Barri** and Hrishikesh Sharma, "Probabilistic Models for Critical Load Factors of Multi-Storey Rigid Frame Structures Subjected to Blast Loading", (***Under Preparation***).
2. **Chinna Seethayya Barri** and Hrishikesh Sharma, "Probabilistic Models for Progressive Collapse Resistance Factors of Multi-Storey Rigid Frame Structures", (***Under Preparation***).
3. **Chinna Seethayya Barri** and Hrishikesh Sharma, "Numerical evaluation of effect of Charge Shape on RC Frame Subjected to Blast Loading", (***Under Preparation***)
4. **Chinna Seethayya Barri** and Hrishikesh Sharma, "Development and Comparison of Quadratic Blast Profile and Its Response Spectrum with Friedlander's Profile", (***Under Preparation***)
5. **Chinna Seethayya Barri** and Hrishikesh Sharma, "Modal Analysis of Multi-Storey Shear Buildings Using Modified Building Shape Function", (***Under Preparation***)
6. **Chinna Seethayya Barri** and Hrishikesh Sharma, "Equivalent SDOF Design of Multi-Storey Shear Buildings Subjected to Blast Loading", (***Under Preparation***)

REFERENCES

1. Abdollahzadeh, Gholamreza, Hadi Faghihmaleki, and Mehrdad Avazeh. (2020). Progressive Collapse Risk and Reliability of Buildings Encountering Limited Gas–Pipe Explosion after Moderate Earthquakes. *SN Applied Sciences* 2(4):1–13.
2. Abebe, Solomon and Tesfaye Alemu Mohammed. (2022). Performance Assessment of Reinforced Concrete Frame under Close-In Blast Loading. *Advances in Civil Engineering* 2022.
3. Abedini, M., Chunwei Zhang, J. Mehrmashhadi, and E. Akhlaghi. (2020). Comparison of ALE, LBE and Pressure Time History Methods to Evaluate Extreme Loading Effects in RC Column. *Structures* 28(August):456–66.
4. Abedini, Masoud and Azrul A. Mutalib. (2020). Investigation into Damage Criterion and Failure Modes of RC Structures When Subjected to Extreme Dynamic Loads. *Archives of Computational Methods in Engineering* 27(2):501–15.
5. Abedini, Masoud and Chunwei Zhang. (2021). Performance Assessment of Concrete and Steel Material Models in LS-DYNA for Enhanced Numerical Simulation, A State of the Art Review. *Archives of Computational Methods in Engineering* 28(4):2921–42.
6. Agrawal, Dhiraj, Abhishek Gulhane, and M. D. Goel. (2019). *Progressive Collapse Analysis of Composite Structure*. Springer Singapore.
7. Akhlaghi, Ebrahim. (2020). Numerical Simulation of Air Shock Wave Propagation Effects in Reinforced Concrete Columns. *Journal of Modeling and Optimization* 12(1):12–22.
8. Alashker, Yasser, D. Ph, Sherif El-tawil, D. Ph, M. Asce, Fahim Sadek, D. Ph, and M. Asce. (2010). Progressive Collapse Resistance of Steel-Concrete Composite Floors. (October):1187–96.
9. Alshaikh, Ibrahim M. H., B. H. Ab. Bakar, Emad A. H. Alwesabi, and Hazizan Md Akil.

(2020). Experimental Investigation of the Progressive Collapse of Reinforced Concrete Structures: An Overview. *Structures* 25(March):881–900.

10. Amiri, Setareh, Hamed Saffari, and Javad Mashhadi. (2018). Assessment of Dynamic Increase Factor for Progressive Collapse Analysis of RC Structures. *Engineering Failure Analysis* 84(June 2017):300–310.
11. Anas, S. M., Mehtab Alam, and Mohammad Umair. (2021). Experimental and Numerical Investigations on Performance of Reinforced Concrete Slabs under Explosive-Induced Air-Blast Loading: A State-of-the-Art Review. *Structures* 31(January):428–61.
12. UFC. (2005). *UNIFIED FACILITIES CRITERIA (UFC) STRUCTURES TO RESIST THE EFFECTS OF ACCIDENTAL EXPLOSIONS APPROVED FOR PUBLIC RELEASE; DISTRIBUTION UNLIMITED.*
13. Danesh Noursadeh. (2017). Response of Building Structure and Its Components to Blast Loads by Danesh Nourzadeh A Thesis Submitted to the Faculty of Graduate and Postdoctoral Affairs in Partial Fulfillment of the Requirements for the Degree of Doctor of Philosophy in Civil Engineer. (March).
14. Ardila-Giraldo, Oscar A. and Santiago Pujol. (2021). Initial Shear Demand in Beams and One-Way Slabs Subjected to Blast Load. *Structures* 32(January 2020):1679–91.
15. Artero-Guerrero, J., J. Pernas-Sánchez, and F. Teixeira-Dias. (2017). Blast Wave Dynamics: The Influence of the Shape of the Explosive. *Journal of Hazardous Materials* 331:189–99.
16. Azim, Iftikhar, Jian Yang, Sanjeev Bhatta, Feiliang Wang, and Qing feng Liu. (2020). Factors Influencing the Progressive Collapse Resistance of RC Frame Structures. *Journal of Building Engineering* 27(April 2019):100986.
17. Bao, Yihai, Sashi K. Kunnath, Sherif El-Tawil, and H. S. Lew. (2008). Macromodel-Based Simulation of Progressive Collapse: RC Frame Structures. *Journal of Structural*

Engineering 134(7):1079–91.

18. Barmaki, Samad, Mohammad R. Sheidaii, and Omid Azizpour. (2020). Progressive Collapse Resistance of Bolted Extended End-Plate Moment Connections. *International Journal of Steel Structures* 20(4):1165–79.
19. Baylot, James T. and Tommy L. Bevins. (2007). Effect of Responding and Failing Structural Components on the Airblast Pressures and Loads on and inside of the Structure. *Computers and Structures* 85(11–14):891–910.
20. Bozdogan, Kanat Burak. (2009). AN APPROXIMATE METHOD FOR STATIC AND DYNAMIC ANALYSES OF SYMMETRIC WALL-FRAME BUILDINGS. 290(September 2007):279–90.
21. Brode, Harold L. (1955). Numerical Solutions of Spherical Blast Waves. *Journal of Applied Physics* 26(6):766–75.
22. Brooks, N. B. and N. M. Newmark. (1953). The Response of Simple Structures to Dynamic Loads. 071(064):61.
23. Caçoilo, A., R. Mourão, F. Teixeira-Dias, D. Lecompte, and D. Rush. (2021). Structural Response of Corrugated Plates under Blast Loading: The Influence of the Pressure-Time History. *Structures* 30(January):531–45.
24. Camarda, Charles. (2015). Mode Shape Derivatives. (February 1986).
25. Cankaya, Mehmet Alper, Izmir Katip, and Celebi Universitesi. (2020). Modeling and Behavior of Reinforced Concrete Panels Subjected to Blast Load Modeling and Behavior of Reinforced Concrete Panels Subjected to Blast Load. (February).
26. Catovic, Alan, Elvedin Kljuno, and Alan Catovic. (2021). Review of the Estimation Methods for External Blast Loads on Structures. 9(1):104–26.
27. Chauhan, Akshay Kumar and Akash Malik. (2021). Review on Performance of Reinforced Concrete Building Structures under Blast Load. 5(12):68–72.

28. Chen, G. Q., J. X. Lu, and H. Wu. (2023). Dynamic Behavior and Retrofitting of RC Frame Building under Vehicular Bomb Explosion. *Engineering Failure Analysis* 143(November 2022).
29. Chiquito, M., R. Castedo, A. P. Santos, L. M. López, and A. Pérez-Caldentey. (2021). Numerical Modelling and Experimental Validation of the Behaviour of Brick Masonry Walls Subjected to Blast Loading. *International Journal of Impact Engineering* 148(September 2020).
30. Chopra, Anil K. (2012). *Dynamics of Structures : Theory and Applications to Earthquake Engineering, 4/E*.
31. Choubey, Bishwajeet, Sekhar Chandra Dutta, Ganga Kasi V. Prakhya, Parthasarathi Mandal, and Rajesh Kumar Tanwar. (2020). Blast Pressure Analysis Due to Confined Explosion-after Effects. *Structures* 28(May):521–36.
32. Christian, Abraham, Lado Riannevo Chandra, Satadru Das Adhikary, and Khim Chye Gary Ong. (2016). Influence of Charge Shape and Orientation on the Response of Steel-Concrete Composite Panels. *International Journal of Engineering and Technology Innovation* 6(4):284–93.
33. Clutter, J. Keith and Kim W. King. (2016). Effect of Charge Shape on Blast Containment Chamber Survivability. *International Journal of Protective Structures* 7(3):389–408.
34. Cormie, David, Geoff Mays, and Peter Smith. (2019). *Blast Effects on Buildings*.
35. Crawford, John E., Hyung-Jin Choi, and Timothy R. Brewer. (2015). Evaluating Disproportionate Collapse Vulnerability. *International Journal of Protective Structures* 6(2):323–56.
36. Cuomo, M. and S. Lanza. (2020). Design of a Membrane Structure Subjected to Blast Load. *Lecture Notes in Mechanical Engineering* (March):1441–58.
37. Datta, Gaurav, Soumya Bhattacharjya, and Subrata Chakraborty. (2021). A

Metamodeling-Based Robust Optimisation Approach for Structures Subjected to Random Underground Blast Excitation. *Structures* 33(June):3615–32.

38. Dib, Nancy, Gérard Philippe Zéhil, and Samuel Rigby. (2022). On the Blast-Wave Shielding Effect of Porous Buildings. *Journal of Fluids and Structures* 115:103787.
39. Dimopoulos, Christoforos A., Fabio Freddi, Theodore L. Karavasilis, and George Vasdravellis. (2020). Progressive Collapse Resistance of Steel Self-Centering MRFs Including the Effects of the Composite Floor. *Engineering Structures* 208(April):109923.
40. Ding, Yang, Xuan Zhang, Yanchao Shi, and Huishen Zhang. (2022). Prediction of Far-Field Blast Loads from Large TNT-Equivalent Explosives on Gabled Frames. *Journal of Constructional Steel Research* 190(January):107120.
41. Ditali, Sabatino, Fulvio Ragno, and Roberto Fiore. (2018). Simplified Criteria for the Application of Blast Loads from Accidental Explosions in Plant Design. in *CHEMICAL ENGINEERING TRANSACTIONS*. Vol. 67.
42. Domenico, Dario De, D. Ph, Emanuele Gandelli, and D. Ph. (2021). Advanced Modeling of SMA Flag-Shaped Hysteresis for Nonlinear Time-History Analysis in SAP2000. 147(11):1–6.
43. Draganić, Hrvoje, Goran Gazić, Sanja Lukić, and Mario Jeleč. (2021). Experimental Investigation on Blast Load Resistance of Reinforced Concrete Slabs Retrofitted with Epoxy Resin Impregnated Glass Fiber Textiles. *Composite Structures* 274(June).
44. Edskär, Ida and Ida Edskär. (2010). *Modal Analysis , Dynamic Properties and Horizontal Stabilisation of Timber Buildings*.
45. El-Tawil, Sherif and Honghao Li. (2013). Progressive Collapse Research: Current State and Future Needs. *Advanced Materials Research* 639–640(1):3–12.
46. El-Tawil, Sherif, Honghao Li, and Sashi Kunnath. (2014). Computational Simulation of Gravity-Induced Progressive Collapse of Steel-Frame Buildings: Current Trends and

Future Research Needs. *Journal of Structural Engineering* 140(8):1–12.

47. Elsanadedy, H. M., T. H. Almusallam, Y. R. Alharbi, Y. A. Al-Salloum, and H. Abbas. (2014). Progressive Collapse Potential of a Typical Steel Building Due to Blast Attacks. *Journal of Constructional Steel Research* 101(May 2018):143–57.
48. Elsanadedy, Hussein, Mohammad Khawaji, Husain Abbas, Tarek Almusallam, and Yousef Al-Salloum. (2023). Numerical Modeling for Assessing Progressive Collapse Risk of RC Buildings Exposed to Blast Loads. *Structures* 48(January):1190–1208.
49. Eslami, Mohammadreza, Khalid M. Mosalam, Shalva Marjanishvili, Brian Katz, Weichiang Pang, and Venkatesh Kodur. (2020). Prediction of Blast Pressure-Duration Capacity of Monolithic Thermally Tempered Glass Panes. *International Journal of Impact Engineering* 136(June 2019):103433.
50. Esparza, Edward D. (1992). Spherical Equivalency of Cylindrical Charges in Free-Air. *25th Department of Defense Explosives Safety Seminar* I(ADA260984):403–28.
51. Fahmed, Kunwer, Alam Ariyana, and Mirza Amir Beg. (2021). Performannce Base Analysis of Multy Storied Building. (August).
52. Farahani, Ahmad, Ali Kheyroddin, and Mohammad Kazem Sharbatdar. (2018). Finding Critical Element in the Progressive Collapse of RC Structures Using Sensitivity Analysis. *Civil Engineering Journal* 4(12):3038.
53. Feng, Fei Fan, Hyeon Jong Hwang, and Wei Jian Yi. (2020). Static and Dynamic Loading Tests for Precast Concrete Moment Frames under Progressive Collapse. *Engineering Structures* 213(April):110612.
54. Feng, Wanhui, Baiyu Chen, Fei Yang, Feng Liu, Lijuan Li, Lin Jing, and Hongzhong Li. (2021). Numerical Study on Blast Responses of Rubberized Concrete Slabs Using the Karagozian and Case Concrete Model. *Journal of Building Engineering* 33(December 2019):101610.

55. Francioli, Mattia, Francesco Petrini, and Franco Bontempi. (2023). Structural Robustness Analysis of RC Frames under Seismic and Blast Chained Loads Scenarios. *Journal of Building Engineering* 67(July 2022):105970.

56. Gajewski, T. and P. W. Sielicki. (2020). Experimental Study of Blast Loading behind a Building Corner. *Shock Waves* 30(4):385–94.

57. Gantes, Charis J. and Nikos G. Pnevmatikos. (2004a). Elastic-Plastic Response Spectra for Exponential Blast Loading. *International Journal of Impact Engineering* 30(3):323–43.

58. Gantes, Charis J. and Nikos G. Pnevmatikos. (2004b). Elastic-Plastic Response Spectra for Exponential Blast Loading. *International Journal of Impact Engineering* 30(3):323–43.

59. Gao, Chu, Xiang zhen Kong, Qin Fang, Jian Hong, and Yin Wang. (2021). Numerical Investigation on Free Air Blast Loads Generated from Center-Initiated Cylindrical Charges with Varied Aspect Ratio in Arbitrary Orientation. *Defence Technology* (xxxx).

60. Geetha, D. (2017). MODAL ANALYSIS OF MULTISTOREY RECTANGULAR BUILDINGS WITH 1 : 2 : 2 . 5 PLAN RATIOS. 1461–66.

61. Ghaderi, Peiman, Daniel Ferreira, Eduardo Cavaco, and Válter Lúcio. (2020). Progressive Collapse Prevention Design of Framed RC Structures-Cost–Benefit Analysis. *Journal of Failure Analysis and Prevention* 20(4):1244–57.

62. Ghobadi, Mohammad Soheil and Hamed Yavari. (2020). Progressive Collapse Vulnerability Assessment of Irregular Voided Buildings Located in Seismic-Prone Areas. *Structures* 25(March):785–97.

63. Gholipour, Gholamreza, Chunwei Zhang, and Asma Alsadat Mousavi. (2020). Numerical Analysis of Axially Loaded RC Columns Subjected to the Combination of Impact and Blast Loads. *Engineering Structures* 219(April):110924.

64. He, Yaobei, Shaobo Geng, Yaxin Wei, Gan Luo, Xin Gong, and Huifeng Mao. (2021). Equivalent SDOF Load Transformation Factors for One-Way Members Subjected to Air Blast Loading. *Advances in Civil Engineering* 2021:1–26.

65. Hu, Ye, Li Chen, Qin Fang, and Hengbo Xiang. (2018). Blast Loading Model of the RC Column under Close-in Explosion Induced by the Double-End-Initiation Explosive Cylinder. *Engineering Structures* 175(April):304–21.

66. Hu, Yi and Junhai Zhao. (2020). Layout of Cross Braces on Progressive Collapse Analysis of a 3D 12-Story Steel Composite Frame Structures. *Journal of Engineering Research (Kuwait)* 8(2):45–58.

67. Huo, Runke, Shuguang Li, Zhanping Song, Yoshiaki Fujii, Shan Lei, Jianchao Mao, Sisi Tian, and Zizhen Miao. (2019). Analysis of Vibration Response Law of Multistory Building under Tunnel Blasting Loads. *Advances in Civil Engineering* 2019.

68. Ibrahim, Yasser E., Mostafa A. Ismail, and Marwa Nabil. (2017). Response of Reinforced Concrete Frame Structures under Blast Loading. *Procedia Engineering* 171:890–98.

69. Jacinto, Abel Carlos, Ricardo Daniel Ambrosini, and Rodolfo Francisco Danesi. (2001). Experimental and Computational Analysis of Plates under Air Blast Loading. *International Journal of Impact Engineering* 25(10):927–47.

70. Jayasooriya, Ruwan, David P. Thambiratnam, Nimal J. Perera, and Vladis Kosse. (2011). Blast and Residual Capacity Analysis of Reinforced Concrete Framed Buildings. *Engineering Structures* 33(12):3483–95.

71. Jing, Lin, Kai Liu, Xingya Su, and Xin Guo. (2021). Experimental and Numerical Study of Square Sandwich Panels with Layered-Gradient Foam Cores to Air-Blast Loading. *Thin-Walled Structures* 161(January):107445.

72. Ju, Seok Jun and Hyo Gyoung Kwak. (2021). Moment-Curvature Approach for Blast Analysis of RC Frames with Multitudinous Members. *Journal of Building Engineering*

42(September 2020):102463.

73. Karimiyan, Somayyeh. (2020). Collapse Distribution Scenario in Seismic Progressive Collapse of RC Buildings Caused by Internal Column Elimination. *Iranian Journal of Science and Technology - Transactions of Civil Engineering* 44(0123456789):241–52.
74. Kennett, Milagros, Eric Letvin, Michael Chipley, and Terrance Ryan. (2005). Risk Assessment: A How-to Guide to Mitigate Potential Terrorist Attacks against Buildings. *Fema 452* (January):1–248.
75. Khandelwal, Kapil and Sherif El-Tawil. (2011). Pushdown Resistance as a Measure of Robustness in Progressive Collapse Analysis. *Engineering Structures* 33(9):2653–61.
76. Khandelwal, Kapil, Sherif El-Tawil, and Fahim Sadek. (2009). Progressive Collapse Analysis of Seismically Designed Steel Braced Frames. *Journal of Constructional Steel Research* 65(3):699–708.
77. Kiakojouri, Foad, Valerio De Biagi, Bernardino Chiaia, and Mohammad Reza Sheidaii. (2020). Progressive Collapse of Framed Building Structures: Current Knowledge and Future Prospects. *Engineering Structures* 206(December 2019):110061.
78. Kiakojouri, Foad, Mohammad Reza Sheidaii, Valerio De Biagi, and Bernardino Chiaia. (2021a). Blast-Induced Progressive Collapse of Steel Moment-Resisting Frames: Numerical Studies and a Framework for Updating the Alternate Load Path Method. *Engineering Structures* 242(April):112541.
79. Kiakojouri, Foad, Mohammad Reza Sheidaii, Valerio De Biagi, and Bernardino Chiaia. (2021b). Progressive Collapse of Structures: A Discussion on Annotated Nomenclature. *Structures* 29(February):1417–23.
80. Knock, C. and N. Davies. (2013). Blast Waves from Cylindrical Charges. *Shock Waves* 23(4):337–43.
81. Knock, Clare and Nigel Davies. (2011). Predicting the Impulse from the Curved Surface

of Detonating Cylindrical Charges. *Propellants, Explosives, Pyrotechnics* 36(2):105–9.

82. Kristoffersen, Martin, Knut Ove Hauge, Arianna Minoretti, and Tore Børvik. (2021). Experimental and Numerical Studies of Tubular Concrete Structures Subjected to Blast Loading. *Engineering Structures* 233(7491).
83. Kulariya, Mahipal and Sandip Kumar Saha. (2022). Performance Evaluation of Hillside Buildings under Blast and Blast-Induced Ground Motion. *Journal of Performance of Constructed Facilities* 36(5):1–16.
84. Kumar, V., K. V. Kartik, and M. A. Iqbal. (2020). Experimental and Numerical Investigation of Reinforced Concrete Slabs under Blast Loading. *Engineering Structures* 206(December 2019):110125.
85. Lam, Nelson (The University of Melbourne), Priyan (The University of Melbourne) Mendis, and Tuan (The University of Melbourne) Ngo. (2004). Response Spectrum Solutions for Blast Loading. *Electronic Journal of Structural Engineering* 4(January):28–44.
86. Langran-Wheeler, C., A. Tyas, S. Rigby, CS Stephens, S. Clarke, and J. Warren. (2017). Characterisation of Reflected Blast Loads in the Very Near-Field From Non-Spherical Explosive Charges. *Isiems 2017* (Tham 2008).
87. Larcher, Martin. (2008). Pressure-Time Functions for the Description of Air Blast Waves. (JRC46829).
88. Li, Bing, Tso Chien Pan, and Anand Nair. (2009). A Case Study of the Effect of Cladding Panels on the Response of Reinforced Concrete Frames Subjected to Distant Blast Loadings. *Nuclear Engineering and Design* 239(3):455–69.
89. Li, Ying, Zhaoyue Chen, Xianben Ren, Ran Tao, Ruxin Gao, and Daining Fang. (2020). Experimental and Numerical Study on Damage Mode of RC Slabs under Combined Blast and Fragment Loading. *International Journal of Impact Engineering* 142(March):103579.

90. Liao, Yu, Shaoqing Shi, Shou Chen, Xinwen Ming, and Liangbin Ge. (2022). Numerical Evaluation of the Retrofit Effectiveness for Polyurea-Woven Glass Fiber Mesh Composite Retrofitted RC Slab Subjected to Blast Loading. *Structures* 36(November 2021):215–32.
91. Lin, Kaiqi, Yi Li, Xinzheng Lu, and Hong Guan. (2017). Effects of Seismic and Progressive Collapse Designs on the Vulnerability of RC Frame Structures. *Journal of Performance of Constructed Facilities* 31(1):04016079.
92. Liu, Chengqing and Dengjia Fang. (2020). Robustness Analysis of Vertical Resistance to Progressive Collapse of Diagrid Structures in Tall Buildings. *Structural Design of Tall and Special Buildings* 29(13):1–13.
93. LUKIĆ, SANJA, HRVOJE DRAGANIĆ, GORAN GAZIĆ, and IVAN RADIĆ. (2020). Statistical Analysis of Blast Wave Decay Coefficient and Maximum Pressure Based on Experimental Results. *Structures Under Shock and Impact XVI* 1(August):65–78.
94. Maazoun, Azer, Stijn Matthys, Bachir Belkassem, Oussama Atoui, and David Lecompte. (2021). Experimental Study of the Bond Interaction between CFRP and Concrete under Blast Loading. *Composite Structures* 277(September 2020):114608.
95. Malekinejad, Mohsen and Reza Rahgozar. (2012). A Simple Analytic Method for Computing the Natural Frequencies and Mode Shapes of Tall Buildings. *Applied Mathematical Modelling* 36(8):3419–32.
96. Masoero, E., P. Darò, and B. M. Chiaia. (2013). Progressive Collapse of 2D Framed Structures: An Analytical Model. *Engineering Structures* 54:94–102.
97. Mello, Lívia, Jia-Liang Le, and Roberto Ballarini. (2020). Numerical Modeling of Delayed Progressive Collapse of Reinforced Concrete Structures. *Journal of Engineering Mechanics* 146(10):04020113.
98. Mishra, Neeti and Omprakash Netula. (2021). Behaviour of Reinforced Concrete Framed Structure Subjected to Blast Loading. *International Journal of Advanced Research in*

Engineering and Technology (IJARET) 12(1):173–81.

99. Mohammadzadeh, Behzad, Junsuk Kang, and Seokbeen Im. (2020). Blast Loaded Plates: Simplified Analytical Nonlinear Dynamic Approach. *Structures* 28(July):2034–46.
100. Mourid, El Houcine, Said Mamouri, and Adnan Ibrahimbegovic. (2020). Progressive Collapse of 2D Reinforced Concrete Structures under Sudden Column Removal. *Frontiers of Structural and Civil Engineering* 14(6):1387–1402.
101. Naji, Arash. (2019). Comparison of Column Removal Methods in Progressive Collapse Analysis of Reinforced Concrete Moment-Resisting Frames. *Practice Periodical on Structural Design and Construction* 24(4):04019017.
102. Nassr, Amr A., A. Ghani Razaqpur, Michael J. Tait, Manuel Campidelli, and Simon Foo. (2012). Single and Multi Degree of Freedom Analysis of Steel Beams under Blast Loading. *Nuclear Engineering and Design* 242:63–77.
103. Netherton, Michael D. and Mark G. Stewart. (2010). Blast Load Variability and Accuracy of Blast Load Prediction Models. *International Journal of Protective Structures* 1(4):543–70.
104. Ngo, Tuan, Raymond Lumantarna, Andrew Whittaker, and Priyan Mendis. (2015). Quantification of the Blast-Loading Parameters of Large-Scale Explosions. *Journal of Structural Engineering* 141(10):04015009.
105. Nouri, Gholamreza, Abolfazl Yoosefpoor Avandari, and Jamal Barmah. (2021). Evaluation of RC Beam-Column Retrofitting Methods against Near-Field Blast Loading. *Journal of Performance of Constructed Facilities* 35(2):04020150.
106. Pannell, Jordan J., George Panoutsos, Sam B. Cooke, Dan J. Pope, and Sam E. Rigby. (2021). Predicting Specific Impulse Distributions for Spherical Explosives in the Extreme Near-Field Using a Gaussian Function. *International Journal of Protective Structures* 1–23.

107. Paripour, Mohammad Bagher, Ahmet Budak, and Oğuz Akın Düzgün. (2021). Investigation of Progressive Collapse Resistance Mechanism in Reinforced Concrete Beam–Column Assembly. *Iranian Journal of Science and Technology - Transactions of Civil Engineering* 45(1):505–12.

108. Pathak, Shashank and G. V. Ramana. (2020). Probabilistic Characterization of Nuclear-Blast Loads. *Journal of Structural Engineering* 146(5):04020055.

109. Paz, Mario and Stanley Halperson. (1980). Structural Dynamics: Theory and Computation. *Journal of Engineering Materials and Technology* 102(3):315–315.

110. Prakash, M. and K. S. Satyanarayanan. (2020). Experimental Study on Progressive Collapse of Reinforced Concrete Frames under a Corner Column Removal Scenario. *Materials Today: Proceedings* 40(xxxx):S69–74.

111. Qian, Kai, Xi Lan, Zhi Li, Yi Li, and Feng Fu. (2020). Progressive Collapse Resistance of Two-Storey Seismic Configured Steel Sub-Frames Using Welded Connections. *Journal of Constructional Steel Research* 170.

112. Radnic, J., R. Markic, M. Glibic, N. Grgić, and I. Banović. (2016). Comparison of Numerical Models for Nonlinear Static Analysis of Planar Concrete Frames Based on 1D and 2D Finite Elements. Pp. 472–82 in *Materialwissenschaft und Werkstofftechnik*. Vol. 47. Wiley-VCH Verlag.

113. Rajkumar, D., R. Senthil, B. Bala Murali Kumar, K. AkshayaGomathi, and S. Mahesh Velan. (2020). Numerical Study on Parametric Analysis of Reinforced Concrete Column under Blast Loading. *Journal of Performance of Constructed Facilities* 34(1):04019102.

114. Ravikumar, Rohit. (2021). A Simplified Procedure for Determining Critical Column in Progressive Collapse Analysis of RC Structures. *International Journal for Research in Applied Science and Engineering Technology* 9(3):623–28.

115. Rigby, Sam E., Tyas, Andrew, Bennett, Terry, Clarke, Sam D. , Fay, Stephen D. (2014).

International Journal of Protective Structures. *International Journal of Protective Structures* 5(1):1–20.

116. Rigby, S.E., C. Osborne, G. S. Langdon, S. B. Cooke, and D. J. Pope. (2021). Spherical Equivalence of Cylindrical Explosives: Effect of Charge Shape on Deflection of Blast-Loaded Plates. *International Journal of Impact Engineering* 155(0):103892.
117. Rigby, S. E., C. Osborne, G. S. Langdon, S. B. Cooke, and D. J. Pope. (2021). Spherical Equivalence of Cylindrical Explosives: Effect of Charge Shape on Deflection of Blast-Loaded Plates. *International Journal of Impact Engineering* 155(February):103892.
118. Roy, Tathagata and Vasant Matsagar. (2021). Mechanics of Damage in Reinforced Concrete Member under Post-Blast Fire Scenario. *Structures* 31(January):740–60.
119. Sabale, Arati Avinash and Rohan Kumar Choudhary. (2021). Comparison of Static and Dynamic Analysis of Multi-Storied. (August).
120. Schenker, András, Ido Anteby, Erez Gal, Yosef Kivity, Eyal Nizri, Oren Sadot, Ron Michaelis, Oran Levintant, and Gabi Ben-Dor. (2008). Full-Scale Field Tests of Concrete Slabs Subjected to Blast Loads. *International Journal of Impact Engineering* 35(3):184–98.
121. Schmidt, Jon A. (2007). *Title: Blast Design-Equivalent Static Methods Author*.
122. Shan, Sidi and Shuang Li. (2020). Fire-Induced Progressive Collapse Mechanisms of Steel Frames with Partial Infill Walls. *Structures* 25(March):347–59.
123. Sharapov, Dmitriy A., Tesfaldet H. Gebre, Yusuf M. Ali, Д. А. Шарапов, Т. Х. Гебре, and Ю. М. Али. (2021). The Effect of Story Drift in a Multi-Story Building under the Influence of an Earthquake. 17(3):270–77.
124. Sherkar, Pushkaraj, Jinwon Shin, Andrew Whittaker, and Amjad Aref. (2016). Influence of Charge Shape and Point of Detonation on Blast-Resistant Design. *Journal of Structural Engineering* 142(2):04015109.

125. Shi Yanchao, Y., Zhong Xian Li, and Hong Hao. (2010). A New Method for Progressive Collapse Analysis of RC Frames under Blast Loading. *Engineering Structures* 32(6):1691–1703.

126. Shirbhate, P. A. and M. D. Goel. (2020). A Critical Review of Blast Wave Parameters and Approaches for Blast Load Mitigation. *Archives of Computational Methods in Engineering* (May).

127. Simoens, Bart and Michel Lefebvre. (2015). Influence of the Shape of an Explosive Charge: Quantification of the Modification of the Pressure Field. *Central European Journal of Energetic Materials* 12(2):195–213.

128. Singh, Karandeep, Paolo Gardoni, and Flavio Stochino. (2020). Probabilistic Models for Blast Parameters and Fragility Estimates of Steel Columns Subject to Blast Loads. *Engineering Structures* 222(November 2019):110944.

129. Stewart, Mark G., Michael D. Netherton, and Hayden Baldacchino. (2020). Observed Airblast Variability and Model Error from Repeatable Explosive Field Trials. *International Journal of Protective Structures* 11(2):235–57.

130. Stochino, Flavio, Alessandro Attoli, and Giovanna Concu. (2020). Fragility Curves for RC Structure under Blast Load Considering the Influence of Seismic Demand. *Applied Sciences (Switzerland)* 10(2).

131. Stochino, Flavio, Armin Tabandeh, Paolo Gardoni, and Mauro Sassu. (2021). Physics-Based Probabilistic Demand Model and Reliability Analysis for Reinforced Concrete Beams under Blast Loads. *Engineering Structures* 248(June):112932.

132. Sun, Jinshan, Yongsheng Jia, Yingkang Yao, and Xianqi Xie. (2020). Experimental Investigation of Stress Transients of Blasted RC Columns in the Blasting Demolition of Buildings. *Engineering Structures* 210(February):110417.

133. Syed, Zubair Iman, Priyan Mendis, and Shaikh Atikur Rahman. (2016). Effect of Large

Negative Phase of Blast Loading on Structural Response of RC Elements. *MATEC Web of Conferences* 47:02015.

134. Talaat, Mennatullah, Ebtisam Yehia, Sherif A. Mazek, Magdy M. M. Genidi, and Alaa G. Sherif. (2022). Finite Element Analysis of RC Buildings Subjected to Blast Loading. *Ain Shams Engineering Journal* 13(4):101689.
135. Taranath, Bungale S., S. E. John, and A. Martin. (2010). *WIND and EARTHQUAKE RESISTANT BUILDINGS STRUCTURAL ANALYSIS AND DESIGN*.
136. Tavakoli, H. R. and F. Kiakojouri. (2013). Influence of Sudden Column Loss on Dynamic Response of Steel Moment Frames under Blast Loading. *International Journal of Engineering, Transactions B: Applications* 26(2):197–205.
137. Taylor, G. I. (2006). The Diffraction of Sound Pulses I. Diffraction by a Semi-Infinite Plane. *Proceedings of the Royal Society of London. Series A. Mathematical and Physical Sciences* 186(1006):322–44.
138. Teich, Martien and Norbert Gebbeken. (2010). The Influence of the Underpressure Phase on the Dynamic Response of Structures Subjected to Blast Loads. *International Journal of Protective Structures* 1(2):219–34.
139. Tolani, Sunita, Shiv Dayal Bharti, Mahendra Kumar Shrimali, and Tushar Kanti Datta. (2020a). Effect of Surface Blast on Multistory Buildings. *Journal of Performance of Constructed Facilities* 34(2):1–15.
140. Tolani, Sunita, Shiv Dayal Bharti, Mahendra Kumar Shrimali, and Tushar Kanti Datta. (2020b). Effect of Surface Blast on Multistory Buildings. *Journal of Performance of Constructed Facilities* 34(2):04020015.
141. Tolani, Sunita, Shiv Dayal Bharti, Mahendra Kumar Shrimali, and Tushar Kanti Datta. (2022). Response Behavior of Buildings under the Simultaneous Actions of Surface Blast and Progressive Collapse. *Journal of Performance of Constructed Facilities* 36(2).

142. Toy, Ahmet Tuğrul and Barış Sevim. (2022). Structural Response of Multi-Story Building Subjected to Blast Load. *Journal of Structural Engineering & Applied Mechanics* 5(1):13–21.

143. Di Trapani, Fabio, Luca Giordano, and Giuseppe Mancini. (2020). Progressive Collapse Response of Reinforced Concrete Frame Structures with Masonry Infills. *Journal of Engineering Mechanics* 146(3):04020002.

144. Tyas, Andrew, Sam Rigby, and Sam Clarke. (2019). Reflected Blast Loads from Long Cylinders in the Near-Field. (November).

145. Ullah, Aleem, Furqan Ahmad, Heung Woon Jang, Sung Wook Kim, and Jung Wuk Hong. (2017). Review of Analytical and Empirical Estimations for Incident Blast Pressure. *KSCE Journal of Civil Engineering* 21(6):2211–25.

146. Vapper, Meelis and Kaspar Lasn. (2020). Blast Protection of Concrete Columns with Thin Strips of GFRP Overlay. *Structures* 25(March):491–99.

147. Vieira, A. de A., S. P. Triantafyllou, and D. A. Bournas. (2020). Strengthening of RC Frame Subassemblies against Progressive Collapse Using TRM and NSM Reinforcement. *Engineering Structures* 207(October 2019):110002.

148. Vivek, Padmanabha and T. G. Sitharam. (2020). *Granular Materials Under Shock and Blast Loading*.

149. Wang, W., D. Zhang, F. Lu, S. C. Wang, and F. Tang. (2012). A New Non-Uniform Blast Load Model for SDOF Method of One-Way Reinforced Concrete Slab. in *EPJ Web of Conferences*. Vol. 26.

150. Wang, Wenming. (2020). Strain Rate Effect on the Progressive Collapse Analysis of RC Frame Structure under Earthquake. *Advances in Civil Engineering* 2020.

151. Wu, Chengqing, Gianni Fattori, Andrew Whittaker, and Deric John Oehlers. (2010). Investigation of Air-Blast Effects from Spherical-and Cylindrical-Shaped Charges.

International Journal of Protective Structures 1(3):345–62.

152. Xiao, Weifang, Matthias Andrae, and Norbert Gebbeken. (2020a). Effect of Charge Shape and Initiation Configuration of Explosive Cylinders Detonating in Free Air on Blast-Resistant Design. *Journal of Structural Engineering* 146(8):04020146.
153. Xiao, Weifang, Matthias Andrae, and Norbert Gebbeken. (2020b). Influence of Charge Shape and Point of Detonation of High Explosive Cylinders Detonated on Ground Surface on Blast-Resistant Design. *International Journal of Mechanical Sciences* 181(April):105697.
154. Xiao, Weifang, Matthias Andrae, Michael Steyerer, and Norbert Gebbeken. (2021a). Investigations of Blast Loads on a Two-Storeyed Building with a Gable Roof: Full-Scale Experiments and Numerical Study. *Journal of Building Engineering* 43(August):103111.
155. Xiao, Weifang, Matthias Andrae, Michael Steyerer, and Norbert Gebbeken. (2021b). Investigations of Blast Loads on a Two-Storeyed Building with a Gable Roof: Full-Scale Experiments and Numerical Study. *Journal of Building Engineering* 43(March):103111.
156. Xu, Shilang, Bokun Chen, Qinghua Li, Fei Zhou, Xing Yin, Xiao Jiang, and Ping Wu. (2022). Experimental and Numerical Investigations on Ultra-High Toughness Cementitious Composite Slabs Subjected to Close-in Blast Loadings. *Cement and Concrete Composites* 126(September 2021):104339.
157. Yadav, Ankur. (2021). Response of RC Structure Exposed to Explosion. 10(05):1048–58.
158. Yan, Junbo, Yan Liu, Zixi Xu, Zhen Li, and Fenglei Huang. (2020). Experimental and Numerical Analysis of CFRP Strengthened RC Columns Subjected to Close-in Blast Loading. *International Journal of Impact Engineering* 146(September):103720.
159. Zhang, Chunwei, M. Abedini, and J. Mehrmashhadi. (2020). Development of Pressure-Impulse Models and Residual Capacity Assessment of RC Columns Using High Fidelity Arbitrary Lagrangian-Eulerian Simulation. *Engineering Structures* 224(May):111219.

160. Zhang, Chunwei and Masoud Abedini. (2021). Time-History Blast Response and Failure Mechanism of RC Columns Using Lagrangian Formulation. *Structures* 34(November 2020):3087–98.

161. Zhang, Chunwei, Gholamreza Gholipour, and Asma Alsadat Mousavi. (2020). Blast Loads Induced Responses of RC Structural Members: State-of-the-Art Review. *Composites Part B: Engineering* 195(April):108066.

162. Zhang, Qiang and Yaozhuang Li. (2020). Experimental and Modeling Study on the Progressive Collapse Resistance of a Reinforced Concrete Frame Structure under a Middle Column Removal Scenario. *Structural Design of Tall and Special Buildings* 29(2):1–21.

163. Zhang, Qiang, Yan-Gang Zhao, K. Kolozvari, and Lei Xu. (2020). Simplified Model for Assessing Progressive Collapse Resistance of Reinforced Concrete Frames under an Interior Column Loss. *Engineering Structures* 215(April):110688.

164. Zhang, Xuan, Yang Ding, and Yanchao Shi. (2021). Numerical Simulation of Far-Field Blast Loads Arising from Large TNT Equivalent Explosives. *Journal of Loss Prevention in the Process Industries* 70(February):104432.

165. Zhao, Nan, Shujian Yao, Duo Zhang, Fangyun Lu, and Chengming Sun. (2020). Experimental and Numerical Studies on the Dynamic Response of Stiffened Plates under Confined Blast Loads. *Thin-Walled Structures* 154(February):106839.

166. Zheng, Kai and Xiangzhao Xu. (2021). Experimental and Numerical Study on the Mechanical Behavior of Composite Steel Structure under Explosion Load. *Materials* 14(2):1–24.

167. Zhou, Fengjun, Yunhou Sun, Xuetao Sun, and Lei Zheng. (2015). Research on the Close-In Flow Field Characteristics of Spherical TNT Charge Bursting in Real Air. *International Journal of Protective Structures* 6(2):379–88.

168. Zhu, Wei, Guang yan Huang, Han Liu, Wei Lai, Xiao bin Bian, and Shun shan Feng. (2020). Experimental and Numerical Investigation of a Hollow Cylindrical Water Based Barrier against Internal Blast Induced Fragment Loading. *International Journal of Impact Engineering* 138(January):103503.

APPENDIX A

A1. Exterior Column Axial Load Factors

Rigid Frame	ECA
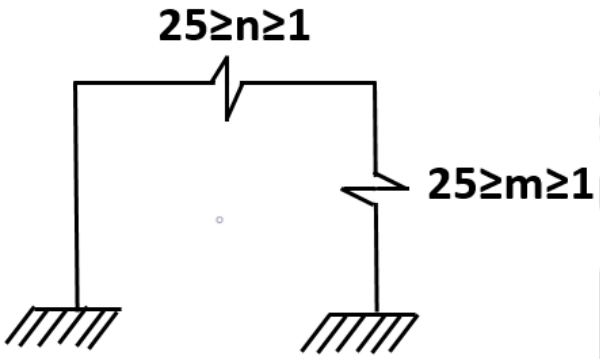	$z0 + Bm^C + Dn^E + Fm^C n^E$

A2. Exterior Column Shear Load Factors

Rigid Frame	ECS
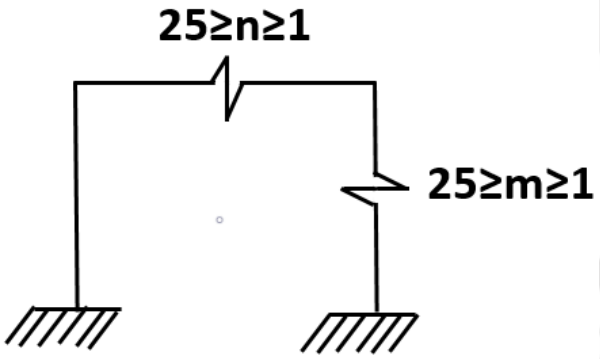	$z0 + Bm^C + Dn^E + Fm^C n^E$

A3. Exterior Column Bending Load Factors

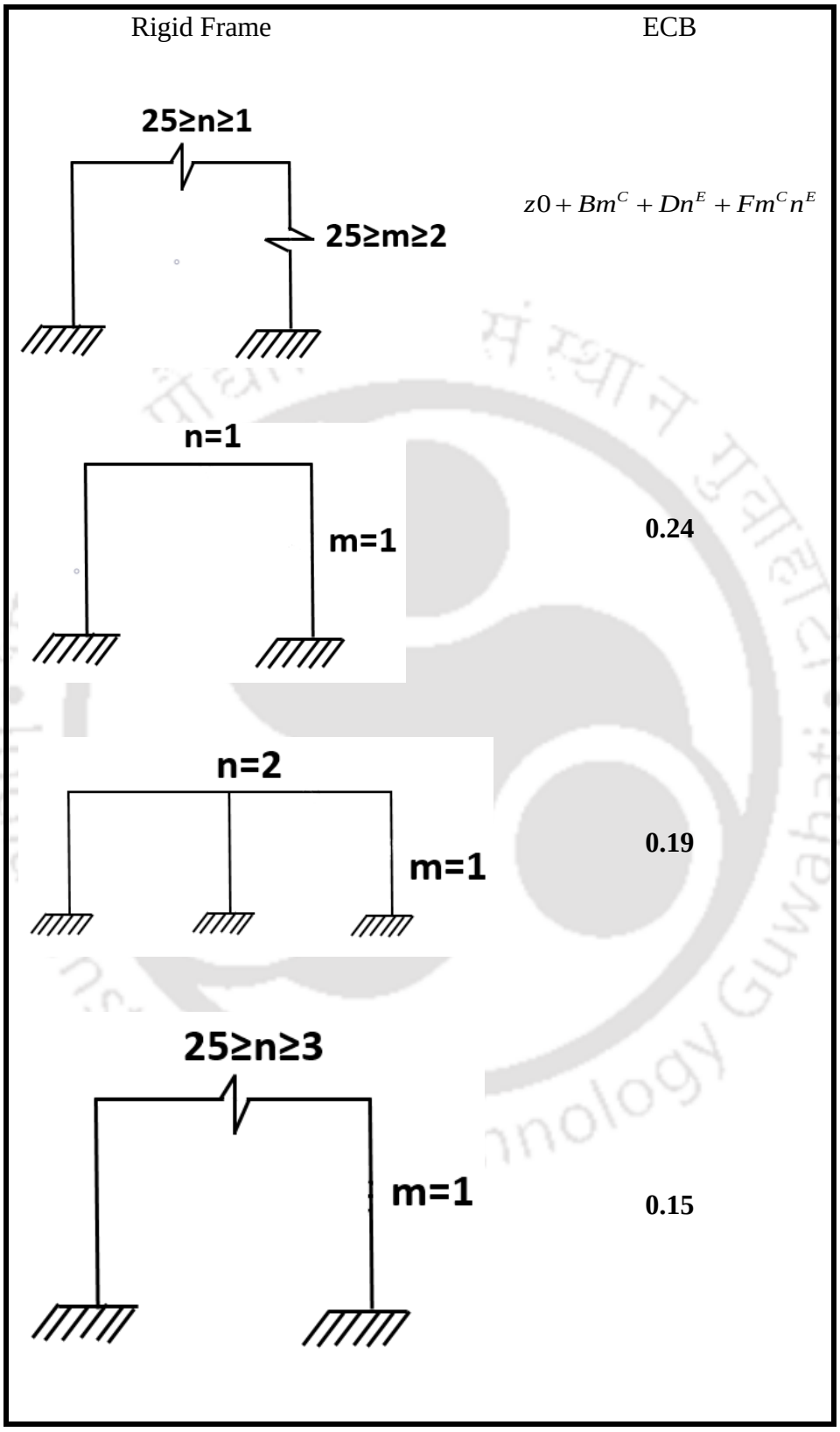

A4. Interior Column Axial Load Factors

Rigid Frame	ICA
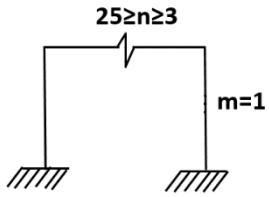	**0.02**
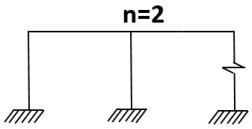	**0.03**
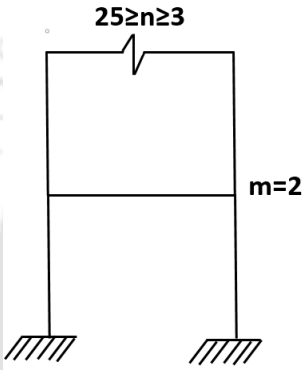	**0.04**
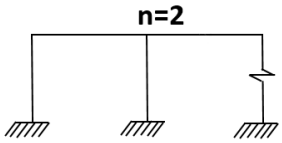	**0.05**
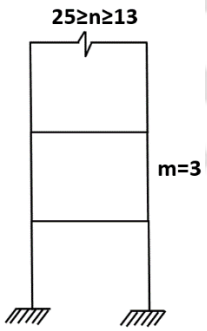	**0.05**
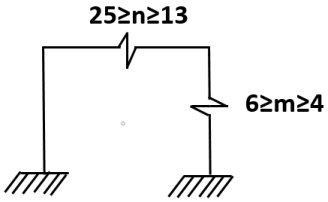	**0.06**

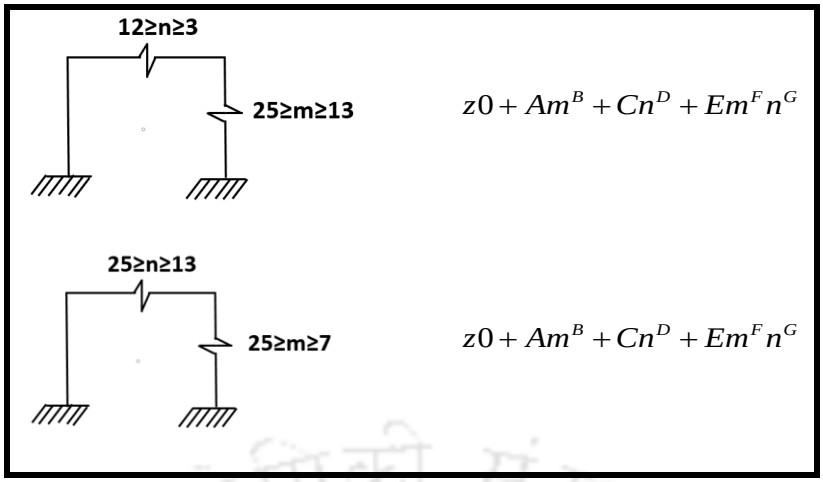

A5. Interior Column Shear Load Factors

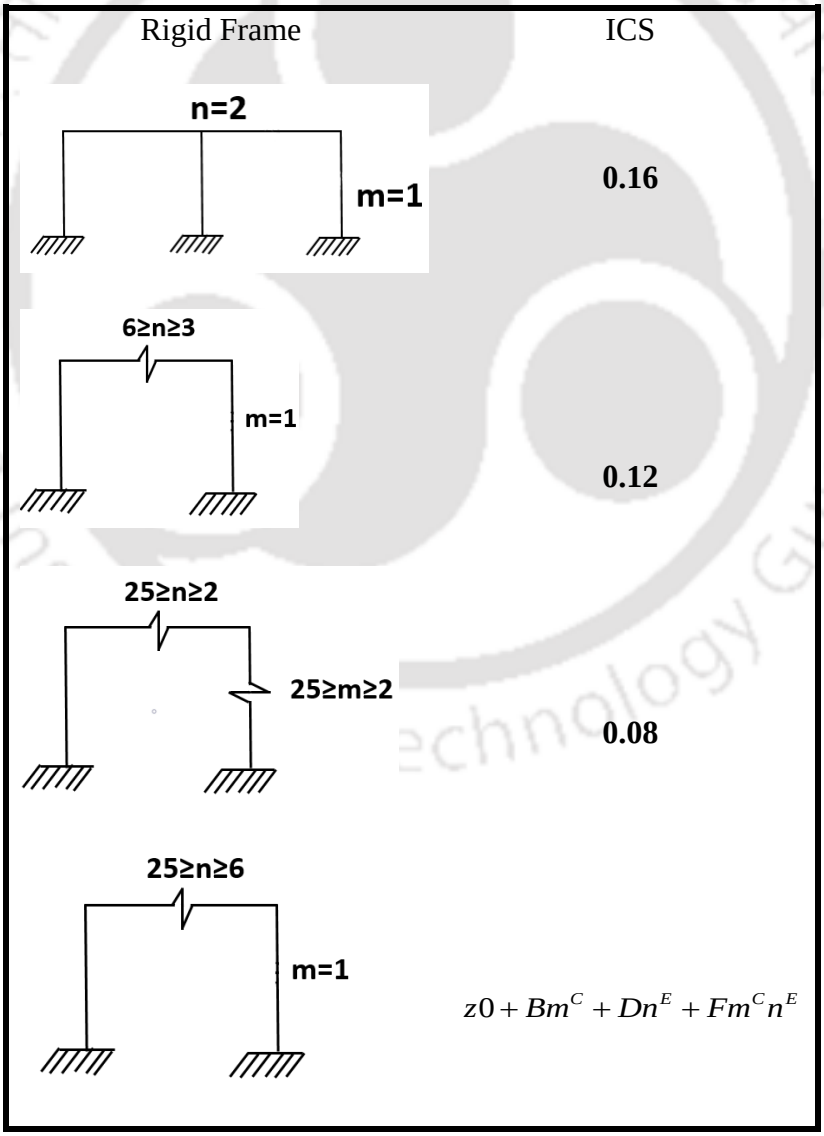

A6. Interior Column Bending Load Factors

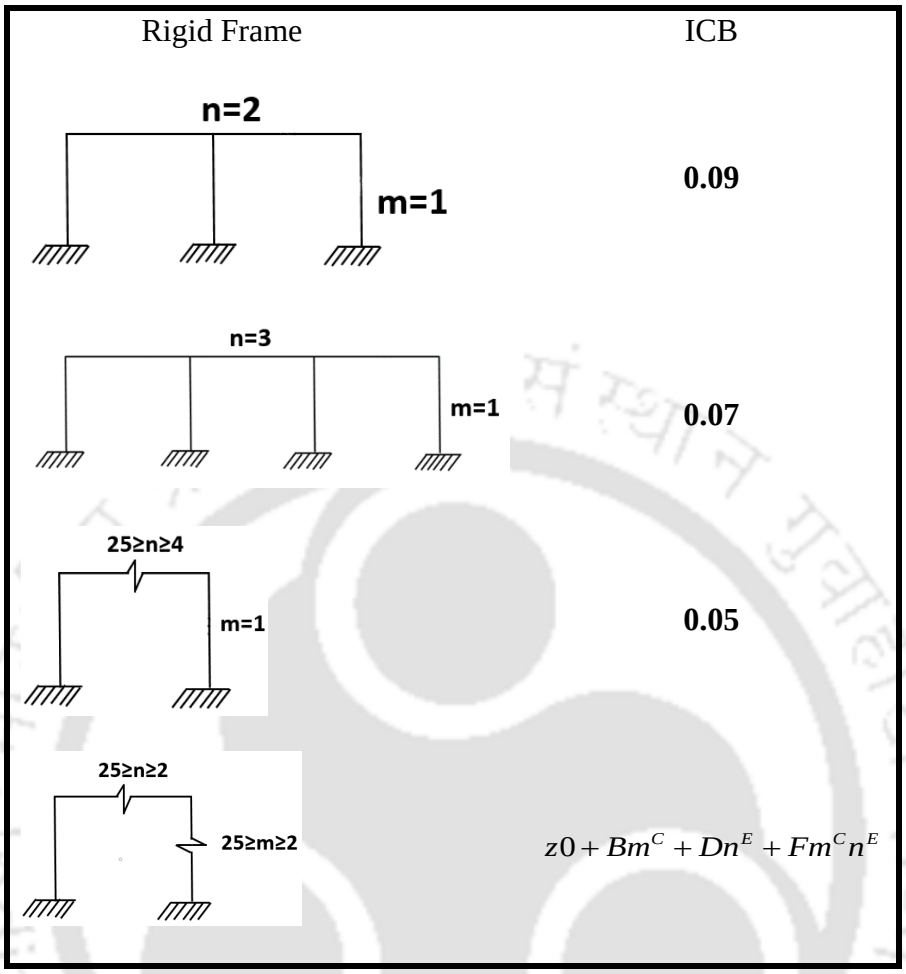

A7. Exterior Beam Axial Load Factors

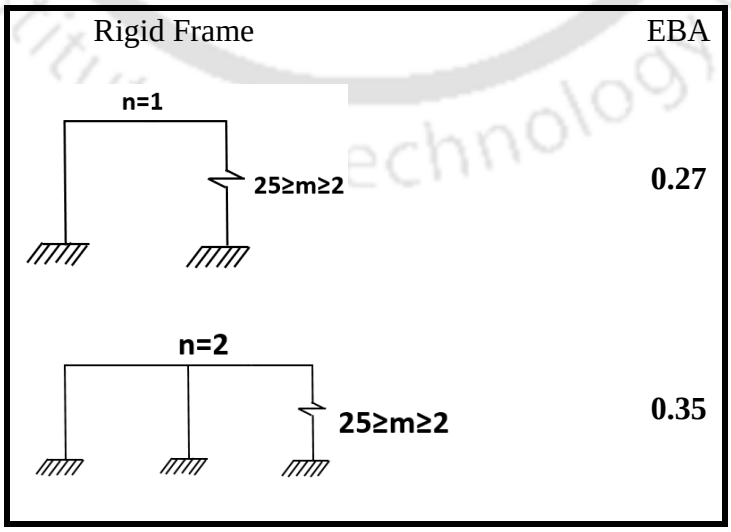

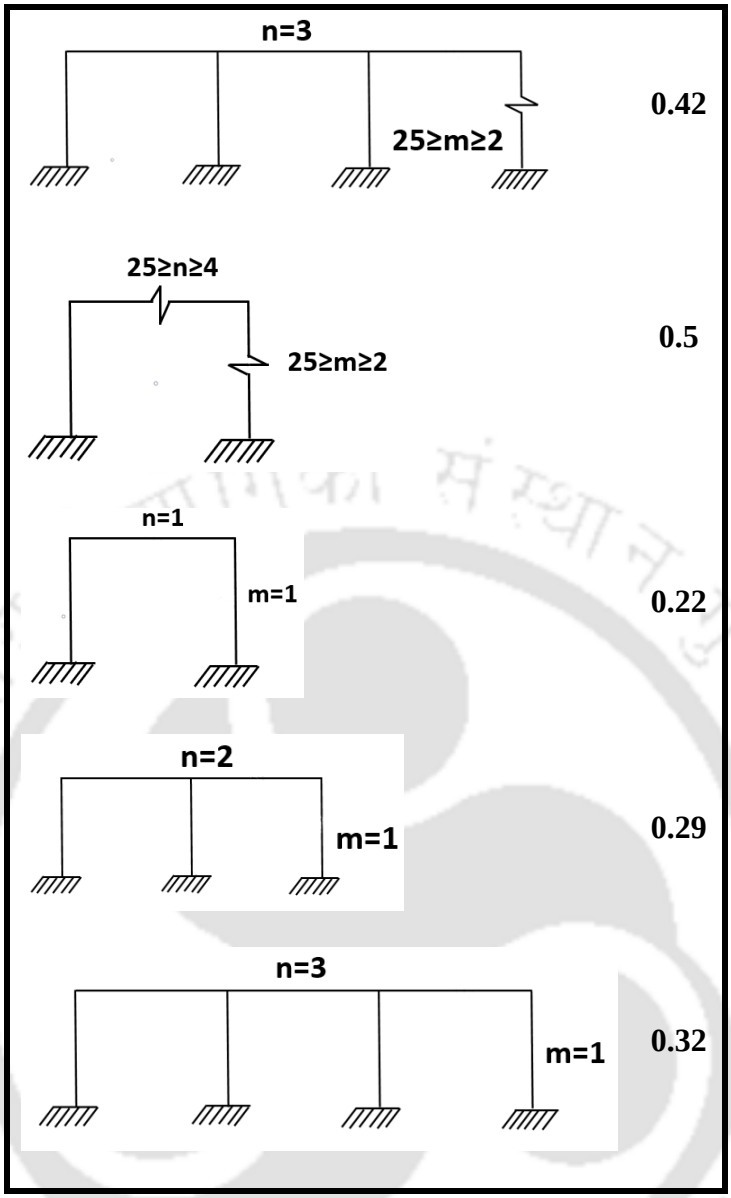

A8. Exterior Beam Shear Load Factors

Rigid Frame	EBS
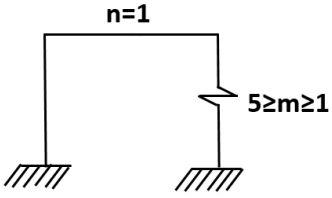	$-0.055m^2 + 0.517m - 0.326$

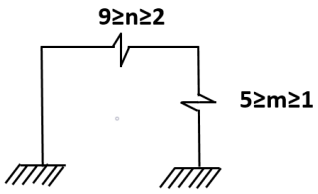

$$z0 + Am^B + Cn^D + Em^F n^G$$

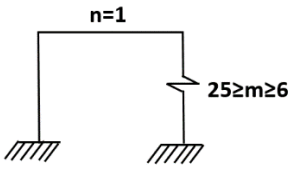

0.94

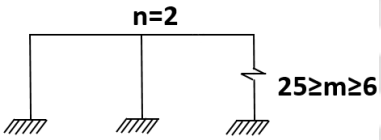

0.49

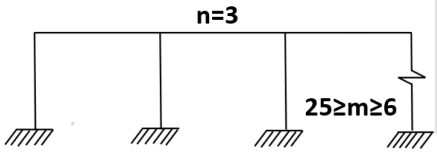

0.31

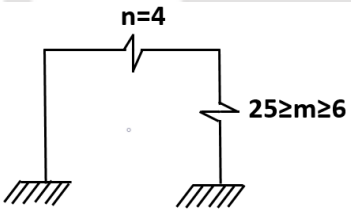

0.22

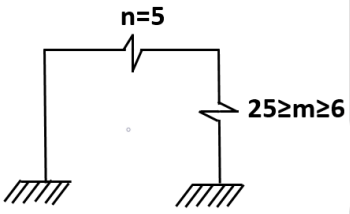

0.17

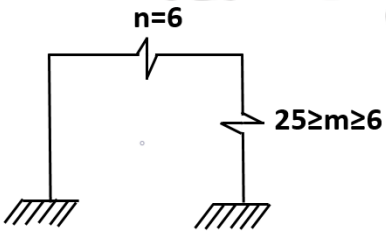

0.14

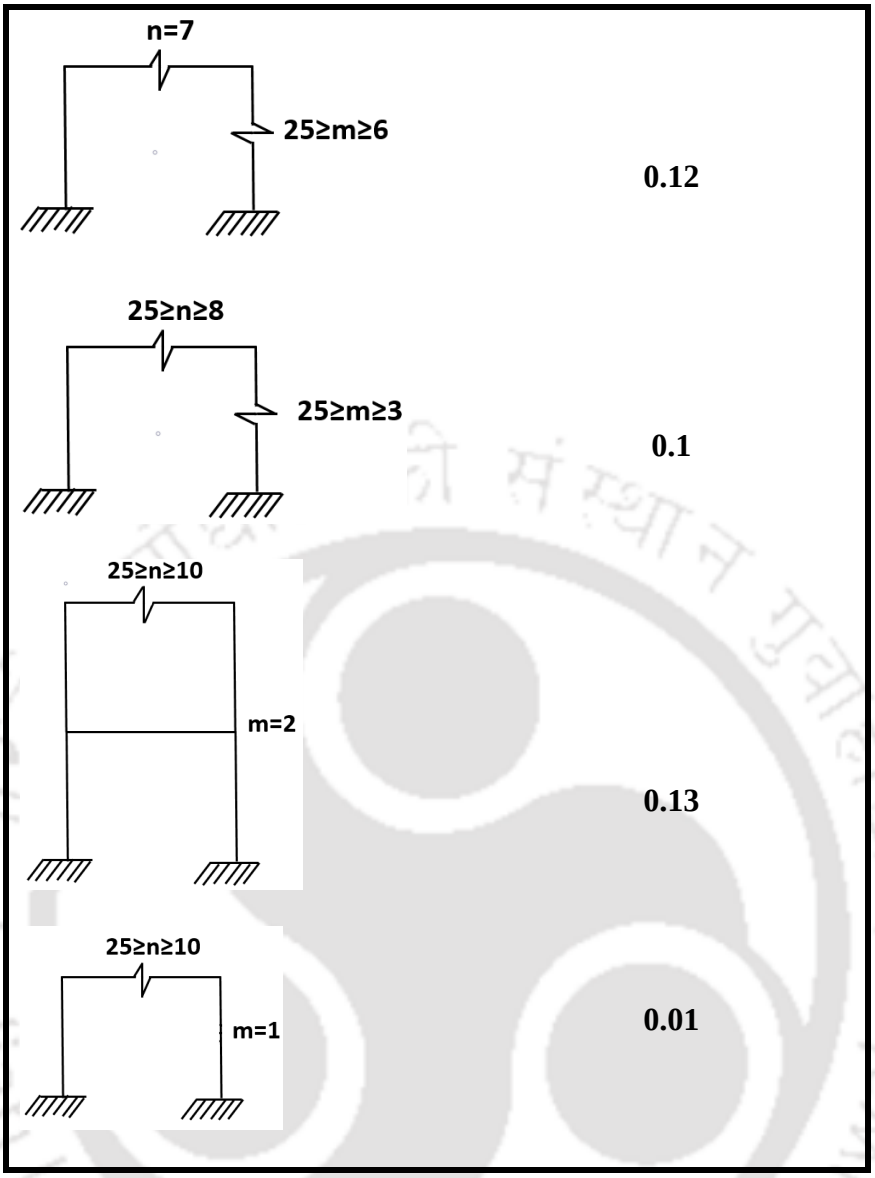

A9. Exterior Beam Bending Load Factors

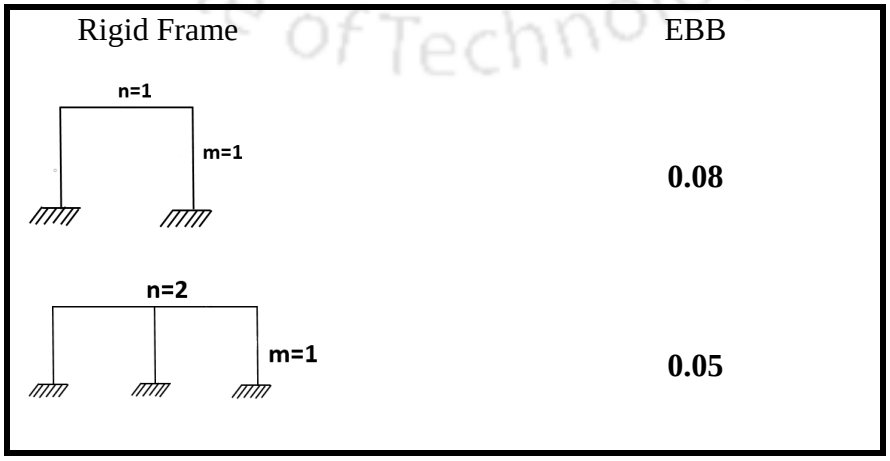

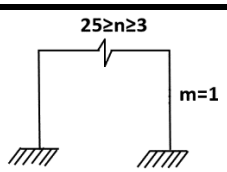

0.02

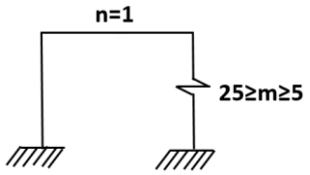

0.47

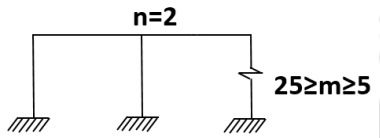

0.27

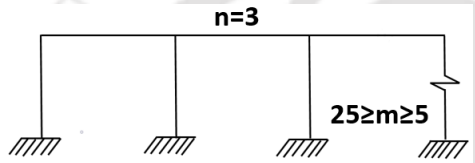

0.18

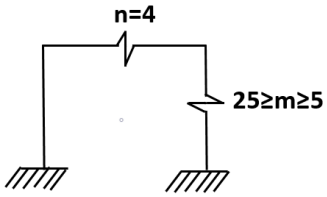

0.13

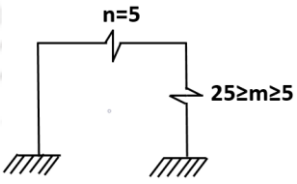

0.1

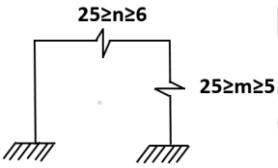

0.08

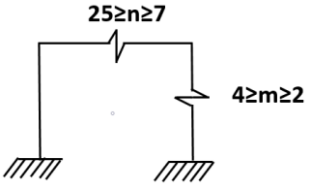

0.09

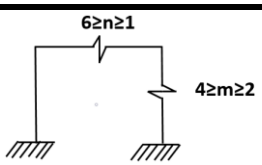

$$z0 + Bm^C + Dn^E + Fm^C n^E$$

A10. Interior Beam Axial Load Factors

Rigid Frame	IBA
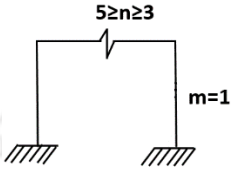	**0.23**
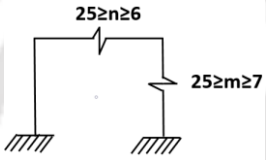	**0.45**
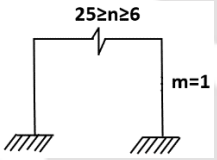	**0.27**
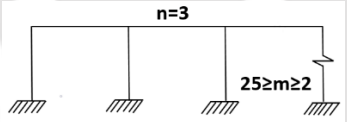	**0.25**
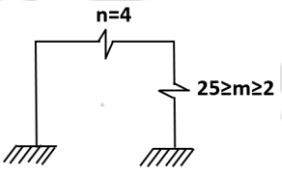	**0.33**
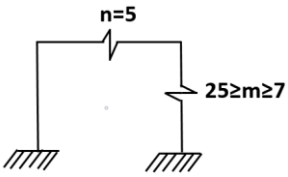	**0.39**

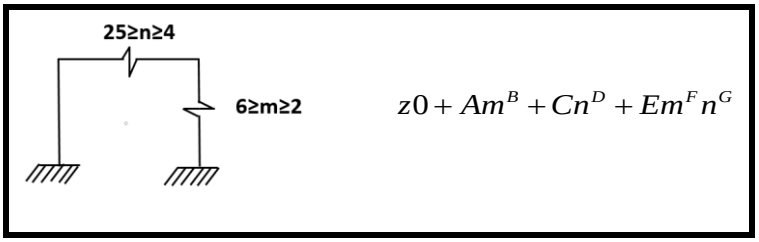

A11. Interior Beam Shear Load Factors

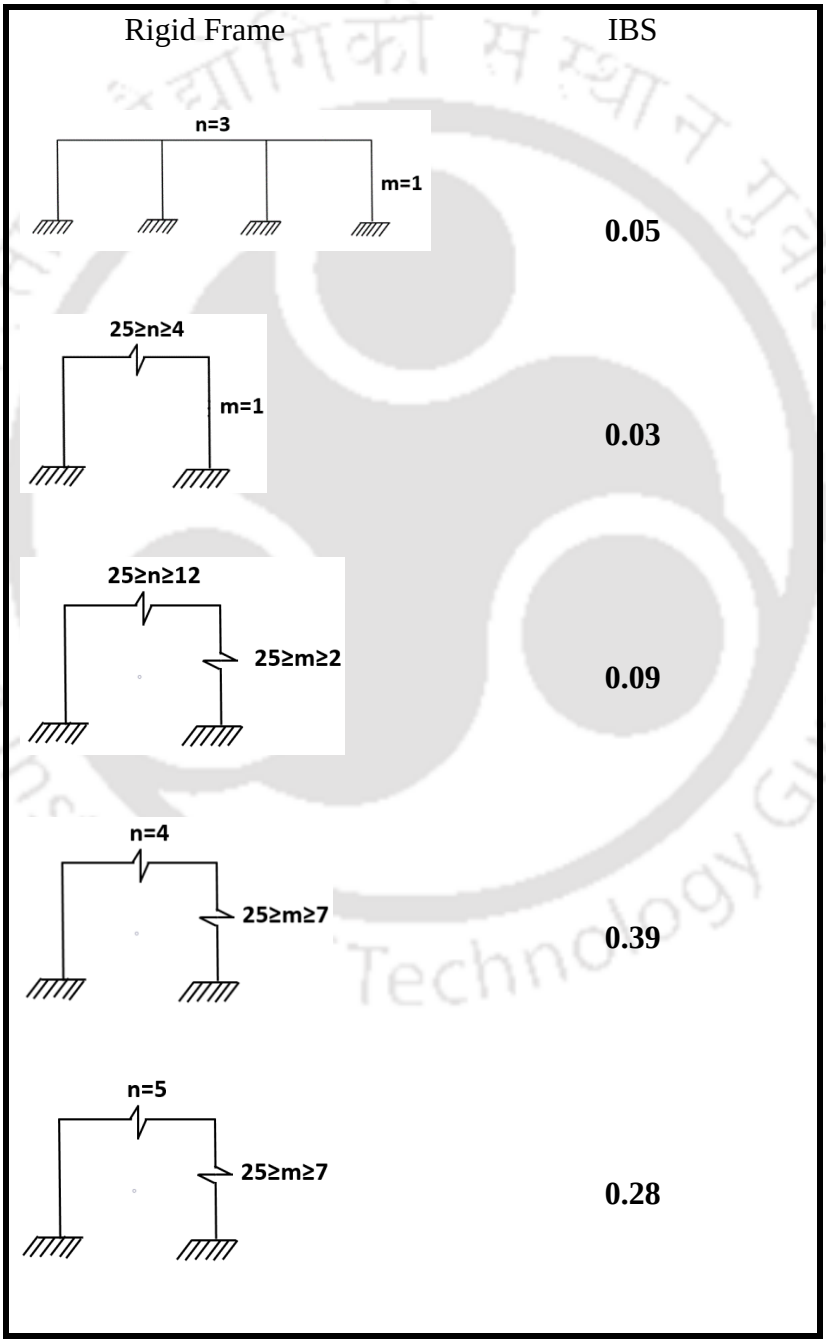

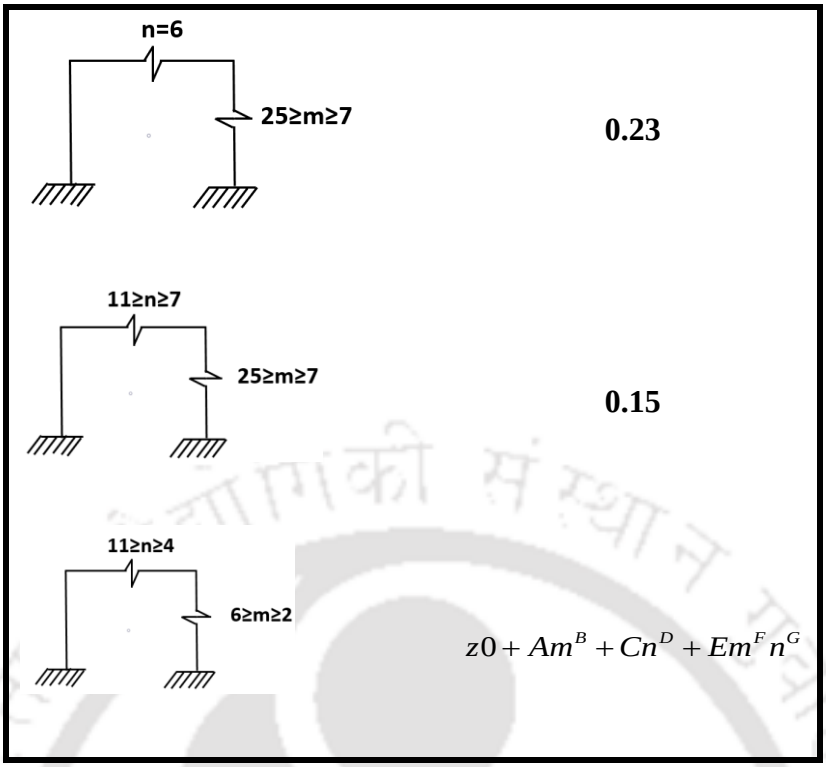

A12. Interior Beam Bending Load Factors

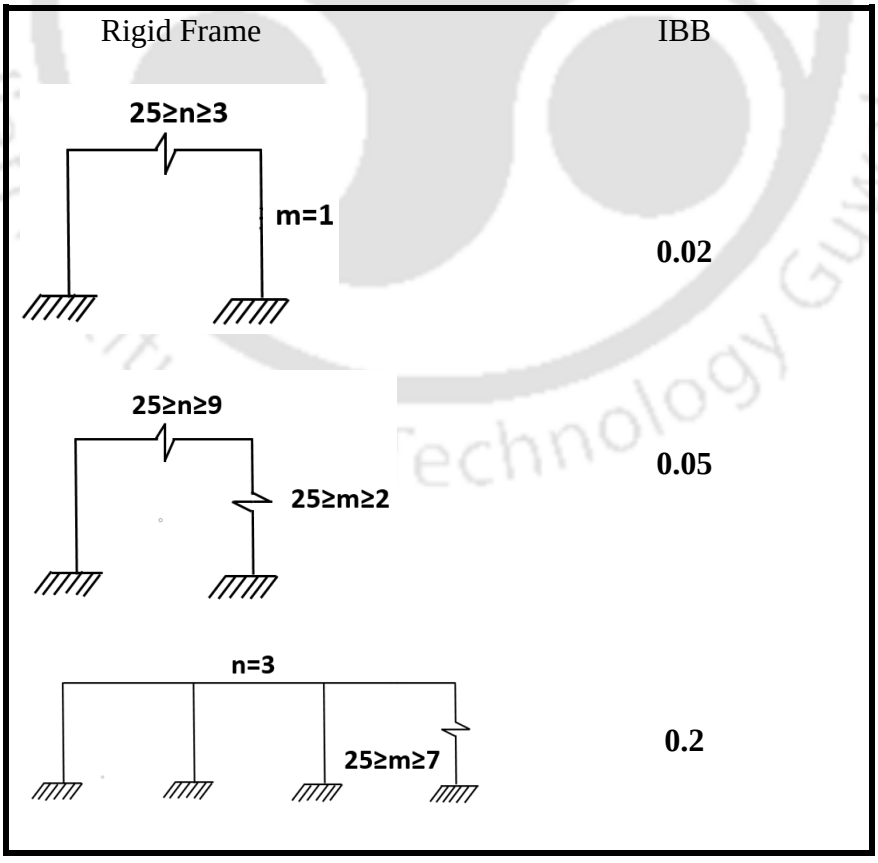

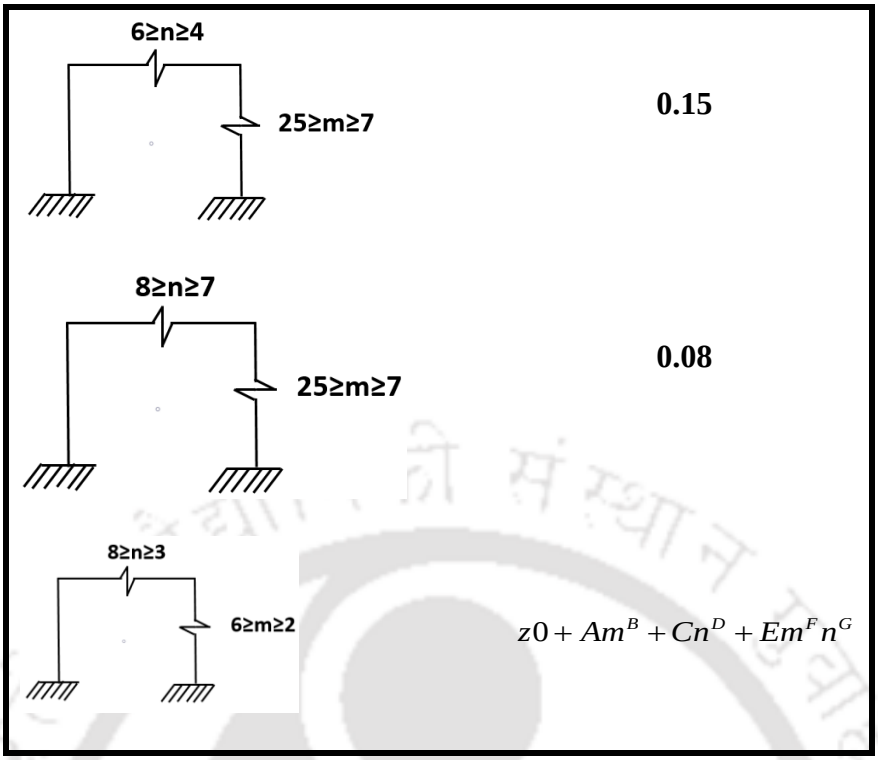

APPENDIX B

B1. Column Axial Resistance Factors

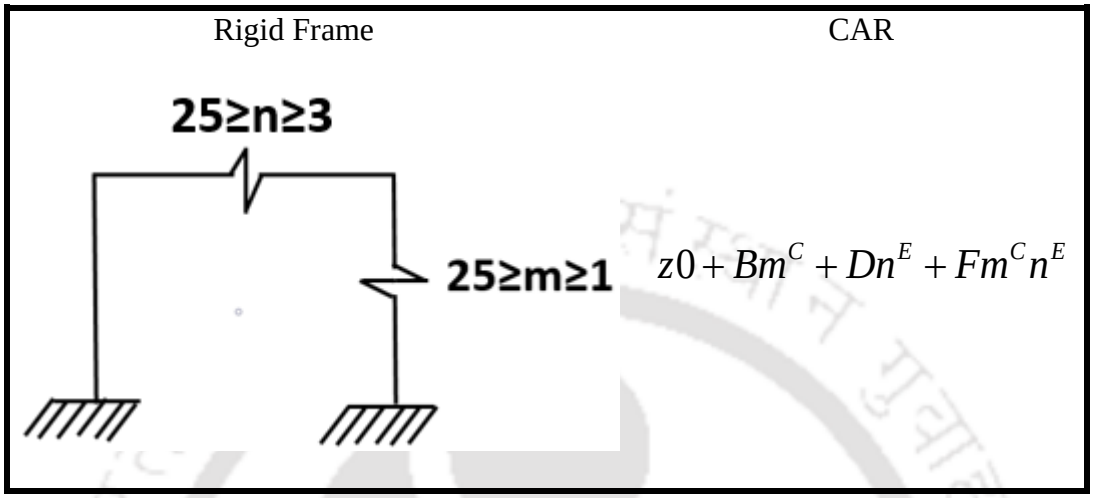

B2. Column Shear Resistance Factors

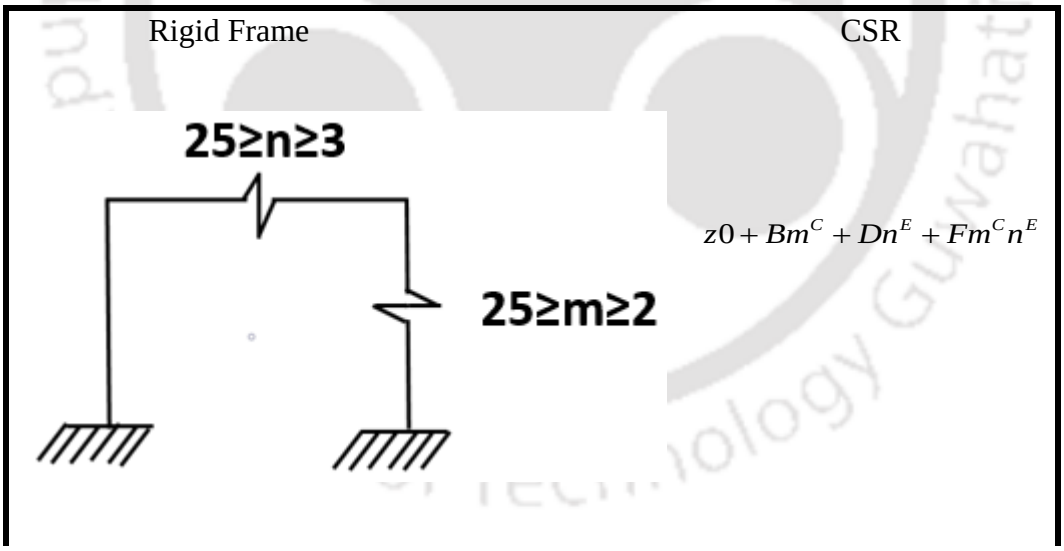

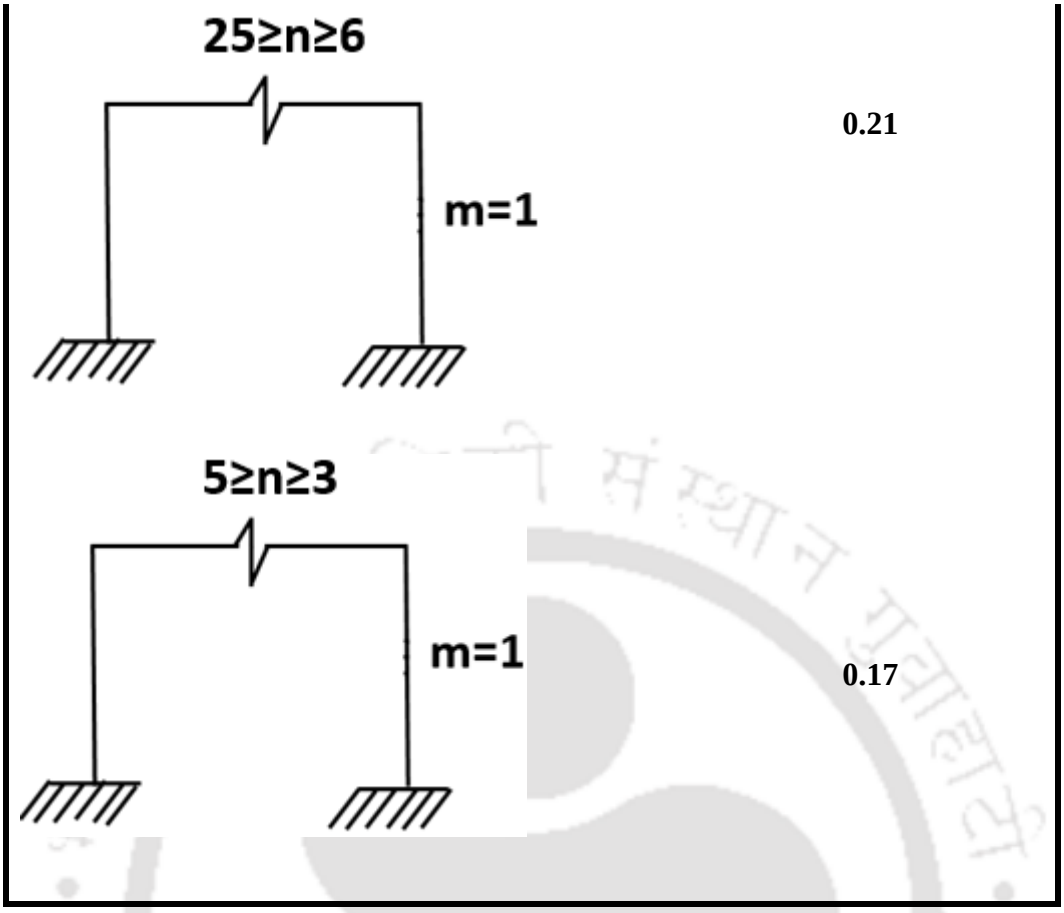

B3. Column Bending Resistance Factors

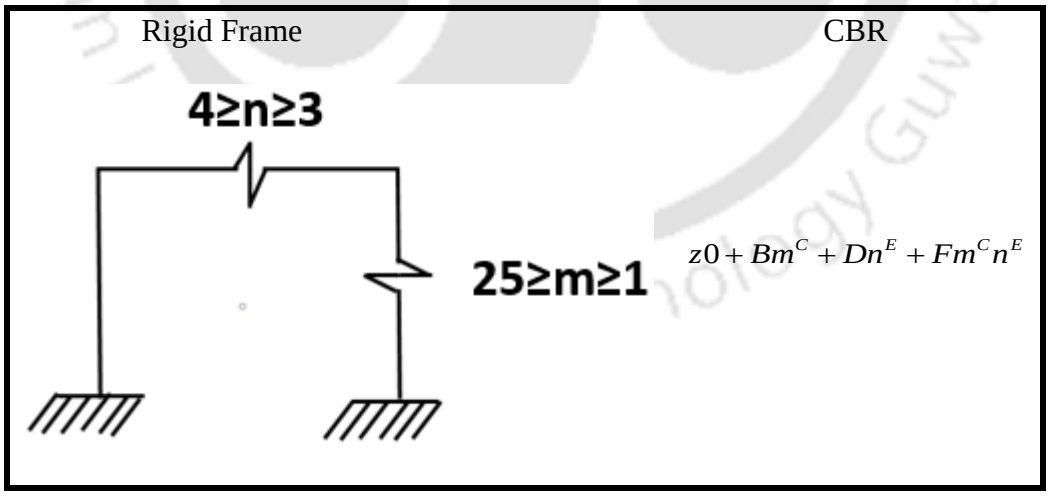

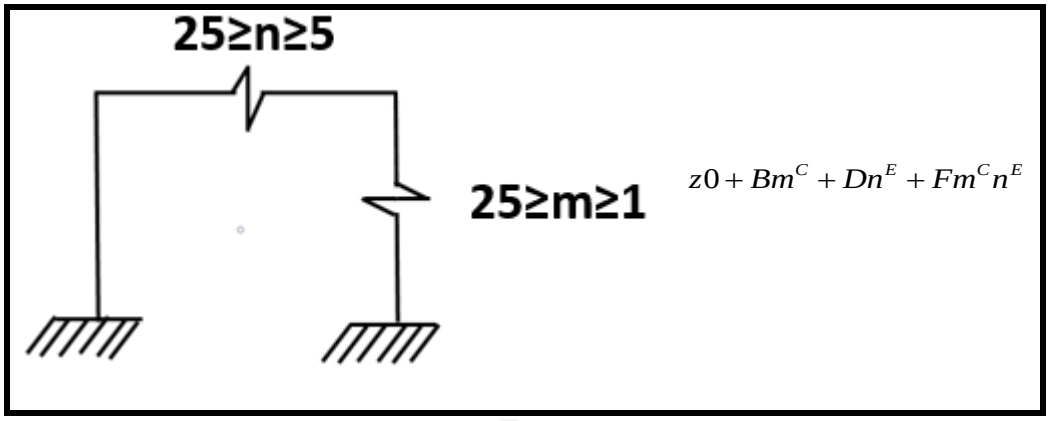

B4. Beam Axial Resistance Factors

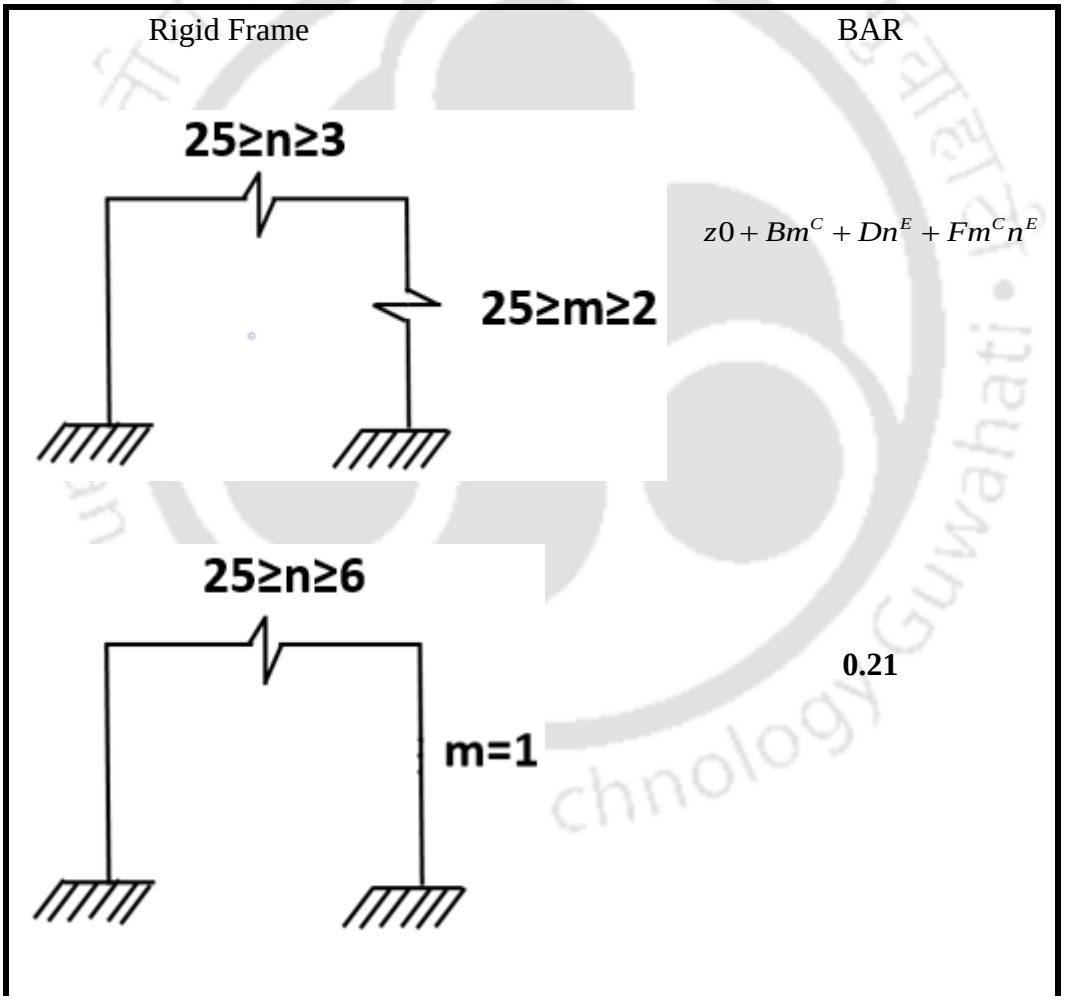

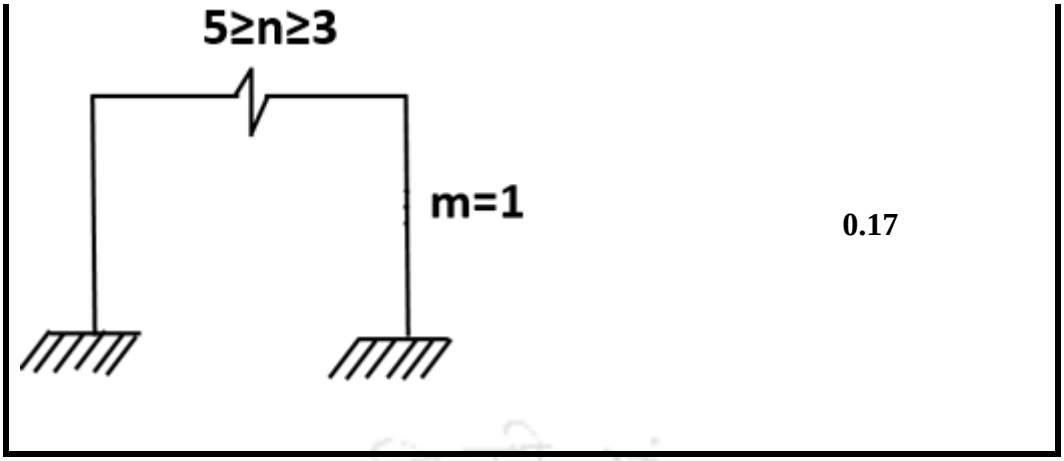

B5. Beam Shear Resistance Factors

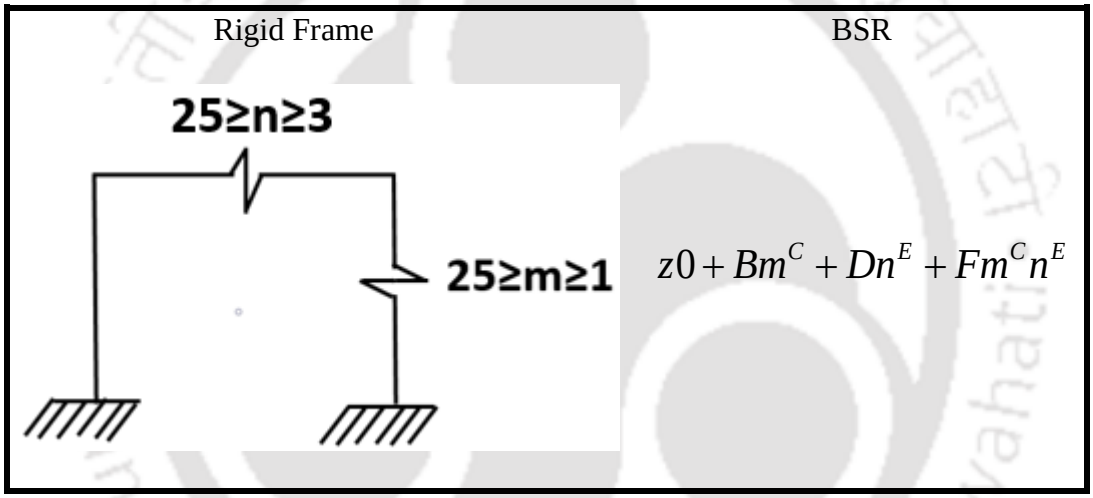

B6. Beam Bending Resistance Factors

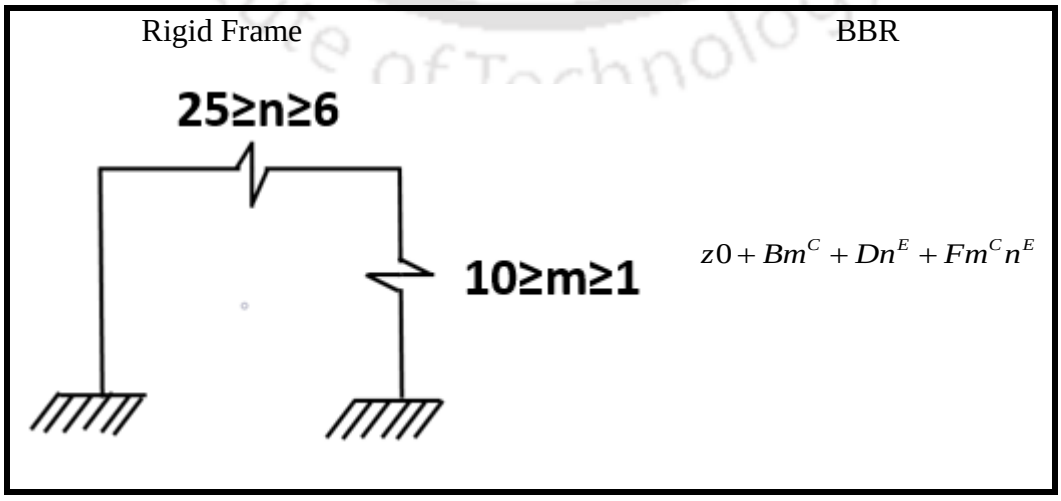

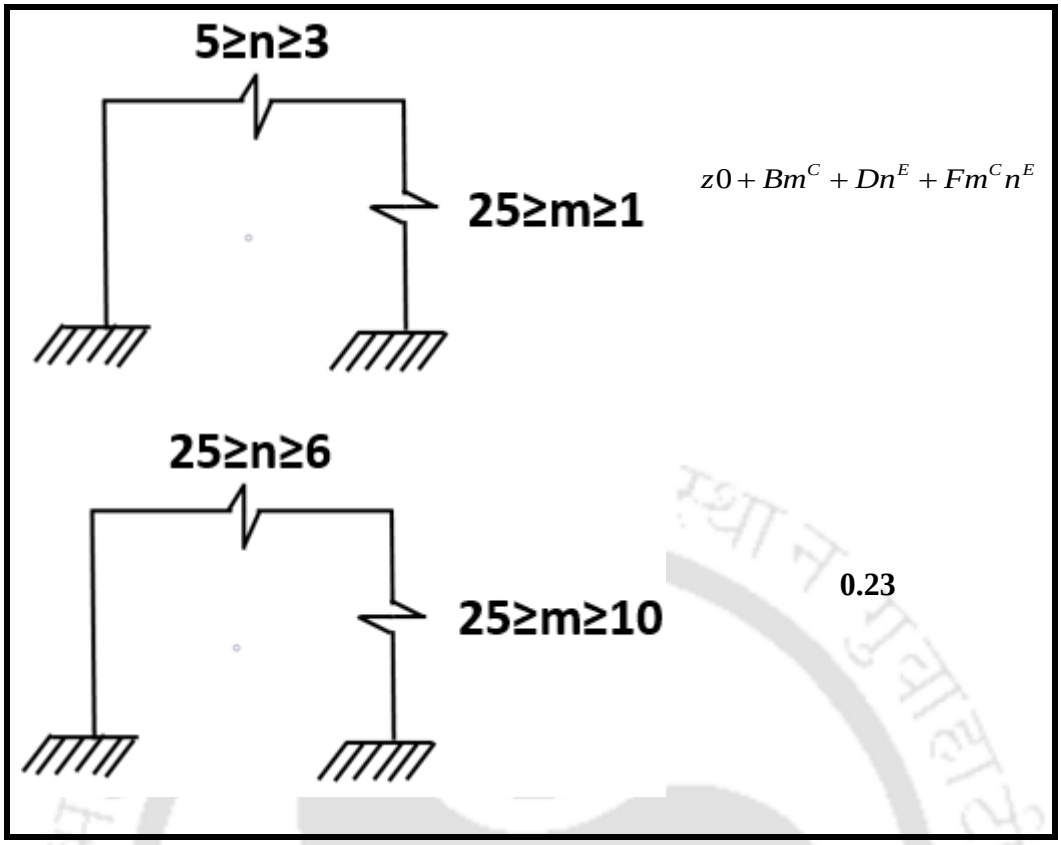
5≥n≥3
25≥m≥1
$z0 + Bm^C + Dn^E + Fm^C n^E$
25≥n≥6
25≥m≥10
0.23